Fragile yet Ductile

Structural Aspects of Reinforced Glass Beams

Proefschrift

ter verkrijging van de graad van doctor

aan de Technische Universiteit Delft,

op gezag van de Rector Magnificus prof. ir. K.C.A.M. Luyben,

voorzitter van het College voor Promoties,

in het openbaar te verdedigen op maandag 18 april 2011 om 12:30 uur

door

Pieter Christiaan LOUTER

bouwkundig ingenieur,

geboren te Papendrecht

Voor

mijn ouders
en Valesca

Preface

Fragile! ... is a warning message often used for postal packages to indicate the fragile nature of their content. The warning especially applies for packages containing glass objects. As is generally known, glass is highly sensitive to impact and fails in a brittle manner, leaving sharp and harmful fragments. Handling glass therefore urges for caution.

The application of glass as load-bearing material in buildings is – taking the before mentioned warning message into account – not an obvious choice. Nonetheless, glass is increasingly applied in contemporary architecture for structural components such as beams and columns. However, since glass is essentially an unsafe structural material, specific measures should be taken to avoid any harmful situations in case of glass breakage.

This PhD research investigates a specific safety concept for structural glass beams. This safety concept makes use of a small reinforcement section that is bonded to the glass beam. In case of incidental glass breakage, the reinforcement section bridges the crack and provides the beam a significant residual strength. Despite the crack in the glass, the beams are still able to carry load. Furthermore, instead of failing in a brittle manner, the so-called reinforced glass beams show ductile (*or:* 'plastic deformable') post-breakage response.

The addition of the reinforcement to the glass beams does not change the properties of the glass itself, which therefore remains *fragile*. However, the reinforcement significantly enhances the safety performance of the beams and even provides a *ductile* post-breakage response. Therefore the following, more reassuring, 'warning' message applies for reinforced glass beams … *Fragile yet Ductile!*

Acknowledgements

I really enjoyed working on this PhD research. Not in the least because of the valuable collaboration with colleagues, companies and students. Moreover, my friends and family have been of great support. I would like to thank every one of them, some of whom I would like to mention in particular.

I would like to thank Jan Rots (promotor) and Fred Veer (co-promotor) for providing the opportunity to work on the PhD research, and to offer a high degree of liberty in performing the research and in pursuing various activities associated to it. In addition, I would like to thank Fred for his dedicated mentorship, his inventive insights and his promptness in commenting on any paper resulting from the research.

Moreover, the members of the PhD committee, Jan Rots, Fred Veer, Rob Nijsse, Jan Belis, Jens Schneider, Paulo Cruz, Mauro Overend and Rinze Benedictus are gratefully acknowledged. It has been an honour to receive your expertise comments on the concept dissertation and to discuss the dissertation in detail. I would like to thank you all.

The chair of Mechanics in Buildings, of which I was a staff member during the research, has been a very pleasant and stimulating environment to work in. I would like to thank my colleague Gerrie Hobbelman for his sound explanations of all technical questions posed to him. Moreover, I would like to thank all the other colleagues of the chair – in particular my PhD-colleagues and roommates Freek Bos, Ilse de Vent en Julia Schönwälder – and the PhD colleagues of the department of Building Technology for the discussions and chats over coffee or lunch, and for the occasional games of chess (before the chess-board was turned into ashes).

The technical expertise of Kees Baardolf was the basis of every experiment performed during my PhD research. His flexibility and swiftness in fabricating test-setups has been of extremely high value for the research and of great support to me. I would like to thank Kees and also Louis – who joined later on – for their open-minded-approach in tackling all the technical issues, and for the joy they bring to the work in the laboratory. In addition, I would like to thank all the colleagues at the Stevin Laboratory (CiTG) and the Materials Laboratory (3ME) for their help in performing the experiments.

The input and support of glass supplier Van Noordenne Groep, interlayer manufacturer DuPont and adhesive manufacturer DELO is highly appreciated. These companies have offered all the materials needed for this research, which is gratefully acknowledged. In addition and on a personal level, I would like to thank Gerrit van Noordenne, Ton Romein, Frans van der Pol and Cor Kluver (Van Noordenne Groep); Björn Sandèn, Joris Bohets, Jan de Loose and Yvan van Geenhoven (DuPont) and Günther Witek (DELO) for their assistance and enthusiastic collaboration.

viii

In terms of research collaboration, the input of various researchers and students is acknowledged. The work performed in collaboration with the 'computation colleagues' at the faculty of Civil Engineering and Geosciences, Anne van de Graaf and Max Hendriks has been of great help. Moreover, the collaboration with Jan Belis and Dieter Callewaert at Ghent University in testing specimens at high temperature and in lateral torsional buckling has been of great value. In addition I would like to thank Jan for his hospitality during my visits in Ghent and for commenting on a great deal of the pre-concept dissertation. Furthermore, the MSc thesis projects of Linda Schetters (TUe), Job van Heusden, Martien Rademakers, Calvin Leung and Daniele Trovato on a topic associated with this PhD work has provided valuable insights. I would like to thank you all for the pleasant collaboration.

In addition, I would like to thank Jean-Paul Lebet, director of the ICOM Steel Structures Laboratory, for providing me additional time to finalize my dissertation and for providing the opportunity to continue my research in the field of glass at the EPFL.

Special thanks go to my appreciated friends and colleagues Freek Bos and Richard Pijpers for being 'paranimf' during the defence ceremony. Freek was my close colleague and companion in the glass research. Together we have been deliberating various times on glass related issues, which was from time-to-time conveniently combined with our travelling to glass conferences and meetings. In addition to being a 'paranimf', I would like to thank you very much for commenting on the concept dissertation and for our enjoyable partnership in the glass research and organization of the Challenging Glass conferences. Richard was, as a PhD-researcher in the field of steel, often the neighbouring conductor of experiments in the laboratory. Several steel and glass specimens have been tested side-by-side. In addition to being a 'paranimf', I would like to thank you very much for the various discussions we had about the PhD research and all the issues related to it.

I would like to thank all my friends for their companionship. Playing music together, having a drink in town, playing sports at Wednesday-evening, and various other activities offered a welcome distraction from the ordinary. Moreover, I would like to thank Marjolein, Richard, Noortje, Thijs, Eline and Erik for our very relaxing holidays.

My dear family is always of great support to me. I would like to thank my parents and Piety, Thierry, Nicole, Annemie, Pieter, and the 6 kids for providing a relaxed and safe harbour and for offering a helping hand whenever needed.

But most of all, I would like to thank my dear Valesca for her cheerfulness, care, patience and love. You really are the joy in my live.

Thank you all!

Christian Louter

Lausanne, Switzerland, March 2011

Summary: Fragile yet Ductile

In contemporary architecture there is an increasing demand for transparency. Apart from its traditional and ongoing use as an infill panel, glass is increasingly used for structural components, such as beams, columns and walls. However, due to its brittle nature and the difficulties in predicting its failure, glass is essentially an unsafe structural material.

This research focuses on a specific safety concept for structural glass beams. This safety concept makes use of a small reinforcement section that is bonded at/in the tensile zone of the glass beam. Upon fracture of the glass, the reinforcement bridges the crack and transfers the tensile forces. Together with a compressive force in the un-cracked compression zone in the glass, an internal couple is generated which enables the cracked beam to still carry load.

This safety concept has been explored in preceding research at the TU Delft. The current research has started from these exploratory studies and investigates the structural response of reinforced glass beams in more detail. Through experimental investigations the effects of various parameters on the structural response of reinforced glass beams are investigated. Furthermore, by means of analytical and numerical modelling the structural response of reinforced glass beams is described.

Experimental investigations

The experimental investigations focus on the effects of the parameters *bond system*, *temperature*, *thermal cycling*, *humidity*, *load duration*, *reinforcement material*, *reinforcement percentage* and *beam size* on the structural response of reinforced glass beams. This is done by means of pull-out tests to investigate the pull-out strength of the reinforcement, and by means of bending tests to investigate the structural response of reinforced glass beams.

Two specific bond systems are investigated, namely the UV-curing acrylate adhesive GB368 (GB) and the ionomer SentryGlas® (SG) interlayer. Furthermore, two specific beam geometries are investigated, namely triple-layer annealed float glass beams with a stainless steel reinforcement section bonded (with the GB or SG) at the inner recessed tensile edge, and double-layer annealed float glass beams with GFRP (Glass Fiber Reinforced Polymer) reinforcement rods embedded in the SG interlayer.

From the experimental investigations into the effects of *bond system*, *temperature*, *thermal cycling* and *humidity* it is observed that they have a specific effect on the extent of bond failure, and thus on the debonding of reinforcement, at the post-breakage stage. In this respect the SG interlayer performed very well. Despite the observed reduction in bond strength of the SG interlayer at low temperature, at high temperature, after thermal cycling and after humidity exposure, the extent of bond failure remained limited. The SG-laminated beams never demonstrated full debonding of reinforcement, whereas this failure mode frequently occurred for the GB-bonded beams.

From the experimental investigations into the effects of *load-duration*, it is observed that creep of the SG bond causes creep of cracked SG-laminated reinforced glass beams. However, even after 3 to 15 months of being loaded at 80% of the predicted ultimate failure load, the cracked beams did not collapse. This indicates that for practical applications of reinforced glass beams, there will be sufficient time for the building users to notice the failure and to take measures.

From the experimental investigations into the effects of *reinforcement material* it is observed that the *stainless steel* reinforced beams display ductile post-breakage response due to plastic deformation of the reinforcement, whereas the *GFRP* reinforced beams show semi-ductile post-breakage response. Since the GFRP reinforcement lacks any yield mechanism, it is assumed that this semi-ductility originates from repetitive cracking of the glass and local debonding of the reinforcement.

From the experimental investigations into the effects of *reinforcement percentage* it is observed that it has a specific effect on the height of the initial cracks in the glass. Increasing the amount of reinforcement at the lower (tensile) edge of the beam lowers its neutral axis, which results in a reduced height of the (initial) cracks in the glass. Furthermore, increasing the amount of reinforcement in the section effectively increases the post-breakage strength and stiffness of the beams, due to an increased total tensile load capacity of the reinforcement.

From the experimental investigations into the effects of *beam size* it is observed that apart from the obvious size-related difference in load-carrying capacity, the investigated 1.5 and 3.2 m SG-laminated reinforced beams demonstrate similar structural response in terms of cracking of the glass and in terms of ductile post-breakage response. However, the 1.5 m beams profited from an additional load-carrying mechanism that was generated by crack-bridging glass fragments that transferred forces over the cracks through shear in the SG interlayer, whereas this additional load-carrying mechanism was largely absent for the 3.2 m beams. No specific explanation for this difference was found.

Analytical and numerical modelling

By means of analytical and numerical modelling the structural response of reinforced glass beams is described. The analytical model is developed in this research in analogy with reinforced concrete. The 2D numerical model – built in DIANA – makes use of a novel sequentially linear analysis (SLA) technique and saw-tooth reduction diagrams to simulate cracking of the glass and plastic deformation of the reinforcement.

From the analytical and numerical models it is observed that their results are in rather good agreement with the experimental results. The analytical and numerical models assume a solid cross-section without any layering of the glass. Since the GB-bonded beams demonstrate rather monolithic behaviour of the adhesively bonded glass layers – with cracks that run through the full width of the laminate – the model results are in good agreement with the experimental results of the GB-bonded beams. For the SG-laminated beams, which show less monolithic behaviour of the laminate due the crack blocking properties of the SG interlayer, the post-breakage strength is underestimated by the models. Since the cracks in the SG-laminated beams generally do not run through the full width of the laminate, an additional load-carrying mechanism is generated by crack-bridging glass fragments in neighbouring glass layers that transfer tensile forces over the crack through shear in the SG interlayer. This mechanism is not yet incorporated in the models. Furthermore, bond-slip of the reinforcement is not incorporated by the models as they neglect the bond between the glass and the reinforcement. Local debonding of reinforcement and ultimate failure due to full debonding of reinforcement is thus not yet described by the models. Moreover, the cracking sequences resulting from the numerical model are currently only indicative and insufficiently consistent with the experimental results.

Conclusions

From the *experimental investigations* performed in this research it is concluded that reinforcing an annealed float glass beam, in order to obtain safe post-breakage behaviour, is a feasible and demonstrably safe concept. The experiments have demonstrated that significant post-breakage strength and stiffness can be obtained through the addition of a reinforcement section at the tensile zone of the glass beam.

Furthermore, it is concluded that between the GB-bonded and SG-laminated specimens, the SG-laminated specimens performed best[i]. The SG-laminated beams demonstrated only limited debonding of reinforcement at the post-breakage stage, whereas the GB-bonded beams often show full debonding of reinforcement and thus collapse.

---

[i] The in this research observed performance levels of the investigated bond systems should not be interpreted for applications outside the scope of this research. For applications outside the scope of this research, different conditions may apply – such as a different bond geometry, loading condition, manufacturing technique, etc. – which may lead to a different performance of the bond system than is observed in this research.

Moreover, it is concluded that the SG-laminated reinforced glass beams are the most feasible to be applied in practice. Even at high and low service temperatures, after thermal cycling and for long-duration post-breakage loading, the SG-laminated reinforced glass beams demonstrate redundant post-breakage performance.

However, it should be noted that the effect of humidity on the structural response is not yet sufficiently understood to be able to apply the SG-laminated reinforced glass beams in (highly) humid environments.

Additionally, it is concluded that the SG interlayer is well-suited for the production of the reinforced glass beams. Due to the low viscosity of the SG interlayer during the autoclave process, the SG interlayer easily adjusts to its surroundings, which allows it to adapt to dimensional tolerances. Furthermore, it allows for embedment of reinforcement in the SG interlayer.

From the *analytical modelling* it is concluded that the analogy with reinforced concrete is valid. Furthermore, it is concluded that the analytical model offers an easy-to-use and fairly accurate tool to describe the overall structural response of reinforced glass beams.

From the *numerical modelling* it is concluded that the sequentially linear elastic analysis (SLA) method and the associated saw-tooth reduction diagrams offer a suitable technique for the simulation of glass fracture and plastic deformation of reinforcement. It provides a stable simulation technique which is capable of accurately simulating the repetitive peaks in the post-breakage response of reinforced glass beams without running into convergence problems. The numerical results are in rather good agreement with the experimental results.

Recommendations

From this research several recommendations for future research follow.

Firstly, it is recommended to perform additional studies into the *effects of various parameters* on the structural response of reinforced glass beams. Especially the effects of the parameter *humidity* on SG-laminated reinforced glass beams are of importance. It should be verified whether the observed delamination of one humidity-exposed SG-laminate originates from the humidity exposure procedure or from other causes. Additionally, the effects of the parameter *beam size* on the structural response are of interest. Further studies should verify whether the effects of beam size are still rather limited for beams larger than the currently investigated 3.2 m beams. Given the rapid developments in the field of oversized glass beams, this is particularly important. Furthermore, the effects of the parameter *glass type* on the structural response should be addressed. The application of stronger glass types than the currently applied annealed float glass might on the one hand significantly reduce the cross-section dimensions of the beam, but might on the other hand also lead to a completely different post-breakage response. Moreover, it is recommended to investigate to what extent there is a

strengthening effect of the reinforcement. Besides a strengthening effect on the initial resistance of the (un-cracked) beam, the reinforcement might also enhance the local strength of the glass by locally bridging the flaws in the glass. This bridging effect might reduce the stress peaks at the flaw tip and might cause an increase of the tensile bending strength of the glass. Also the *simultaneous effects* of various parameters on the structural response could be examined. The current research has only focused on individual parameters, while a combination of parameters could have more severe effects.

Secondly, it is recommended to further develop *the analytical and the numerical model* to improve their accuracy in describing the structural response of reinforced glass beams. For the analytical model it is expected that its results can be improved by implementing the bond between glass and the reinforcement in the model, to predict bond-slip of the reinforcement. This could possibly be done by extending the model with equations for describing the shear stress in the bond by which bond failure could be predicted. For the numerical model it is expected that its results could be enhanced by incorporating layering of the glass and bond-slip of the reinforcement, which could both be done by means of interface elements and by upgrading the currently applied 2D model to a 3D model. However, the SLA technique is currently not suited for interface elements and for 3D modelling and should therefore be further developed. Additionally, it is expected that the application of sophisticated meshing alternatives and the application of rotating crack formulations could further improve the simulation of the crack path in the glass.

Thirdly, it is recommended to investigate the possibilities of *embedded reinforcement* in structural glass beams in more detail. From the current research it is observed that the embedment of reinforcement offers various structural and architectural benefits that could be further exploited.

Fourthly, it is recommended to investigate the *post-breakage lateral stability* of reinforced glass beams in more detail. Especially for laterally unsupported bending components, such as facade fins, the post-breakage stability is of importance.

Finally, it is recommended to also further investigate the *alternative concept of post-tensioned* glass beams. In post-tensioned beams the use of the tension component seems to be more efficient than in a reinforced glass beam. Exploratory studies into post-tensioned glass beams, given in Appendix IV, show promising results.

Samenvatting: Fragiel maar toch Ductiel

In de hedendaagse architectuur de vraag naar transparantie neemt toe. Glas wordt, naast het traditionele gebruik als gevelpaneel, steeds meer gebruikt voor constructieve componenten, zoals liggers, kolommen en wanden. Echter, vanwege de brosse breuk en de moeilijkheden bij het voorspellen van het faalgedrag is glas in essentie een onveilig constructiemateriaal.

Het voorliggend onderzoek richt zich op een specifiek veiligheidsconcept voor constructief glazen liggers. In dit veiligheidsconcept wordt gebruik gemaakt van een klein wapeningsprofiel dat aan/in de trekzone van de glazen ligger wordt verlijmd of gelamineerd. Bij breuk van het glas zal het wapeningsprofiel de ontstane scheur in het glas overbruggen en daarmee de trekkrachten opnemen. Samen met een drukkracht in de ongescheurde drukzone van de ligger, wordt een intern koppel gegenereerd waardoor de ligger nog steeds in staat is belasting te dragen.

De werking van dit veiligheidsconcept is reeds verkend in voorgaand onderzoek aan de TU Delft. Het huidige onderzoek is gestart uit deze verkennende studies en onderzoekt het constructief gedrag van de gewapende glazen liggers in meer detail. Door middel van experimenteel onderzoek worden de effecten van verschillende parameters op het constructief gedrag van de gewapende glazen liggers onderzocht. Tevens wordt middels analytische en numerieke modellen het constructief gedrag van de liggers beschreven.

Experimenteel onderzoek

Het experimenteel onderzoek richt zich op verschillende parameters die het gedrag van de liggers kan beïnvloeden, zoals het *lijm/lamineer systeem*, *omgevings temperatuur*, *wisselende temperatuursbelasting*, *vocht*, *belastingsduur*, *wapeningsmateriaal*, *wapeningspercentage* en *liggerformaat*. Deze parameters worden onderzocht middels 'uittrek-proeven' die zich richten op de aanhechting tussen de wapening en het glas, en middels 'buigproeven' die zich richten op het constructief gedrag van de liggers.

Twee verschillende systemen om de wapening aan het glas te verbinden zijn onderzocht, namelijk een lijmmethode die gebruik maakt van een UV-uithardende acrylaatlijm (GB) en een lamineermethode die gebruik maakt van de polymeer tussenlaag SentryGlas® (SG). Tevens zijn twee verschillende ligger configuraties getest, namelijk drielaags glazen liggers met een roestvaststalen (rvs) wapening verlijmd/gelamineerd (met GB of SG) ter plaatse van de terugliggende middelste glaslaag, en dubbellaags glazen liggers met glasvezelversterkte kunststof (gvvk) wapeningsstrengen die tussen de twee glaslagen zijn gelamineerd met behulp van de SG tussenlaag.

Het experimenteel onderzoek naar de effecten van de parameters *lijm/lamineer systeem*, *omgevings temperatuur*, *wisselende temperatuursbelasting* en *vocht* laat zien dat deze parameters specifiek effect hebben op de mate van onthechting tussen het glas en de wapening tijdens het post-breuk gedrag van de ligger. In dit opzicht presteerde de SG tussenlaag zeer goed. Ondanks de geoberseerde verminderde hechtsterkte van de SG bij lage temperatuur, bij hoge temperatuur, na wisselende temperatuursbelasting and na expositie aan vocht, bleef de mate van ontheching tussen het glas en de wapening beperkt. The SG-gelamineerde liggers vertoonden geen volledige onthechting van de wapening, terwijl dit wel vaak het geval was voor de GB-verlijmde liggers.

Het experimenteel onderzoek naar de effecten van de parameter *belastingsduur* laat zien dat kruip van de SG tussenlaag leidt tot kruip van gescheurde SG-gelamineerde gewapende glazen liggers. Echter, zelfs na een belastingsduur van 3 tot 15 maanden op een belastingsniveau van 80% van de voorspelde bezwijkbelasting, zijn de gescheurde liggers niet bezweken. Dit is een goede indicatie dat er in praktijk-toepassingen voldoende tijd zal zijn voor de gebouw-gebruikers om eventuele breuk van de gewapende glazen liggers te detecteren en om vervolgens maatregelen te nemen.

Het experimenteel onderzoek naar de effecten van de parameter *wapeningsmateriaal* laat zien dat rvs-gewapende liggers ductiel post-breuk gedrag vertonen door plastische vervorming van de wapening, terwijl gvvk-gewapende liggers semi-ductiel post-breuk gedrag vertonen. Aangezien de gvvk (glasvezelversterkte kunststof) wapeningsstrengen geen plasticiteit vertonen, wordt verondersteld dat dit semi-ductiel gedrag zijn oorsprong heeft in het herhaaldelijk ontstaan van scheuren in het glas en de lokale onthechting van de wapening.

Het experimenteel onderzoek naar de effecten van de parameter *wapeningspercentage* laat zien dat deze parameter een specifiek effect heeft op de hoogte van de initiële scheuren in het glas. Een hoger wapeningspercentage, dus meer wapening, resulteert in lagere scheurhoogten. De grotere hoeveelheid wapening zorgt voor een verlaging van de neutrale liggeras en een verkleining van de scheuropening, waardoor de scheur minder ver propageert. Tevens zorgt de grotere hoeveelheid wapening voor een grotere reststerkte en stijfheid van de ligger.

Het experimenteel onderzoek naar de effecten van *ligger formaat* laat zien dat, afgezien van het voor de hand liggende verschil in draagvermogen, de 1,5 m en 3,2 m lange SG-gelamineerde gewapende glazen liggers sterke gelijkenissen vertonen in scheurgedrag en post-breuk gedrag. Echter, de 1,5 m liggers profiteerden van een bijkomend draagmechanisme dat werd gegenereerd door scheuroverbruggende glasfragmenten die krachten over de scheur leiden door schuifkrachten in de SG tussenlaag, terwijl dit mechanisme niet bij de 3,2 m liggers optrad. Een specifieke oorzaak voor dit verschil is niet gevonden.

Analytische en numerieke modellering

De analytische en numerieke studies richten zich op het modelleren van het constructief gedrag van de gewapende glazen liggers. Het analytisch model is ontwikkeld in dit onderzoek in analogie met gewapend beton. Het numerieke 2D model maakt gebruik van een innovatieve sequentieel linear elastische analyse techniek en zogenoemde zaagtand-diagrammen waarmee het scheuren van het glas en het plastisch vervormen van de wapening kan worden gesimuleerd.

De resultaten van zowel het analytische model als het numerieke model komen redelijk goed overeen met de experimentele resultaten. In beide modellen wordt uitgegaan van een massieve glasdoorsnede en wordt de gelaagdheid van het glas niet verondersteld. Hierdoor zijn de resultaten met name in overeenstemming met de GB-gelijmde liggers die door de relatief starre lijm zich vrijwel monolitisch gedragen en daardoor scheuren vertonen die door de volle breedte van het laminaat groeien. Voor de SG-gelamineerde liggers, die door de scheurstoppende werking van de SG tussenlaag minder monolitisch gedrag vertonen, wordt de post-breuk sterkte door de modellen onderschat. Aangezien de scheuren in de SG-gelamineerde liggers niet over de volle breedte van het laminaat lopen, kan een bijkomend draagmechanism worden ontwikkeld door scheur-overbruggende glasfragmenten die trekkrachten over de scheur leiden door afschuiving in de SG tussenlaag. Dit bijkomende draagmechanisme wordt door de modellen niet meegenomen. Tevens wordt de lijmverbinding/tussenlaag tussen het glas en de wapening niet meegenomen in de modellen. Hierdoor kunnen de modellen eventuele locale danwel volledige onthechting van de wapening niet simuleren.

Conclusies

Op basis van de experimenten verricht in dit onderzoek, wordt geconcludeerd dat het wapenen van een glazen ligger (uitgegloeid floatglas), met als doel het verkrijgen van een veilig post-breuk gedrag, een haalbaar en aantoonbaar veilig concept is. De experimenten tonen aan dat een significante post-breuk sterkte en stijfheid kan worden verkregen door het aanbrengen van een wapening in de trekzone van de glazen ligger.

Tevens wordt geconcludeerd dat van de onderzochte GB-verlijmde en SG-gelamineerde proefstukken, de SG-gelamineerde proefstukken het best presteren[i]. De SG-gelamineerde liggers vertoonden slechts in zeer beperkte mate onthechting van de wapening, terwijl de GB-gelijmde liggers veelal volledige onthechting van de wapening vertoonden met volledig bezwijken van de liggers tot gevolg.

---

[i] De in dit onderzoek geobserveerde prestaties van de lijm/lamineer systemen, geven geen garanties voor toepassingen buiten het aandachtsgebied van dit onderzoek. Voor toepassingen anders dan hier onderzocht zullen andere condities gelden – zoals een andere geometrie, belastingsgeval, productietechniek, etc. – waardoor de prestatie van het lijm/lamineer systeem anders kan zijn dan hier gepresenteerd.

Bovendien wordt geconcludeerd dat de SG-gelamineerde gewapende glazen liggers het meest haalbaar zijn om in praktijk te worden toegepast. Zelfs bij hoge en lage omgevingstemperaturen, na wisselende temperatuursbelasting en voor langdurige post-breuk belasting, vertonen de SG-gelamineerde liggers zeer veilig gedrag. Echter, het moet worden opgemerkt dat de effecten van vocht nog niet voldoende bekend zijn om de liggers in (extreem) vochtige omgevingen te kunnen toepassen.

Daarnaast wordt geconcludeerd dat de SG tussenlaag zeer geschikt is voor de productie van gewapende glazen liggers. Door de lage viscositeit van de SG tussenlaag tijdens het autoclaaf lamineerproces, vormt de SG tussenlaag zich gemakkelijk naar zijn omgeving, waardoor maattoleranties op het glas en/of de wapening geen probleem vormen. Bovendien maakt deze lage viscositeit inbedding van wapeningsstrengen in de SG tussenlaag mogelijk.

Op basis van de analytische modelleringen verricht in dit onderzoek wordt geconcludeerd dat de analogie met gewapend beton valide is. Verder wordt geconcludeerd dat het analytische model een tamelijk eenvoudige methode biedt waarmee het constructief gedrag van de gewapende glazen liggers tot op zekere hoogte accuraat beschreven kan worden.

Op basis van de numerieke modelleringen verricht in dit onderzoek wordt geconcludeerd dat de sequentieel linear elastische analyse methode en de daarmee samenhangende zaagtand diagrammen een geschikte methode bieden voor het simuleren van het scheuren van het glas en het plastisch vervormen van de wapening. Tevens kan worden geconcludeerd dat het numerieke model het constructief gedrag van de liggers, en met name de achtereenvolgende pieken in het post-breuk gedrag, redelijk gedetailleerd kan beschrijven zonder daarbij op convergentie problemen te stuiten.

Echter, het moet worden opgemerkt dat zowel in het analytische als het numerieke model momenteel de gelaagdheid van het glas en de aanhechting tussen het glas en de wapening niet is meegenomen. Verder moet worden opgemerkt dat de scheurpatronen die door het numerieke model worden gegenereerd momenteel slechts indicatief van aard zijn en onvoldoende overeenkomen met de experimentele resultaten.

Aanbevelingen

Op basis van dit onderzoek worden enkele aanbevelingen voor vervolgonderzoek gegeven.

Ten eerste wordt aanbevolen om aanvullend onderzoek te verrichten naar de effecten van verschillende parameters op het constructief gedrag van gewapende glazen liggers. Met name de effecten van de parameter *vocht* op SG-gelamineerde liggers zijn van belang. Er moet worden nagegaan of de waargenomen delaminatie van een aan vocht

blootgestelde SG-gelamineerde ligger het gevolg is van de hoge vochtigheid of van andere oorzaken. Bovendien zijn de effecten van de parameter *ligger formaat* op het constructief gedrag van belang. Vervolgstudies zullen moeten aantonen of de effecten van liggerformaat nog steeds vrij beperkt zijn voor liggers groter dan de momenteel onderzochte 3,2 m balken. Gezien de snelle ontwikkelingen op het gebied van overmaatse glazen liggers is dit van specifiek belang. Tevens zullen de effecten van de parameter *glas type* op het constructief gedrag nader moeten worden onderzocht. De toepassing van sterkere glassoorten dan het momenteel toegepaste uitgegloeide floatglas zou aan de ene kant de afmetingen van de liggerdoorsnede aanzienlijk kunnen reduceren, maar kan aan de andere kant ook leiden tot een volstrekt ander post-breuk gedrag van de liggers. Bovendien wordt aanbevolen om te onderzoeken in welke mate de wapening bijdraagt aan een versterking van de ligger. Naast een versterkend effect op de stijfheid van de (on-gescheurde) ligger, zorgt de wapening wellicht ook voor een verhoging van de lokale sterkte van het glas door het lokaal het overbruggen van microscheuren in het glas. Dit laatste kan leiden tot een vermindering van de spanningspieken aan de scheurtip en daarmee tot een toename van de buigtreksterkte van het glas. Ten slotte kan de gelijktijdige invloed van verschillende parameters op het constructief gedrag van de liggers worden worden onderzocht. Het huidige onderzoek heeft zich alleen gericht op de individuele parameters, terwijl een combinatie van parameters tot andere resultaten zou kunnen leiden.

Ten tweede wordt aanbevolen om het analytische en numerieke model verder te ontwikkelen en daarmee de resulterende beschrijvingen van het constrief gedrag van de gewapende glazen liggers verder te verbeteren. De verwachting is dat het implementeren van een interface tussen de wapening en het glas en tussen de individuele glaslagen kan leiden tot een meer accurate beschrijving van het constructief gedrag van de gewapende glazen liggers.

Ten derde wordt aanbevolen om de mogelijkheden van het inbedden van wapening in de tussenlaag van gelamineerde glazen liggers in meer detail te onderzoeken. De huidige onderzoeksresultaten tonen aan dat het inbedden van wapening diverse constructieve en architectonische voordelen biedt, die verder kunnen worden benut.

Ten vierde wordt aanbevolen om de zijdelingse stabiliteit van gescheurde gewapende glazen liggers in meer detail te onderzoeken. Speciaal voor lateraal ongesteunde buigcomponenten, zoals gevelvinnen, is de post-breuk stabiliteit van belang.

Ten slotte wordt aanbevolen om verder onderzoek te verrichten naar het alternatieve concept van nagespannen glazen liggers. In nagespannen glazen liggers kan door de aangebrachte naspankracht meer efficient gebruik worden gemaakt van het toegevoegde trekelement dan in gewapende glazen liggers. Verkennende onderzoeken op dit gebied, zoals getoond in Appendix IV, laten veelbelovende resultaten zien.

xx

Table of Contents

PART II   **Theoretical framework**

PART V   **Retrospect and prospect**

Chapter 11
Conclusions   **233**

Chapter 12
Recommendations   **241**

APPENDICES

List of symbols and abbreviations

symbol	description
A	area
A_{gl}	glass area
A_i	area of the considered component
A_{re}	reinforcement area
E	Young's modulus
E_i	Young's modulus of the considered component
EI	bending stiffness
$EI_{composite}$	composite/initial bending stiffness
F	force
G_f	fracture energy
I	moment of inertia
$I_{yy,i}$	moment of inertia of the considered component
M	moment
N_{gl}	axial force in the glass
N_{re}	axial force in the reinforcement
S	linear moment of area
T_g	glass transition temperature
T_m	melting temperature
V	shear force
W	moment of resistance
a	internal lever arm; distance between the compressive and tensile force
a_{setup}	distance between the loading and support point in a bending setup
b	width
b_{beam}	width of the beam

b_{bond}	width of bond line
b_{gl}	width of the glass
d	distance from compressive beam edge to reinforcement axis
$f_{gl,c}$	compressive strength glass
$f_{gl,t}$	tensile strength glass
$f_{re,t}$	tensile strength reinforcement
$f_{re,y}$	yield strength reinforcement
h	height
h_{beam}	height of the beam
h_{cbw}	crack band width
h_{gl}	height of the glass
i	considered component in the section (either glass or reinforcement)
l	length
l_{beam}	length of the beam
l_{setup}	distance between the beam supports in a test setup
n	total number of components in the section
t	thickness
t_{bond}	thickness of the bond (i.e. adhesive or interlayer thickness)
w	crack opening
x_B	height of the compression zone at stage B
x_C	height of the compression zone at stage C
z	distance to the neutral axis
z_c	distance from the compressive beam edge to neutral beam axis
z_i	distance between axis of the component and the neutral beam axis
z_{re}	distance from the reinforcement axis to the neutral beam axis
z_t	distance from the tensile beam edge to the neutral beam axis

β	shear reduction factor
δ	displacement
ε	strain
ε_{gl}	compressive strain glass
ε'_{gl}	tensile strain glass
$\varepsilon_{gl,t}$	ultimate tensile strain glass
$\varepsilon_{gl,c}$	ultimate compressive strain glass
$\varepsilon_{re,y}$	yield strain reinforcement
$\varepsilon_{re,r}$	strain at rupture
κ	curvature
ρ	density
σ	stress
τ	shear stress
υ	poisson's ratio
φ	angle of rotation

abbreviation	description
GB	GlasBond; GB 368; acrylate adhesive
HE	humidity exposure
LD	long-duration
RT	room temperature
SG	SentryGlas; polymer interlayer
TC	thermal cycling
mg	mesh geometry
r	rectangular
rs	reduction steps
tr	triangular

Part I

Introduction

Part I

Introduction

Chapter 1

Introduction to
the research

Part II

Theoretical
framework

Chapter 2

Structural
glass beams

Chapter 3

The reinforced
glass beam
concept

Chapter 4

Materials
applied in this
research

Part III

Experimental,
analytical and
numerical
investigations

Chapter 5

Experimental
investigations
into the effects
of
bond type,
temperature,
thermal cycling,
humidity and
load duration
on the structural
response

Chapter 6

Experimental
investigations
into the effects
of
reinforcement
percentage
and beam size
on the structural
response

Chapter 7

Experimental
investigations
into the
structural
response of SG-
laminated glass
beams with
embedded glass
fibre
reinforcement

Chapter 8

Analytical and
numerical
modelling of
the structural
response

Part IV

Integrated
discussion of
the research
results

Chapter 9

Integrated
discussion on the
structural aspects of
reinforced glass
beams

Chapter 10

Integrated
discussion on the
production and
design aspects of
reinforced glass
beams

Part V

Retrospect
and
prospect

Chapter 11

Conclusions

Chapter 12

Recommendations

Chapter 1
Introduction to the research

This chapter provides an introduction to the research. The research topic and the research aspects are briefly introduced. Furthermore, an outline of the dissertation is provided.

Abstract

In contemporary architecture there is an increasing demand for transparency. Glass is desired as a load-bearing material for structural components, such as beams, columns, and walls. However, due to its brittleness and un-predictable failure behaviour, glass is considered a structurally unsafe material. To overcome the problem of brittle failure, this research focuses on a specific safety concept for structural glass beams. This safety concept embodies the addition of a reinforcement section at/in the tensile zone of the glass beam. It intends to increase the residual resistance of the beam at the cracked stage through a composite action of the glass and reinforcement. Preceding exploratory investigations at TU Delft has demonstrated the potential of this reinforced glass beam concept. The beams showed ductile post-breakage response and significant post-breakage strength. The current research has started from these exploratory studies and investigates the reinforced glass beam concept in more detail. It consists of *experimental* investigations into the effects of *bond system*, *temperature*, *thermal cycling*, *humidity*, *load duration*, *reinforcement material*, *reinforcement percentage* and *beam size* on the structural response of reinforced glass beams. Furthermore, it consists of *analytical* and *numerical* studies into the prediction of the structural response of reinforced glass beams. The objective of this research is to increase the understanding of the structural response and structural functioning of reinforced glass beams.

1.1.   Problem definition

1.1.1.   *Glass as a structural material*

The application of glass as a structural material in contemporary architecture is steadily increasing. Besides its traditional use as an infill panel, glass has evolved over the last few decades to a load-bearing material for various structural elements; such as beams, columns and walls. These structural elements are employed for e.g. roof structures, façade structures, conservatories, footbridges or staircases [Nijsse, 2003; Schittich et al., 2007; Wigginton, 1996; Wurm, 2007].

However, due to its brittle failure, glass is essentially an unsafe structural building material. Unlike for instance steel that shows noticeable ductile deformation before ultimate failure occurs, glass lacks this ability to deform in a ductile manner. It fails sudden and without any warning. Furthermore, due to its inability to redistribute stresses by local yielding of the material, glass is highly sensitive to peak stresses. Excessive local stressing of the glass results in cracking of the glass. Moreover, glass is strong in compression, but weak in tension, which limits its applicability as a tension component.

To overcome the problem of unsafe structural behaviour of glass, two measures – adopted from the car industry – are commonly applied for structural glass components, see Chapter 2. Firstly, a tempering process is applied to increase the (tensile) strength of the glass. Due to this increase in strength, the resistance of the component is enhanced. Secondly, foil or resin interlayers are applied to compose components that consist of multiple glass layers ('laminated glass'). If one of the glass layers fails, the others will still be able to carry load. Both measures are focused on minimizing the probability of complete failure – i.e. failure of all glass layers of the component – and thus to prevent from collapse of the structural glass component.

However, despite these measures, complete failure of the structural glass component may still occur due to unforeseen events. The multiple glass layers of the component may for instance crack due to severe or repetitive impact (e.g. vandalism), or due to simultaneous high local stressing of all glass layers as a result of assembly errors (most notably at the supports or at the joints). Additional safety measures or safety concepts to enhance the redundancy of structural glass components are therefore strongly recommended.

This research project focuses on a specific safety concept for structural glass beams. The safety concept embodies the addition of a reinforcement section to the glass beam and intends to increase the residual resistance of the beam through a composite action of the glass and reinforcement. The so-called 'reinforced glass beam' concept has been developed within the structural glass research program at TU Delft over the past few years, see Chapter 3, and is explained in more detail in the following section.

1.1.2.   Reinforced glass beam concept

The reinforced glass beam concept has been developed from a different perspective than common safety measures. Rather than minimizing the probability of glass failure, it focuses on minimizing the consequences of glass failure. Even if all glass layers of the beam laminate are broken, the beam should not collapse and should still be able to carry load. The concept thus aims for high residual resistance of structural glass beams.

This high residual resistance is obtained by bonding a reinforcement section at the tensile edge of the glass beam. In case of glass fracture the reinforcement acts as a crack bridge, thereby halting the crack growth in the glass and transferring the tensile force over the crack, see Figure 1.1. The tensile force in the reinforcement together with a compression force in the (non-cracked) compression zone generates an internal load-carrying mechanism which enables the beam to still carry load even if all glass layers are cracked[i]. This significantly enhances the safety performance of the beam.
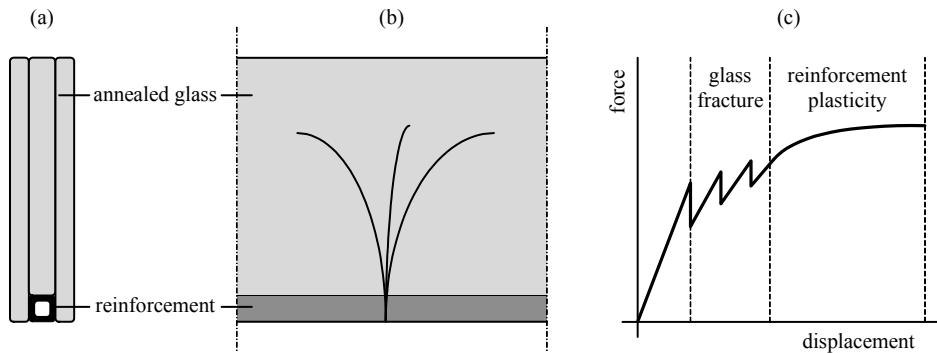
Figure 1.1: Schematic representation of the functioning of the reinforced glass beam concept;
(a) cross-section of a reinforced glass beam; (b) side-view of a cracked reinforced glass beam;
(c) intended force-displacement diagram, which shows a significant post-breakage strength.

---

[i] A more extensive description of the functioning of the reinforced glass beam concepts is provided in Chapter 3, section 3.2.

Preceding research at the TU Delft [Louter et al., 2005; Veer et al., 2003a, b] explored the reinforced glass beam concept[i]. The stainless steel reinforced glass beams that were investigated in preceding research showed high residual strength and ductility at the post-breakage stage. These promising results are further sustained by other research projects that focus(ed) on glass beams with either carbon-fiber, timber, reinforced-concrete, or steel reinforcement [Cruz & Pequeno, 2008a; Freitag, 2004; Kreher, 2004; Nielsen & Olesen, 2007; Palumbo, Palumbo & Mazzuchelli, 2005; Weller, Meier & Weimar, 2010]. These research projects focused on the structural response of reinforced glass beams. From the results of 3-point and 4-point bending tests it is observed that the reinforced glass beams show significantly enhanced safety performance compared to common (un-reinforced) structural glass beams.

However, not all (structural) aspects of reinforced glass beams are yet fully understood and investigated. The effects of for instance temperature, humidity and long-term post-breakage loading on the structural response of reinforced glass beams are not yet (extensively) investigated. These effects may be crucial for the safety performance of the reinforced glass beam, as it may influence the intermediary bond between glass and reinforcement and the structural functioning of the system.

The current research project therefore focuses on a further broadening of the knowledge and understanding of the structural response of reinforced glass beams. Various parameters that are expected to influence the structural response of reinforced glass beams are experimentally investigated. Furthermore, analytical and numerical investigations are performed into the prediction of the structural response of reinforced glass beams. The following section provides an overview of the research aspects, the investigated parameters and the applied methodology.

---

[i] An overview of the evolution of the reinforced glass beam concept studied at TU Delft is provided in Chapter 3, section 3.3.

1.2.   Research aspects and methodology

The experimental, analytical and numerical investigations performed in this research are explained in more detail in the following subsections.

1.2.1.   Experimental investigations

The experimental investigations focus on the effects of various parameters on the structural response of reinforced glass beams. These parameters have been investigated by means of pull-out tests, to investigate the pull-out strength of the reinforcement, and by means of bending tests, to investigate the structural response of reinforced glass beam specimens. The investigated parameters are listed below:

a)   Bond system

To investigate the effect of bond system on the structural response of reinforced glass beams, two different systems are applied in this research as an intermediary bond system between the glass and the reinforcement, and between the individual glass layers of the specimens. These bond systems are a UV-curing acrylate adhesive Glasbond 368 (GB) from DELO and the ionomer SentryGlas® (SG) interlayer from DuPont. Both bond systems provide a fully transparent bond. It is expected that differences in material properties between both bond systems may have an effect on the interaction between the glass and the reinforcement and thus on the structural response of the reinforced glass beams.

b)   Temperature

The effects of temperature are investigated in order to determine whether the reinforced glass beams are redundant at all temperature levels that can occur during their service life. It is expected that differences in the response of the polymer intermediary bond at different temperatures may influence the interaction between the glass and the reinforcement and thus may influence the structural response of the reinforced glass beams. The effects of temperature are investigated by means of pull-out tests at -20, +23, +60 and +80°C and by means of bending tests at -20, +23 and +60°C, see Chapter 5.

c)   Thermal cycling

The effects of thermal cycling are investigated in order to determine whether repetitive changes in serviceability temperature, e.g. due to changing day and night conditions, have an effect on the performance of the reinforced glass beams. It is expected that the repetitive straining of the intermediary bond, due to a difference in thermal expansion between the glass and the reinforcement, might influence its bond strength, which might subsequently affect the structural performance of the reinforced glass beams. To investigate the effect of thermal cycling, the pull-out specimens and beam specimens have exposed to 150 cycles between -20 and +30°C before being tested, see Chapter 5.

d)   Humidity

The effects of humidity are investigated in order to determine whether humid environments or water condensation have an effect on the structural performance of reinforced glass beams. To investigate the effects of humidity, the pull-out and beam specimens have been exposed for 4 weeks to 100% relative humidity at 50°C prior to the tests, see Chapter 5.

e)   Load duration

The effects of load duration are investigated in order to determine whether cracked reinforced glass beams can carry the required load for a sufficient period of time. In practical applications this long-duration redundancy is required to provide the building user(s) sufficient time to notice the failure and to take measures. To investigate the effect of load duration, long-duration pull-out tests and long-duration bending tests (post-breakage loading) have been performed. The pull-out tests stretch over a loading time of 4 weeks and the bending tests over a loading time of 3 to 15 months, see Chapter 5.

f)   Reinforcement material

The effects of reinforcement material are investigated by means of bending tests on glass beams provided with either *stainless steel* or *glass fiber* reinforcement. The former has been applied by means of square sections that are integrated at the inner recessed edge of triple-layer glass beams. The latter has been applied by means of GFRP (Glass Fiber Reinforced Polymer) rods that are embedded in the SG interlayer of double-layer glass beams, see Chapter 5 and 7. It is expected that differences in material properties of the reinforcement materials will result in a different structural response of the beams.

g)   Reinforcement percentage

The effects of reinforcement percentage are investigated by means of bending tests on two series of glass beams with identical beam dimensions, but with varying reinforcement sections. Whereas the first beam series is provided with a *hollow* stainless steel reinforcement section the second beam series is provided with a *solid* stainless steel reinforcement section, see Chapter 6.

h)   Beam size

The effects of beam size are investigated by means of bending tests on 'small' 1.5 m and 'large' 3.2 m SG-laminated reinforced glass beams, see Chapter 6.

1.2.2. Analytical and numerical investigations

The analytical and numerical investigations are focused on the prediction of the structural response of reinforced glass beams.

The analytical investigations focus on the prediction of the structural response by means of an analytical model which is developed in this research based on the reinforced concrete theory. Since the structural functioning of the reinforced glass concept is very similar to the reinforced concrete technology, the transfer of the reinforced concrete theory towards the reinforced glass concept is expected to be valid. Based on the reinforced concrete theory, a number of equations are derived which can be used to construct a moment-curvature (M-κ) or a force-displacement (F-δ) curve. To validate the analytical model, the predicted results are compared with the experimental results.

The numerical investigations make use of a 2D model and a sequentially linear analysis (SLA) technique to describe the structural response of reinforced glass beams. The SLA approach, which is currently under development at TU Delft, is especially suited for modelling the response of brittle materials. It makes use of saw-tooth reduction curves through which the strength and stiffness properties of critical elements in the model are repetitively updated in order to simulate cracking of the material. In this research the method is applied to simulate both cracking of the glass and plastic deformation of the reinforcement. The validity of this method for describing the structural response – especially the post-breakage response – of reinforced glass beams is investigated. Load-displacement curves and cracking responses are derived from the numerical model and compared with the experimental results. Furthermore, the effects of various model parameters – such as mesh size, number of saw-tooth reduction steps and shear reduction factor – on the predicted results are investigated.

1.3. Objective

The goal of this research is to increase the understanding of the structural response and structural functioning of reinforced glass beams.

1.4.   Outline of the dissertation

Figure 1.2 presents the outline of this dissertation. The dissertation consists of 5 parts, each with its specific focus.

Part I provides the *'Introduction'* to the research and contains the current Chapter 1.

Part II focuses on the *'Theoretical framework'* of this research. Firstly, some examples of structural glass beams and some examples of commonly applied safety measures are provided, see Chapter 2. Secondly, the theory behind the reinforced glass concept is elucidated and an overview of similar research projects by others is provided, see Chapter 3. Finally, the material properties of the three constituent components – glass, reinforcement and intermediary bond – are presented, see Chapter 4.

Part II presents the *'Experimental, analytical and numerical investigations'* done within the framework of this study. Firstly, the experimental investigations into the effects of bond type, temperature, thermal cycling and load duration on the structural response of reinforced glass beams are presented, see Chapter 5. Secondly, the experimental investigations into the effects of reinforcement percentage and beam size on the structural response of reinforced glass beams are presented, see Chapter 6. Thirdly, the experimental investigations into the structural response of glass beams with glass fiber reinforcement embedded in the interlayer are presented, see Chapter 7. Finally, the analytical and investigations into the description of the structural response of reinforced glass beams are provided, see Chapter 8.

Part III presents an *'Integrated discussion of the research results'*. It provides an integrated discussion on the structural aspects of reinforced glass beams, see Chapter 9. Furthermore, it provides an integrated discussion on the production and design aspects of reinforced glass beams, see Chapter 10.

Part IV look in *'Retrospect and prospect'* at the research results presented in the preceding parts. It provides the conclusions from the research, see Chapter 11, and provides recommendations for future studies, see Chapter 12.

Part I Introduction	**Chapter 1** Introduction to the research

Part II Theoretical framework	**Chapter 2** Structural glass beams	**Chapter 3** The reinforced glass beam concept	**Chapter 4** Materials applied in this research

Part III Experimental, analytical and numerical investigations	**Chapter 5** Experimental investigations into the effects of bond type, temperature, thermal cycling, humidity and load duration on the structural response	**Chapter 6** Experimental investigations into the effects of reinforcement percentage and beam size on the structural response	**Chapter 7** Experimental investigations into the structural response of SG-laminated glass beams with embedded glass fibre reinforcement	**Chapter 8** Analytical and numerical modelling of the structural response

Part IV Integrated discussion of the research results	**Chapter 9** Integrated discussion on the structural aspects of reinforced glass beams	**Chapter 10** Integrated discussion on the production and design aspects of reinforced glass beams

Part V Retrospect and prospect	**Chapter 11** Conclusions	**Chapter 12** Recommendations

Figure 1.2: Outline of the dissertation.

PART II

Theoretical framework

Part I

Introduction

Chapter 1

Introduction to
the research

Part II

Theoretical
framework

Chapter 2

Structural
glass beams

Chapter 3

The reinforced
glass beam
concept

Chapter 4

Materials
applied in this
research

Part III

Experimental,
analytical and
numerical
investigations

Chapter 5

Experimental
investigations
into the effects
of
bond type,
temperature,
thermal cycling,
humidity and
load duration
on the structural
response

Chapter 6

Experimental
investigations
into the effects
of
reinforcement
percentage
and beam size
on the structural
response

Chapter 7

Experimental
investigations
into the
structural
response of SG-
laminated glass
beams with
embedded glass
fibre
reinforcement

Chapter 8

Analytical and
numerical
modelling of
the structural
response

Part IV

Integrated
discussion of
the research
results

Chapter 9

Integrated
discussion on the
structural aspects of
reinforced glass
beams

Chapter 10

Integrated
discussion on the
production and
design aspects of
reinforced glass
beams

Part V

Retrospect
and
prospect

Chapter 11

Conclusions

Chapter 12

Recommendations

Chapter 2
Structural glass beams

This chapter provides some examples of structural glass beams applied in practice. Furthermore, it briefly describes a commonly applied safety concept for structural glass beams.

Abstract

The application of glass as a structural material is a rather novel field and has only started some decades ago. Over the years glass has been applied for various structural glass components such as columns, beams and walls. For the current research the application of structural glass beams is of specific interest. Basically, three beam categories can be distinguished, namely continuous glass beams, segmented glass beams and splice-laminated glass beams. Continuous glass beams consist of one single piece of (laminated) glass, that spans the full length of the beam. Segmented glass beams consist of multiple (laminated) glass segments that are joined with (mechanical) connections, to create a greater span. Splice-laminated beams consist of multiple glass sheets that are laminated in overlap, to create greater a span than the length of the individual glass sheets. The commonly applied safety concept for structural glass beams is the application of strengthened and laminated glass. This safety concept is focused on minimizing the probability of full glass failure and consequent collapse of the beam. However, the chance of full glass failure cannot be fully eliminate and might still occur due to unforeseen events. Additional or other safety concepts are therefore strongly recommended.

2.1.   Introduction

The application of glass as a structural material is a relatively new field. It is only some decades ago that glass – besides its traditional and ongoing use as an infill material – has emerged as a structural building material. Especially the pioneering work done in the 1980's and 1990's in the field of structural glass by engineers Peter Rice, Rob Nijsse and Tim Macfarlane contributed to the evolution of glass as a structural material [Nijsse, 2003; Macfarlane, 1999; Rice & Dutton, 1995].

Over the years glass has been applied for various structural components such as beams, columns and walls. These components are applied in various structures, such as façade structures, roof structures, small bridge-walkways and staircases.

For the current research the use of glass as a bending component, such as a glass roof beam or a glass façade beam/fin, is of specific interest. Section 2.2 therefore provides some examples of glass beam applications. Subsequently, section 2.3 briefly describes a commonly applied safety concept for structural glass beam applications.

2.2.   Examples of structural glass beam applications

This section provides some of examples of structural glass beam applications, such as glass roof beams and glass façade fins/beam. Three categories of structural glass beams are defined, namely continuous glass beams, segmented glass beams and splice-laminated glass beams. The different types will be explained in more detail in the following subsections.

2.2.1. *Continuous glass beams*

The continuous glass beam type refers to beams that are made of one single and continuous piece of (laminated) glass. Although the beams may consist of multiple glass layers, that are joined using foil or resin interlayers, each individual glass layer spans the full length of the beam. Initially, the maximum length of such beams was limited to about 4.5 to 6 m [Nijsse, 2003], due to size restrictions of standard glass sheets and size restrictions in the (autoclave) lamination process. However, currently the boundaries of both the obtainable glass sizes and the lamination possibilities are pushed forward, which enables the manufacturing of oversized (> 6m) glass beams.

An early application of (continous) structural glass beams is given in Figure 2.1, which shows the glass beams of the Louvre extension. Additional (early) examples are provided in Figure 2.2 and 2.3, which show the glass roof beams applied for the ING office building and the glass beams applied in the glass extensions made for the Broadfield House Glass Museum.
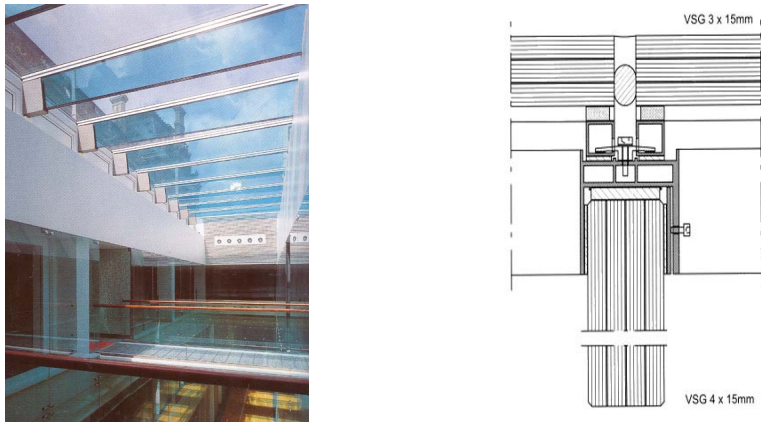
Figure 2.1: Glass beams applied in the Louvre extensions, Paris, France; Engineer: RFR.
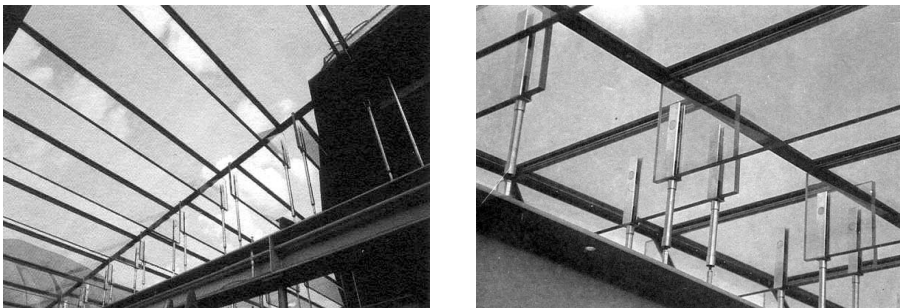
Figure 2.2: Glass beams applied in the ING headoffice, Budapest, Hungary; Engineer: ABT.

Figure 2.3: Glass beams applied in the Broadfield museum; Engineer: Dewhurst Macfarlane.

2.2.2. *Segmented glass beams*

To obtain greater lengths, structural glass beams can be composed of multiple (laminated) glass segments that are joined using e.g. bolted connections. An early example of a project that features such segmented glass beams is the Yurakucho canopy, see Figure 2.4. In this project the 9 m cantilevering beams consist of triangular glass and acrylic segments that are bolted together [Macfarlane, 1999]. The acrylic segments are applied to obtain a redundancy for seismic loads. A later example of an application of segmented glass beams is shown in Figure 2.5, which shows the atrium roof covering of the IHK in Munich [Betsch, 2004]. This atrium roof covering consists of 12 m glass primary beams that are composed of multiple triangular laminated glass segments that are bolted together. Another exemplary application of segmented glass beams is given in Figure 2.6, which shows the atrium roof covering of the Medical School in Glasgow. The largest beam of this triangular (in plan) roof covering spans 15.5 m and is composed of four segments of resin laminated glass, which are joined used bolted friction grip joints.
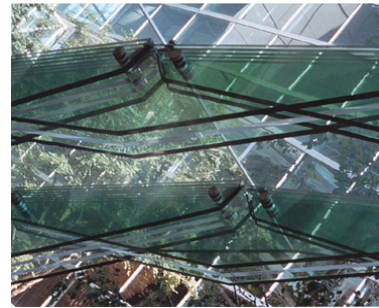
Figure 2.4: Segmented 9 m glass beams applied in the Yurakucho metro station entrance covering, Japan; Engineer: Dewhurst Macfarlane

Figure 2.5: Segmented 14 m glass beams applied in the atrium roof covering of the Industrie Handelskammer building in Munich, Germany [Betsch, 2004].
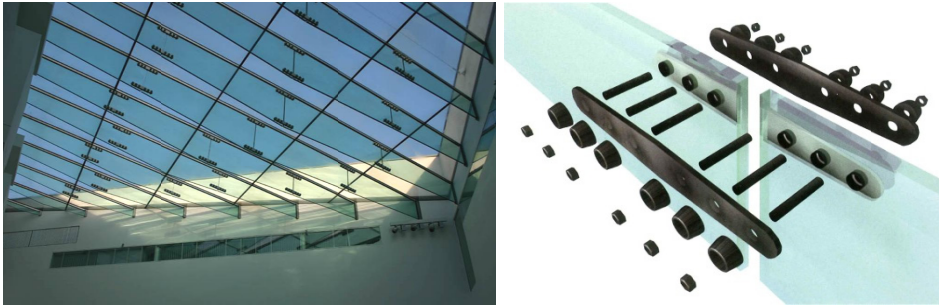
Figure 2.6: Segmented 15.5 m glass beams applied in the atrium roof of the Medical School building in Glasgow, Scotland. Engineer: Arup.

2.2.3.   *Splice-laminated glass beams*

Another method to obtain greater beam lengths, is to splice laminate the beam. This way the beam consists of multiple glass sheets that are laminated in overlap to greater a beam with a larger length than each of the individual glass sheets. An example of a splice-laminated glass fin is presented in Figure 2.7(a), which shows the iconic glass cube of the Apple Store on the 5th Avenue in New York. The 10 m vertical glass fins have been splice-laminated according to the segmentation scheme shown in Figure 2.7(b).

(a)   (b)
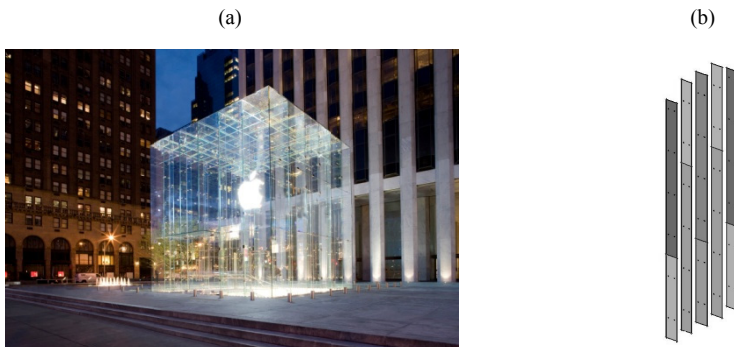
Figure 2.7: Splice-laminated glass fins applied in the glass cube of the Apple store at the 5th avenue in New York; [O'Callaghan, 2008]; Engineer: Eckersley O'Callaghan.

2.3.   Safety concepts for structural glass beams

To design a safe glass beam one has to overcome the fundamental problem of the brittle failure of glass. Unlike a steel beam that will visually deform upon overloading, glass has no built-in warning mechanism; it can only deform elastically or fracture. To overcome the problem of unsafe structural behavior of glass, two measures are commonly applied for structural glass beams.

Firstly, tempered glass is often applied for structural glass beams. By means of a heat treatment process – as is explained in Chapter 4 – the strength of the glass, and thus the practical strength of the glass beam, is increased. This increase in strength decreases its sensitivity to several common failure causes[i], such as thermal breakage and peak stresses [Bos, 2009].

Secondly, structural glass beams are generally composed of multiple glass layers, which are laminated using a foil or resin interlayer. The purpose of this laminated glass, is that if one of the layers fails due to an impact or whatever cause, the remaining layers will still be able to carry the load. Furthermore, the broken glass will stick to the interlayer, which prevents from falling glass and human injury.

Both measures minimize the probability of total glass failure, i.e. failure of the full beam component. However, despite these measures, complete failure of the structural glass component may still occur due to unforeseen events. The multiple glass layers of the component may for instance crack due to severe or repetitive impact (e.g. vandalism), or due to simultaneous high local stressing of all glass layers as a result of assembly errors (most notably at the supports or at the joints). Additional safety measures or safety concepts to enhance the redundancy of structural glass components are therefore strongly recommended.

For further reading on safety concepts in structural glass engineering, is referred to Bos [Bos, 2007; Bos, 2009]. Bos provides an extensive discussion on safety concepts in structural glass engineering. This topic is therefore not further addressed in the current thesis.

---

[i] However, it should be noted that for tempered glass there is a probability of 'spontaneous' glass failure due to nickel sulfide inclusions, see Chapter 4, section 4.2.5.

Chapter 3
The reinforced glass beam concept

This chapter provides more background information on the reinforced glass beam concept that has been introduced in Chapter 1. It explains the intended functioning of the system and provides an overview of the evolution of the concept at TU Delft. Furthermore, it provides an overview of similar concepts studied by others. The properties of the constituent components of the reinforced glass beam concept – glass, reinforcement and intermediary bond – are presented and discussed in the following chapter.

Abstract

The reinforced glass beam concept intends to generate a significant post-breakage resistance for structural glass beams. This is achieved through the addition of reinforcement that is bonded at/in the tensile zone of the beam. Upon fracture of the glass the reinforcement bridges the crack in the glass and will thereby transfer the tensile forces over the crack. Together with a compression force in the un-cracked compression zone in the glass, an internal couple will be generated, which will enable the beam to still carry load. The reinforced glass beam concept has been explored in preceding research at TU Delft. It was first introduced in 2003 by means of 2.25 m glass-polycarbonate beams that were additionally reinforced with a small stainless steel section. From there the concept evolved to 7.2 m adhesively bonded full-section stainless steel reinforced glass beams that have been applied in an all glass pavilion that was built at the TU Delft. Apart from the research at TU Delft, several other research programmes are focused on composite glass beam concepts. Similar to the reinforced glass beam concept investigated at TU Delft these concepts focus on enhancing the (residual) resistance of glass beams or glass plates through the addition of a secondary material. The majority of the concepts focus on a combination of steel and glass, but also other additive materials such as carbon-fiber, timber or reinforced-concrete are applied. From the results of the preceding research at TU Delft and the results of the similar research projects by others, it is observed that the reinforced glass beam concept is a promising concept. However, the effects of various environmental and geometrical parameters on the structural response seem largely unknown. The current research therefore investigates the effects of various parameters – which are: bond system, temperature, thermal cycling, humidity, load duration, reinforcement material, reinforcement percentage and beam size – on the structural response of reinforced glass beams in more detail.

3.1.   Introduction

This Chapter provides more in depth information on the reinforced glass beam concept. Firstly, the intended functioning of the reinforced glass beam concept is described in section 3.2. Secondly, the evolution of the reinforced glass beam concept as it is studied at the TU Delft is presented in section 3.3. Thirdly, an overview of concepts similar to the reinforced glass beam concept is provided in section 3.4. Finally, a brief evaluation of the subjects discussed in this Chapter is provided in section 3.5.

3.2.   The functioning of the reinforced glass beam concept

The aim of the reinforced glass beam concept is to generate a significant post-breakage resistance for structural glass beams. This is achieved through the addition of reinforcement that is bonded at the tensile zone of the beam. The reinforcement is connected to the glass through an intermediary bond. In case of glass fracture the crack in the glass will be bridged by the reinforcement, see Figure 3.1. The effect of the reinforcement is twofold. Firstly, due to the dissipation of fracture energy by deformation of the reinforcement, the crack propagation in the glass will be halted. Hence the cracks will not run over the full height of the beam, but will be stopped upon reaching the compression zone. Secondly, the reinforcement will transfer the tensile force over the crack and will transfer it back into the glass through the intermediary bond. Together with a compressive force in the un-cracked compression zone of the beam, this tensile force in the reinforcement generates an internal moment capacity which enables the beam to still carry load. This way a significant post-breakage strength is obtained.
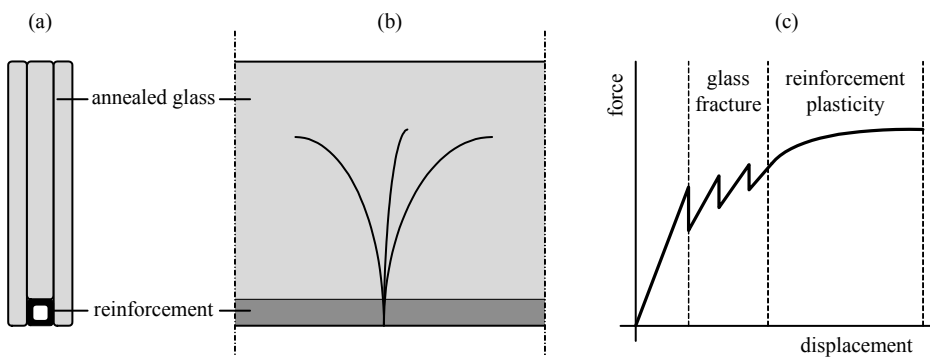
Figure 3.1 (re-print of Figure 1.1): Schematic representation of the functioning of the reinforced glass beam concept (a) cross-section of reinforced glass beam; (b) side-view of a cracked reinforced glass beam; (c) force-displacement diagram of reinforced glass beam loaded in displacement controlled bending.

3.3.   The evolution of the reinforced glass beam concept studied at TU Delft

The reinforced glass beam concept has been studied at the TU Delft since 2003. The concept was first introduced by Veer [Veer et al., 2003a] who developed and tested glass-polycarbonate laminated beams with an additional reinforcement section at the tensile edge. Subsequently, the concept was further developed through intermediary steps of a reinforced box-section aquarium [Veer, 2003b], a reinforced box-section beam and a reinforced and post-tensioned glass T-section beam [Louter, 2004; Bos et al., 2004] into reinforced glass full-section beams [Louter et al., 2005]. The latter were applied in the All Transparent Pavilion [Bos et al., 2005b] which was built in 2004 by the structural glass research group at the Faculty of Architecture of the TU Delft to demonstrate several structural glass safety and connection principles that had been developed within the research group [Veer, 2005].

The current research has started from there and investigates the structural response of reinforced glass beams in more detail. The following sub-sections briefly present the reinforced glass beams investigated prior to this research and describe the evolution of the concept.

3.3.1.   Glass-PC laminated beam with additional reinforcement section

In 2003 Veer [Veer et al., 2003a] developed and tested glass-polycarbonate laminated beams that were provided with an additional reinforcement section positioned at the tensile edge. The beams consisted of continuous polycarbonate sheets, annealed float glass segments and an L-shaped stainless steel reinforcement section, which were adhesively bonded, see Figure 3.2.
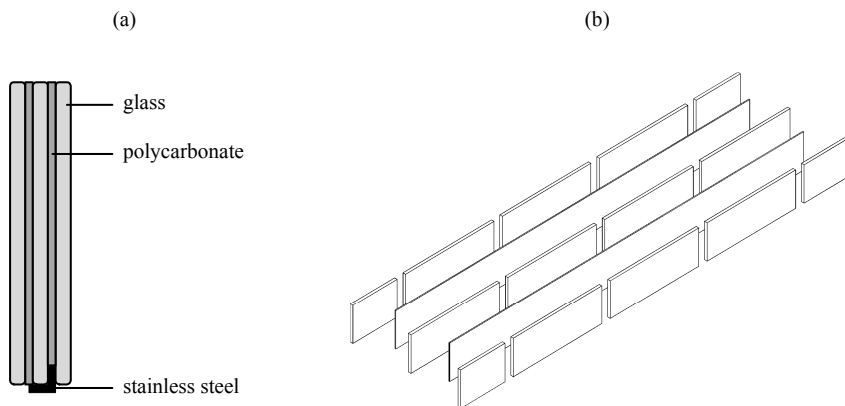
Figure 3.2: (a) Schematic cross-section of the glass-PC laminated beam with additional reinforcement section. Image based on [Veer et al., 2003a]. (b) Segmentation scheme applied for the glass-polycarbonate beam.

The glass-polycarbonate laminate had already been developed in preceding research [Veer et al., 2003a] in a quest for highly transparent glass beams with safe failure behaviour [Veer, 2005]. This safe failure behaviour was generated by the polycarbonate, which provided the beam residual resistance and ductile post-breakage response upon glass fracture.

The L-shaped stainless steel reinforcement section has been added to the laminate at a later stage. The purpose of this reinforcement section was to increase the level of residual resistance and to prevent rupture of the polycarbonate sheets, which had been encountered in preceding research.

From the results of bending tests on the glass-polycarbonate beam provided with the additional reinforcement, it was observed and concluded that reinforcing a glass beam with a metal reinforcement section is feasible and that it significantly improves its post-breakage response.

3.3.2.   *Reinforced glass box-section aquarium*

The concept of adding a metal reinforcement section at the tensile edge of a glass beam was further explored by Veer and Gross in 2003 [Veer et al., 2003b]. They designed and built an 8 m reinforced glass aquarium that was intended for an exhibition on glass and which was to be suspended in the air from both ends, see Figure 3.3.

The aquarium acted as a box-section glass beam and consisted of annealed float glass and two stainless steel box sections which were all adhesively bonded using the GB 368 UV-curing acrylate adhesive from DELO. The polycarbonate, which was previously used to function as a crack bridge, was omitted from the beam design. The stainless steel reinforcement sections now served as a crack bridge.

(a)   (b)

glass
(adhesively bonded)

stainless steel

Figure 3.3: Reinforced glass box-section aquarium [Veer et al., 2003b]; (a) schematic representation of the cross-section of the aquarium; (b) artist impression of the 8 m aquarium suspended in the air.

Since the aquarium exceeded the maximum 6 m glass size, the side and the bottom panels were segmented. The side panels were bonded in overlap to create the full 8 m span. The top panel of the aquarium was removed from point-to-point to allow air to enter the aquarium.

In the end, the 8 m aquarium was not exploited for the exhibition. It was therefore decided to test the 8 m aquarium in three-point bending. The results of the bending test showed gradual instead of brittle failure. Furthermore, the 8m box section aquarium showed some level of post-breakage resistance.

The aquarium project demonstrated that it was feasible to construct a safe beam out of annealed float glass segments, stainless steel reinforcement and an intermediary adhesive bond.

3.3.3. *Reinforced glass box-section beam*

Taking the design of the aquarium as a starting point, Louter [Louter, 2004] designed and built a 3 m prototype of a box-section reinforced glass beam, see Figure 3.4. The prototype served as a scale 1:4 model of a 12 m glass beam.

Similar to the aquarium, this box section beam was composed of annealed float glass and two stainless steel box sections which were all adhesively bonded using the GB 368 acrylate adhesive from DELO. During the construction of the beam prototype it was found that the beam design was highly sensitive to dimensional inaccuracies. Especially at the linear edge joints between the webs and the flanges, dimensional inaccuracies on the glass caused alignment problems. The relatively thin acrylate adhesive bond had no gap-filling capacity was not able to compensate for the dimensional inaccuracies.

(a)   (b)
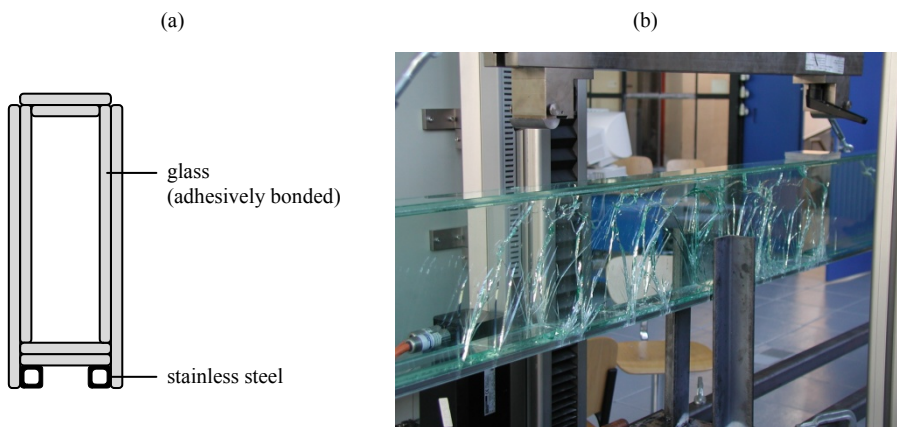
Figure 3.4: Reinforced glass box-section beam [Louter, 2004];
(a) schematic representation of the cross- section; (b) beam during the four-point-bending test.

Nonetheless, the 3 m prototype was successfully constructed and subsequently tested in four-point bending. The beam showed a significant residual resistance which amounted to about 140% of the initial failure load. For the first time in the evolution of the reinforced glass beam concept, it was demonstrated that the post-breakage resistance could exceed the initial failure strength.

3.3.4.   *Post-tensioned glass T-section beam*

Based on the knowledge gained from the construction and testing of the box-section glass beam, Louter [Louter, 2004] designed and built a 3 m prototype of a T-section glass beam which was both reinforced and post-tensioned, see Figure 3.5. The beam design is briefly described below. The general concept of post-tensioned glass beams and exploratory investigations done alongside the current research are more extensively discussed in Appendix IV.

The design of the T-section beam aimed at avoiding the dimensional inaccuracy problems that had been encountered at the construction of the box-section glass beam. Furthermore, the design aimed at enhanced strength compared to the previously tested box-section beam.

This resulted in an adhesively bonded T-section glass beam composed of an annealed float glass web and flange. The web and flange were both segmented and bonded in overlap. Furthermore, their free edges were grinded in a parabolic curve. A curved stainless steel box section was integrated in the web of the beam, through which a high strength steel tendon was fed and subsequently tensioned at the beam ends. For this tensioning, steel heads with intermediary EPDM (Ethylene Propylene Diene Monomer) pads were positioned at the beam ends.

The T-section beam design allowed for dimensional inaccuracies to be 'absorbed' at the free edges of the web and flange, thereby preventing assembly problems at the adhesively bonded linear joint between the web and the flange. Furthermore, the post-tensioning tendon exerted a compressive force at the beam ends and provided an upward lift, which enhanced the strength of the beam.

A four-point bending test on the 3m prototype demonstrated enhanced initial and post-breakage strength of the T-section beam compared to the box-section beam. The beam showed gradual failure response. However, due to the persisting post-tensioning force, the beam showed explosive final failure of the glass at the compression zone and consequent collapse of the beam.

The construction and testing of the T-section glass beam provided significant additional knowledge on the manufacturing and structural functioning of such beams, which could be implemented in the further development of the reinforced glass beam concept.

(a)   (b)

glass
(adhesively bonded)

stainless steel
hollow section
post-tensioning
tendon

(c)

(d)

post-tensioning tendon
placed in a hollow section
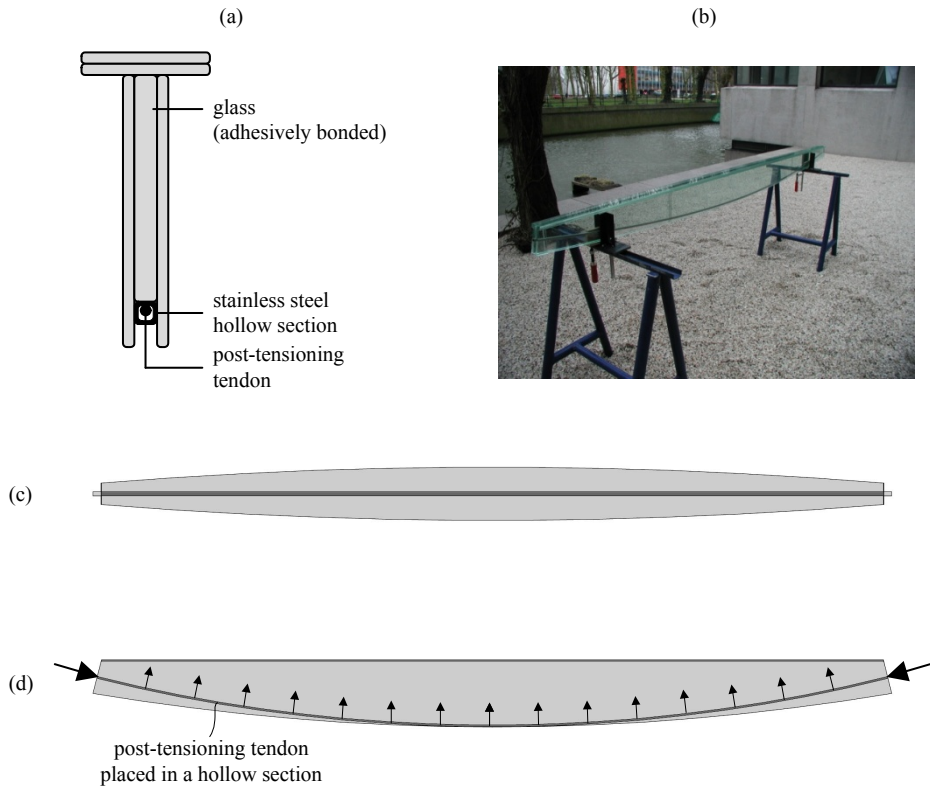
Figure 3.5: Post-tensioned T-section glass beam[i] [Louter, 2004];
(a) cross-section; (b) photograph of beam prototype; (c) top view; (d) side view.

3.3.5. *Reinforced glass full-section beams for the All Transparent Pavilion*

In 2004 it was decided to build a temporary 'All Transparent Pavilion' [Bos et al., 2005b] to demonstrate the then current state-of-play of the structural glass research group at the Faculty of Architecture of the TU Delft, see Figure 3.6. Several innovative concepts that were developed by the research group were incorporated in a glass pavilion that was designed and built by a group[ii] of researchers and students. The design of the pavilion made use of annealed float glass and consisted of double-walled resin-filled glass columns, reinforced glass primary beams, laminated glass secondary beams, acrylic joints, adhesively bonded metal joints and laminated glass facade and roof

---

[i] More images of the post-tensioned glass beam are available in Appendix IV, which provides a discussion on the post-tensioned glass beam concept .

[ii] The following people were directly involved in the design and construction of the pavilion: Fred Veer, Freek Bos, Christian Louter, Jan Belis, Elke van Nieuwenhuijzen, Gerrie Hobbelman, Ton Romein, Henk Rijgersberg, Kees Baardolf, Julian Hoogmans, Jordy de Raay, Sabine de Richemont, Desiree Schouten, Remko Siemerink, Marten Valk, Thijs Welman, Wijnand Wesselink.

sheeting [Belis et al., 2005; Bos et al., 2005a, b; Louter et al., 2005; Van NieuwenhuijzenBos & Veer, 2005; Veer, 2005]. However, it should be noted that for the final construction of the pavilion some of these components were omitted or altered [Bos et al., 2005b].

The design of the primary beams for the pavilion was based on the promising results of the previously investigated reinforced glass beams. The beams were designed and built as 7.2 m reinforced glass full-section beams, which spanned 4.8 m and cantilevered 1.2 m on either side [Louter et al., 2005], see Figure 3.6. The beams consisted of four layers of annealed float glass segments which were adhesively bonded in overlap using the GB 368 acrylate adhesive from DELO. Due to the cantilevering parts of the beam, tensile stresses occurred at both edges of the glass beam, requiring a stainless steel box-section reinforcement on either side. Similar to the T-section beam the reinforcement sections were integrated in the web of the beam. At the tapered cantilever parts only two out of the four glass layers and only the upper reinforcement were continued.

(a)   (b)

(c)   (d)
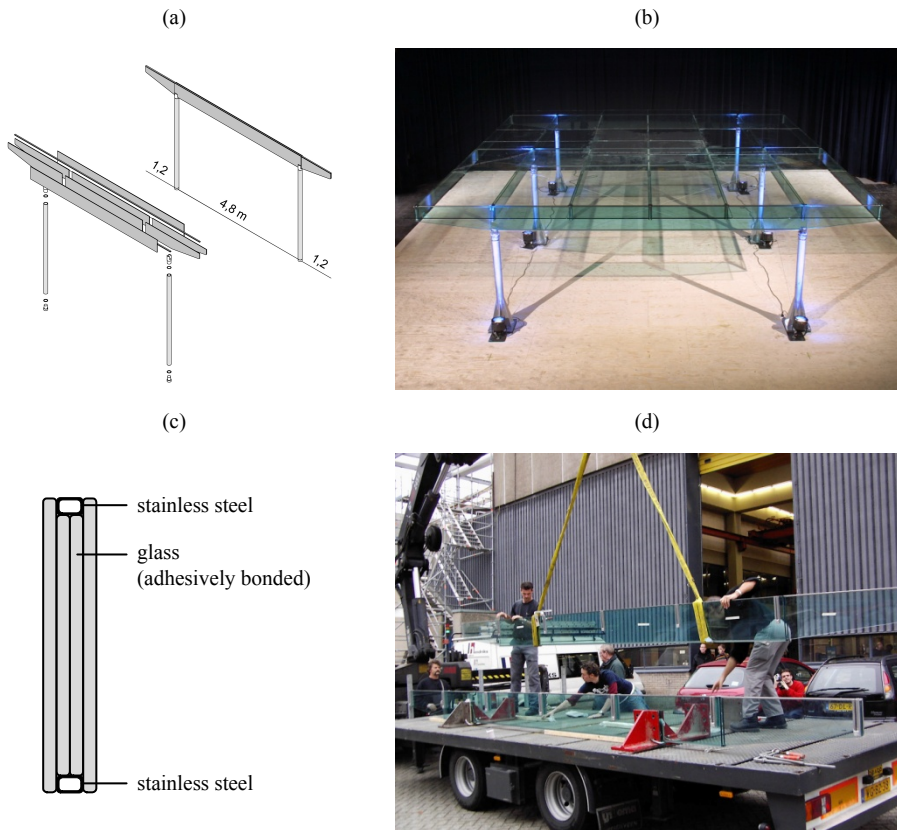
Figure 3.6: Reinforced glass beams for the All Transparent Pavilion [Louter et al., 2005].

Prior to the construction of the All Transparent Pavilion, one prototype of the primary beams was built and tested in three-point bending. Both cantilever parts were tested for the hogging moments and the mid-span was tested for the sagging moments, which resulted in three separate tests on the beam prototype. The cantilever parts showed fairly good response. They showed gradual post-breakage response and some ductility. Especially at mid-span the beam performed well. It showed a significant residual resistance and ductility, see Figure 3.7(a). The post-breakage loading reached 150% of the initial failure load.

(a)   (b)

(c)   (d)
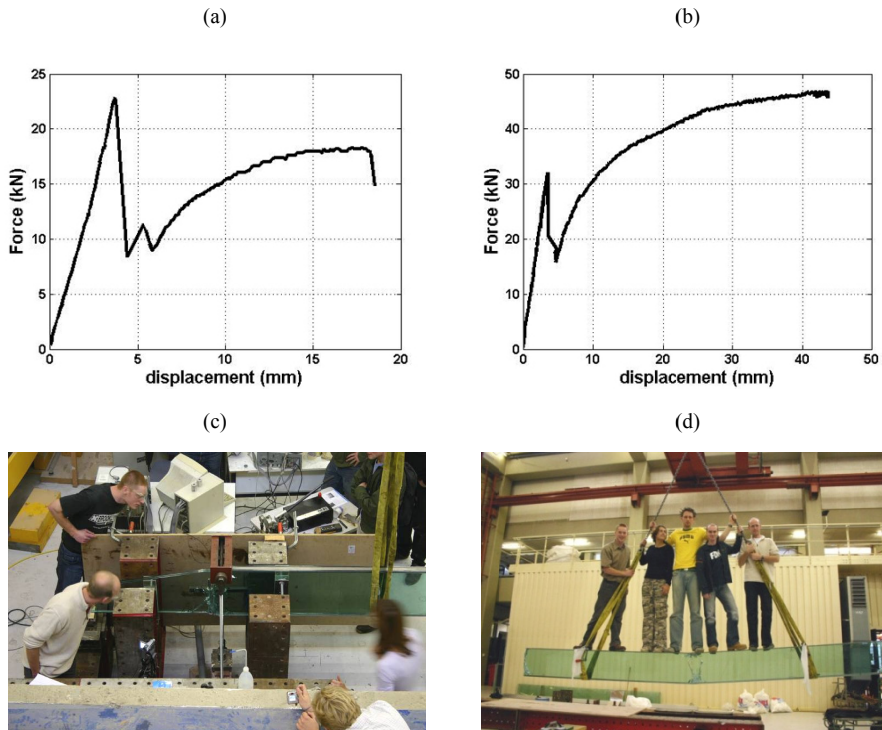
Figure 3.7: Results of bending tests on the prototype reinforced glass beam for the All Transparent Pavilion [Louter et al., 2005]; (a) result of the bending test at the cantilever part; (b) results of the bending test at mid span; (c) beam prototype during the bending test at the cantilever parts; (d) beam prototype after the bending test at mid-span (the cantilever parts have been cut off in the process).

3.3.6.   Sub-studies performed during the current research

As has been indicated before, the current research has started from the aforementioned results. It investigates the structural response of reinforced glass beams in more detail and investigates different aspects that might affect the structural response.

Complementary to the current research, several sub-studies have been performed. These sub-studies have been performed in the scope of MSc-thesis projects. The projects are briefly described below.

In 2005, Van Heusden[i] [Heusden, 2005; Louter et al., 2006b] focused on the possibilities of post-tensioning glass beams. Various methods to introduce the post-tensioning force into the glass were investigated. Furthermore, small scale (80 cm) post-tensioned glass beams were tested, see Figure 3.8.
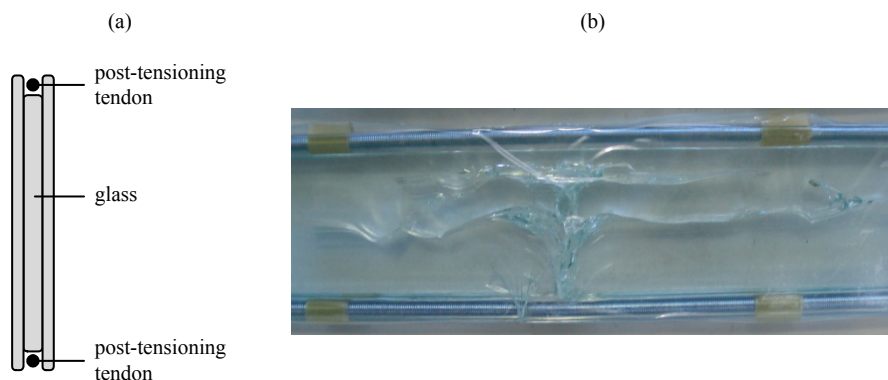
Figure 3.8: Small scale post-tensioned glass beams [Heusden, 2005; Louter et al., 2006b].

In 2007, Schetters[ii] and Louter [Louter et al., 2006a; Schetters, 2007] focused on the development of an 18 m reinforced glass beam. Scale 1:8 prototypes were built and tested, see Figure 3.9. At a later stage also scale 1:4 prototypes have been built and tested [Louter & Veer, 2007a, b]. The final 18 m beam has not (yet) been realized.

---

[i] The MSc project of Van Heusden was supervised by Vamberský & De Boer (Civil Engineering & Geosciences, TU Delft, NL), Louter (Faculty of Architecture, TU Delft, NL) and Versteegen (Pieters Bouwtechniek, Delft, NL).
[ii] The MSc project of Schetters was supervised by Van Herwijnen & Lindner (Faculty of Architecture, Building and Planning, TU Eindhoven, NL) and Veer & Louter (Faculty of Architecture, TU Delft, NL).

(a)   (b)

glass

stainless steel

(c)
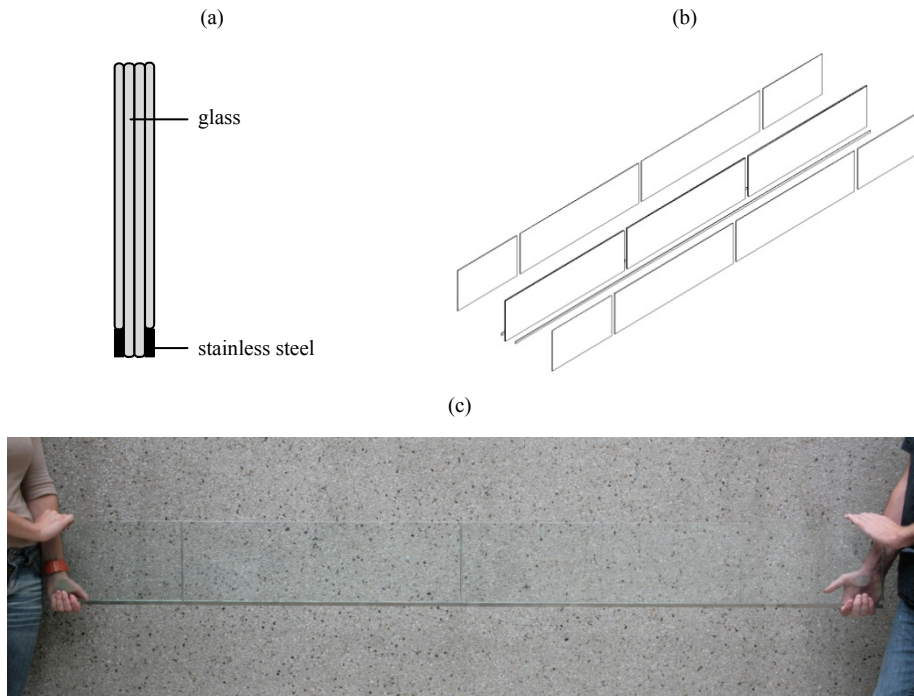
Figure 3.9: Scale 1:8 beams of an 18 m reinforced glass beam [Schetters, 2007; Louter et al., 2006a].

In 2008 & 2009, Rademakers[i] [Rademakers, 2008], Louter [Louter, 2009] and Leung[ii] [Leung, 2010; Louter et al., 2010a] focused on the possibilities of glass fiber reinforcement. Rademakers investigated the possibility of adhesively bonding glass fiber reinforcement in a slit nudge at the edge of a glass beam, see Figure 3.10(a). Alternatively, Louter investigated the possibilities of embedding round glass fiber reinforcement rods in the SG interlayer of glass beams, see Figure 3.10(b) and Chapter 7. Additionally, Leung and Louter investigated the possibilities of embedding rectangular glass fiber reinforcement rods in the SG interlayer, see Figure 3.10(c) and Chapter 7.

---

[i] The MSc project of Rademakers was supervised by Wagemans & Vamberský (Faculty of Civil Engineering & Geosciences, TU Delft, NL) and Louter (Faculty of Architecture, TU Delft, NL).
[ii] The MSc project of Leung was supervised by Vamberský, Kolstein & Hendriks (Faculty of Civil Engineering & Geosciences, TU Delft, NL) and Louter (Faculty of Architecture, TU Delft, NL).

(a)   (b)   (c)

Glass fiber rod bonded	Round glass fiber rods embedded	Flat glass fiber rods embedded in

Glass fiber rod bonded
in slit nudge; developed and
investigated by Rademakers
[Rademakers, 2008]

Round glass fiber rods embedded
in the SG interlayer; developed
and investigated by Louter
[Louter, 2009]

Flat glass fiber rods embedded in
the SG interlayer; developed and
investigated by Leung and Louter
[Leung, 2010; Louter et al., 2009]
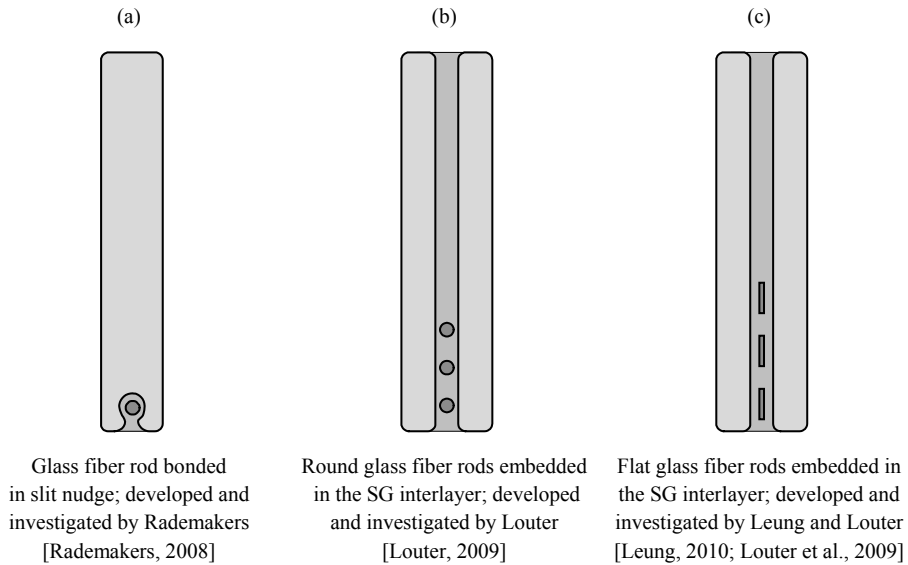
Figure 3.10: Glass beams provided with glass fiber reinforcement rods.

Finally, in 2009, Trovato[i] [Trovato, 2009] performed some initial studies into the possibilities of the novel sequentially linear analysis (SLA) technique for modelling the structural response of reinforced glass beams. At a later stage this technique has been further and more extensively explored by Louter et al. [Louter, Van de Graaf & Rots, 2010] for predicting the structural response of reinforced glass beams, see Chapter 8.

---

[i] The MSc project of Trovato was supervised by Carpinteri & Invernizzi (Politecnico di Torino, IT) and guided by Rots, Hendriks & Van de Graaf (Faculty of Civil Engineering & Geosciences, TU Delft, NL) and Louter (Faculty of Architecture, TU Delft, NL).

3.4.   An overview of similar concepts studied by others

Various authors report on similar concepts as the reinforced glass concept studied at the TU Delft. Like the reinforced glass concept, these concepts focus on enhancing the (residual) resistance of glass beams or glass plates through the addition of a secondary material. The majority of the concepts focus on a combination of steel and glass. However, also other additive materials such as carbon-fiber, timber or reinforced-concrete are applied. The concepts are briefly discussed in the following sub-sections[i].

3.4.1.   Steel-glass beams and plates

Steel-reinforced glass beams have been investigated by Nielsen, Olesen & Ølgaard [Nielsen, 2009; Nielsen & Olesen, 2007; Ølgaard et al. 2008; Ølgaard, Nielsen & Olesen, 2009], see Figure 3.11. The beams consist of annealed float glass – either single-layered or PVB-laminated – and a steel solid section, which has been bonded at the tensile edge using a two-component epoxy resin. The steel is intended to enhance the post-breakage performance of the glass beams and to provide residual resistance. Besides bending tests on the steel-reinforced glass beams, the research of Nielsen, Olesen and Ølgaard include investigations into the properties of the adhesive bond. Furthermore, a theoretical beam model describing the structural response of the beams is derived. Additionally, non-linear FE-modelling is performed using a user-defined subroutine for the glass (cracking) behaviour.

(a)   (b)
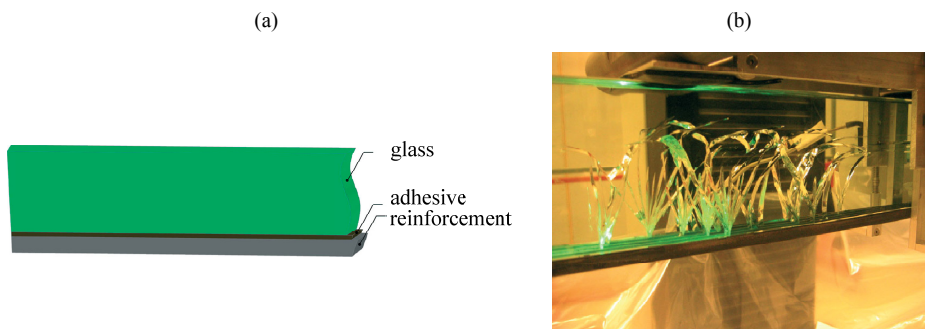
Figure 3.11: Steel-reinforced glass beams investigated by Nielsen, Olesen & Ølgaard;
[Nielsen, 2009; Nielsen & Olesen, 2007; Ølgaard et al. 2008; Ølgaard, Nielsen & Olesen, 2009].

---

[i] It should be noted that the majority of the projects presented in this overview have started during the course of the current research. The overview presented here is therefore mainly illustrative to the topic of the current study, rather than that it has been taken as a starting point for the current research.

Steel-glass hybrid I-section beams are studied by various researchers amongst which Bucak et al.; Feldmann et al.; Netusil & Eliasova; Ungermann & Preckwinkel; Wellershof, Sedlacek & Kasper; see Figure 3.12 to 3.16; [Bucak et al., 2009 a, b; Feldmann, Abeln & Baitinger, 2010; Netusil & Eliasova, 2010 a, b; Wellershof & Sedlacek, 2003; Wellershoff, Sedlacek & Kasper, 2004; Ungermann & Preckwinkel, 2010]. The beams consist of a glass web and steel flanges, which are linearly adhesively bonded. The steel flanges provide lateral stability, additional bending resistance and enhanced post-breakage response. The structural response of the beams is investigated by means of bending tests. Complementary to the bending tests the properties of the linear adhesive bond are investigated through bond tests.

(a)   (b)
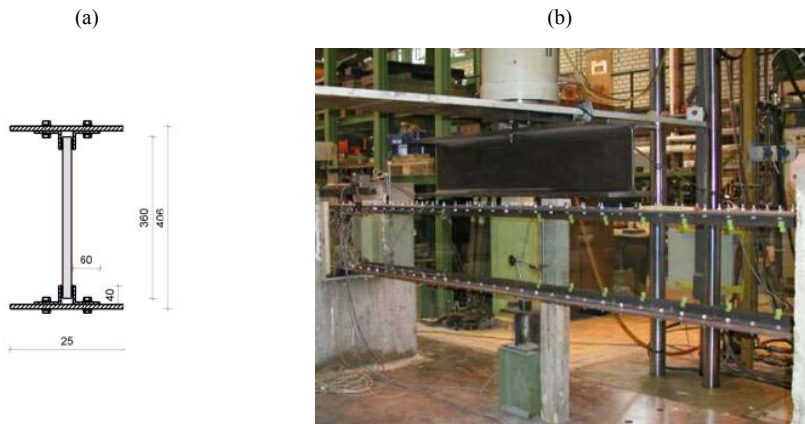
Figure 3.12: Steel-glass I-section beams presented by Wellershof, Sedlacek & Kasper
[Wellershof & Sedlacek, 2003; Wellershoff, Sedlacek & Kasper, 2004];
(a) Cross-section of the steel-glass I-section beam; (b) Steel-glass I-beam in four-point bending.

(a)   (b)

Figure 3.13: Steel-glass hybrid beam investigated by Bucak & Bues [Bucak et al., 2009 a, b].

(a) (b)
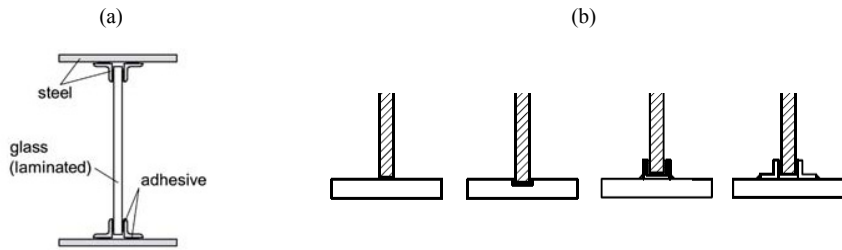
Figure 3.14: Steel-glass I-section beams presented by Feldmann, Abeln, Baitinger
[Feldmann, Abeln, Baitinger, 2010];
(a) Cross-section of the I-section beam; (b) Alternative adhesive joints.

(a) (b)
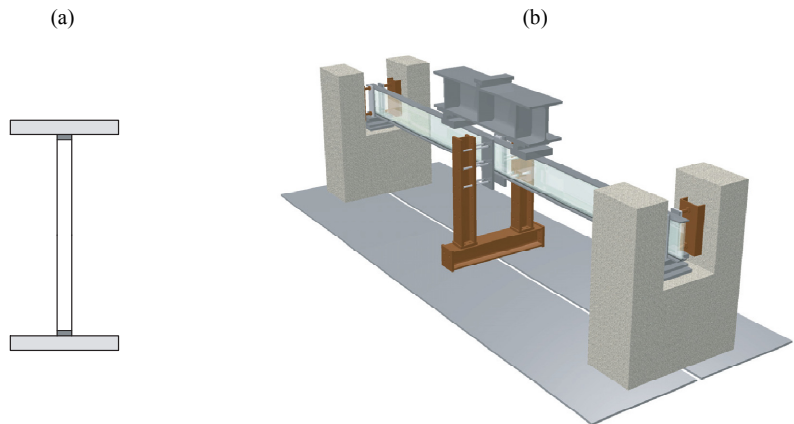
Figure 3.15: steel-glass I-beam presented by Ungermann & Preckwinkel [Ungermann & Preckwinkel, 2010];
(a) Cross-section of the steel-glass I-section beam; (b) Schematic representation of the test setup.

(a) (b)
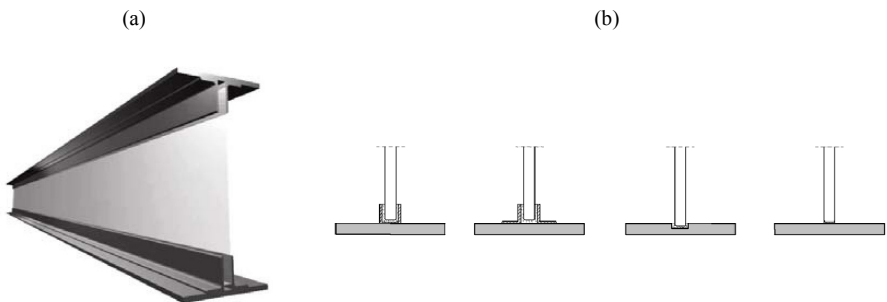
Figure 3.16: Steel-glass I-section beams presented by Netusil & Eliasova [Netusil & Eliasova, 2010 a, b];
(a) overview of the steel-glass I-section beam;
(b) alternative adhesive joints between glass web and steel flanges.

Steel-framed glass beams – developed by Absoluut Glastechniek, The Netherlands – have been studied by Belis et al. [Belis et al., 2009c], see Figure 3.17. The beams consisted of a double-layer fully tempered laminated glass web and a slender surrounding steel framing. The steel framing has been bonded to the glass using a structural sealant. The purpose of the steel framing is to provide ductility and to be able to form larg(er) span glass beams by bolting several framed glass segments together. The beams have been tested in short term and in long term loading. Furthermore, the beams have been applied in roof and facade structures of the renovated Ministry of Finance building in The Hague, The Netherlands.
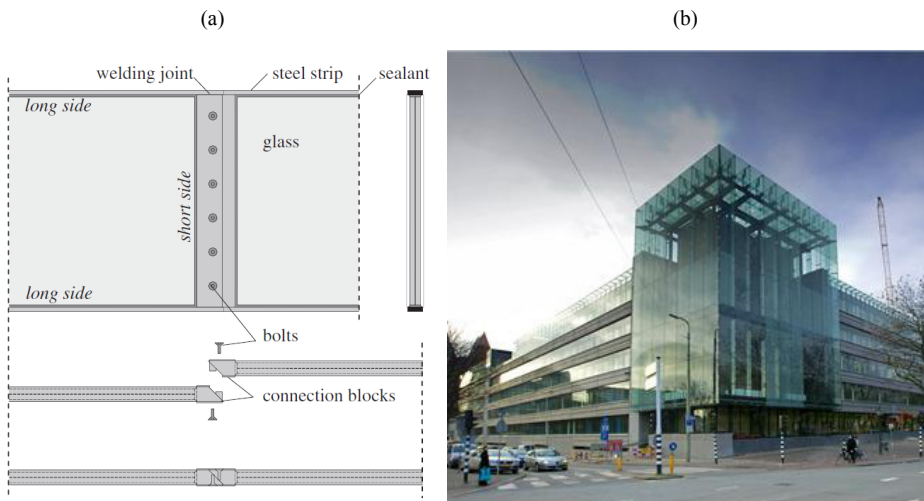
Figure 3.17: Steel-framed glass beams developed by Absoluut Glastechniek and investigated by Belis et al. [Belis et al., 2009c].

Composite steel-glass beams as structural members of facades are investigated by Weller, Meier & Weimar [Weller, Meier & Weimar, 2010], see Figure 3.18. The beams consist of triple-layer PVB-laminated annealed float glass and have been provided with one or two stainless steel section(s) at both edges. The steel has been bonded to the glass using an UV- and light-curing acrylate adhesive. The structural response of various beam layouts are investigated by means of in-plane bending tests.
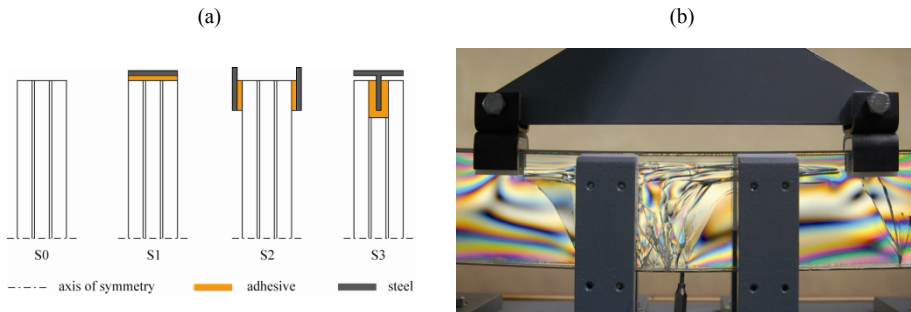
Figure 3.18: Steel-glass hybrid beams investigated by Weller, Meier & Weimar
[Weller, Meier & Weimar, 2010].
(a) alternative cross-section designs; (b) steel-glass hybrid beam during test.

Hybrid pre-stressed steel-glass beams are investigated by Froli & Lani [Froli & Lani, 2010a, b], see Figure 3.19. The beams consist of triangular double-layer PVB-laminated chemically tempered glass, stainless steel knots and steel tension cables. The steel cables provide a ductile failure response of the beam. Two prototypes have been constructed and subjected to static and dynamic tests. The structural response is analysed using both 2D and 3D non-linear FEM analyses.

Figure 3.19: Steel-glass hybrid beam Froli & Lani [Froli & Lani, 2010a, b].

Steel-reinforced glass plates have been investigated by Feirabend & Sobek [Feirabend, 2010; Feirabend & Sobek, 2008; Feirabend & Sobek, 2009], see Figure 3.20. Steel wire mesh or perforated thin metal sheet have been embedded in the interlayer of PVB or SG laminated glass units. The laminated glass units consisted of two layers of annealed, heat-strengthened or fully tempered glass. The structural response of the plates is investigated in out-of-plane bending tests at different temperatures (+23, +40 and +70°C).

(a)	(b)
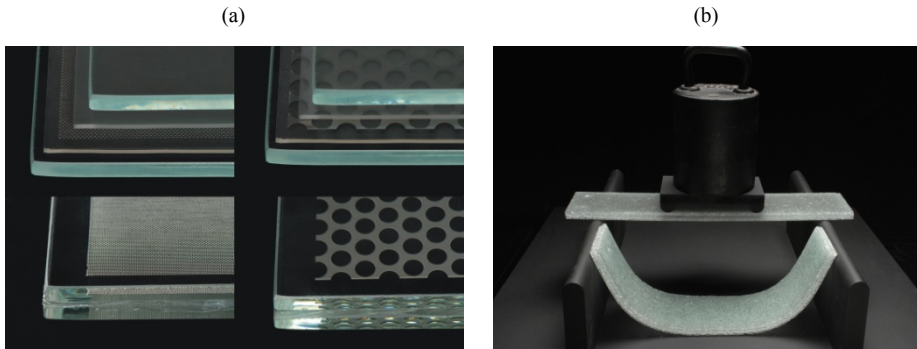
Figure 3.20: Metal wire mesh or perforated thin metal plate reinforcement embedded
in the interlayer of laminated glass, investigated by Feirabend
[Feirabend, 2010; Feirabend & Sobek, 2008; Feirabend & Sobek, 2009];
(a) Overview of reinforced laminated glass samples; (b) laminated glass with and without reinforcement.

Also Carvalho [Carvalho, 2010] studies a concept of steel-reinforced glass plates, see Figure 3.21. Similar to Feirabend, Carvalho applies perforated thin sheet as reinforcement in laminated glass plates. An additional feature of the perforated sheet is that it also functions as a connector to surrounding members.

(a)	(b)
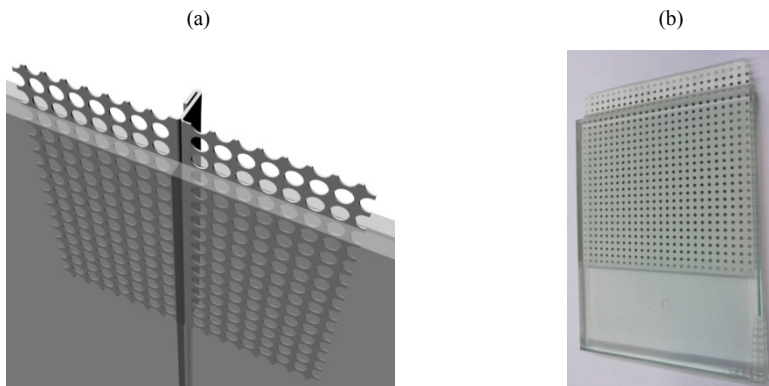
Figure 3.21: Perforated metal sheet embedded in interlayer [Carvalho, 2010].

3.4.2.   CFRP reinforced glass beams

CFRP (Carbon Fiber Reinforced Polymer) reinforced glass beams have been investigated and applied by Palumbo [Palumbo, Palumbo & Mazuchelli, 2005], see Figure 3.22. The beams consisted of laminated annealed float glass and a carbon-fiber reinforced polymer (CFRP) section which was adhesively bonded at the tensile edge. The concept has been experimentally investigated on scaled beam models and has been applied in a roof covering for the 'Loggia de Vicari' in Italy.

Figure 3.22: CFRP reinforced glass beams [Palumbo, Palumbo & Mazuchelli, 2005].

Also Antonelli & Cagnacci [Antonelli et al., 2008; Gacnacci et al., 2008; Gacnacci, Orlando & Spinelli, 2009] investigated carbon-fiber reinforced glass beams, see Figure 3.23. The beams consisted of PVB-laminated annealed float glass and contained a CFRP section integrated at the recessed edges. Different resins (epoxy or polyester) were investigated to apply as a bond between the glass and the CFRP sections. Furthermore, different types of reinforcing bars (smooth or ribbed) were investigated. Bending tests were performed on 3 m beam specimens. Additionally, a facade design that makes use of the CFRP-reinforced beams was proposed.
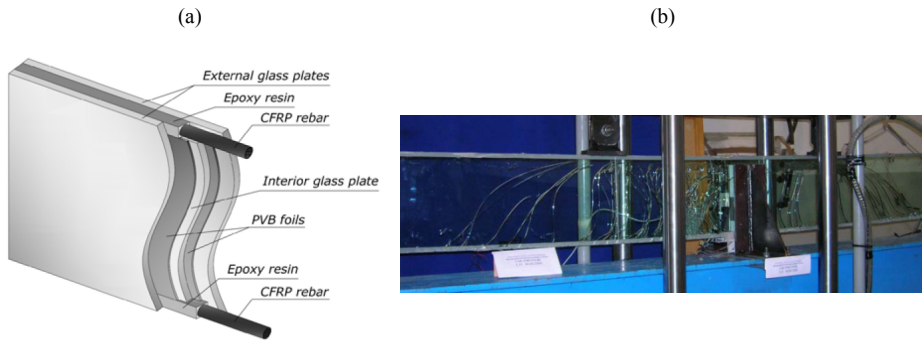
Figure 3.23: CFRP reinforced glass beams, Antonelli & Gacnacci
[Antonelli et al., 2008; Gacnacci et al., 2008; Gacnacci, Orlando & Spinelli, 2009];
(a) layout of the CFRP-reinforced glass beam; (b) CFRP-reinforced glass beam in test setup.

3.4.3.   Timber-glass beams

Timber-glass beams have been investigated by Hamm & Kreher [Hamm, 2000; Kreher, 2004; Kreher, Natterer & Natterer, 2004], see Figure 3.24. The beams consist of a single-layer glass web and timber flanges which are adhesively bonded both at the top and the bottom edge. Annealed, heat-strengthened or fully tempered glass has been applied. The beams have been experimentally investigated and have been applied in a roof structure for a hotel in Switzerland.

(a)   (b)

Figure 3.24: Timber-glass beams investigated by Hamm & Kreher
[Hamm, 2000; Kreher, 2004; Kreher, Natterer & Natterer, 2004];
(a) Cross-section of the timber-glass beams; (b) Timber-glass beams applied in a hotel in Switzerland.

Also Cruz & Pequeno [Cruz & Pequeno, 2008 a, b] have investigated timber-glass beams, see Figure 3.25. The beams consisted of double-layer float glass web(s) and timber flanges. The timber flanges were bonded to the glass using a polymer, silicone or polyurethane adhesive. Different beam spans and different cross-section geometries (I-section and box-section) are investigated. Additionally, a similar concept for timber-glass panels has been investigated [Cruz & Pequeno, 2008c].

(a)   (b)
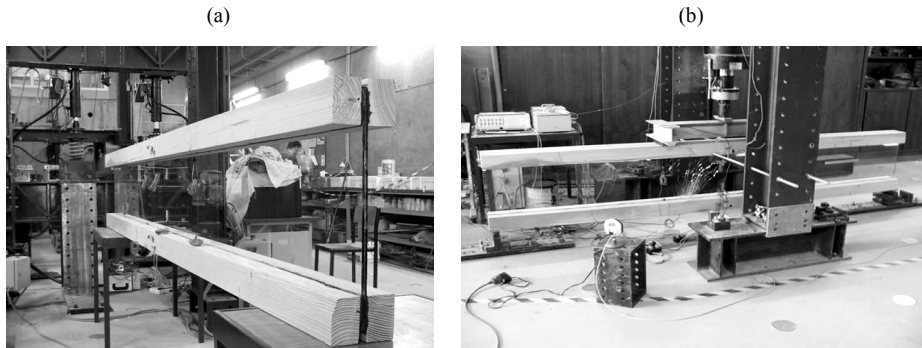
Figure 3.25: Timber-glass beams investigated by Cruz & Pequeno [Cruz & Pequeno, 2008 a, b];
(a) Photograph of the timber-glass beam; (b) Timber-glass beam in test setup.

3.4.4.   *Reinforced-concrete-glass composite beam*

Reinforced-concrete-glass composite beams have been investigated by Freitag [Freitag, 2004], see Figure 3.26. The beams consist of a triple-layer fully tempered laminated glass web and two ultra-high-performance reinforced concrete flanges. The connection between the web and the flanges is made through freshly poured concrete.

(a)   (b)
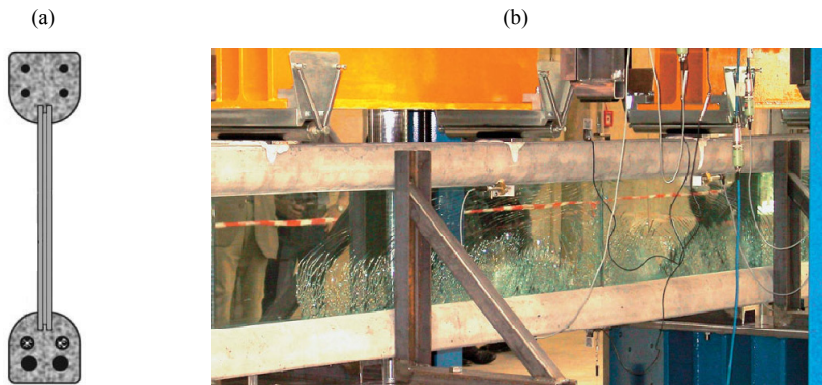
Figure 3.26: Reinforced-concrete-glass composite beams investigated by Freitag [Freitag, 2004].

3.5.   Evaluation

The described evolution of the reinforced glass beam concept at TU Delft, see section 3.3, and the overview of similar concepts studied by others, see section 3.4, indicate that the intended functioning of the reinforced glass beam concept, as described in section 3.2, is feasible.

However, different from the projects presented in the overview, the current study focuses on composite glass beams in which a reinforcement section is integrated in the layout of the beam, rather than that tensile elements have been externally bonded to the glass beam. It is expected that fully integrating the reinforcement in the beam instead of externally bonded it to the beam enhances both the architectural and the structural performance of the beams.

Furthermore, most of the aforementioned research projects only focused on the structural response of the beams in simple bending. The specific effects of parameters such as temperature, thermal cycling, load duration, humidity, beam size, reinforcement material and reinforcement percentage on the beam response seem largely unknown. These aspects are therefore investigated in the current study. Additionally, an analytical model is developed and a novel numerical model is investigated to describe the structural response of reinforced glass beams.

Chapter 4
Materials applied in this research

This chapter provides an overview of the properties of the materials applied in this research. These materials are glass, reinforcement and intermediary bond. They have applied to construct the specimens that are experimentally investigated in the following Chapters 5, 6 and 7.

Abstract

The pull-out and beam specimens that are tested in this research are made of glass, reinforcement and an intermediary bond system. For the glass, annealed float glass is applied. It is expected that due to the limited fracture pattern of this glass type, a high post-breakage strength of the reinforced glass beams is obtained. For the reinforcement two materials are applied, namely stainless steel and glass fiber. The stainless steel offers durability, high strength and ductility. The glass fiber reinforcement, which has been applied by means of glass fiber reinforced polymer (GFRP) rods, offers high strength – even higher than stainless steel – and a semi-transparent appearance. For the intermediary bond two different bond systems are applied, namely a UV-curing acrylate adhesive from DELO and the SG interlayer from DuPont. Both systems offer a fully transparent bond. The properties of the glass, reinforcement materials and intermediary bond systems are presented in this chapter.

4.1.   Introduction

The pull-out and beam specimens that are investigated in this research consist of glass, reinforcement and an intermediary bond.

For the glass, ordinary annealed float glass is applied. It is expected that by the application of this glass type, which fails in large fragements, the largest post-breakage strength of the beams is obtained.

For the reinforcement two different materials are applied, namely stainless steel and glass fiber. The stainless steel has been selected for its high tensile strength and its ductility. These properties are expected to positively contribute to the post-breakage strength and ductility of the reinforced glass beams. The glass fiber, which is applied by means of glass fiber reinforced polymer (GFRP) rods, has been selected for its high strength – even higher than stainless steel – and its (semi-)transparency. These properties are expected to enhance the post-breakage strength and the transparency of the beams respectively.

For the intermediary bond, two different systems have been selected, namely the UV-curing acrylate Glasbond 368 (GB) adhesive from DELO [DELO, 2009] and the ionomer interlayer SentryGlas® (SG) from DuPont [DuPont, 2009]. The former has been selected because of the broad experience and promising results obtained during the development of the reinforced glass beam concept at TU Delft [Richemont & Veer, 2007; Veer, 2005; Veer, Janssen & Nägele, 2005; Veer & Zuidema, 2008], see Chapter 3, section 3.3. The latter has been selected for its promising results in bonding metal components to glass [Belis et al., 2009a; O'Callaghan, 2008; Peters et al., 2007]. Both bond systems provide a fully transparent bond.

The material properties of the glass, the reinforcement materials and the intermediary bond systems are discussed in the following sections.

4.2.   Glass

Annealed float glass is applied in this research. The following sub-sections present the production process, the chemical composition and the mechanical properties of the applied glass type. Furthermore, the possibilities of strengthening glass through a heat-treatment process, and layering glass by means of a lamination process are discussed. Finally, the choice for the selected glass type for this research is explained.

4.2.1.   Production process

The float process is currently the primary production process for flat glass[i]. A schematic representation of the float glass process is provided in Figure 4.1. In this continuous[ii] float glass process the raw materials are melted in a furnace at 1550°C. Subsequently, the molten glass is poured at 1000°C onto a bath of molten tin[iii]. The glass floats[iv] on the tin forming a glass ribbon with perfectly smooth surfaces[v]. By means of top rollers the thickness[vi] of the glass is adjusted. At the end of the tin bath the glass has cooled down to 600°C and is drawn into an oven called the annealing lehr. In this oven the glass is slowly cooled down to 100°C, to prevent from residual stresses in the glass. After the glass has left the annealing lehr the glass is inspected by an automated process for visual defects, which are subsequently removed in the cutting process. Finally, the glass is cut to its final size. The maximum standard size of glass is 6*3.21 m. However, it is also possible to obtain greater lengths[vii].

raw material

1550°C   1000°C   600°C   500°C   100°C

melter   tin bath   annealing lehr   inspection   cutting
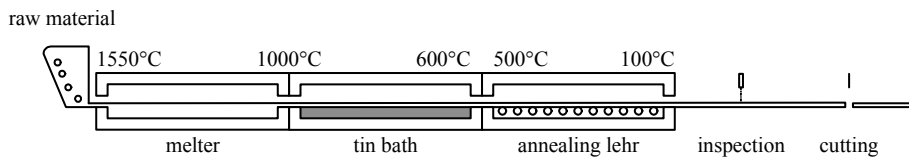
Figure 4.1: Schematic representation of the float glass process; based on [Wörner, Schneider & Fink, 2001].

---

[i] The float glass production process has been introduced by the Pilkington Brothers in 1959. It provided a cheaper and better quality alternative to the other mass production processes of flat glass developed by that time, such as the Fourcault, Pittsburgh and Libbey-Owens processes.

[ii] A float glass production plant operates 24 hours a day, 7 days a week. The process is only seldomly disrupted.

[iii] Oxidation of the tin is prevented by an inert atmosphere consisting of hydrogen and nitrogen.

[iv] The name of the 'float process' refers to this floating of the molten glass on the tin bath.

[v] The surface facing the tin is, in the final product, referred to as 'tin side', whereas the other surface is referred to as 'air side'. The tin side can be detected by means of UV radiation; it then appears bluish.

[vi] Float glass is produced in standard thicknesses of 2, 3, 4, 5, 6, 8, 10, 12, 15, 19 and 25 mm. The practical thicknesses (for building applications) range from 4 to 19 mm.

[vii] The possibilities of obtaining larger lengths of glass are currently rapidly increasing. Also the possibilities for further processing, such as lamination, of oversized glass panels are rapidly increasing. This is illustrated by the 21 m splice laminated glass beam and the 18 m insulated glass unit presented at Glasstec 2010 fair in Düsseldorf.

4.2.2. Composition

A glass is often referred to as an inorganic product of fusion which has been cooled to a rigid condition without crystallization[i] [Haldimann, Luible & Overend, 2008]. This means that during the cooling process from a liquid to a solid, glasses do not convert to a crystalline state, see Figure 4.2. Instead of forming a crystalline structure, the liquid turns – over a specific glass transformation temperature range or region, see Figure 4.2 – into a frozen solid with an amorphous structure. Glass is therefore also referred to as a super-cooled liquid.
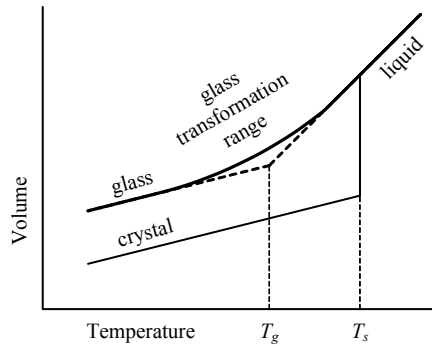
Figure 4.2: Schematic representation of the volume's dependence on temperature for a glass and a crystalline material; based on [Shelby, 2005]; T_g = glass transition temperature; T_s = melting temperature.

In this research soda-lime silica glass, which is the most commonly used glass type in the building industry, is applied. This glass type is a mixture of silica sand, lime, soda, magnesia and alumina, see Table 4.1. Its structure consists of an irregular network of tetrahedral modules – each composed of one silicium atom and four oxide atoms – and intermediate alkaline parts, see Figure 4.3.

For a more extensive description of glass(es), their composition and their formation is referred to [Shelby, 2005].

---

[i] It is noted, however, that this 'definition' of a glass applies for most glasses, but not for all. Other processes can be applied such as vapor deposition, sol-gel processing of solutions, and neutron irradiation of crystalline materials [Shelby. 2005]. Furthermore, glasses can theoretically be produced from any material.
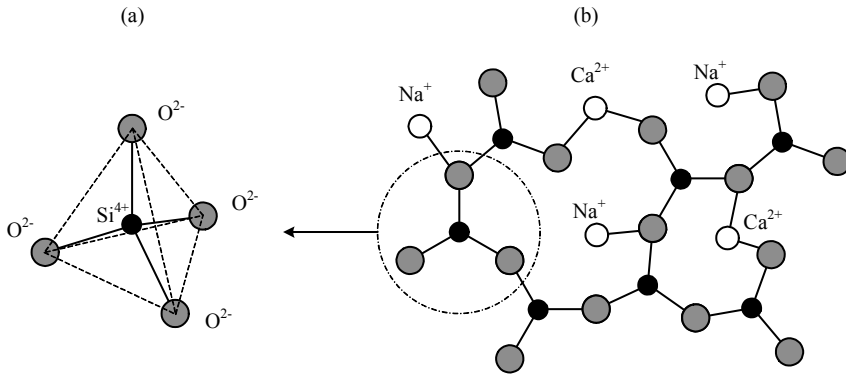
Figure 4.3: Schematic representation of the structure of soda-lime silica glass; figure based on [Bos, 2009];
(a) Schematic 3D representation of a tetrahedral module built from one silicium and four oxide atoms;
(b) Schematic 2D representation of the irregular network of soda lime silica glass.

Table 4.1: Chemical composition of soda-lime silica glass according to [EN 572-1: 2004].

		mass [%]
Silica sand	SiO_2	69-74%
Lime (calcium oxide)	CaO	5-14%
Soda	Na_2O	10-16%
Magnesia	MgO	0-6%
Alumina	Al_2O_3	0-3%
Others	-	0-5%

4.2.3.   Mechanical and physical properties

A selection of material properties of soda-lime silicate glass is presented in Table 4.2. The density of glass is similar to the density of concrete and its Young's modulus is similar to the Young's modulus of aluminium. Glass shows linear-elastic, isotropic behaviour and exhibits brittle failure, see Figure 4.4. Since glass is not able to redistribute stresses by means of plastic deformation, it is highly sensitive to stress concentration. The strength of glass is not a material constant, but depends on various parameters, as will be explained in the following section.

Table 4.2: Properties of (annealed) soda-lime silicate glass, according to [EN 572-1: 2004]

Property	symbol	unit	value
Density	ρ	kg/m^3	2500
Hardness (Knoop)	$HK_{0,1/20}$	GPa	6
Young's modulus	E	GPa	70
Poisson's ratio	v	-	0.2 [a]
Tensile bending strength	f_t	MPa	45 [b]
Specific thermal capacity	c_p	J·kg^{-1}·K^{-1}	720
Thermal expansion coefficient (between 20 and 300°C)	α	K^{-1}	$9*10^{-6}$
Thermal conductivity	λ	W·m^{-1}·K^{-1}	1
Mean refractive index to visible radiation (380 to 780 nm)	N	-	1.5

[a]   in research and application, values between 0.22 and 0.24 are commonly used [Haldimann, Luible & Overend, 2008].

[b]   the strength of glass is not a material constant, see section 4.2.4.
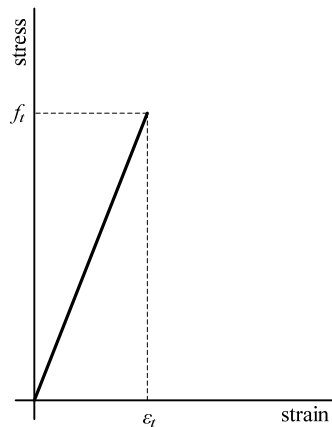
Figure 4.4: Schematic representation of the stress-strain diagram of glass in tensile loading.

4.2.4.   Strength of glass

Glass has a high theoretical/intrinsic strength, which is determined by the forces of the interatomic bonds. According to *Orowan*, the theoretical failure stress σ_m of a material, which is the stress necessary to break a bond, is given by Equation 4.1. Following this equation, the theoretical strength of a typical silica glass (E = 70 GPa; γ = 3 Jm^{-2}; r_0 = 0.2 nm) amounts to 32 GPa.

$$\sigma_m = \sqrt{\frac{E\gamma}{r_0}} \qquad\qquad (4.1)$$

with:

E = Young's modulus

γ = fracture surface energy

r_0 = equilibrium spacing of the atoms

However, the practical tensile bending strength of annealed soda-lime silicate glass is much lower[i]. *Griffith*[ii] attributed this difference between the theoretical and the practical strength to randomly distributed microscopic flaws at the glass surface. These so-called *Griffith flaws* act as (tensile) stress concentrators from which fracture of the glass starts. They are already present in the material after the production process. Additional flaws may occur during further processing and handling of the glass and during its further service-life due to e.g. scratching, debris, impact etc. The strength of a glass specimen is related to the depth of the (critical) flaw. A larger flaw depth results in a lower strength. Furthermore, as the flaws are assumed to be randomly spread over the glass surface, the chance of the presence of a large (critical) flaw, thus a lower failure strength, increases with increasing specimen sizes.

---

[i] EN 572-1: 2004 gives a characteristic tensile bending strength of 45 MPa.
[ii] [Griffith, 1920] as quoted in [Haldimann, Luible & Overend, 2008].

The flaws display a time-dependent behaviour when loaded in tension. This phenomenon of slow crack growth (or: *sub-critical crack growth*) originates from *stress corrosion*[i,ii,iii] in the glass. In the presence of humidity, stress corrosion causes flaws to grow slowly when they are exposed to a positive crack opening stress[iv]. This means that a glass specimen that is stressed below its momentary strength will still fail after the time necessary for the most critical flaw to grow to its critical size at that particular stress level [Haldimann, Luible & Overend, 2008].

The chemical process associated with stress corrosion is commonly explained as the *classical stress corrosion theory*[v], which embodies the chemical reaction of a water molecule with silica at the (stressed) crack tip, see Figure 4.5 and Equation 4.2. This chemical reaction both sharpens and lengthens the crack tip, which leads to an increase in stress around the crack tip.

$$Si\text{-}O\text{-}Si + H_2O \quad \rightarrow \quad Si\text{-}OH + HO\text{-}Si \tag{4.2}$$
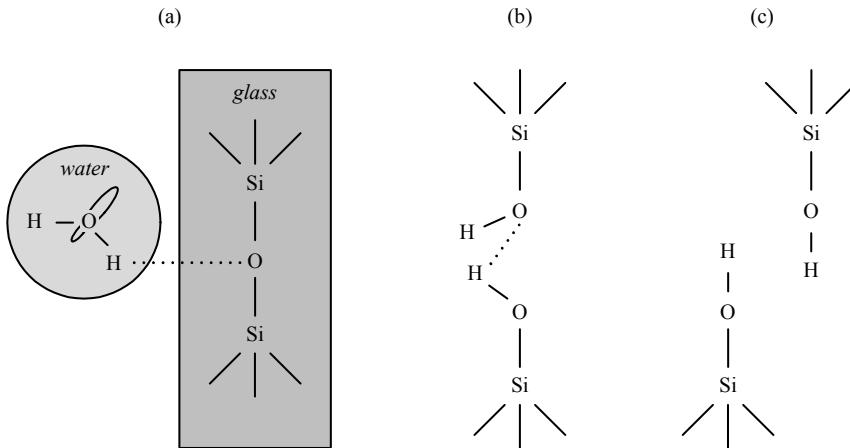
Figure 4.5: Schematic representation of the stress corrosion process; based on [Haldimann, 2006]; (a) adsorption of water to Si-O bond, (b) concerted reaction involving simultaneous proton and electron transfer, and (c) formation of surface hydroxyl groups.

---

[i] This process was already discovered in 1899 by Grenet [Grenet, 1899], as quoted in [Haldimann, 2006].
[ii] For an in-depth reading on stress corrosion in glass is referred to [Charles & Hillig, 1962; Gy, 2003; Michalske & Freiman, 1983; Wiederhorn & Bolz, 1970], as quoted in [Haldimann, 2006].
[iii] 'Stress corrosion' is also referred to as 'static fatigue'. However, the latter might be confusing as 'fatigue' is, especially in civil engineering, often associated with cyclic loading [Haldimann, 2006].
[iv] i.e. tensile stress
[v] Developed by Levengood, Charles & Hillig and Michalske & Freiman respectively [Charles & Hillig, 1962; Levengood, 1958; Michalske & Freiman, 1983], as quoted in [Haldimann, Luible & Overend, 2008].

Figure 4.7 shows a schematic representation of the relation between *crack velocity v* and the *stress intensity factor K_I* [i]. Such a *v-K* diagram is often used for glass lifetime prediction. The stress intensity factor K_I has been introduced by *Irwin* and represents the elastic stress intensity near the crack tip. For mode I loading[ii] the stress intensity factor is given by Equation 4.3:

$$K_I = Y\sigma_n\sqrt{\pi a} \tag{4.3}$$

with:

Y = geometry factor[iii]

σ_n = nominal tensile stress normal the crack's plane

a = crack size; i.e. crack depth or half of the crack length, as given in Figure 4.6.

(a)   (b)
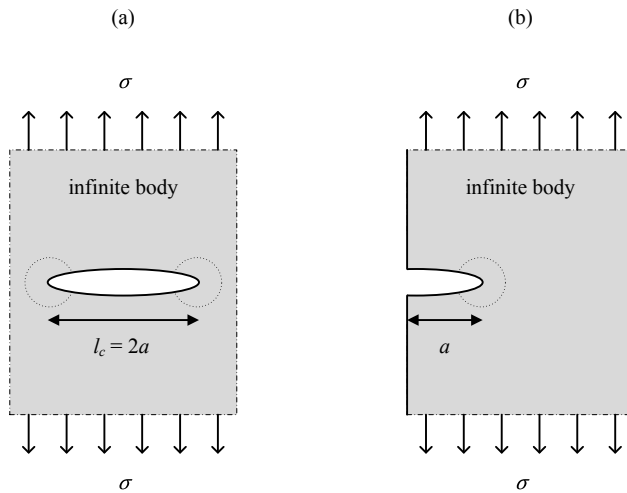
Figure 4.6: Schematic representation of (a) volume crack and (b) surface crack; based on [Bos, 2009].

---

[i] Stress intensity for mode I loading, as indicated by the suffix 'I'.

[ii] In Linear Elastic Fracture Mechanics (LEFM) three fracture modes are distinguished; Mode I (opening mode) corresponds to normal separation of the crack walls under the action of tensile stress; Mode II (sliding mode) corresponds to longitudinal shearing of the crack walls in a direction normal to the crack front; Mode III (tearing mode) corresponds to lateral shearing parallel to the crack front; [Lawn, 1993].

[iii] The geometry factor Y depends on the crack's depth and geometry, the specimen geometry, the stress field and the proximity of the crack to the specimen boundaries. A long, straight-fronted plane edge crack in a semi-infinite specimen has a geometry factor of Y = 1.12. For half-penny shaped cracks in a semi-infinite specimen the geometry factor amounts to 0.637 to 0.713 [Haldimann, Luible & Overend, 2008]. The latter is often assumed in glass.
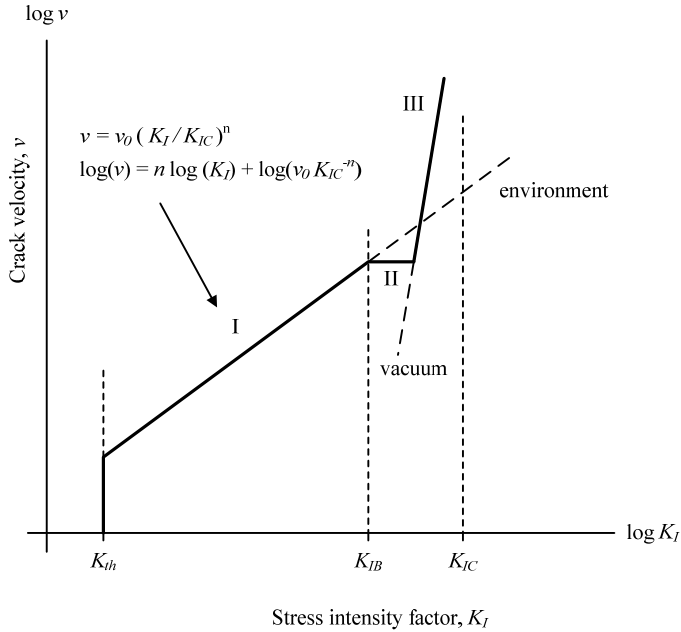
Figure 4.7: Schematic representation of the relation between *crack velocity v* and *stress intensity K_I*.

Rapid crack growth[i], and consequently failure of the glass, occurs when K_I reaches or exceeds the *critical stress intensity[ii]* K_{Ic}. This criterium is known as *Irwin's fracture criterion* and is given by Equation 4.4:

$$K_I \geq K_{Ic} \tag{4.4}$$

with:

K_{Ic} = critical stress intensity factor[iii]

---

[i] i.e. high velocity crack growth
[ii] or: fracture toughness
[iii] An overview of published K_{Ic} values for modern soda lime silica glasses is presented in [Haldimann, Luible & Overend, 2008]. They indicate that a value of 0.75 MPa m$^{0.5}$ can be used for all practical purposes.

This is also seen in the *v, K* diagram presented in Figure 4.7. In region III, where the *stress intensity factor K_I* approaches the *fracture toughness K_{Ic}* the *crack velocity v* is independent of the environment and approaches a characteristic crack propagation speed very rapidly [Haldimann, Luible & Overend, 2008]. In inert environments the steep curve in region III would extrapolate linearly to lower crack velocity. In normal environments, however, the behaviour strongly depends on the environmental conditions, which results in a different curve, as can be seen at region I in Figure 4.7. In this region the relation between crack velocity and stress intensity is given by Equation 4.5:

$$v = v_0 \left(\frac{K_I}{K_{Ic}}\right)^n \qquad\qquad (4.5)$$

with:

v_0 = crack velocity parameter [i]

n = parameter [ii]

In region II, the *crack velocity v* is independent of the stress intensity K_I. In this region, the speed of the chemical reaction depends on the supply rate of water from the environment. As it takes time for a water molecule to be transported to the crack tip, a shortage in the supply of water occurs as the crack velocity increases [Wiederhorn & Bolz, 1970]. The *crack velocity v* is, therefore, essentially independent of K_I but depends on the amount of humidity in the environment [Haldimann, 2006]. Below the threshold stress intensity K_{th} no crack growth occurs.

The relation between the *crack velocity v* and the *stress intensity factor K_I*, is influenced by several conditions such as humidity, temperature, corrosive media and pH value, chemical composition of the glass and loading rate [Haldimann, Luible & Overend, 2008]. Increased *humidity* and increased *temperature* causes a parallel shift of the *v, K_I* curve towards higher crack velocities. For increased loading rate the *v, K_I* curve shifts towards lower crack velocities. The latter is explained by Haldimann [Haldimann, 2006] by a shortage in the supply of water to the crack tip for fast loading. As the diffusion process of humidity is not fast enough, the stress corrosion and consequently the sub-critical crack growth is slowed down for high loading rates.

---

[i] The parameter v_0 has to be determined from experiments. For general application v_0 = 6 mm/s should be conservative. For glass elements that are permanently immersed in water a higher value of v_0 = 30 mm/s is more appropriate [Haldimann, Luible & Overend, 2008].
[ii] The parameter n has to be determined from experiments. Commonly, n = 16 is assumed for structural glass applications [Haldimann, Luible & Overend, 2008].

Another aspect of glass is that the fracture strength of glass specimens with induced flaws increases when the glass specimen is left free of stress over a period of time. This phenomenon, which is referred to as *crack healing*, is a consequence of the *crack growth threshold* and a *hysteresis effect* [Haldimann, Luible & Overend, 2008]. Below the *crack growth threshold* no crack growth occurs. This crack growth threshold was originally attributed to crack tip blunting[i] at slow crack velocities, but recent investigations support the hypothesis that the crack growth threshold results from alkali that are leached out of the glass which causes a change in the chemical composition of the glass at the crack tip. Additionally, in alkali containing glasses there is a *hysteresis effect*. This embodies the phenomenon that an aged crack will not re-propagate immediately on reloading. Crack healing strongly depends on the environmental conditions and on the chemical composition of the glass. It is therefore difficult to quantify.

The inherent tensile strength of the edge of a glass pane glass is generally lower than the strength away from the edge. This difference is caused by the more severe surface damage at the edge of the glass pane due to the cutting and machining process. The edge strength of glass strongly depends on the applied edge finishing. Especially for glass beams, which are loaded in plane thereby highly stressing the edge of the glass, a proper edge finishing is therefore required.[ii,iii]

From experimental data a large scatter in the strength of glass is found. This large scatter obviously relates to the various parameters introduced above that influence the strength of glass. The Weibull distribution is often used as a statistical descriptor for the strength of glass. However, this distribution is questioned by several authors[iv] and also other distributions have been suggested.

---

[i] Crack tip blunting refers to rounding of the crack tip.
[ii] In this research all specimens (both the pull-out specimens and the beam specimens) have been made with polished edges.
[iii] For a further reading on the edge strength of glass loaded in plane is referred to [Hess, 2000; Veer, Louter & Bos, 2009].
[iv] For instance: Veer [Veer, 2007; Veer, Louter & Bos, 2009; Veer & Rodichev, 2009] and Calderone & Jacob [Calderone & Jacob, 2001]

4.2.5. *Heat-treated glass*

The practical strength of glass can be enhanced by a heat treatment [i] (or: tempering) process. In this process the glass is heated to approximately 620-675°C and subsequently rapidly cooled by air jets, see Figure 4.8. As the outside surface cools and solidifies more rapidly than the inner core of the glass, a surface compressive residual stress and an interior tensile residual stress results in the glass. The compressive residual (pre-)stress at the glass surface effectively enhances the tensile (bending) resistance of the glass. The flaws at the glass surface can only grow when they are exposed to an effective tensile stress. As long as the surface tensile stress due to actions is smaller than the surface compressive pre-stress, no crack growth will occur.

cleaning   heating   cooling / quenching
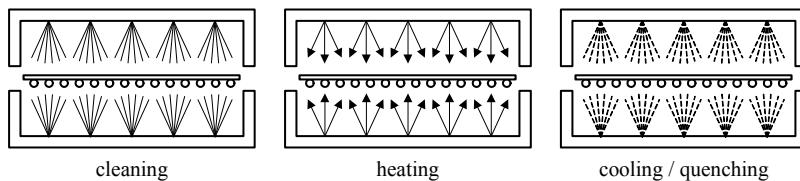
Figure 4.8: Schematic representation of the thermal tempering process;
based on [Wörner, Schneider & Fink, 2001].

---

[i] A different method to enhance the practical strength of glass is a chemical tempering process. This process is based on the exchange of sodium ions in the glass surface by potassium ions. The latter are 30% larger, so that a thin compressive pre-stress layer results at the glass surface. For structural glass applications, however, this process is rarely applied and only for special geometries where heat-tempering cannot be applied [Haldimann, Luible & Overend, 2008].

Any drilling, cutting or grinding of the glass must be done prior to the tempering process. If these mechanical actions are performed after the tempering process, the energy balance between the tensile stress in the core and the compressive stress at the surface will be disturbed, which will result in shattering of the heat-treated glass.

Using the heat treatment process, two types of heat-treated glass can be made, namely fully tempered and heat-strengthened glass, see Table 4.3. Fully tempered glass has the highest level of residual stress. For heat-strengthened glass the cooling rate in the tempering process is lower, which results in a lower level of residual stress.

The fracture pattern of a glass sheet depends on the energy stored in the glass, and thus on the pre-stress and the stress due to actions. Figure 4.9 shows the different fracture patterns for *annealed* glass (as it results from the float process), *heat-strengthened* and *fully tempered* glass. Due to the high pre-stress level in fully tempered glass, this type of glass shows the highest fragmentation and breaks in small fragments (dice), see Figure 4.9 (c). Heat-strengthened glass has a lower pre-stress level and breaks in larger fragments, see Figure 4.9 (b). Annealed glass has no pre-stress and breaks into even larger fragments, see Figure 4.9 (a).

Table 4.3: Characteristic tensile bending strength of annealed, heat-strengthened and fully tempered float glass according to [EN 572-1: 2004; prEN 13474-1, 1999].

	Characteristic tensile bending strength
Annealed	45 MPa
Heat-strengthened	70 MPa
Fully tempered	120 MPa

(a)	(b)	(c)
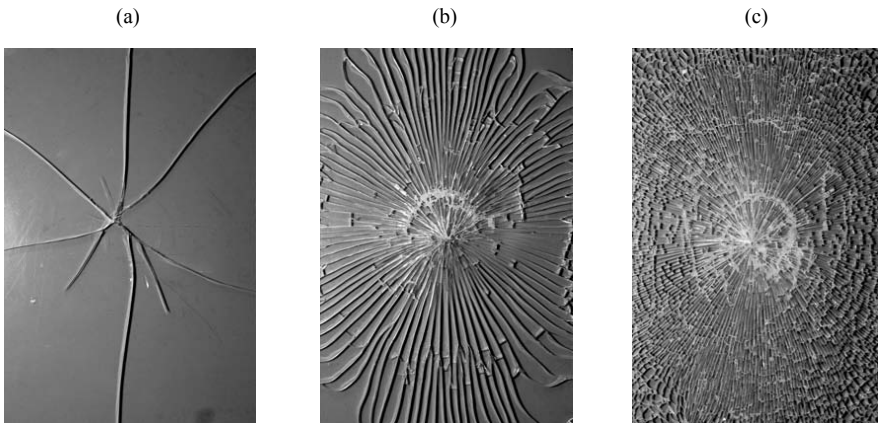
Figure 4.9: Fracture pattern of (a) annealed glass, (b) heat-strengthened and
(c) fully tempered glass; pictures taken from [Haldimann, 2006].

Fully tempered glass has a small probability of 'spontaneous' fracture, due to nickel-sulfide (NiS) inclusions in the glass. These nickel sulfide particles are included in the glass during the production process and cannot be completely avoided. Under influence of temperature, these inclusions can expand in volume due to a phase change. This expansion in combination with the high tensile stress in the core of fully tempered glass can cause 'spontaneous' fracture of the glass. To limit the probability of 'spontaneous' fracture of fully tempered glass, a heat-soak test can be applied to the glass directly after the tempering process. In this heat-soak test the glass is slowly heated to approximately 290°C and maintained at this temperature level for several hours. This accelerates the phase change of any nickel-sulfide inclusion, which will cause failure of glass sheets with critical nickel-sulfide inclusions. However, it should be noted that the heat-soak test can only limit the probability of 'spontaneous' fracture due to nickel-sulfide inclusions, but cannot fully eliminate it.

For further reading on various topics related to heat-treated glass, such as modeling of the tempering process to estimate the resulting residual stresses and issues concerning nickel-sulfide inclusions, is referred to [Bernard, Gy & Daudeville, 2002; Carré & Daudeville, 1998; Kasper & Stadelmann, 2002; Laufs, 2000; Nielsen, 2009; Schneider & Hilcken, 2010].

4.2.6. Laminated glass

Laminated glass consists of two or more glass panes that are bonded together by means of an interlayer. This interlayer can be either an adhesive foil or an adhesive resin. For foil interlayers an autoclave lamination process, which uses heat and pressure to realize the bond, is applied. For adhesive resins a cast-in-place lamination process[i] and a subsequent polymerization by UV-radiation are commonly applied[ii].

Foil interlayers are the most commonly applied interlayers for laminated glass. The main purpose of the foil interlayer is to keep the glass fragments together in case of glass fracture and thus to prevent from human injury. Furthermore, foil laminated glass offers enhanced post-breakage behaviour. As the glass fragments adhere to the foil, a residual structural capacity is obtained through an arching or interlocking effect of the glass fragments. The extent of this post-breakage capacity, however, depends on the applied glass type (annealed, heat-strengthened or fully tempered) and the applied interlayer type.

The most commonly used foil interlayer is PVB (polyvinyl butyral). This interlayer type is widely used in the automotive and building industry. Other examples of foil

---

[i] For the cast-in-place process, the individual panes are kept at a certain distance by means of a double-sided tape along the perimeter of the glass panes. The void/space between the glass panes is filled with adhesive resin and subsequently cured by UV-radiation.

[ii] For the UV-curing adhesive that has been applied in this research, a semi-automated adhesive bonding process has been developed, which is described in Chapter 10.

interlayers are EVA (Ethyl Vinyl Acetate), which are often used in the domain of the solar industry, and SG (SentryGlas®). The latter has been developed by DuPont for hurricane, vandalism and burglary resistant glazing. Compared to common PVB interlayers, this foil is supposed to offer enhanced strength and stiffness [DuPont, 2009].

In this research a UV-curing acrylate adhesive and the SG interlayer have been applied to laminate the specimens. Their properties are described in more detail in section 4.5.

4.2.7.   Selected glass type for this research

For this research annealed glass is selected. Although the tensile strength of annealed glass is smaller than that of heat-strengthened or tempered glass, the application of ordinary annealed float glass is expected to be most advantageous. Due to the absence of residual stresses in the glass, annealed float glass breaks in large fragments. It is expected that these large fragments offer the highest remaining load carrying potential and prevent from total disintegration of the beam upon glass failure. This line of reasoning is supported by the experimental research of Kreher [Kreher, 2004], who investigated the effect of annealed, heat-strengthened and fully tempered glass on the residual resistance of timber-glass composite beams, see section 3.4.3. From that study it is observed that timber-reinforced glass beams made of annealed float glass show the highest residual resistance, see Figure 4.10. For the current research it is therefore decided to focus on the application of annealed float glass in reinforced glass beams.
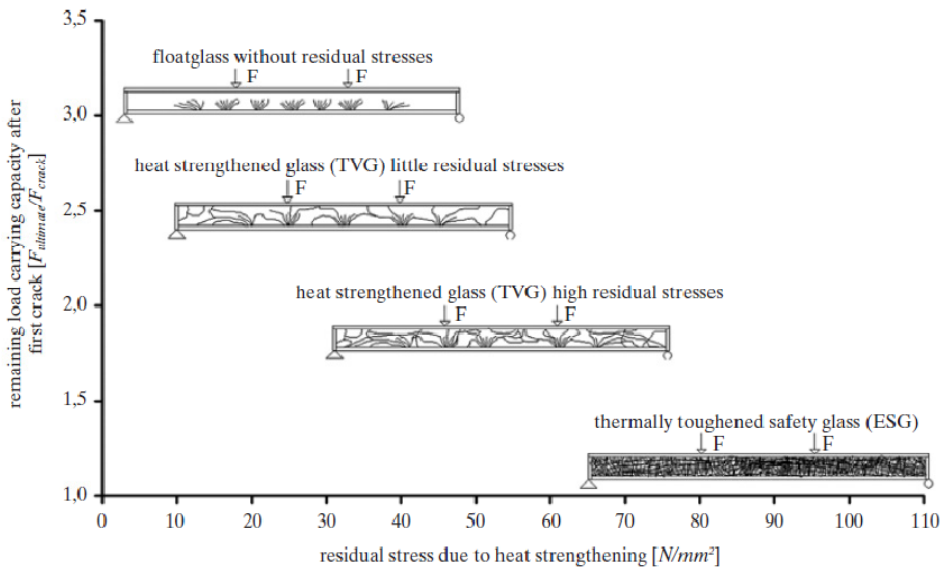
Figure 4.10: Relation of residual (internal) pre-stress and remaining load-carrying capacity for timber-reinforced glass beams; toughened glass = fully tempered glass; taken from [Kreher, 2004].

4.3.   Reinforcement

In the current research stainless steel and glass fiber are investigated as reinforcement materials for structural glass beams.

The stainless steel is applied as a square hollow or solid section, which is bonded at the inner recessed edge of triple-layer annealed float glass beams using the GB adhesive or the SG interlayer, see Chapter 5 and 6. Since the edges of glass are always distinct, bonding a stainless steel section at the edge does not significantly affect the transparency of the beam.

The glass fiber has been applied by means of pultruded GFRP (glass fiber reinforced polymer) rods, which have been embedded in the interlayer of double-layer SG-laminated annealed float glass beams, see Chapter 7.

The material properties of stainless steel and glass fiber (i.e. GFRP rods) are described in the following sub-sections.

4.3.1.   Stainless steel

Stainless steels are a large family of iron-chromium (Fe-Cr) based alloys that are essentially low-carbon steels[i] containing a high percentage of chromium [Cardarelli, 2008]. This addition of chromium makes them corrosion resistant in a variety of environments. The chromium content of the steel allows the formation of a protective chromium-rich oxide film[ii] on the surface of the steel. To obtain sufficient corrosion resistance there has to be a concentration of chromium present in the alloy of at least 10.5 wt% [EN 10088-1: 2005]. Increasing the concentration of chromium will further enhance the corrosion resistance of the steel. Furthermore, other alloys additions, like nickel (Ni), molybdenum (Mo), titanium (Ti), sulfur (S), and Copper (Cu) can be made to tailor the chemical composition in order to meet the needs of different corrosion conditions, operating temperature ranges, and strength requirements or to improve weldability, machinability, and work hardening [Cardarelli, 2008].

---

[i] Low-carbon steels, or mild steels, contain up to 0.30 wt.% carbon. They are characterized by a low tensile strength and a high ductility. Carbon is the principal hardening and strengthening element in steel. Actually, carbon increases hardness and strength and decreases weldability and ductility [Cardarelli, 2008].
[ii] If damaged mechanically or chemically, this oxide-film is self-healing when small traces of oxygen are present in the corrosive medium [Cardarelli, 2008].

For this research a specific grade of stainless steel has been applied, namely stainless grade AISI 304[i, ii]. This stainless steel grade belongs to the class of austenitic stainless steels, which are the largest and most popular family of stainless steels[iii] [Cardarelli, 2008]. Austenitic stainless steels typically contain 18-25 wt.% chromium (Cr) and 8-20 wt.% Nickel (Ni) and a carbon content of usually less than 0.15 wt.%. Within the family of austenitic stainless steels grade AISI 304 is in terms of total industrial usage, the most commonly used[iv]. The chemical composition of AISI 304 is given in Table 4.4.

Table 4.4: Composition of austenitic stainless steel type AISI 304 (EN name designation = X5CrNi18-10; EN number designation = 1.4301); composition according to [EN 10088-1: 2005].

	C	Si	Mn	P	S	N	Cr	Ni
wt.%	≤ 0.07	≤ 1.00	≤ 2.00	0.045	≤ 0.015	≤ 0.11	17.5 to 19.5	8.0 to 10.5

Important for this research is the behaviour of the stainless steel reinforcement in tension. Figure 4.11 displays a typical tensile stress-strain curve for stainless steels. The rounded stress-strain curve does not demonstrate a distinctive yield stress point at which the behaviour changes from elastic to plastic deformation. The yield strength is therefore defined by the stress at which the stainless steel has suffered a permanent strain of 0.2%. After this 0.2% yield strength point ($f_{y, 0.2\%}$) the stress-strain curve shows plastic deformation with an increase in strength up to a maximum or ultimate tensile strength (f_t) followed by a decrease in strength until the material reaches its final break point. For AISI 304 the tensile strength and other properties are listed in Table 4.5.

For further reading on stainless steels is referred to [Beddoes, 1999; Bhadeshia & Honeycombe, 2006; Cardarelli, 2008].

---

[i] AISI is the abbreviation of *American Iron and Steel Institute*; the AISI 300 series are wrought austenitic stainless steels, i.e. alloys of iron-chromium-nickel.

[ii] In Europe a different name and number designation is applied than in the AISI system. For AISI 304 the equivalent European designations are as follows; EN name designation = X5CrNi18-10; EN number designation (Werkstoffnr.) = 1.4301. An easy tool to find the equivalent designations is provided at http://www.euro-inox.org/technical_tables.

[iii] The five distinct stainless steel classes are martensitic, ferritic, austenitic, duplex and precipitation-hardening stainless steels. The classes are indentified by the alloying elements that affect their microstructure, after which they are named [Cardarelli, 2008].

[iv] Another common austenitic stainless steel type is AISI 316, which has a better corrosion resistance than AISI 304. However, for this research the AISI 316 was not applicable, since the required reinforcement sizes were not available in AISI 316.
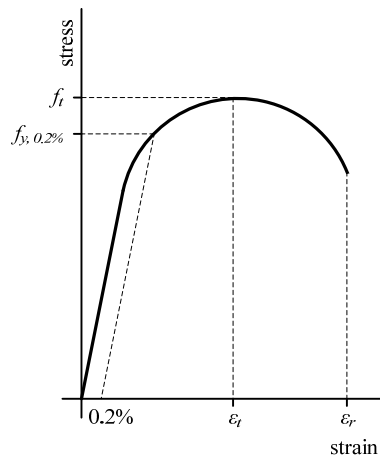
Figure 4.11: Schematic representation of the typical tensile stress-strain diagram for stainless steels; based on [Beddoes, 1999].

Table 4.5: Properties of austenitic stainless steel type AISI 304 (EN name designation = X5CrNi18-10; EN number designation = 1.4301); properties according to [EN 10088-1: 2005; EN 10088-2: 2005].

Density	ρ	kg/dm^3	7.9
Modulus of Elasticity at 20°C	E	GPa	200
Yield strength 0.2% proof	$f_{y,0.2\%}$	MPa	210-230
Ultimate tensile strength	f_t	MPa	520-750
Elongation at fracture	ε_r	%	45
Mean coefficient of thermal expansion between 20°C and 100°C	α	10^{-6} *K^{-1}	16.0
Thermal conductivity at 20°C	k	W/mK	15
Specific thermal capacity at 20°C	C	J/kg K	500
Electrical resistivity at 20°C	R	Ω·mm^2/m	0.73
Magnetizable	-	-	no

4.3.2.   Glass fiber

Continuous glass fibers are made by drawing molten glass through a bushing, see Figure 4.12, giving glass fiber filaments with a diameter from 4 and 40 µm. Subsequently, the glass fibers are sprayed with water, to cool them down, and provided with a coating ('size'). The purpose of the 'size' is twofold; 1) it serves to protect the glass fibers from mechanical damage during the further processing; 2) it serves as a bonding agent when the fibers are further processed in a polymer matrix to form a composite material (GFRP). The individual glass fiber filaments that result from this process are gathered to form strands that are winded on a rotating drum.

There are several grades of glass fiber, differing in composition and mechanical properties. E-glass[i] fibers are the most commonly produced glasses for reinforcement applications and the most economically attractive. S-glass[ii] fibers have better mechanical properties than E-glass fibers, but are more expensive. C-glass[iii] has better corrosion resistance than E-glass; and AR-glass[iv] resists alkalis, allowing it to be used to reinforce cement.

Glass fibers show linear elastic behaviour and brittle failure. The flaws in glass fibers are less and less deep than in e.g. float glass, which explains their relatively high tensile strength. In this research E-glass and S-glass fibers are applied. Their composition and properties are listed in Table 4.6 and 4.7.

In this research the glass fibers are applied by means of glass fiber reinforced polymer (GFRP) rods. Two different types of GFRP pultruded rods have been used. The first are round (Ø 2 mm) rods made of E-glass fibers with a surrounding polyester resin. The second are flat (0.8*6 mm) rods made of S-glass fibers with a surrounding epoxy resin. The rods contain a volume fraction of 63 and 65% respectively, which means that either 63 or 65% of the rod consists of glass fiber and the resulting part of resin. Both GFRP pultruded rods have a semi-transparent appearance.

The GFRP rods are made by means of a pultrusion process, see Figure 4.13. In this process glass fiber rovings are pulled through a device with liquid resin to impregnate the fibers. Subsequently, the impregnated fibers are drawn through a die and the resin is heat-set to obtain the final shape of the GFRP rod. Afterwards the rods are cut to a pre-defined length.

For further reading on glass fibers and GFRP is referred to [Hartman, Greenwood & Miller, 1996; Loewenstein, 1993; Lubin, 1969; Wallenberger & Bingham, 2010].

---

[i] The designation E stands for electrical as E-glass is a good electrical insulator besides having good strength and a reasonable Young's modulus.
[ii] S stands for high strength as S-glass has a higher strength than others.
[iii] C stands for chemical durability as C-glass has a better resistance to chemical corrosion.
[iv] AR stands for alkali resistance.

Table 4.6: Compositional ranges (wt%) of E-glass and S-glass,
according to [Hartmann, Greenwood & Miller, 1996].

	SiO_2	Al_2O_3	B_2O_3	CaO	MgO	Na_2O+K_2O	TiO_2	Fe_2O_3
E-glass	52-56	12-16	5-10	16-25	0-5	0-2	0-0.8	0-0.4
S-glass[a]	64-66	24-25	-	0-0.18	9.5-10.2	0-0.2	-	0-0.1

[a]   In [Hartmann, Greenwood & Miller, 1996] is referred to S2-glass®

Table 4.7: Properties of E-glass and S-glass;
according to [Hartmann, Greenwood & Miller, 1996].

			E-glass	S-glass[a]
Density		kg/m³	2580	2460
Refractive index			1.558	1.521
Tensile strength (filament strength)	σ_{fil}	MPa	3445 [b]	4890 [b]
E-modulus	-	GPa	72.3	86.9
Elongation at break			4.8	5.7
Thermal expansion coefficient		ppm°C	5.4	1.6

[a]   In [Hartmann, Greenwood & Miller, 1996] is referred to S2-glass®

[b]   According to [Hartmann, Greenwood & Miller, 1996] the strengths of the strands are usually 20-30%
       lower than the strength of the individual filaments, due to surface defects introduced during the strand-
       forming process.
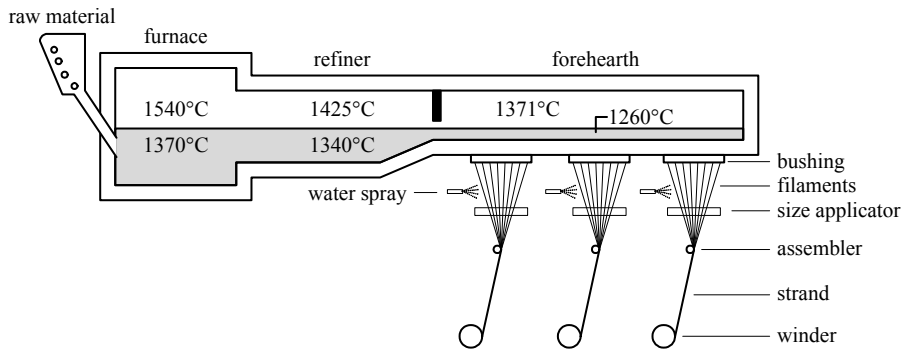
Figure 4.12: Schematic representation of the fiberglass production process;
based on [Wallenberger & Bingham, 2010].
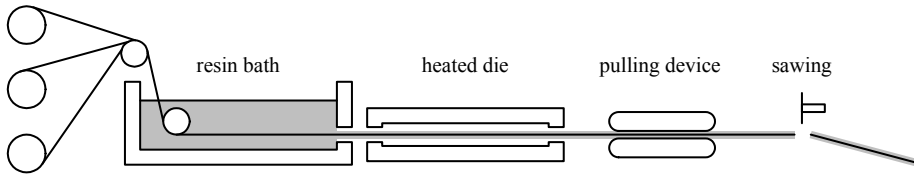
Figure 4.13: Schematic representation of the pultrusion process.

4.4.   Bond systems

For the bond between the glass and the reinforcement two different bond systems are applied in this research, namely the UV-curing acrylate Glasbond 368 (GB) adhesive from DELO and the SentryGlas® (SG) interlayer from DuPont. Their characteristics are described in the following subsections.

Table 4.8: Indicative properties of the GB adhesive and the SG interlayer;
according to [DELO, 2009; DuPont, 2009].

Property	Unit	DELO GB368	SentryGlas®
Tensile strength	N/mm^2	20	34.5
Elastic modulus	N/mm^2	900	300 [a]
Density	g/cm^3	1.0	0.95
Glass-aluminum shear strength	N/mm^2	23	n/a
Glass transition temperature	°C	102	~55-60 [b]
Elongation at tear	%	17	400
Density	kg/m^3	1000	950

[a]   Strongly dependent on temperature and load duration. An overview of values for the Young's modulus, shear modulus and poisson ratio of SentryGlas® at different temperatures and for different load durations is given by [Stelzer, 2010].

[b]   as reported by [Bucak & Meissner, 2005].

4.4.1.   GB adhesive

The Glasbond (GB) 368 adhesive is a one-component, UV- and light curing acrylate[i] adhesive [DELO, 2009]. The adhesive is transparent (clear) and belongs to the family of Photobond adhesives from DELO. These adhesives are used for a rather broad range of applications, such as bonding electronic parts, bonding aluminium door hinges to shower cabins, or bonding stainless steel point-fixings to glass panels. According to the datasheet [DELO, 2009], the GB368 is especially used for interior glass-glass, glass-metal and glass-plastic bonding.

The GB adhesive is cured within seconds, by illumination of UV- or visible light in a wavelength range of 320-420 nm. This rapid curing of UV-curing adhesives makes them attractive from a manufacturing point of view. The properties of the GB adhesive are listed in Table 4.8.

In this research the GB adhesive is applied to simultaneously bond the glass layers of the specimens and to bond the stainless steel reinforcement to the glass. For this, a semi-automated bonding process is developed in this research, which provides a rather constant bond thickness of $t \approx 0.1$ mm. This adhesive bonding process is explained in more detail in Chapter 10. To enhance the bond strength, the GB-bonded specimens have consistently been made – on advice of the adhesive manufacturer – with the air side of the glass facing the reinforcement sections; i.e. the reinforcement sections have been bonded to the air side of the glass.

The DELO UV-curing adhesives are subject of a limited number of research programs. For further reading on the performance of these adhesives is referred to [Puller, 2008; Tasche, 2008; Veer & Zuidema, 2008; Vogt, 2009; Weller & Tasche, 2009]. For a more general reading on adhesives, adhesive types, adhesive properties, bonding processes, design rules and adhesive applications is referred to [Adams & Wake, 1984; Brockmann et al., 2009; Ebnesajjad, 2008; ISE, 1999; Petrie, 2007].

---

[i] The datasheet of DELO [DELO, 2009] states that the adhesive is a modified urethane acrylate.

4.4.2.   SG interlayer

The SentryGlas[®][i] (SG) interlayer is a semi-crystalline thermoplastic polymer[ii] sheet[iii] material [Bucak & Meissner, 2005] that has been developed by DuPont for hurricane, vandalism and burglary resistant laminated glass [Bennison et al., 2002]. Compared to 'ordinary' interlayer materials, the SG offers enhanced strength and stiffness[iv] [Stelzer, 2010]. This effectively enhances the performance of the SG-laminated glass both in the un-fractured and the fractured state [Stelzer, 2010]. The material properties of the SG are provided in Table 4.8.

SG-laminated glass is produced by means of an autoclave lamination process. This process uses heat and (atmospheric) pressure to realize the connection between the glass and the SG. During the process the initially translucent sheet material turns transparent and a fully transparent bond in the final laminated glass product is obtained.

Recent studies and realized projects have demonstrated that the SG interlayer can – besides bonding glass to glass – be applied to bond metal to glass [Belis et al., 2009a; O'Callaghan, 2008; Peters et al., 2007]. This feature of the SG interlayer has for instance been applied in various Apple Store staircases, see Chapter 2, and in the Seele staircase that was presented at the Glasstec 2006 in Düsseldorf. In the latter project, for instance, the connection between the glass treads and the glass side beams of the staircase have been realized by means of an intermediary metal connector that has been laminated/bonded to the glass side walls using the SG interlayer.

In the current research the SG interlayer is exploited to simultaneously laminate the glass layers of the specimens and to bond the stainless steel or GFRP reinforcement to the glass. For this, standard 0.89 or 1.52 mm SG interlayer sheets[v] have been applied. A standard vacuum bag lamination procedure has been applied, which is discussed in more detail in Chapter 10. To enhance the adhesion, the specimens for this research have – on advice of the interlayer manufacturer – consistently been laminated with the tin side of the glass facing the reinforcement section; i.e. the reinforcement has – where possible – been laminated to the tin side of the glass.

---

[i] The interlayer material was introduced in the early nineties by the name SentryGlas[®], which was later changed in SentryGlas[®] Plus with the introduction of an improved version of the product. Nowadays, the product is again called SentryGlas[®].

[ii] SentryGlas is also often referred to as 'ionoplast' [Stelzer, 2010], which seems to be a contraction of 'ionomer' and 'thermoplast'.

[iii] Unlike e.g. PVB (polyvinylbutyral) that is available as a flexible foil material and distributed on rolls, the rather stiff SentryGlas interlayer is currently available as a sheet material with maximum sizes of 2.5*5.69 m. This sheet material is preferably transported in flat position. The manufacturer is currently working on a version of the SentryGlas that can be distributed on a roll, which eases its transport and storage.

[iv] The manufacturer even claims that the SentryGlas interlayer is 100 times stiffer and 5 times stronger than traditional interlayers [DuPont, 2010].

[v] Standard thicknesses of SG interlayer sheets are 0.89, 1.52 and 2.28 mm.

The SG interlayer has been and is subject of various research programs that focus on for instance the shear transfer capacity of the SG in various loading conditions and the durability of the SG interlayer. For further reading on these topics is referred to [Belis et al., 2009b; Bucak & Meissner, 2005; Callewaert et al., 2008; Delincé et al., 2008a, b; Louter, 2010b; Meissner & Sackmann, 2006].

4.4.3.   Polymer behaviour

Both the GB adhesive and the SG interlayer are polymer materials. A brief introduction into polymer materials and their behaviour is therefore provided in this section.

Polymers[i] consist of large chain-like molecules (or: *macromolecules*) composed of repeating simple monomer units. The monomer units within the macromolecules are chemically bonded. The macromolecules can be linked to one another via either physical (Van der Waals bonds) and/or chemical bonds (cross-links), which results in different chemical and physical structures, see Figure 4.14. Compared to the physical bonds, the chemical bonding forces are up to 10^3 times stronger. Furthermore, the physical bonds are reversible when subjected to heat, solvents, or mechanical forces, whereas the chemical bonds are irreversible [Ehrenstein, 2001].

| (a) | (b) | (c) | (d) |
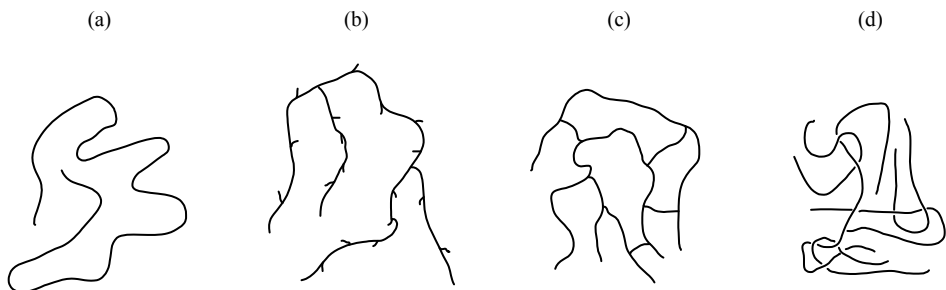
Figure 4.14: Schematic representation of the structure of polymer materials; based on [Ehrenstein, 2001]; (a) linear; (b) branched; (c) cross-linked; (d) entangled.

---

[i] 'Polymer' = 'many units' in Greek.

Polymers can be classified according to their molecular structure in 'thermoplastics', 'thermosets' and 'elastomers':

- Thermoplastics

  Thermoplastics consist of physically bound linear or branched macromolecules [Ehrenstein, 2001]. Due to the absence of cross-links, thermoplastics soften when heated and harden again upon cooling [Callister, 2000]. Thermoplastics are made by chain polymerization. Their structure may be amorphous or partly crystalline (semi-crystalline). Due to a range of molecular weights and a variety of configurations of the molecules (amorphous or semi-crystalline) the thermoplastics do not have a sharp melting point, but show decreasing viscosity over a range of temperature [Ashby & Jones, 2006].

- Thermosets

  Thermosets solidify via a chemical reaction between different components, e.g. resin, hardener, as well as various accelerators and additives. Since the result is usually a heavily cross-linked and intertwined structure, thermosets are also described as network polymers [Ashby & Jones, 2006]. Their structure is almost always amorphous. Thermosets will, once having solidified, not soften or melt when heated [Callister, 2000]. When heated the secondary (physical) bonds between the macromolecules melt, causing a drop of the E-modulus of the polymer. However, the cross-links prevent true melting or viscous flow of the polymer. Further heating will cause the polymer to decompose [Ashby & Jones, 2006].

- Elastomers

  Elastomers consist of chemically cross-linked macromolecules that form a loosely bound network structure with a rather low cross-link density [Ehrenstein, 2001]. Elastomers can experience large and reversible elastic deformations [Callister, 2000]. Due to the cross-links, which provide the 'memory' of the material, the elastomers return to their original shape on unloading [Ashby & Jones, 2006]. Similar to thermosets, elastomers do not flow when heated, due to the presence of the chemical cross-links.

The mechanical behaviour of polymers is highly sensitive to external influences such as temperature, time, loading rate, environment (humidity, oxygen, organic solvents, etc.) and UV-radiation [Ehrenstein, 2001]. When loaded, three different deformation types, which have to be superimposed, are distinguished for polymers:

- Instantaneous elastic deformation (reversible), due to instantaneous modification of the atomic distances and the distortion of the valence angles between fixed chemical bonds, see Figure 4.15 (a).

- Time-dependent viscoelastic deformation or relaxation (reversible), due to stretching of the molecular chains, see Figure 4.15 (b).

- Time-dependent viscous (viscoplastic) deformation (irreversible), due to movement (relocation) of the molecular chains, see Figure 4.15 (c).
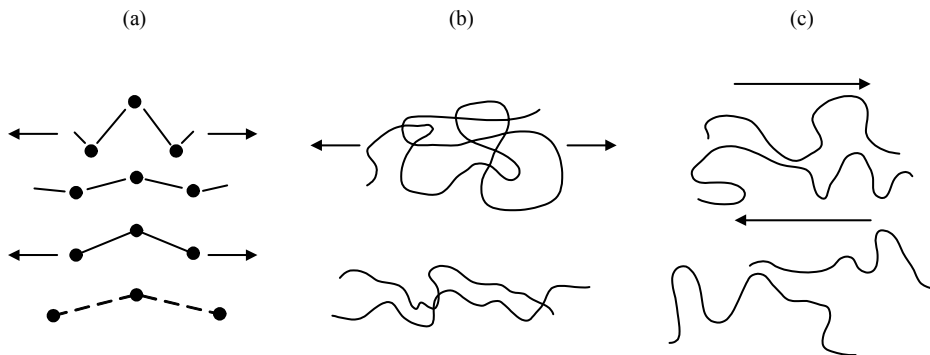
Figure 4.15: Schematic representation of elastic, viscoelastic and viscous deformation in polymers;
based on [Ehrenstein, 2001];
(a) elastic deformation, valence angle and distance distortions;
(b) viscoelastic/relaxation, chain elongation and orientation;
(c) viscous, displacement with relative relocation.

These deformations are strongly related to the material temperature as well as the rate and magnitude of the applied load. In this respect the glass transition temperature T_g is of specific influence on the performance. The glass transition (or: softening) temperature is the temperature of largest change of stiffness prior to melting. Below the glass transition temperature or for high loading rates polymers exhibit rigid and brittle behaviour. This rigid and brittle response is caused by the inability of the molecules to relocate fast enough. Reversely, polymers exhibit tough and ductile behaviour at temperatures above the glass transition temperature or for slow loading rates.

Furthermore, the network structure and the cross-linking degree influence the behaviour of the polymer. The behaviour of the heavily cross-linked and intertwined thermosets tends to be more brittle at ambient temperatures. And semi-crystalline thermoplastics are generally tougher than amorphous thermoplastics.

Humidity and water absorption can, especially for polyamides, influence the mechanical behaviour of polymers. Water absorption can cause a lowering of the glass transition temperature. This will influence the mechanical behaviour at ambient temperature and will affect the material stiffness, the yield stress, strain at failure and the toughness.

UV-radiation can cause a chemical degradation (accelerated oxidation) and embrittlement of polymers. To limit or prevent this 'aging' of the polymer, the internal compositional stability of the polymer can be enhanced by the addition of stabilizers. To limit the effect of UV-radiation, *light stabilizers* are added to the polymer.

For further reading on polymer materials is referred to [Ashby & Jones, 2006; Callister, 2000; Ehrenstein, 2001].

PART III

Experimental, analytical and numerical investigations

Part I

Introduction

Chapter 1

Introduction to
the research

Part II

Theoretical
framework

Chapter 2

Structural
glass beams

Chapter 3

The reinforced
glass beam
concept

Chapter 4

Materials
applied in this
research

Part III

Experimental,
analytical and
numerical
investigations

Chapter 5

Experimental
investigations
into the effects
of
bond type,
temperature,
thermal cycling,
humidity and
load duration
on the structural
response

Chapter 6

Experimental
investigations
into the effects
of
reinforcement
percentage
and beam size
on the structural
response

Chapter 7

Experimental
investigations
into the
structural
response of SG-
laminated glass
beams with
embedded glass
fibre
reinforcement

Chapter 8

Analytical and
numerical
modelling of
the structural
response

Part IV

Integrated
discussion of
the research
results

Chapter 9

Integrated
discussion on the
structural aspects of
reinforced glass
beams

Chapter 10

Integrated
discussion on the
production and
design aspects of
reinforced glass
beams

Part V

Retrospect
and
prospect

Chapter 11

Conclusions

Chapter 12

Recommendations

Chapter 5
Experimental investigations into
the effects of bond system, temperature,
thermal cycling, humidity and load duration
on the structural response

As introduced in Chapter 1, the current chapter investigates the effects of bond system, temperature, thermal cycling, humidity and load duration on the structural response of reinforced glass beams. The findings of this investigation are implemented in the integrated discussion of the research results, presented in Chapter 9 and Chapter 10.

Abstract

This chapter investigates the effects of the parameters *bond system*, *temperature*, *thermal cycling*, *humidity* and *load duration* on the structural response of reinforced glass beams. To do so, a series of pull-out tests – to investigate the shear strength of the bond between the glass and the reinforcement – and a series of bending tests – to investigate the structural response of reinforced glass beams – have been performed at different temperature levels, after thermal cycling, after humidity exposure and for long-duration loading. Both test series have been performed for specimens manufactured with either the acrylate adhesive DELO Photobond Glasbond 368 (GB) or the ionomer interlayer SentryGlas® (SG). The test results show that temperature, thermal cycling, humidity and load duration have a specific effect on the bond strength of both bond systems. Furthermore, the results show that they have a specific effect on the structural response of the GB-bonded and SG-laminated reinforced glass beams. However, these effects are less pronounced for the SG-laminated specimens than for the GB-bonded specimens. Especially the SG-laminated beams showed good results in terms of post-breakage strength and ductility at the post-breakage stage. It is therefore concluded that the performance of the SG-laminated reinforced glass beams is superior to the performance of the GB-bonded reinforced glass beams. However, it should be noted that for the SG-laminated specimens some delamination occurred, presumably as a result of humidity exposure. This should be investigated in more detail.

Background information

Material support and assistance

- Van Noordenne Groep,
  Hardinxveld Giessendam, The Netherlands

- DELO Industrial Adhesives,
  Windach, Germany

- Dupont de Nemours, Glass Laminating Solutions,
  Mechelen, Belgium.

Technical support and assistance

- Kees Baardolf,
  Building Technology Laboratory,
  Faculty of Architecture, TU Delft, The Netherlands

Test facilities

Pull-out and room temperature bending tests:

- Materials Laboratory,
  Faculty of Mechanical, Maritime and Materials Engineering,
  TU Delft, The Netherlands

Low temperature bending tests:

- Building Technology Laboratory,
  Faculty of Architecture, TU Delft, The Netherlands

- Stevin Laboratory,
  Faculty of Civil Engineering and Geosciences, TU Delft, The Netherlands

High temperature bending tests:

- Laboratory for Research on Structural Models,
  Department of Structural Engineering, Ghent University, Belgium

Research conducted in collaboration with

Room temperature bending tests:

- Freek Bos,
  Faculty of Architecture, TU Delft, The Netherlands

High temperature bending tests:

- Jan Belis, Dieter Callewaert,
  Laboratory for Research on Structural Models,
  Department of Structural Engineering, Ghent University, Belgium

5.1.   Introduction

This chapter investigates the effects of the parameters *bond system*, *temperature*, *thermal cycling*, *humidity* and *load duration* on the structural response of reinforced glass beams. This is done through two series of tests. Firstly, a series of pull-out tests – to investigate the pull-out strength of the reinforcement – has been performed at -20, +23, +60 and +80˚C, after thermal cycling, after humidity exposure and for long-duration loading. Secondly, a series of bending tests – to investigate the structural beam response – have been performed at -20, +23 and +60˚C, after thermal cycling, after humidity exposure and for long-duration loading. Both test series have been performed for specimens manufactured with either the acrylate adhesive DELO Photobond Glasbond 368 (GB), or the ionomer interlayer SentryGlas® (SG).

The investigated temperature range has been adopted from the ETAG 002 [EOTA, 1999] guideline, which describes adhesion tests such as shear and rupture tests for structural silicone sealants at -20, +23 and +80°C. However, because of practical limitations the high temperature bending tests could not be executed at +80°C and have therefore been performed at +60°C. Consequently, the pull-out test temperature range has been extended with a testing temperature of +60°C, to complete a full range of -20, +23, +60 and +80°C. For Nordic countries the ETAG guideline suggests a lower test temperature of -40°C. However, this temperature level was not possible for the current study because of practical limitations.

The thermal cycling procedure has been executed between -20 and +30°C. This temperature range has not been based on a standard or guideline, but was predominated by the ultimate temperature range of the applied thermal cycling machine. The specimens have been subjected to 150 cycles of 8 hours each.

The humidity exposure procedure has been based on standard EN 12543-4 [EN 12543-4, 1998], which describes test methods for the durability of laminated glass. The prescribed exposure time of 2 weeks at +50°C and 100% rH (condensation) has for the current study been extended to 4 weeks.

The long-duration tests have been executed on a custom-made load-controlled test rig. For the pull-out tests, loading times up to 4 weeks have been applied. For the bending tests, loading times up to 15 months have been applied.

The following sections 5.2, 5.3, 5.4 and 5.5 describe the specimens, the pre-conditioning methods and the test methods in more details. Subsequently, section 5.6, 5.7, 5.8 and 5.9 provide and discuss the test results. Finally, conclusions from this research are provided in section 5.10.

5.2.   Test specimens

Table 5.1 and 5.2 list the number of specimens that were made for the pull-out and bending test series. The geometry and materials used for the pull-out and beam specimens are described in the following sub-sections.

Table 5.1: Overview of the number of pull-out specimens per test series.

Test name	Pre-conditioning	Test temperature	Number of spec.	
			GB	SG
-20°C	5 days at -23°C	-20°C	3	3
+23°C	5 days at RT	RT	3	3
+60°C	5 days at +63°C	+60°C	3	3
+80°C	5 days at +83°C	+80°C	3	3
TC	150 cycles between -20 and +30°C.	RT	3	3
HE	4 weeks at 50°C, 100% rH	RT	3	3
LD	5 days at RT [a]	RT	n/a	3

HE = Humidity Exposure

LD = Long-Duration

RT = room temperature

TC = Thermal Cycling

Table 5.2: Overview of the number of beam specimens per test series.

Test name	Pre-conditioning	Test temperature	Number of spec.	
			GB	SG
-20°C	7 days at -30°C	-20°C	5	5
+23°C	7 days at RT	RT	5	5
+60°C	24 hours at +60°C	+60°C	5	5
TC	150 cycles between-20 and +30°C.	RT	3	3
HE	4 weeks at +50°C, 100% rH	RT	n/a	3
LD	7 days at RT	RT	n/a	3

HE = Humidity Exposure

LD = Long-Duration

RT = room temperature

TC = Thermal Cycling

5.2.1. *Materials*

The pull-out and beam specimens were made of annealed glass, metal inserts and either the GB adhesive or the SG interlayer as an intermediary bond.

For the glass ordinary annealed float glass was used, which was cut and ground by a commercial supplier. The material properties of the glass are described in Chapter 4.

For the metal inserts stainless steel AISI 304 was applied. It was applied as a hollow section with section dimensions of 10*10*1 mm. The material properties of the stainless steel are described in Chapter 4.

The GB adhesive was cured in a thickness of $t \approx 0.1$ mm. For the SG interlayer standard sheets with a thickness of $t = 1.52$ mm were applied.

The applied assembly and production processes are described in Chapter 10.

5.2.2.   *Pull-out specimens*

The GB-bonded and SG-laminated pull-out specimens consisted of small triple-layer glass sandwiches with a stainless steel insert, see Figure 5.1. The middle glass layer was split in two equal parts to provide a cavity for the centred stainless steel hollow section. The cavity was made approximately 2 mm wider on either side of the stainless steel hollow section, to avoid any contact between the metal insert and the middle glass layers. In other words, the stainless steel hollow section was been bonded to both outer glass layers.
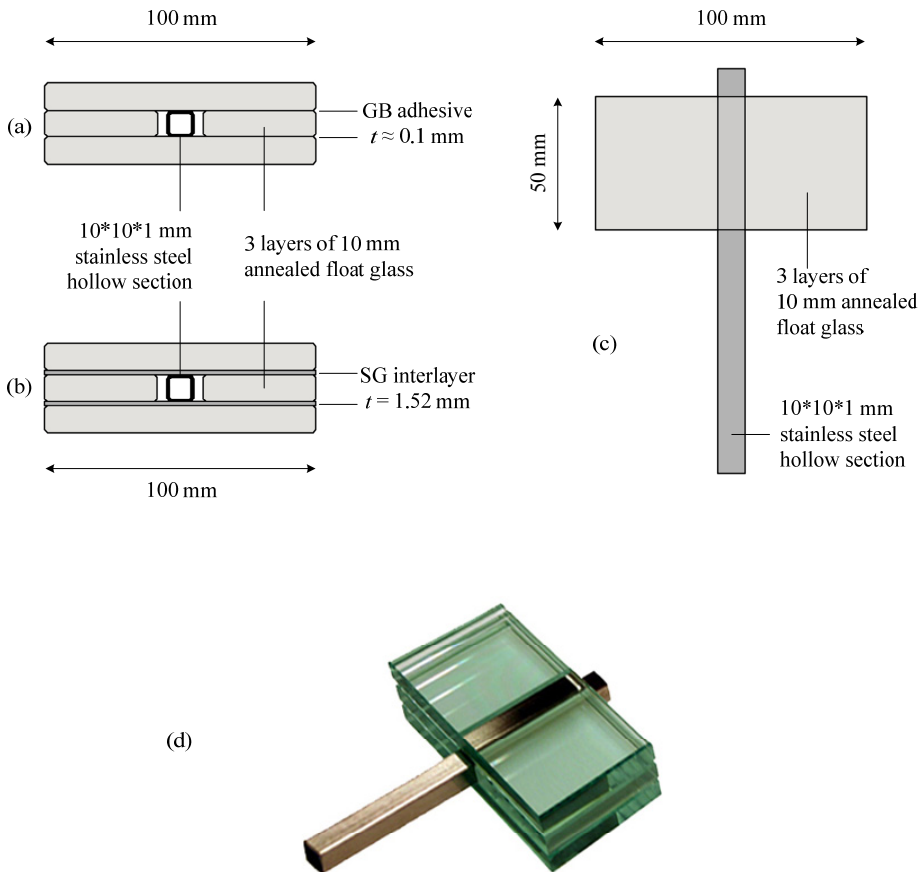
Figure 5.1: Pull-out specimens; (a) cross-section of the GB-bonded pull-out specimens; (b) cross-section of the SG-laminated specimens; (c) front view pull-out specimens; (d) photograph of assembled specimen.

5.2.3. *Beam specimens*

The GB-bonded and SG-laminated beam specimens consisted of triple-layer glass sandwiches with a stainless steel hollow reinforcement section bonded at the inner recessed edge, see Figure 5.2. The stainless steel reinforcement section had the same section dimensions as the metal insert that was applied in the pull-out specimens. In the beam specimens the stainless steel hollow section was bonded to the inner glass layer [i] and to both outer glass layers. This way, a 3-face bond was obtained.

| (a) | (b) |
| GB-bonded beam specimens | SG-laminated beam specimens |

annealed float glass:
6*125*1500 mm
6*125*1500 mm
10*115*1500 mm

GB adhesive
$t \approx 0.1$ mm

SG interlayer
$t = 1.52$ mm

stainless steel
hollow section
10*10*1 mm

125 mm
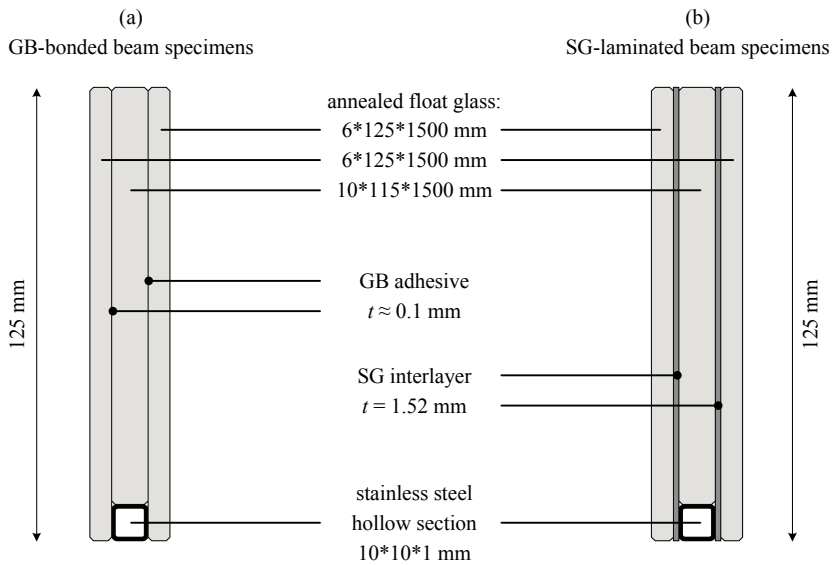
Figure 5.2: Cross section of the 1.5 m long reinforced glass beam specimens;
(a) GB-bonded beam specimens (b) SG-laminated beam specimens.

---

[i] For the GB-bonded beam specimens the bond between the reinforcement and the middle glass layer was realized by applying adhesive at this position. For the SG-laminated beam specimens no extra SG interlayer strip was applied between the reinforcement and the middle glass layer. However, due to the low viscosity of the SG during the lamination process, the SG interlayer had seeped between the reinforcement and the middle glass layer, thereby creating a bond at this position.

5.3.   Pre-conditioning

Prior to the tests, the pull-out and beam specimens were pre-conditioned in different manners. The following sub-sections describe these different pre-conditioning procedures.

5.3.1.   Temperature pre-conditioning

Prior to the -20, +60 and +80˚C pull-out tests, the pull-out specimens were conditioned for 5 days at either -23, +63 or +83°C (±1°C) in a refrigerator or oven respectively. The conditioning temperature was selected 3°C lower or higher than the test temperature to compensate for any heat gain or heat loss during the mounting of the test specimens in the test setup, which took about 2 minutes per specimen. Prior to the +23°C and the long-duration pull-out tests, the pull-out specimens were kept for 5 days at room temperature (RT) in the same room as the test setup.

Prior to the -20°C bending tests, the beam specimens were conditioned for 7 days in a refrigerator at -30°C (±3°C). The conditioning temperature was selected 10 degrees lower than the test temperature to compensate for any heat gain during transport and mounting of the specimen in the test setup, which took about 5 minutes per specimen. Prior to the +23˚C and long-duration bending tests, the beam specimens were kept for 7 days at room temperature (RT) in the same room as the test setup. Prior to the bending tests performed at +60˚C the beam specimens were stored for 24 to 36 hours at +60°C in a climate chamber. Since also the testing took place in this climate chamber no temperature difference occurred in transporting and mounting the specimens in the test setup.

5.3.2.   Thermal cycling procedure

The thermal cycling (TC) pull-out and beam specimens were exposed to 150 temperature cycles between -20 and +30°C in a thermal cycling cabinet, see Tables 5.1 and 5.2, before they were tested at room temperature (RT). To obtain the thermal cycling temperature range – which was measured by a thermo couple placed inside the stainless steel hollow sections of the specimens[i] – the targeted air temperature inside the cabinet was altered between -27.5 and +32.5°C every 4 hours, see the block diagram in Figure 5.3(b). During the thermal cycling procedure the targeted air temperature, the effective air temperature, the relative humidity and the thermo couple measurements were recorded, see Figure 5.3(b). After removing the specimens from the slab-tester they were kept for 24 hours at room temperature in the same room as the test setup, before they were tested at room temperature.

---

[i] It should be noted that the measured temperature, inside the metal inserts of the pull-out and beam specimens, was not used as a feed-back signal to the thermal cycling cabinet. The thermal cycling cabinet consistently cycled between -27.5 and +32.5 without being steered by the measured temperature inside the specimens.
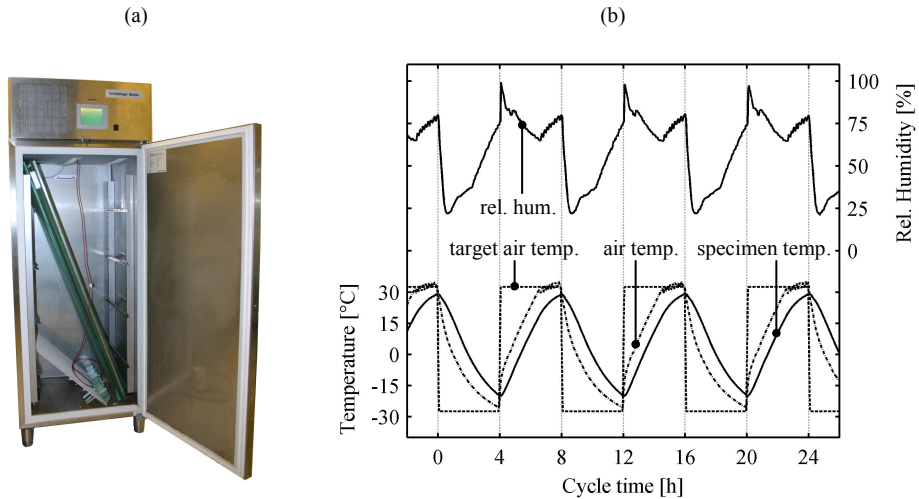
Figure 5.3: Thermal cycling procedure; (a) Specimens in thermal cycling cabinet. (b) Diagram of the applied 8 hour thermal cycle between -20 and +30; the diagram shows 3 complete cycles within 24 hours; The specimens were exposed to 150 cycles in total.

5.3.3.   *Humidity exposure procedure*

For the humidity exposure (HE) test series, the pull-out and beam specimens were exposed to humidity before they were tested at room temperature (RT). The applied humidity exposure procedure was largely based on standard EN 12543-4 [EN 12543-4, 1998], which describes test methods for the durability of laminated glass. Section 5.3.1 of this standard describes a 'humidity test with condensation' by suspending specimens over water in a closed container for 2 weeks while maintaining the temperature of the air in the container at +50˚C (+5˚C). The test mainly focuses on the occurrence of air inclusions[i], delamination and cloudiness[ii] within the laminate due to the humidity exposure.

---

[i] EN 12543-4 [EN 12543-4, 1998] uses the word 'bubbles'.
[ii] Cloudiness is sometimes also referred to as 'haze'.

For the current study some minor adjustments were made to the humidity exposure procedure described in EN 12543-4 [EN 12543-4, 1998]. The pull-out and beam specimens were suspended over water in a custom-made insulated and closed container, see Figure 5.4, for 4 instead of 2 weeks. Furthermore, the water, instead of the air, was kept at a constant temperature level of +55˚C. This resulted in an air temperature of +52˚C (±2˚C) and a relative humidity of 100% (condensation) within the container. After removing the specimens from the humidity exposure container they were kept for 24 hours (±4 hours) at room temperature in the same room as the test setup, before they were tested at room temperature.

(a)   (b)

beam specimens
on rack

water at 55°C

pull-out specimens
on rack

beam specimens   pull-out specimens
on rack   on rack

thermal
insulation

water temperature
control

water at 55°C
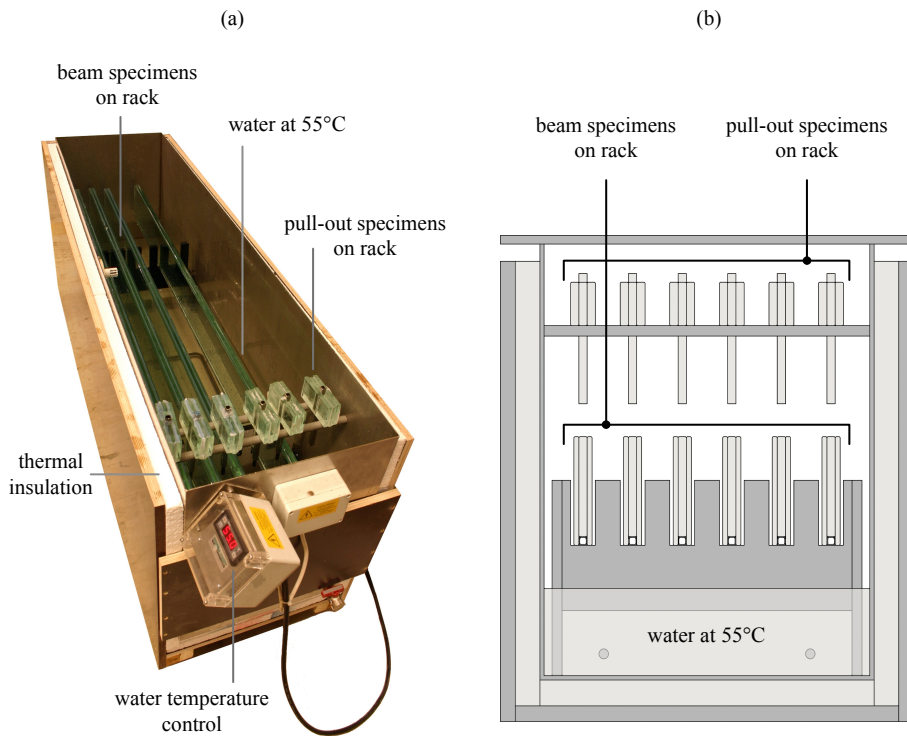
Figure 5.4: Custom-made humidity exposure setup; (a) Photograph of the humidity exposure container (without cover) with the pull-out specimens and beam specimens on a rack, suspended over heated water (+55°C); (b) Cross-section of the humidity exposure container.

5.4.   Pull-out test setups

The test setups of the pull-out tests are described in the following sub-sections.

5.4.1.   Pull-out test setup at room temperature

The room temperature (RT) pull-out tests – i.e. the +23˚C, thermal cycling (TC) and humidity exposure (HE) test series, see Table 5.1[i] – were performed on a standard Zwick Z100 testing machine. This machine was provided with a custom-made steel bracket to host the pull-out specimens, see Figure 5.5. The metal insertion of the pull-out specimens was clamped in the lower clamping wedges of the testing machine, as illustrated in Figure 5.5. Subsequently, the upper steel bracket containing the glass laminate was moved upwards at a constant displacement rate of 2 mm/minute. Consequently, the metal insert was pulled out of the glass laminate. During the tests the load and the displacement of the crosshead, see Figure 5.5, were measured at an interval of 0.01 seconds.
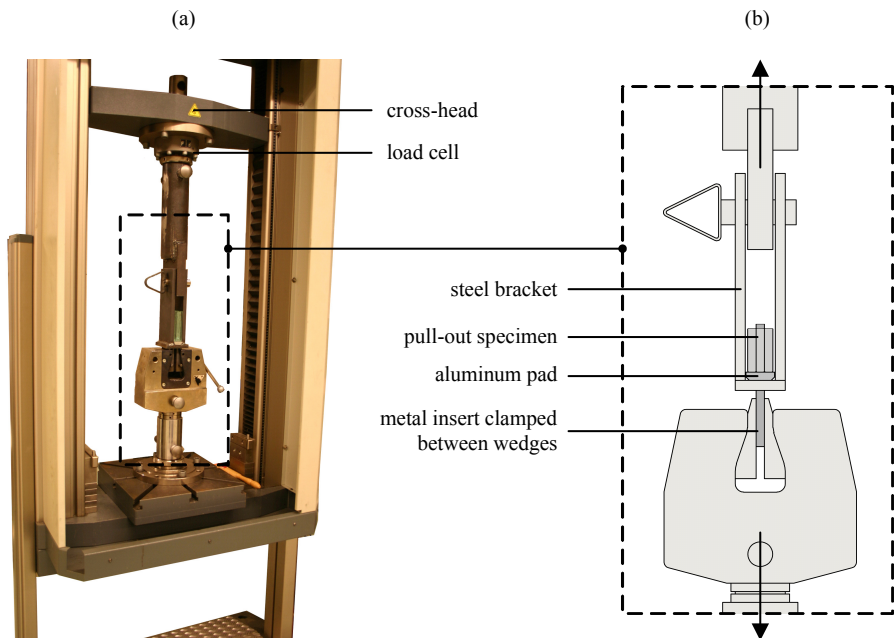
Figure 5.5: Pull-out test setup at room temperature; (a) Photograph of the pull-out test setup; (b) Schematic presentation of a close-up of the pull-out test setup, with a pull-out specimen that is mounted in the upper custom-made steel bracket and clamped in the lower clamping wedges.

---

[i] The long-duration loading pull-out tests were performed with a custom-made test rig, see section 5.4.3.

5.4.2.   Pull-out test setup at -20, +60 and +80°C

For the -20, +60 and +80°C pull-out tests a climate box was positioned around the test setup that is described in the previous section, see Figure 5.6. This climate box was either cooled with vaporized liquid nitrogen or heated with an electric heating element. A fan at the back side of the climate box generated an air flow throughout the climate box which ensured a relatively even temperature level throughout the climate chamber. During the tests the air temperature in the climate box was measured and automatically maintained at a temperature of -20, +60 and +80°C (±1°C) respectively. Similar to the room temperature pull-out tests the specimens were tested at a constant displacement rate of 2 mm/minute. Furthermore, again similar to the room temperature pull-out tests, the load and the displacement of the crosshead were measured at an interval of 0.01 seconds.

(a)   (b)

Figure 5.6: Pull-out test setup for the -20, +60 and+80°C test series; photographs of the test setup;
(a) The climate box was cooled to -20°C with vaporized liquid nitrogen (the door was closed during the test);
(b) The climate box was heated to +60 and +80°C with an electric heating element
(not visible on the photograph).

5.4.3.   Pull-out test setup for long-duration loading.

The long-duration (LD) pull-out tests were performed at a custom-made load-controlled test setup, see Figure 5.7(a), (b), and were conducted at room temperature (RT). Similar to the temperature tests the pull-out specimens were positioned in a steel bracket and the metal insert was fixed to the test setup by means of a threaded rod which had been welded to the metal insert prior to the lamination process. Within the test setup the steel bracket was connected to a cantilever. By manually adding weight to the counterpart of the cantilever the tensile load on the pull-out specimen was increased and consequently the metal insert was pulled out of the laminate.

Firstly, the pull-out specimens were loaded up to 20% of the predicted failure load, which had been estimated from the +23°C pull-out tests (21.8 kN, see Table 5.3 in section 5.6.1) and were left statically loaded. Subsequently, the load was increased by 20% of the predicted failure load every week, see Figure 5.7(c).

During the tests, the load on the pull-out specimens and the vertical displacement of the steel bracket relative to the fixed end of the metal insert were measured and recorded at a time interval of 100 seconds.
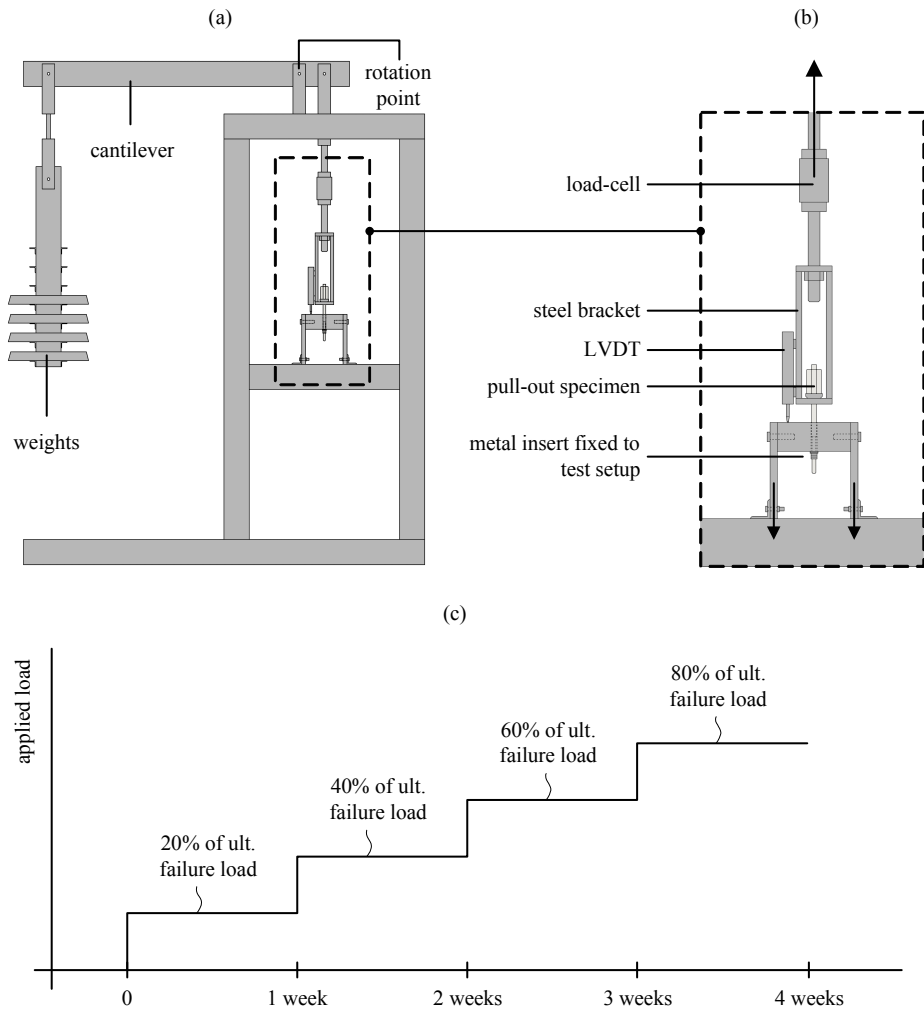
Figure 5.7: Long-duration pull-out test setup; (a) Schematic representation of the test rig; (b) Close-up of the test rig; (c) Loading scheme in time.

5.5.   Bending test setups

The test setups of the bending tests are described in the following sub-sections.

5.5.1.   *Bending test setup at room temperature*

The room temperature bending tests – i.e. the +23˚C, thermal cycling (TC) and humidity exposure (HE) test series, see Table 5.2[i] – were performed on a universal testing machine[ii] which was provided with a custom-made support frame. The support, load and lateral support span corresponded to the values depicted in Figure 5.8. The beams were loaded at a vertical displacement rate of 2 mm/minute. During the bending tests the inflicted load and the vertical displacement of the cross-head, see Figure 5.8, were measured at a time interval of 0.01 seconds.
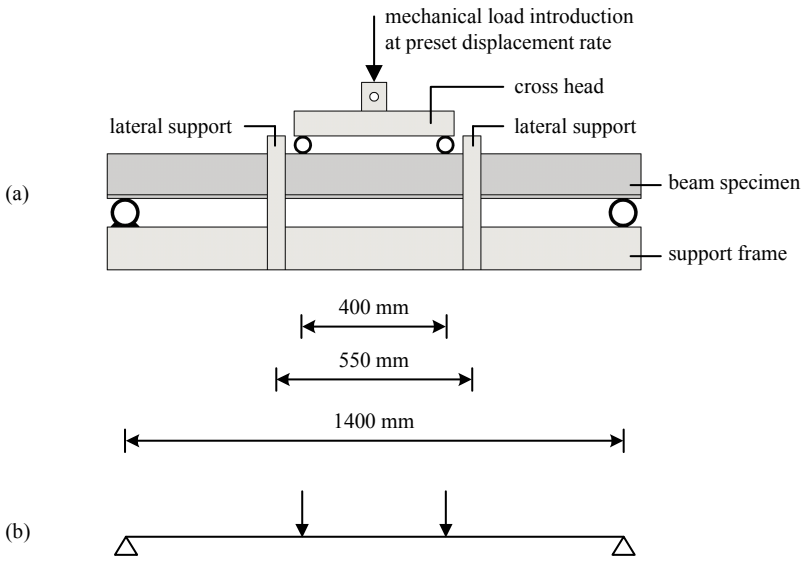
Figure 5.8: Custom-made support frame applied for the bending tests.

---

[i] The long-duration loading bending tests were performed with a custom-made test rig, see section 5.5.4.

[ii] For the +23°C bending tests a Zwick Z100 mechanical test machine was used. For the TC and HE bending tests an Instron mechanical test machine was used.

5.5.2.   Bending test setup at -20°C

For the -20°C bending tests, see Table 5.2, a climate box was positioned around the beams, see Figure 5.9. This climate box was cooled with vaporized liquid nitrogen. The temperature inside the box was measured and targeted at -20°C (±5°C) by manually opening and closing the valve of the liquid nitrogen inlet. Furthermore, the support frame, the load rate, the measurements and the measurement time interval was identical to the room temperature tests.
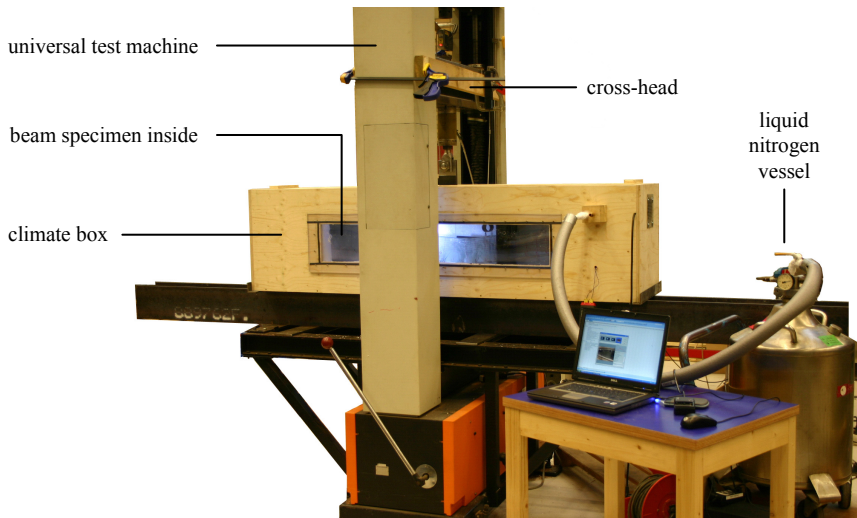
Figure 5.9: Bending test setup at -20°C. A wooden climate box was put around the beam.
The climate box was cooled with vaporized liquid nitrogen to -20°C.

5.5.3.   Bending test setup at +60°C

The +60°C bending tests, see Table 5.2, were performed in a large-scale climate chamber, see Figure 5.10. In the test setup the load was applied manually using a hydraulic jack. Similar to the room temperature bending tests, the applied load and the vertical displacement of the beams at mid-span were measured at a time interval of 0.01 seconds.

Figure 5.10: Bending test setup at +60°C, within a climate chamber.
(a) outside view (photograph: Dieter Callewaert); (b) inside view of the climate chamber with the test setup.

5.5.4.   *Bending test setup for long-duration loading*

The long-duration (LD) bending tests were performed at room temperature (RT) in a load-controlled bending test setup, which was similar to the one applied for the long-duration pull-out tests. The beam specimen was positioned up-side-down in the test setup and loaded by means of a cantilever mechanism, see Figure 5.11. The load was manually increased by adding weight at the counterpart of the cantilever. Firstly, the specimen was loaded until initial glass fracture occurs. Subsequently, the specimens were kept statically loaded at this loading level for 4 weeks. Afterwards the load was increased to 60 and 80% of the predicted ultimate failure load, which has been estimated from the (short-term) +23°C bending tests (17.5 kN, see Table 5.4 in section 5.7.1), with an intermediate waiting time of 4 weeks. After 20 weeks, calculated from the start of the test, the specimen were unloaded and reloaded again after 24 hours to 80% of the predicted ultimate failure load. During the tests the load and the vertical displacement of the beam specimens at mid-span were measured and recorded at a time interval of 100 seconds. Furthermore, the specimens were frequently visually inspected for crack initiation and crack propagation.

(a)

(b)
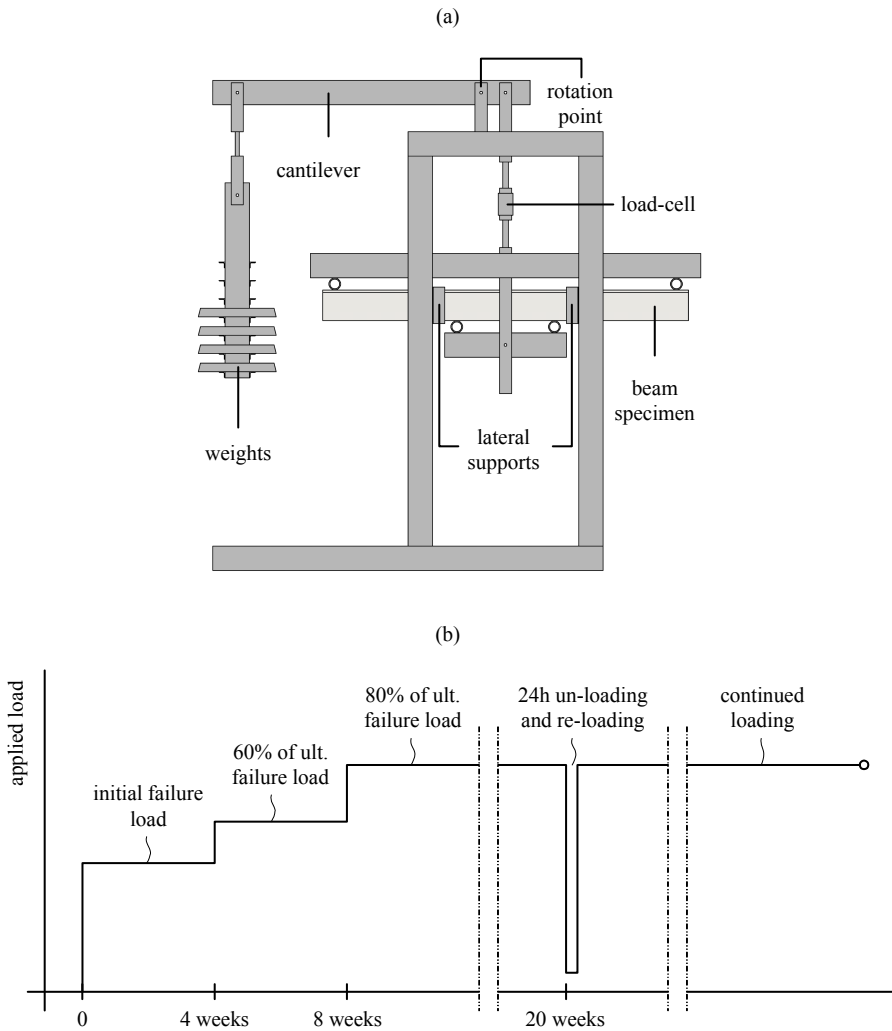
Figure 5.11: Long-duration loading bending test setup; (a) Schematic representation of the custom-made test rig, with the weights at the counterpart of cantilever loading mechanism; (b) Loading scheme in time.

5.6.   Pull-out test results

The results of the pull-out tests are presented in the following sub-sections[i].

5.6.1.   *Pull-out test results at -20, +23, +60, +80˚C, after TC and after HE.*

The numerical results of the -20, +23, +60 and +80°C pull-out tests are presented in Table 5.3. Additionally, Figure 5.12 shows the load-displacement diagrams of the pull-out tests.

The pull-out specimens demonstrated an increasing loading capacity until bond failure occurred. This caused either a sudden or more gradual drop in load. For some specimens a limited residual pull-out resistance remained, see Figure 5.12.

Table 5.3: Experimental results of the pull-out tests performed at -20, +23 and +60°C, after thermal cycling (TC) and after humidity exposure (HE)..

Test name		GB-bonded pull-out test results						SG-laminated pull-out test results					
		-20 °C	+23 °C	+60 °C	+80 °C	TC[a]	HE[b]	-20 °C	+23 °C	+60 °C	+80 °C	TC[a]	HE[b]
Maximum load													
mean [c]	[kN]	10.5	16.7	4.7	2.6	7.1	6.4	24.2	21.8	11.1	3.2	6.2	12.1
st.dev.	[kN]	1.0	0.2	0.2	0.1	4.9	0.3	4.3	1.2	0.9	0.2	0.3	1.8
rel.st.dev.	[%]	9.3	1.1	3.3	3.4	68.9[d]	5.1	17.8	5.3	8.1	4.9	5.1	15.2

[a]   TC = Thermal Cycling;

[b]   HE = Humidity Exposure

[c]   The mean results are displayed in the table; the full results are given in Appendix I.

[d]   The dispersion in the results is extremely large for this series.
Care should therefore be taken in interpreting these results.

---

[i] For the full results is referred to Appendix I.

GB-bonded pull-out specimens   SG-laminated pull-out specimens
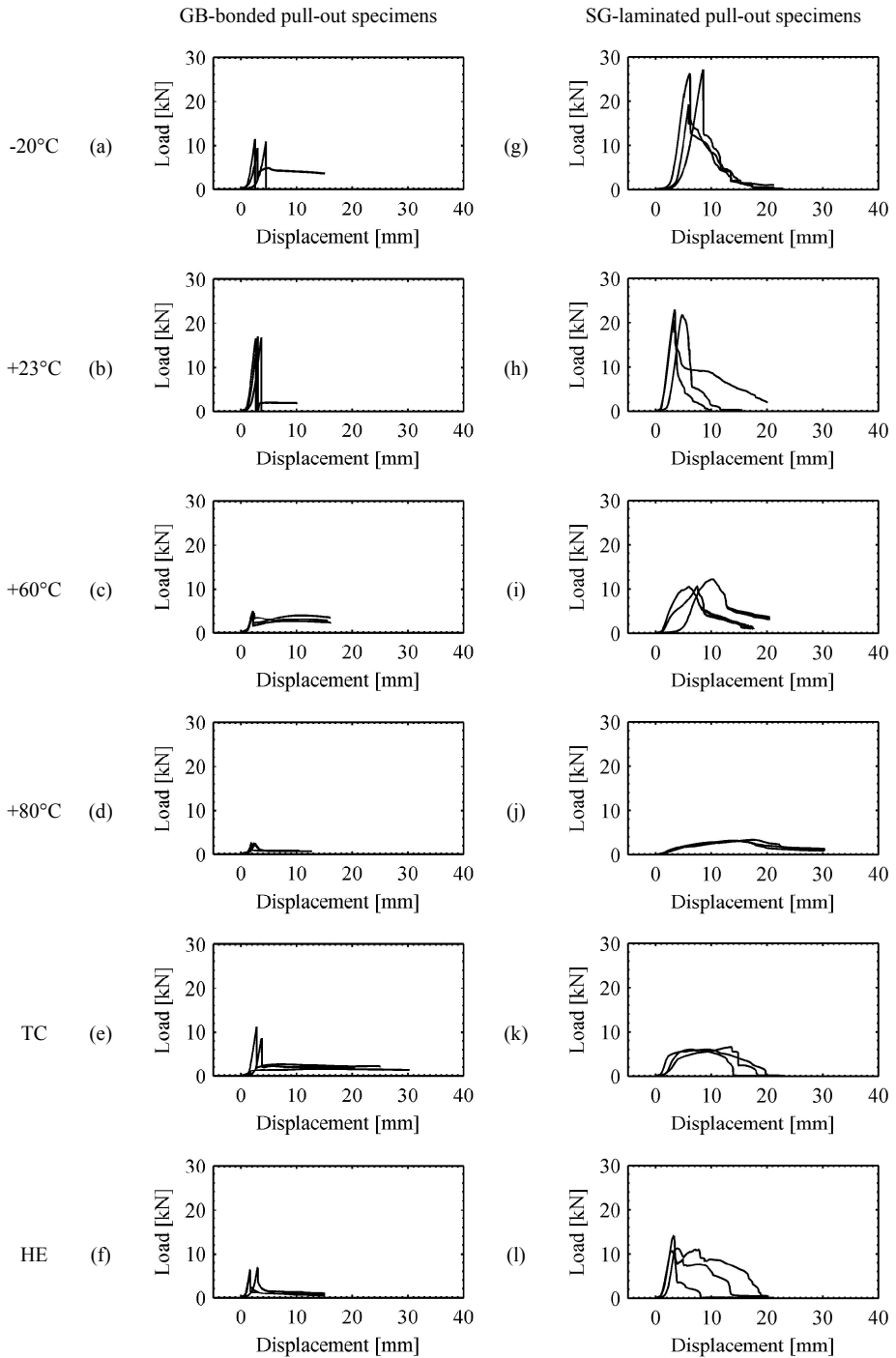
Figure 5.12: Load-displacement diagrams of the pull-out tests; TC = thermal cycling HE = hum. exposure.

5.6.2.   Pull-out test results for long-duration loading.

Figure 5.13 displays a plot of the applied load and the measured displacement versus the elapsed time of an exemplary long-duration loaded SG-laminated pull-out specimen. The load has been increased by 20% every week, until failure of the bond occurred. The results of all the long-duration loaded pull-out specimens are presented in Appendix I.
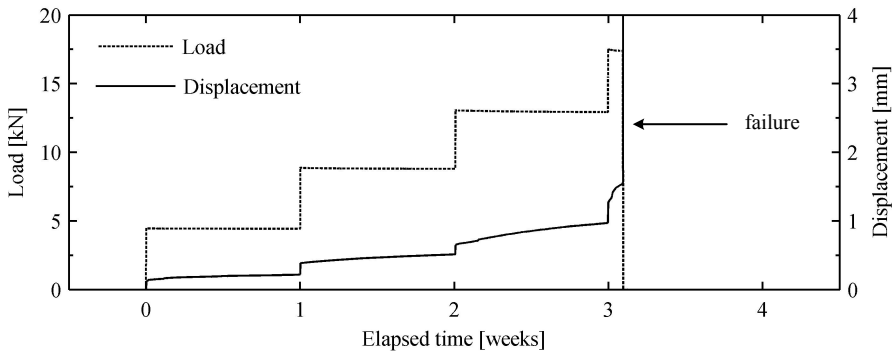
Figure 5.13: Load and displacement plotted versus time, for an exemplary long-duration loaded SG-laminated pull-out specimen. An overview of all experiment results is provided in Appendix I

5.7.   Bending test results

The results of the bending tests are described in the following sub-sections.[i]

5.7.1.   Bending test results at -20, +23, +60˚C, after TC and after HE.

The results of the bending tests are presented in Table 5.4. Additionally Figures 5.14 and 5.15 show the load-displacement diagrams and a sequential set of diagrams demonstrating the crack pattern development numbered 1 to 3 which corresponds to the numbers indicated in the load-displacement diagrams.

The beam specimens typically showed linear elastic response until initial glass failure occurred which caused a drop in load. As loading was continued, the load generally increased again and additional cracks occurred in the glass repetitively causing a drop in load. The bending stiffness gradually decreased and the beams started to show more ductile response. Most GB-bonded beams finally failed due to adhesive failure, which caused slip of reinforcement. Since the tensile force could not be transferred anymore the beams collapsed. For the SG-laminated beams this full debonding of reinforcement did not occur. None of the SG-laminated beams failed within the deformation limit of the test rig, thus their tests had to be stopped prematurely.

---

[i] For the full results and exemplary photo sequences of the bending tests is referred to Appendix I.

Table 5.4: Experimental results of the bending tests performed at -20, +23 and +60°C,
after thermal cycling (TC) and after humidity exposure (HE).

Test name		Bending test on GB-bonded beams					Bending tests on SG-laminated beams				
		-20 °C	+23 °C	+60 °C	TC[a]	HE[b]	-20 °C	+23 °C	+60 °C	TC[a]	HE[b]
Number of spec.		5	5	5	3	0	5	5	5	3	3
Maximum load											
mean[c]	[kN]	13.4	10.3	9.7	10.7	n/a	16.1	11.7	9.1	10.1	13.0
st.dev	[kN]	1.3	0.9	0.8	0.1	n/a	1.8	1.1	1.3	1.7	1.8
rel.st.dev.	[%]	9.9	8.4	8.3	1.3	n/a	11.2	9.5	14.4	16.5	13.7
Post-breakage load											
mean[c]	[kN]	9.7	13.8	9.5	12.7	n/a	15.4	17.5	14.3	16.5	16.7
st.dev.	[kN]	1.2	0.6	0.3	4.0	n/a	0.9	0.5	0.5	0.5	1.0
rel.st.dev.	[%]	12.0	4.1	3.6	31.6	n/a	5.6	2.8	3.7	3.2	6.1
Post-/ini.- fail. load											
mean[c]	[%]	73.1	135.7	98.4	118.8	n/a	96.4	150	159.1	166.6	129.5
st.dev.	[%]	12.6	14.5	7.6	37.2	n/a	7.7	12.0	22.7	21.0	9.2
rel.st.dev.	[%]	17.3	10.7	7.7	31.4	n/a	7.9	7.7	14.2	12.6	7.1

[a]   TC = Thermal Cycling;

[b]   HE = Humidity Exposure

[c]   The mean results are displayed in the table; the full results are given in Appendix I.
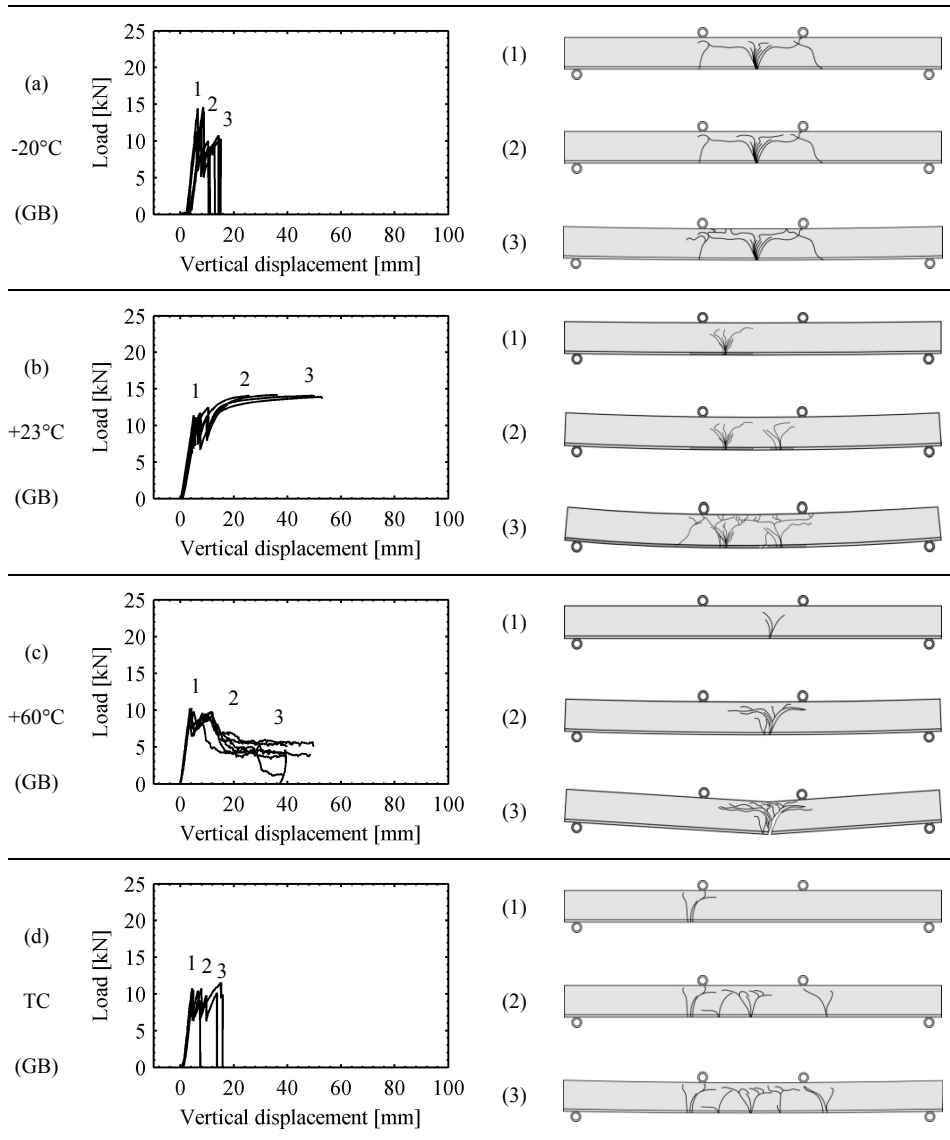
Figure 5.14: Bending test results of the GB-bonded beams; TC = thermal cycling.
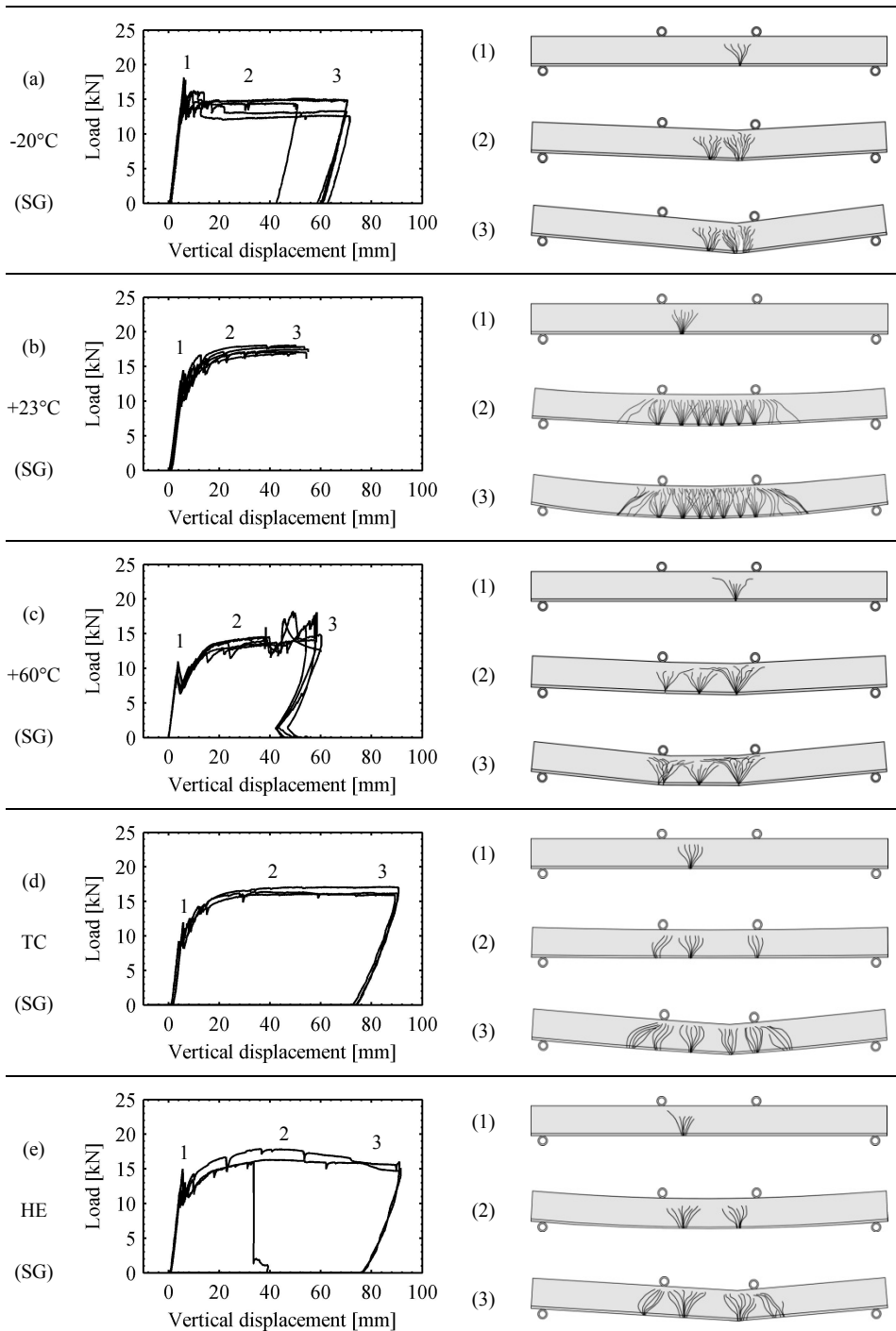
Figure 5.15: Bending test results of the SG-laminated beams; TC = thermal cycl.; HE = humidity exposure.

5.7.2.   *Bending test results for long-duration loading.*

Figure 5.16 shows a plot of the applied load and the measured displacement versus the elapsed time of an exemplary long-duration loaded SG-laminated reinforced glass beam specimen. After 20 weeks of loading the specimen has been unloaded and kept unloaded for 24 hours before being reloaded again. The results of all the long-duration loaded beam specimens are presented in Appendix I.
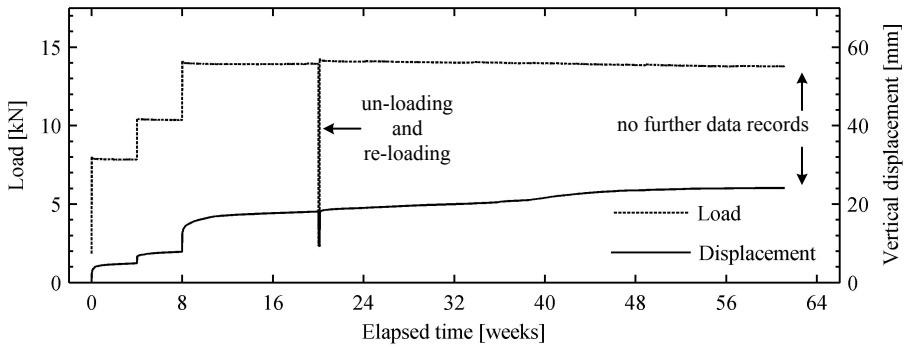
Figure 5.16: Load and displacement plotted versus time, for an exemplary long-duration loaded SG-laminated reinforced glass beam; An overview of all experiment results is provided in Appendix I.

5.8.   Discussion pull-out tests

The results of the pull-out tests clearly demonstrate a temperature, thermal cycling, humidity and load duration effect on the bond strength of both the GB adhesive and the SG interlayer, see Figure 5.17. The following sub-sections discuss these effects. Furthermore, a performance comparison of the GB adhesive and SG interlayer bond is provided.

(a)   (b)

pull-out test results for GB-bonded specimens   pull-out test results for SG-laminated specimens
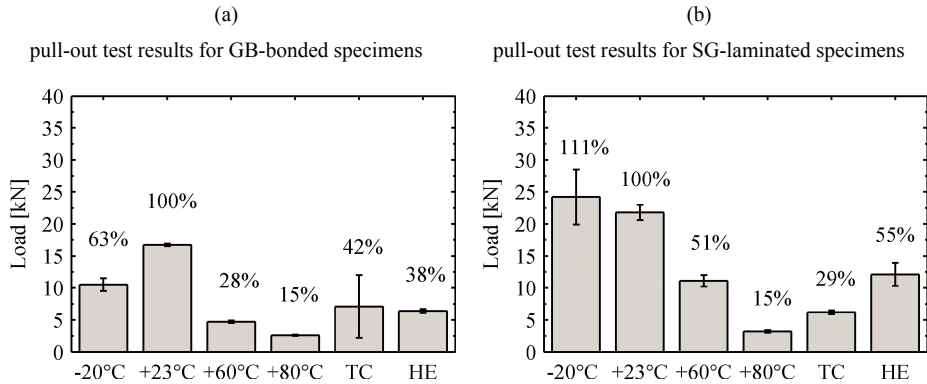
Figure 5.17: Bar graph of the pull-out test results. The mean load value at +23°C is the reference (100%) for each series. It should be noted that the number of specimens per test series is rather small. Furthermore, it should be noted that the thermal cycling (TC) results of the GB-bonded specimens and the -20°C results of the SG-laminated specimens show a large variation. Care should thus be taken in interpreting these results.

5.8.1.   Temperature effects on the bond strength

From the -20, +23, +60 and +80°C pull-out test it is observed that temperature has a significant effect on the bond strength of the GB adhesive and the SG interlayer, see Figure 5.12 and Figure 5.17. At increased test temperatures the bond strength and stiffness of both the GB adhesive and the SG interlayer drops compared to room temperature. At low temperature the bond strength of the GB adhesive drops, whereas it increases for the SG interlayer.

At +60 and +80°C the GB-bonded pull-out specimens demonstrate reduced bond strength and stiffness compared to +23°C, see Figure 5.17(a). This reduction in bond strength and stiffness is the result of a reduced shear stiffness of the adhesive bond at increased temperatures. However, based on the relatively high glass transition temperature of +102°C, as stated by the manufacturer's datasheet, see Chapter 4, one would not expect to encounter such an extreme temperature dependency within the tested temperature range. It should therefore be noted that caution should be taken at interpreting these values of the glass transition temperature as provided by the manufacturer.

Also at -20°C the GB-bonded pull-out specimens demonstrate reduced bond strength compared to +23°C, see Figure 5.17(a). This reduction in bond strength seems not in line with an increased shear stiffness at low temperatures, see Chapter 4. However, it might be that increased shear stiffness at low temperatures, as a result of increased rigidity of the intertwined polymer chain network, combined with the relative small bond thickness ($t \approx 0.1$ mm) results in an extremely rigid bond which is highly susceptible for peak stresses that occur at the perimeter of the bond. Combined with a decreased toughness of the adhesive bond at low temperatures, this leads to bond failure at lower loading levels than has been reached at room temperature.

At +60 and +80°C also the SG-laminated pull-out specimens demonstrate, similar to the GB-bonded pull-out specimens, decreased bond strength and stiffness compared to +23°C, see Figure 5.17(b). This reduction in bond strength and stiffness is in line with a significant reduction in shear stiffness of the SG interlayer at and above its glass transition temperature of ~ +55°C, see Chapter 4.

At -20°C the SG-laminated pull-out specimens demonstrate, contrary to the GB-bonded pull-out specimens, increased bond strength compared to +23°C, see Figure 5.17(b). This increase in bond strength is in line with increased polymer stiffness at lower temperature levels, which seems to effectively increase the shear transfer capacity of the SG interlayer. However, it should be noted that the scatter in the result of the -20°C specimens is relatively large, which urges for caution in interpreting these results. Although a similar increase in bond strength of the SG interlayer at -20°C has been observed for embedded glass fiber rods, see Chapter 7, it is recommended to extend the test series to confirm the tendency of increasing bond strength at lower temperatures.

The different test temperature levels had also a significant effect on the failure mode of the specimens, see Figure 5.19. Whereas the -20 and +23°C specimens show some distinct cracking of the glass, this cracking is fully absent for the +60 and +80°C specimens. The glass breakage at -20 and +23°C is most probably caused by the relatively high shear stiffness and consequent very good load transfer to the glass of both the GB adhesive and SG interlayer at these temperature levels. At +60 and +80°C the shear stiffness of both the GB adhesive and SG interlayer has significantly decreased, which allowed for a friction-slip displacement of the metal insert, without significantly stressing the glass. It is assumed that this friction is generated by an interlocking effect of failed bond remainders.

5.8.2.   *Thermal cycling effects on the bond strength*

From the pull-out tests performed after thermal cycling it is observed that thermal cycling significantly reduces the bond strength of both the GB adhesive and the SG interlayer, see Figure 5.12 and Figure 5.17. Due to the differences in thermal expansion of the glass and the metal insert, the bond is (repetitively) strained during the thermal cycling process. It is assumed that this (repetitive) straining causes damage in the bond which results in a reduction in bond strength.

Furthermore, whereas the GB-bonded pull-out specimens showed no visible damage[i] after the thermal cycling procedure, some SG-laminated pull-out specimens 'spontaneously' delaminated during the thermal cycling procedure, see Figure 5.18. However, this delamination might not only be the result of the repetitive temperature change, but also of the repetitive high air humidity and possible water condensation[ii] on the specimens during the thermal cycling procedure, see Figure 5.3. As will be discussed in section 5.8.3 this high humidity will also affect the bond strength and might cause delamination of the SG interlayer.
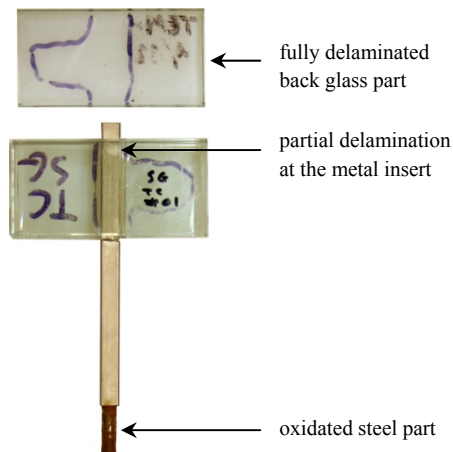
Figure 5.18: Partially delaminated SG-laminated pull-out specimen after the thermal cycling process. The delamination might be the result of thermal cycling combined with high humidity exposure.

5.8.3.   *Humidity effects on the bond strength*

From the pull-out test performed after humidity exposure it is observed that humidity causes a significant reduction in bond strength of both the GB adhesive and the SG interlayer, see Figure 5.12 and Figure 5.17. It is assumed that water molecules penetrate

---

[i] The GB-bonded specimens showed visible damage neither in the glass, nor in the bond.
[ii] Water condensation on the specimens might occur when the air temperature inside the thermal cycling cabinet is rising again, while the specimens are still at a low temperature level due to their thermal mass.

between the substrates and locally break the physical bond between the substrates. After the humidity exposure procedure both the GB-bonded and SG-laminated pull-out specimens demonstrated some white discoloration or 'haze' at the perimeter of the bond line. Furthermore, the SG-laminated specimens showed some local delamination of the glass-to-glass bond. Although no significant delamination or debonding had been observed at the metal insert, the pull-out tests revealed a significant reduction in bond strength.

5.8.4.   Load duration effects on the bond strength

The long-duration loaded pull-out specimens demonstrated creep of the SG interlayer. While the load remained constant, the slip of the metal insert, gradually increased, see Figure 5.13. At higher loading levels a more rapid increase in slip of reinforcement was observed. Moreover, the slip of the metal insert was even further stimulated by partial glass fracture within the specimens. In the end, the maximum loading level amounted to only about 80% of the mean loading level of the SG-laminated pull-out specimens tested at +23°C (21.8 kN, see Table 5.3). The observed creep of the SG interlayer is in line with the visco-elastic properties of this polymer interlayer material, which causes a temperature and load duration dependency of the material, see Chapter 4.

5.8.5.   Performance comparison of GB-bonded and SG-laminated specimens

Overall, the performance of the SG-laminated pull-out specimens was better than the performance of the GB-bonded pull-out specimens[i]. Except for the thermal cycling test series, the SG-laminated pull-out specimens reached higher loading levels than the GB-bonded pull-out specimens. However, it should be noted that for the thermal cycling test series the scatter in the results of the GB-bonded specimens was large, whereas it was highly consistent for the SG-laminated specimens, see Figure 5.17.

Besides the difference in strength performance, the GB-bonded and SG-laminated pull-out specimens demonstrate some differences in failure mode, see Figure 5.19. Firstly, at +23°C the SG-laminated specimens show more extensive glass fracture than the GB-bonded specimens; compare Figure 5.19 (b) and (i). This difference in fracture behaviour is probably caused by higher shear stiffness of the SG interlayer and consequently better load transfer to the glass. Secondly, at -20°C the GB-bonded pull-out specimens demonstrate complete disintegration, whereas this has not been observed for the SG-laminated specimens; compare Figure 5.19 (a) and (h). For the SG-laminated specimens complete disintegration is prevented by the relatively tough foil SG interlayer material, which keeps all glass fragments together. For the GB-bonded specimens this mechanism is absent.

---

[i] It should be noted that the observed performance level of the bond systems only refers to the specific application studied in this research (i.e. reinforced glass beams). The observed performance levels should not be interpreted for applications outside the scope of the current research.

GB-bonded pull-out specimens   SG-laminated pull-out specimens

-20°C	(a)		(h)
+23°C	(b)		(i)
+60°C	(c)		(j)
+80°C	(d)		(k)
TC	(e)		(l)
HE	(f)		(m)
LD	(g)	n /a	(n)
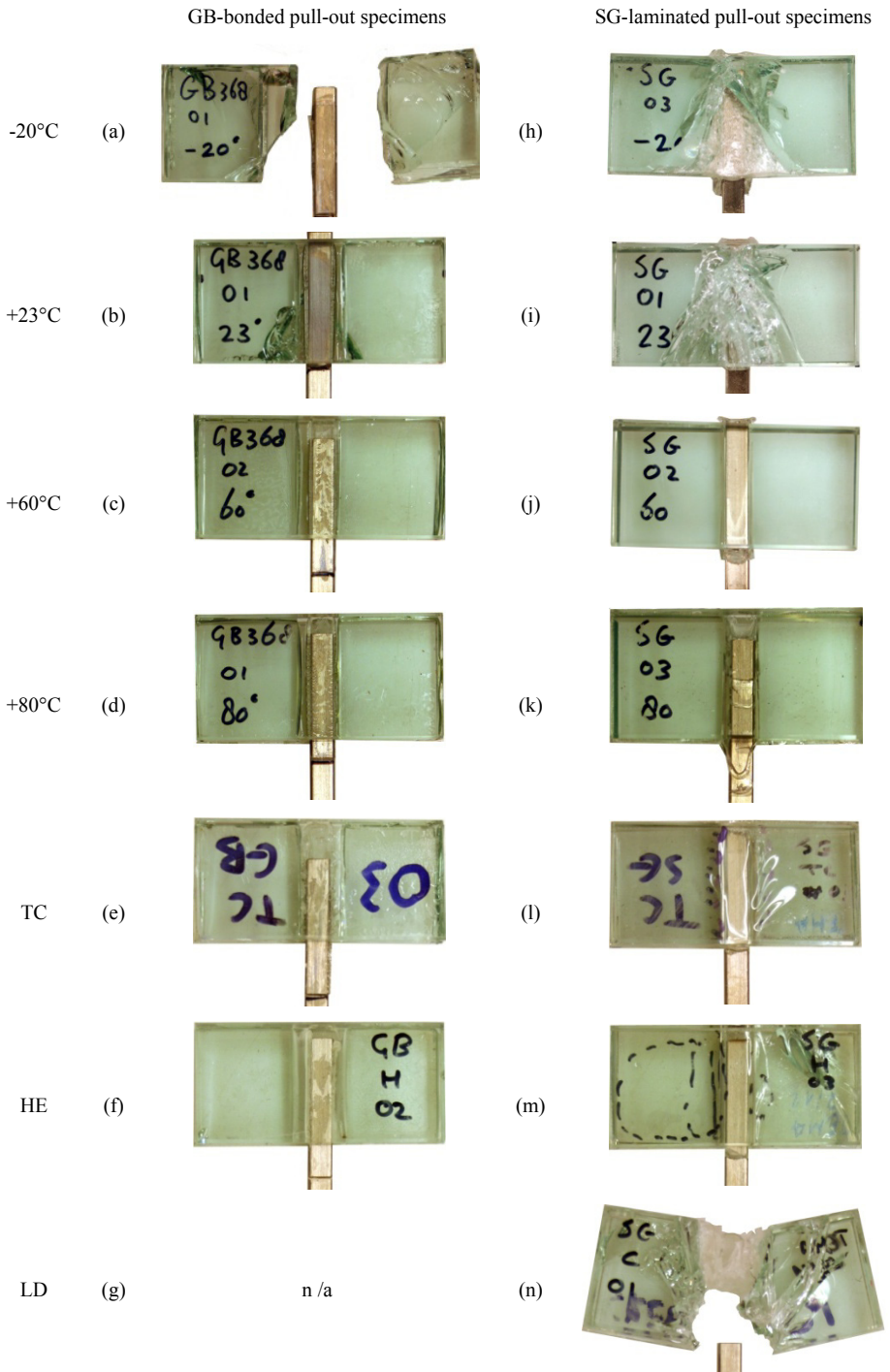
Figure 5.19: Overview of typical failed test specimens per pull-out test series.

5.9.   Discussion bending tests

Similar to the pull-out tests, the bending tests demonstrated a temperature, thermal cycling, humidity and load duration effect on the structural response of the beams, see Figure 5.20. The following sub-sections discuss these effects. Furthermore, a performance comparison of the GB-bonded and SG-laminated reinforced glass beams is provided.
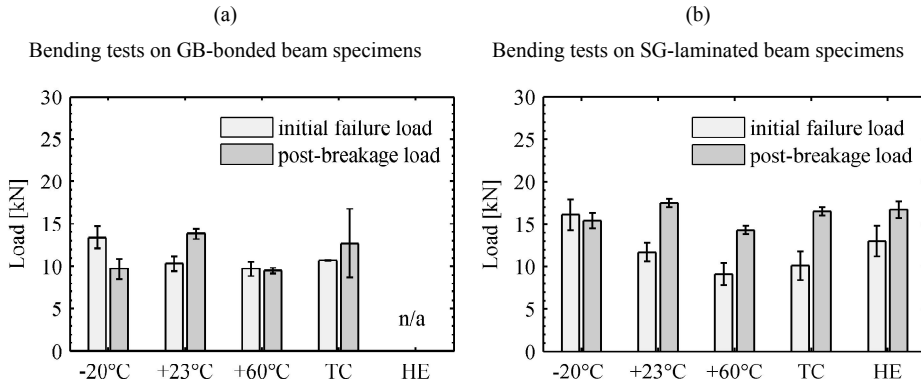
Figure 5.20: Bar graph of the bending test results;
(a) results of the GB-bonded beams; (b) results of the SG-laminated beams.

5.9.1.   Temperature effects on the beam response

At room temperature both the GB-bonded and SG-laminated beams demonstrated their highest post-breakage load, see Table 5.4 and Figures 5.14, 5.15 and 5.20. At this temperature level the bond strength of both the GB and SG is sufficient to effectively activate the reinforcement. Due to plastic deformation of the reinforcement a highly ductile post-breakage beam response is obtained, see Figure 5.14 (b) and 5.15 (b). However, the GB-bonded beams ultimately collapsed due to progressive adhesive failure which caused the reinforcement to detach. As the tensile forces could not be transferred anymore the beams collapsed. For the SG-laminated beams this mechanism did not occur and their reinforcement maintained largely attached to the glass. Their tests had to be stopped upon reaching the ultimate deformation capacity of the test setup.

At -20˚C the GB-bonded beams demonstrated significantly worse post-breakage performance than at +23˚C, see Figure 5.14 and Figure 5.20. Due to reduced bond strength of the GB adhesive at -20˚C – as has been determined by the pull-out tests – and decreased fracture toughness of the GB adhesive, the GB-bonded beams demonstrated excessive debonding of reinforcement upon initial glass failure. This local debonding of reinforcement, which occurred along several centimetres on either side of

the crack origin in the glass, has also been observed at +23˚C, though to a much smaller extent. The excessive debonding of reinforcement at -20˚C limited the reinforcement in arresting cracks in the glass. This resulted in extensive cracking of the glass upon initial failure and larger crack opening displacements, which severely weakened the beams and limited their post-breakage strength. Furthermore, due to reduced adhesive bond strength at -20°C, complete debonding of reinforcement occurred much earlier in the post-breakage stage than at +23°C; compare Figure 5.14 (a) and (b). This caused the beams to collapse at significantly lower loading levels than were observed at +23°C.

Also at +60˚C the GB-bonded beams demonstrated significantly worse post-breakage performance than at +23˚C, see Figure 5.14 and Figure 5.20. Due to reduced bond strength of the GB adhesive at +60˚C – as has been determined by the pull-out tests – more excessive debonding of reinforcement occurred. This caused a reduced post-breakage strength and a premature ultimate failure of the GB-bonded beams. However, unlike the abrupt collapse of the GB-bonded beams tested at -20 and +23˚C, see Figure 5.14, the GB-bonded beams tested at +60˚C demonstrated a gradual reduction in load carrying capacity until a lower threshold in the residual load carrying capacity was reached, see Figure 5.14 (c). This relatively small residual load carrying capacity resulted from a residual friction-grip between glass and reinforcement generated by failed adhesive remainders, as has also been observed at the pull-out tests, see Figure 5.12 (c).

At -20˚C, the SG-laminated beams demonstrated, similar to the GB-bonded beams, reduced post-breakage performance compared to +23˚C, see Figure 5.15 and Figure 5.20. At -20˚C the SG-laminated beams showed some local debonding of reinforcement upon initial glass failure, whereas this occurred only to a very small extent at +23˚C. Since the bond strength of the SG interlayer at -20˚C should not be less than at +23˚C, as has been determined by the pull-out tests, this increased debonding probably originates from decreased fracture toughness of the SG interlayer at -20˚C. This assumption is supported by the results of Bucak and Meissner [Bucak & Meissner, 2005] who observed a similar effect of debonding between glass and polymer at low temperature for a prior generation of the SG interlayer. Due to the local debonding in the SG-laminated beams the reinforcement could arrest the cracks in the glass less effectively. The cracks could open up further, which resulted in concentrated crack growth. Due to this concentrated crack growth a plastic hinge occurred in the SG-laminated beams, which caused the beams to be divided into two hinged parts, see Figure 5.15 (a)(3). Subsequently, the SG ruptured due to decreased flexibility of the SG at -20°C, see Figure 5.21(e). Due to the high bond strength of the SG at -20°C though, as has been observed in the pull-out tests, the reinforcement remained largely attached to the glass, which enabled the beams to generate a highly ductile post-breakage response by plastic deformation of the reinforcement.

Also at +60°C, the SG-laminated beams demonstrated, similar to the GB-bonded beams, reduced post-breakage performance compared to +23°C, see Figure 5.15 and Figure 5.20. Due to reduced bond strength of the SG at +60°C – as has been observed in the pull-out tests – more excessive bond failure and consequently more debonding of reinforcement occurred at the post-breakage stage. Similar to the tests at -20°C, this caused the cracks to open up further, which resulted in concentrated crack growth. Multiple plastic hinges occurred in the beams causing the beams the open up in three parts, see Figure 5.15(c)(3). Despite progressive bond failure, the reinforcement remained largely attached to the glass, which enabled the SG-laminated beams to generate highly ductile post-breakage response by plastic deformation of the reinforcement.

	GB-bonded – beams	SG-laminated – beams

-20°C (a)   (e)

23°C (b)   (f)

60°C (c)   (g)

TC (d)   (h)

HE   n/a   (i)

LD   n/a   (j)
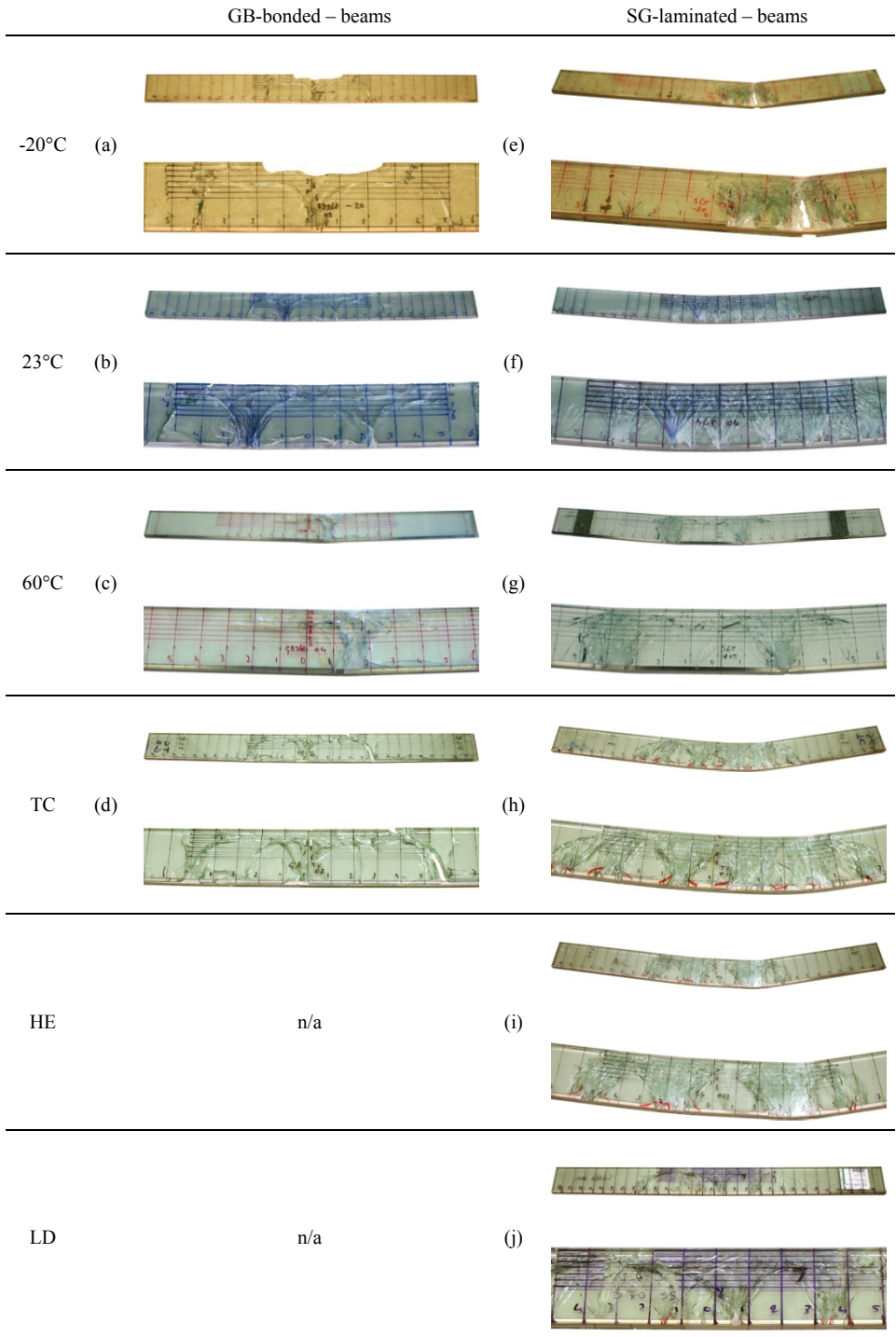
Figure 5.21: Photographs of exemplary failed beams per test series; upper = full beam; lower = close-up.

5.9.2.   *Thermal cycling effects on the beam response*

The effects of thermal cycling on the post-breakage response differed between the GB-bonded and SG-laminated beams. For the GB-bonded beams thermal cycling had a significantly negative effect on the post-breakage performance, whereas this effect was largely absent for the SG-laminated beams, see Figure 5.14(d) and 5.15(d).

The GB-bonded beams tested after thermal cycling showed only limited ductility at the post-breakage stage, see Figure 5.14 (d). Excessive bond failure at the post-breakage stage caused detachment of the reinforcement and consequent collapse of the beams. During the thermal cycling process the adhesive bond had been repetitively strained due to a difference in thermal expansion between the glass and the reinforcement. Due to its relatively small thickness ($t \approx 0.1$ mm), the adhesive bond was probably not sufficiently able to compensate for this difference in thermal expansion, which caused damage to accumulate in the adhesive bond. This accumulated damage weakened the adhesive bond and caused the reinforcement to detach during the bending tests.

The SG-laminated beams tested after thermal cycling demonstrated similar post-breakage response as the SG-laminated beams tested at +23°C without any special exposure, compare Figure 5.15 (b) and (d). Only a slight reduction in post-breakage strength has been observed, see Figure 5.20 (b). However, taking the scatter of the results into account, this reduction in post-breakage strength is regarded insignificant. Probably due to the relatively large thickness ($t = 1.52$ mm) of the SG interlayer, the shear deformation capacity is sufficient to compensate for the difference in thermal expansion between glass, reinforcement and SG interlayer during the thermal cycling process. Remarkably, the significant reduction in bond strength after thermal cycling as has been observed at the pull-out tests, seems to have no significant effect on the beam specimens. This difference is probably related to the size and geometry of the specimens. The metal-to-glass bond length in the beam specimens is very large compared to the bond length in the pull-out specimens. It is assumed that this increased bond length compensates for any possible negative effects of the thermal cycling exposure.

5.9.3.   *Humidity effects on the beam response*

The effects of humidity on the beam response, which in the current research have only been investigated for SG-laminated beams[i], seem limited at first instance. The humidity exposed SG-laminated beams reached post-breakage strength levels reasonably in line with the post-breakage strength values reached by the SG-laminated beams tested at +23°C without special exposure. Furthermore, the SG-laminated beams tested after humidity exposure demonstrated high ductility at the post-breakage stage, see Figure 5.15 (e).

However, one SG-laminated beam partly disintegrated and collapsed during the bending test, at a displacement level of 37 mm, see Figure 5.15(e). Although the specimen did not show any visual defects after the humidity exposure procedure that was done prior to the bending test, one of the outer glass panes largely delaminated during the bending test, see Figure 5.22. As a result of this delamination the lateral stability of the beam was significantly reduced, which caused the beam to buckle, see Figure 5.22(b). Apparently, the humidity had severely affected the bond strength of the SG interlayer. Both the glass-to-glass and metal-to-glass bond had failed. Additional research will be necessary to verify whether this was an incidental problem related to possible manufacturing errors or whether this problem is more consistent and related to sensitivity of the SG bond to humidity.

Overall, the effect of humidity was – apart from the delamination of one beam – larger for the pull-out specimens than for the beam specimens. It is assumed that this difference is related to the geometry and size of the specimens. In the pull-out specimens the bond area is relatively small compared to the bond area in the beam specimens. Furthermore, in the pull-out specimens the perimeter of the SG bond is more exposed than in the beam specimens, see Figure 5.23. The perimeter effect of humidity penetration is therefore assumedly more significant for the pull-out specimens than for the beam specimens.

---

[i] In the current research no GB-bonded beams have been tested for humidity effects. However, preceding research [Louter, Veer & Belis, 2008], in which GB-bonded beams were exposed for 8 weeks to salt-water spraying according to ASTM standard B 117-03 [ASTM, B 117-03], showed no significant effect of humidity on the structural response of the GB-bonded beams.
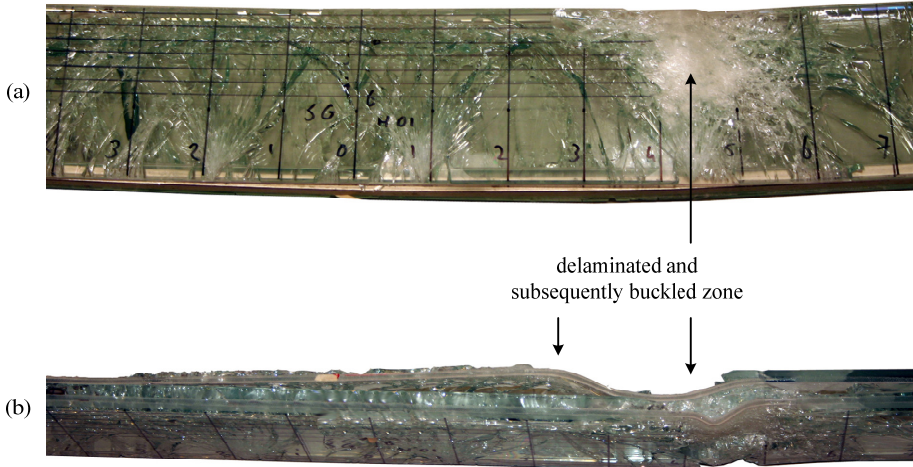
Figure 5.22: Delaminated SG-laminated reinforced glass beam; (a) top view; (b) side view.
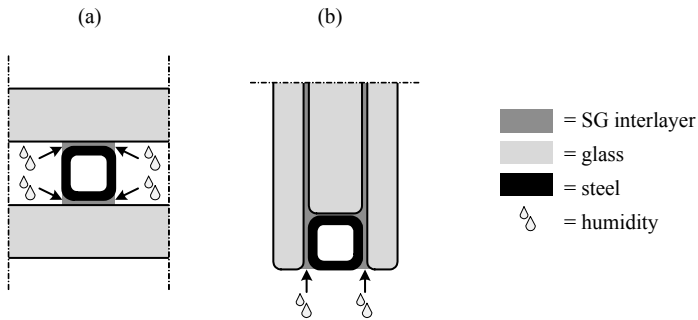
Figure 5.23: Perimeter effect of humidity;
(a) cross-section pull-out specimens; (b) cross-section beam specimens.

5.9.4.   *Load-duration effects on the beam response*

The long-duration bending tests, which in the current study have only been performed for SG-laminated beams, reveal a creep deformation of the beams at the post-breakage stage. The vertical displacement of the beams gradually increased while the load remained constant, see Figure 5.16. During the long-duration bending tests three processes have been visually observed, which explain this gradual increase in vertical displacement (or: creep) of the SG-laminated beams at constant loading levels.

Firstly, a very slow movement of the reinforcement along the glass was observed at the post-breakage stage. Due to this movement of reinforcement the resistance of the beam was reduced, which caused an increase in vertical displacement of the beam. The slow movement of reinforcement is caused by a creep deformation of the SG interlayer, as has also been observed in the long-duration pull-out tests.

Secondly, a slow propagation of the existing cracks in the glass was observed. This crack propagation was also the result of the creep movement of the reinforcement. Due to creep movement of the reinforcement the existing cracks in the glass could open up further. As a result of this larger crack opening displacement, the tensile stress at the crack tip increased, which stimulated a further propagation of the crack.

Thirdly, it was observed that new cracks occurred while the load remained constant. Again this might have been the result of the creep movement of the reinforcement along the glass. Due to creep movement of the reinforcement the overall resistance of the beam decreased, which caused – at a constant loading level – an increased stressing of the glass. Additionally, the occurrence of new cracks in the glass might be the result of stress-corrosion in the glass, see Chapter 4.

Apart from the observed creep, the semi-permanently loaded SG-laminated beams showed similar cracking behaviour and beam response as the SG-laminated beams tested at +23°C. The cracking process was stretched over a longer period of time, but in the end a similar cracking pattern resulted.

Furthermore, despite the observed vertical creep, the SG-laminated beams were able to carry load without collapsing. Even after being unloaded and reloaded again after 20 weeks, see Figure 5.16, the beams could withstand the load for a significant period of time. One beam specimen has even been tested up to 15 months. The beam did not collapse within that time frame. For building applications this seems to provide sufficient time for the building users to detect the crack(s) in the beam and to take semi-permanent supporting measures or to replace the beam.

5.9.5.   *Performance comparison of GB-bonded and SG-laminated beams*

Overall, the SG-laminated beams performed better than the GB-bonded beams[i]. For the tests at -20, +23, +60°C and after thermal cycling, which have been performed for both the GB-bonded and SG-laminated beams, the SG-laminated beams reached significantly higher post-failure strength levels. Furthermore, the SG-laminated beams consistently showed ductile post-breakage response, whereas for the GB-bonded beams this was only the case at +23°C, see Figure 5.14 and 5.15.

---

[i] The in this research observed performance levels of the investigated bond systems should not be interpreted for applications outside the scope of this research. For applications outside the scope of this research, different conditions may apply – such as a different bond geometry, loading condition, manufacturing technique, etc. – which may lead to a different performance of the bond system than is observed in this research.

This difference in post-breakage performance between the GB-bonded and SG-laminated beams is partly due to the higher bond strength and toughness of the SG interlayer compared to the GB adhesive. Due to the high bond strength and toughness of the SG interlayer, the reinforcement in the SG-laminated beams could be activated more effectively than in the GB-bonded beams. Upon initial glass failure the SG-laminated beams demonstrated less local debonding of the reinforcement, which enabled the reinforcement to arrest the cracks in the glass more efficiently. Furthermore, due to the higher bond strength, the SG-laminated beams showed less additional debonding of reinforcement at the post-breakage stage than the GB-bonded beams. For all the SG-laminated beams the reinforcement remained therefore largely attached to the glass, which enabled the beams to generate a highly ductile post-breakage response, whereas most GB-bonded beams finally collapsed due to full debonding of reinforcement.

Additionally, the difference in post-breakage performance between the GB-bonded and SG-laminated beams originates from profitable crack blocking properties of the SG interlayer. The SG interlayer acts – at least at room temperature – as a barrier between the glass layers and will largely prevent cracks to propagate through multiple glass layers. This limits the probability of cracks in one layer to coincide with cracks in the other(s). As a result the SG-laminated beams show a crack pattern of multiple cracks that are (evenly) distributed along the length of the beam and over the different glass layers[i]. The benefit of these non-coinciding cracks is that a crack in one layer is locally bridged by glass fragments in the other layer(s). These bridging glass fragments are able to transfer (tensile) forces over the crack through shear in the SG interlayer. This provides the beam, apart from the reinforcement, with an additional tensile force transferring mechanism which enhances the residual resistance of the beams [Bos, 2009]. For the GB-bonded beams this additional load-carrying mechanism is absent. Due to its low fracture toughness and small thickness, the GB adhesive does not have a crack blocking capacity. The multiple glass layers of a GB-bonded beam therefore act as a monolithic beam, and the crack generally runs through multiple glass layers without being blocked. Since the SG-laminated beams do profit from the additional load-carrying mechanism, they reach – at least at room temperature – higher post-breakage strength levels than the GB-bonded beams. However, it should be noted that the SG-laminated beams largely lose their additional load-carrying mechanism at -20 and +60°C due to the occurrence of plastic hinges in the beams as a result of decreased toughness and decreased bond strength of the SG at -20 and +60°C respectively. This will be explained in more detail in Chapter 9.

---

[i] The cracking behaviour of GB-bonded and SG-laminated beams is schematically presented in Figure 9.4.

5.10.   Conclusions

The following sections provide the conclusions from the pull-out tests and bending tests that have been performed in this chapter to investigate the effects of the parameters *bond system*, *temperature*, *thermal cycling*, *humidity* and *load duration*.

5.10.1.   Temperature effects

From the pull-out tests performed at -20, +23, +60 and +80°C, it is concluded that the bond strength and stiffness of both the GB adhesive and the SG interlayer, is highly temperature dependent. At increased temperature levels the bond strength of both the GB adhesive and the SG interlayer reduces significantly due to a decrease in polymer stiffness. At low temperature levels, however, a difference between both bond systems occurs. Whereas the bond strength of the GB adhesive reduces at -20°C, the SG interlayer shows a small increase in bond strength. The reduced bond strength of the GB adhesive probably originates from an increased rigidity of the GB adhesive bond at low temperatures, which makes the bond more susceptible for peak stresses that occur at the perimeter of the bond line.

From the bending tests performed at -20, +23 and +60°C, it is concluded that temperature levels within the range of -20 to +60°C do not endanger the safety performance of the SG-laminated beams, whereas they do endanger the safety performance of the GB-bonded beams. The SG-laminated beams demonstrated – despite some reduction in post-breakage strength, due to reduced toughness and reduced bond strength of the SG interlayer at -20 and +60°C respectively – high post-breakage strength levels and high ductility at all test temperatures. The GB-bonded beams, however, demonstrated a significant reduction in post-breakage strength and almost no ductility at -20 and +60°C.

5.10.2.   Thermal cycling effects

From the pull-out tests performed after thermal cycling it is concluded that thermal cycling has a negative effect on the bond strength of both the GB adhesive and the SG interlayer. It is assumed that due to (repetitive) straining of the bond during the thermal cycling procedure – as a result of the differences in thermal expansion of the assembled materials – the bond is (increasingly) damaged. This damage significantly reduces the bond strength. For the SG-laminated pull-out specimens this even resulted in spontaneous delamination. It should, however, be noted that this delamination might also have been caused by water condensation on the specimens during the thermal cycling procedure. Nevertheless, it is recommended to investigate the effect of thermal cycling in more detail.

From the bending tests performed after thermal cycling it is concluded that the negative effect of thermal cycling on the post-breakage performance is more significant for the GB-bonded beams than for the SG-laminated beams. The GB-bonded beams

demonstrated after the thermal cycling procedure no ductility at the post-breakage stage. Due to the thermal cycling procedure the bond strength had significantly reduced, which caused full debonding of reinforcement at the post-breakage stage and consequently collapse of the beams. The SG-laminated beams, on the contrary, still demonstrated high post-breakage strength and ductility after the thermal cycling procedure.

5.10.3. Humidity effects

From the pull-out tests performed after humidity exposure it is concluded that humidity exposure significantly reduces the bond strength of both the GB adhesive and the SG interlayer. It is assumed that, in humid environments, water molecules penetrate between the glass and the adhesive/interlayer and break the physical bonds between them.

From the bending tests performed after humidity exposure – conducted for SG-laminated beams only – it is concluded, however, that humidity generally has only a limited effect on the post-breakage performance of the SG-laminated beams. After the humidity exposure the SG-laminated beams still showed high ductility and high post-breakage strength. The observed reduction in bond strength of the SG interlayer for the humidity exposed pull-out specimens was not directly reflected in the test results of the humidity exposed beams. It is assumed that this difference originates from a difference in specimen geometry.

However, it should be noted that one humidity-exposed SG-laminated beam specimen largely delaminated during the test. Although the beam did not show any visual defects after the humidity exposure procedure, such as delamination or haze, the SG bond had apparently significantly degraded during the humidity exposure procedure. This alarming result urges for caution and for more in depth research of the behaviour of the SG-laminated (reinforced) glass beams in humid environments.

5.10.4. Load duration effects

From the pull-out tests performed for long-duration loading – conducted for SG-laminated pull-out specimens only – it is concluded that the SG interlayer shows, in line with its visco-elastic properties, significant creep. At constant loading levels the shear deformation of the SG interlayer gradually increases, which in the end leads to failure of the bond.

From the bending tests performed for long-duration loading – conducted for SG-laminated beams only – it is concluded that the observed creep of the beams, which mainly originated from creep of the SG interlayer, did not endanger their safety performance. Even for load durations up to 15 months the severely cracked SG-laminated beams were able to withstand loads up to 80% of their predicted ultimate failure load.

5.10.5. *Bond system effects*

From the performance comparison of the GB-bonded and SG-laminated specimens, it is concluded that, for the application tested in this research, the performance of the SG interlayer bond is more promising than the performance of the GB adhesive bond[i]. At the pull-out test series the SG interlayer showed, apart from the thermal cycling tests, consistently higher bond strength levels than the GB adhesive. Furthermore, at the bending tests the SG-laminated beams showed consistently higher post-breakage strength values and more ductility at the post-breakage stage than the GB-bonded beams.

However, it should be noted that the SG-laminated specimens showed some specific delamination issues after the thermal cycling (for the pull-out specimens) and the humidity exposure (for the beam specimens) procedures, which indicates a need for caution. From the current research it could not be determined whether the delamination problems originated from possible errors during the manufacturing process or whether this delamination problem is more consistent and possibly caused by humidity. Additional in depth research into this delamination effect is required.

---

[i] The observed performance levels of the investigated bond systems should not be interpreted for applications outside the scope of this research. For applications outside the scope of this research different conditions may apply, which may lead to a different performance of the bond system.

Chapter 6
Experimental investigations into
the effects of reinforcement percentage
and beam size on the structural response

As introduced Chapter 1, the current chapter investigates the effects of reinforcement percentage and beam size on the structural response of reinforced glass beams. It uses the results of the SG-laminated reinforced glass beams tested at room temperature in Chapter 5 and compares these results with additional bending tests on two additional beam series with varying reinforcement percentage and beam size. The findings of this investigation are implemented in the integrated discussion of the research results, presented in Chapter 9 and Chapter 10.

Abstract

This chapter investigates the effects of the parameters *reinforcement percentage* and *beam size* on the structural response of reinforced glass beams. To investigate the effects of reinforcement percentage, two SG-laminated 1.5 m reinforced glass beam series with identical beam dimensions but with either a square hollow section reinforcement or a square solid section reinforcement have been tested in four-point bending. From the test results it is concluded that increasing amount of reinforcement at the tensile edge of the beams does effectively enhance the post-breakage performance. Due to a lowering of the neutral axis of the beam, the height of the (initial) cracks in the glass is reduced. Furthermore, due to an increase in total load capacity of the reinforcement, the post-breakage strength and stiffness of the beams is increased. To investigate the effects of beam size on the structural response, a series of SG-laminated 3.2 m reinforced glass beams has been tested in four-point bending. From a comparison of their test results with the test results of the 1.5 m beams, it is concluded that the effects of beam size on the post-breakage response are only limited. The 'large' 3.2 m beams demonstrated similar structural response and cracking behaviour as the 'small' 1.5 m beams. To simultaneously explore the lateral stability performance of reinforced glass beams, the 3.2 m beams have been tested in a lateral torsional buckling test setup. From this exploratory investigation it is observed that even at the post-breakage stage, when the beams are weakened by (a large number of) cracks in the glass, the beams demonstrate excellent lateral stability performance.

Background information

Material support and assistance

- Van Noordenne Groep,
  Hardinxveld Giessendam, The Netherlands

- Dupont de Nemours, Glass Laminating Solutions,
  Mechelen, Belgium

Technical support and assistance

- Kees Baardolf
  Building Technology Laboratory,
  Faculty of Architecture, TU Delft, The Netherlands

Test facilities

- Building Technology Laboratory,
  Faculty of Architecture, TU Delft, The Netherlands

- Materials Laboratory,
  Faculty of Mechanical, Maritime and Materials Engineering,
  TU Delft, The Netherlands

- Stevin Laboratory,
  Faculty of Civil Engineering and Geosciences, TU Delft, The Netherlands

- Laboratory for Research on Structural Models,
  Department of Structural Engineering, Ghent University, Belgium

Lateral torsional buckling tests conducted in collaboration with

- Jan Belis, Dieter Callewaert,
  Laboratory for Research on Structural Models,
  Department of Structural Engineering, Ghent University, Belgium

6.1.   Introduction

To investigate the effects of the parameters *reinforcement percentage* and *beam size* on the structural response of reinforced glass beams, three different beam series with varying reinforcement sections and beam sizes have been tested in four-point bending. Two SG-laminated 1.5 m reinforced glass beam series with identical beam dimensions but with varying reinforcement sections have been tested to investigate the effects of reinforcement percentage. Additionally, an SG-laminated 3.2 m reinforced glass beam series has been tested to investigate the effects of beam size. To simultaneously explore their lateral stability, the latter beam series has been tested in a lateral torsional buckling test setup.

The geometries of the three different beam series are presented in section 6.2. Thereafter section 6.3 discusses the four-point bending test setups and test procedures. The results of the tests are presented and discussed in section 6.4 and section 6.5 respectively. Finally, conclusions from this investigation are provided in section 6.6.

6.2.   Test specimens
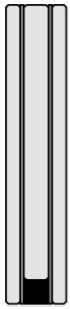
Three different beam series were studied in this research. Their cross-section geometries are presented in Figure 6.1. The general layout of the three beam geometries were similar; they all consisted of triple-layer annealed float glass laminates with a square stainless steel reinforcement section bonded at the inner recessed edge. All beam specimens were laminated by commercial suppliers using standard 1.52 mm SG interlayer sheets[i].

The beams of series I had a length of 1.5 m and nominal cross-section dimensions of 25.04*125 mm. The beams were provided with a square hollow section reinforcement (10*10*1 mm, A_{re} = 36 mm^2).

The beams of series II had, similar to the series I beams, a length of 1.5 m and nominal cross-section dimensions of 25.04*125 mm. Different from the series I beams, however, they were provided with a square solid section reinforcement (10*10 mm, A_{re} = 100 mm^2). This solid section reinforcement had the same outer dimensions as the hollow section reinforcement applied for series I beams. Thus the bond area between the glass and the reinforcement was equal for series I and II.

The beams of series III had a length of 3.2 m and nominal cross-section dimensions of 34.04*285 mm. The beams were provided with a square hollow section reinforcement (15*15*1.5 mm, A_{re} = 81 mm^2). Compared to the series I, the beams of series III were scaled by approximately a factor 2.

---

[i] Standard thicknesses of SG interlayer sheets are 0.89, 1.52 and 2.28 mm.

			Series I	Series II	Series III	ratio I:III
Number of specimens		-	5	3	3	
Section dimensions outer glass layers	$b*h$	[mm]	6*125	6*125	8*285	
Section dimensions inner glass layer	$b*h$	[mm]	10*115	10*115	15*270	
Section dimensions reinforcement	$b*h\,(*t)$	[mm]	10*10*1	10*10	15*15*1.5	
Thickness SG interlayer	t_{bond}	[mm]	1.52	1.52	1.52	
Beam width	b_{beam}	[mm]	25.04 [i]	25.04 [i]	34.04 [i]	1 : 1.4
Beam height	h_{beam}	[mm]	125	125	285	1 : 2.3
Beam length	l_{beam}	[mm]	1500	1500	3200	1 : 2.1
Reinforcement area	A_{re}	[mm^2]	36	100	81	1 : 2.3
Glass area	A_{gl}	[mm^2]	2650	2650	8610	1 : 3.2
Initial bending stiffness [ii]	$EI_{composite}$	[Nmm^2]	2.51*10^{11}	2.91*10^{11}	4.18*10^{12}	1 : 16.7

[i]   Width including 2 SG interlayers with a nominal thickness of t = 1.52 mm each (before lamination).

[ii]   Calculated according to Equation 8.2, see Chapter 8.

Figure 6.1: Cross-sections of the three different beam series; nominal dimensions.

6.3.   Test setup

Three different four-point bending test setups were applied in this research.

The series I beams (1.5 m, with hollow section reinforcement) were tested at a Zwick Z100 testing machine which was provided with a custom-made support frame, see Figure 6.2 and Chapter 5. The series I beams were loaded at a constant vertical displacement rate of 2 mm/minute. During the test the applied force and the vertical displacement of the cross-head were measured.

The series II beams (1.5 m, with solid section reinforcement) were tested at a universal Instron mechanical testing machine which has been provided with the same custom-made support frame as for the series I beams, see Figure 6.2. The series II beams were loaded at a constant displacement rate of 2 mm/minute until initial failure. Thereafter the test speed was stepwise increased to 5 and 10 mm/minute respectively, to limit the test duration. During the test the applied force and the vertical displacement of the cross-head were measured.

The series III beams (3.2 m) were tested in four-point bending in a lateral buckling test setup which allowed for out-of-plane bending of the beam specimens, see Figure 6.3. The beam specimens were supported by fork bearings, which could rotate freely around their vertical axis to allow the beam to laterally deflect. Furthermore, the loading mechanism, which was pulling the beam downwards, was provided with hinged load introduction points and a roller mechanism, see Figure 6.3, which allowed the mechanism to fully follow any lateral movement of the beam. During the tests the load was manually applied using a hydraulic jack. The applied force and both the vertical and horizontal displacements were measured during the tests.

load span = 400 mm
lateral support span = 550 mm
support span = 1400 mm
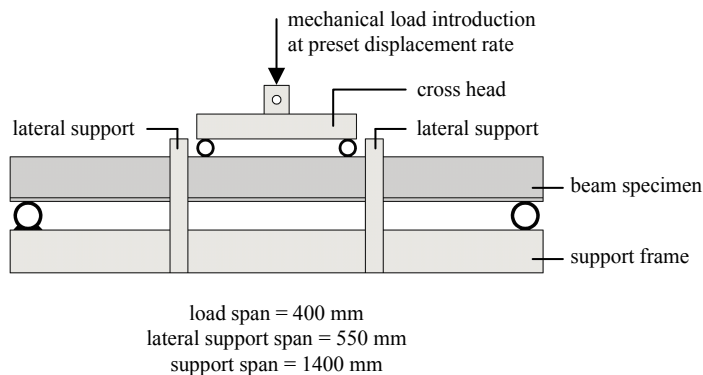
Figure 6.2: Schematic representation of the test setup used for the bending test
on the 1.5 m series I and II beams.

(a)   (b)
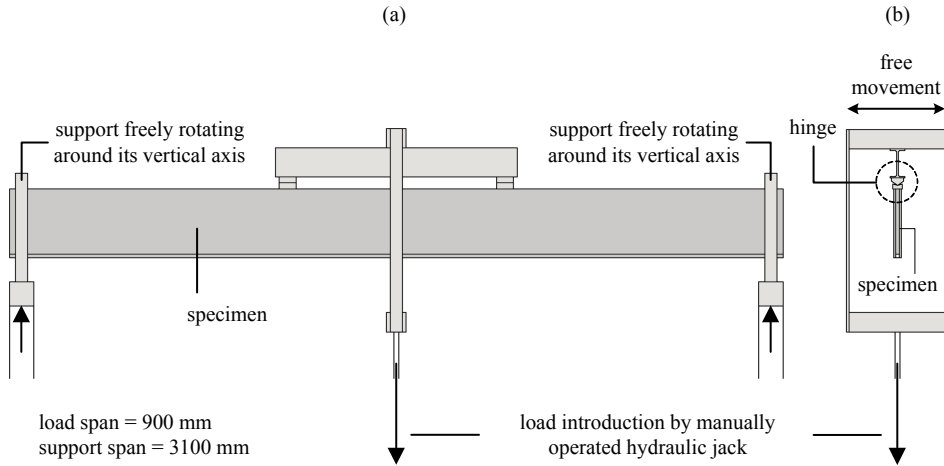
Figure 6.3: Lateral torsional buckling test setup for the 3.2 m series III beams;
(a) side view; (b) cross-sectional view.

6.4.   Results

The results of the four-point bending tests on the series I, II and III beams are presented in Table 6.1[i]. Additionally Figure 6.4 shows the load-displacement diagrams and a sequential set of diagrams showing the crack pattern development numbered 1 to 3. This sequence number is also indicated in the load-displacement diagrams.

The series I beams (1.5 m, with hollow section reinforcement) typically demonstrated linear elastic response until initial glass failure, followed by a ductile post-breakage response. Multiple V-shaped cracks occurred in the glass, which were more or less evenly distributed along the length of the beam. Outside the maximum bending moment zone typical diagonal shear cracks occurred. For all series I beams the test procedure had to be aborted upon reaching the maximum displacement of the test rig, which was about 60 mm. Consequently, none of the series I beams could be tested to complete collapse.

The series II beams (1.5 m, with solid section reinforcement) also demonstrated initial linear elastic response followed by a ductile post-breakage response. However, compared to the series I beams, the series II beams reached significantly higher post-breakage strength values. Similar to the series I beams the series II beams demonstrated a dense fracture pattern of multiple V-shaped cracks and diagonal shear cracks. The series II beams finally failed due to explosive glass failure underneath one of the load introduction points.

---

[i] For the full results and exemplary photo sequences of the bending tests is referred to Appendix I.

The series III beams (3.2 m) demonstrated similar structural response as the series I beams (1.5 m). After an initial linear elastic stage, the beams showed ductile post-breakage response. Again a dense fracture pattern of multiple V-shaped cracks and diagonal shear cracks occurred. Only one specimen was tested to full destruction. This beam collapsed due to failure of the laminate along a diagonal shear crack. The other tests had to be stopped upon reaching the ultimate displacement limit of the hydraulic jack.

Table 6.1: Experimental results of the bending tests on the series I, II and III beams.

		Series I	Series II	Series III
Initial failure load				
mean [a]	[kN]	11.7	16.9	32.9
st.dev.	[kN]	1.1	0.7	2.0
rel.st.dev.	[%]	9.5	3.9	6.1
Maximum post-breakage load				
mean [a]	[kN]	17.5	40.6	36.4
st.dev.	[kN]	0.5	0.1	1.7
rel.st.dev.	[%]	2.8	0.4	4.8
Max.post-breakage load / initial load				
mean [a]	[%]	150.0	240.7	110.7
st.dev.	[%]	12.0	9.2	2.5
rel.st.dev.	[%]	7.7	3.8	2.3

[a]   The mean are results are displayed in the table; the full results are given in Appendix I.

Load-displacement diagrams   Cracking sequences
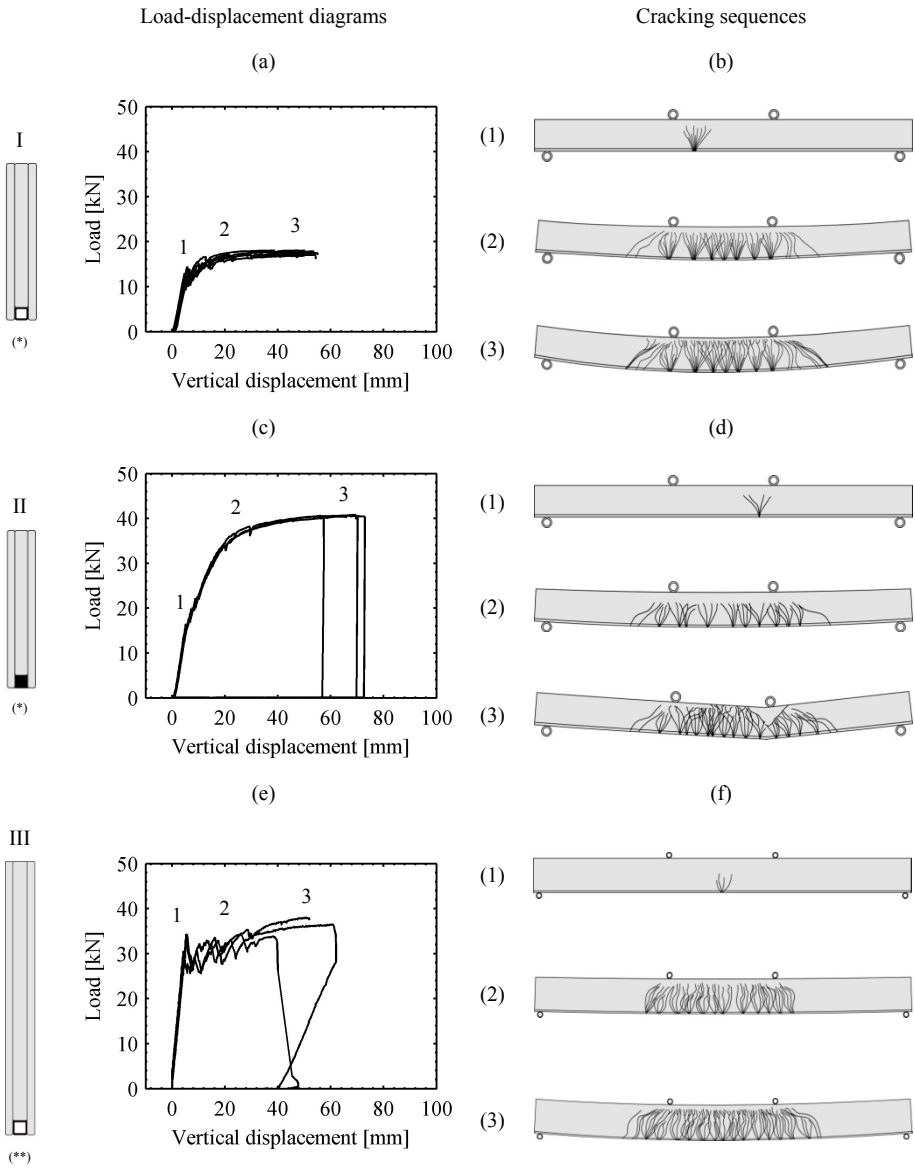
Figure 6.4: Load-displacement diagrams and cracking sequences of the series I, II and III beams.

[*] laterally supported; [**] laterally unsupported

6.5. Discussion

The effects of reinforcement percentage and beam size on the structural response are separately discussed in the following subsections. Additionally, the lateral stability performance of the series III beams is discussed.

6.5.1. Effects of reinforcement percentage

The effects of reinforcement percentage on the structural response of reinforced glass beams can be derived from a comparison of the results of the series I beams (1.5 m, with hollow section reinforcement) with the series II beams (1.5 m, with solid section reinforcement), see Figure 6.4 (a), (b) and (c), (d). From this comparison the following is observed.

Firstly, it is observed that the initial crack height in the series II beams (1.5 m, with solid section reinforcement) is less than in the series I beams (1.5 m, with hollow section reinforcement). The initial crack in the series I beams travels on average 74 % of the beam height, whereas it travels on average only 64 % of the beam height in the series II beams. This difference is caused by the increased amount of reinforcement in the series II beams, which lowers the 'neutral axis' of the beams both at the uncracked and the cracked stage. Due to the lowering of the neutral axis, the height of the (initial) cracks in the glass is reduced. This reduced crack height (or: increased height of the compression zone) also results from the analytical model presented in Chapter 8 of this thesis. Equation 8.4 can be used to determine the height of the uncracked compression zone of the beam, and thereby the height of the crack in the glass. For the beam geometries studied in the current chapter Equation 8.4 yields a crack height of 77% of the beam height for the series I beams and a crack height of 65% of the beam height for the series II beams. These analytical values are rather close to the experimental values mentioned at the beginning of this paragraph.

Secondly, it is observed that the series II beams (1.5 m, with solid section reinforcement) demonstrate a higher strength and stiffness at the post-breakage stage than the series I beams (1.5 m, with hollow section reinforcement). Again this difference is directly related to the higher percentage of reinforcement in the series II beams. The increased total tensile force that can be carried by the reinforcement effectively enhances the post-breakage strength of the reinforced glass beams. Furthermore, due to the increased amount of reinforcement, the strain in the reinforcement is smaller, which results in stiffer post-breakage response of the beams[i]. This increased post-breakage strength and stiffness of the series II beams is also described by the analytical model presented in Chapter 8 of this thesis. As is plotted in Figure 8.17 of that chapter, the analytical results are in fairly good agreement with the experimental results.

---

[i] However, when the reinforcement starts to plastically deform, the stiffness of the beam will decrease.

Thirdly, it is observed that there is no noticeable difference in local debonding of reinforcement between the series I and the series II beams. It was expected that a higher amount of reinforcement with a same bond area between the glass and the reinforcement would result in higher stressing of the bond, and thus possibly more debonding of the reinforcement. However, this did not occur. From Equation 6.1 it can be calculated, though, that the shear stress (τ) in the bond between the glass and the reinforcement is – for the same loading levels, and thus for the same shear force (V) – about 2 times higher in the series II beams than in the series I beams. This confirms the expected increased stressing of the bond.

$$\tau = \frac{V \cdot S}{b_{bond} \cdot I_{yy}} = \frac{V \cdot A_{re} \cdot z_{re}}{b_{bond} \cdot I_{yy}} \tag{6.1}$$

with:

V = shear force

S = linear moment of area

A_{re} = cross-sectional area of the reinforcement

z_{re} = distance of reinforcement to the neutral axis

b_{bond} = width bond line

I_{yy} = moment of inertia

However, between the loading points of the four-point bending test setup, the shear force (V) is theoretically "0" and thus Equation 6.1 yields "0". Between the loading points, a different mechanism applies, and the stress in the bond on either side of a crack in the glass is governed by the local transfer of the tensile force from the reinforcement to the glass. As the cross-sectional area of reinforcement (A_{re}) and thus the stiffness of the reinforcement in the series II beams is higher, the local elongation (strain) of the reinforcement is limited. It is assumed that this limited elongation of reinforcement causes less straining of the bond and thus possibly less debonding of reinforcement, which is the opposite from what was expected. However, more in depth calculations should further investigate this.

6.5.2.   *Effects of beam size*

The effects of beam size on the structural response of reinforced glass beams can be derived from a comparison of the results of the bending tests on the series I beams (1.5 m) with the results of the series III beams (3.2 m), see Figure 6.4 (a), (b) and (e), (f). From this comparison the following is observed.

Firstly, the series I beams (1.5 m) and the series III beams (3.2 m) display similar cracking behaviour. Both beam series show a rather dense crack pattern of V-shaped bending cracks and some diagonal shear cracks. From this observation it is assumed that the beam size does not have a significant effect on the cracking behaviour of the beams.

Secondly, a difference in post-breakage behaviour between the series I beams (1.5 m) and the series III beams (3.2 m) is observed. Obviously the 'large' series III beams reached higher post-breakage strength levels than the 'small' series I beams due to an increased load-carrying capacity which is directly related to their size. However, apart from this difference in strength, another difference occurred in post-breakage behaviour. As has been explained in Chapter 5, the SG-laminated reinforced glass beams profit – at room temperature – from an additional load-carrying mechanism at the post-breakage stage. This additional load-carrying mechanism originates from unbroken glass segments overlapping local cracks in the neighbouring glass layers thereby transferring bending induced forces through shear in the SG interlayer. Due to this additional load carrying mechanism the series I beams reach higher post-breakage strength levels than is given by the analytical model presented in Chapter 8. This analytical model assumes that the post-breakage strength is only generated by a compression force in the glass and a tensile force in the reinforcement. It disregards the layering of the glass beam and thereby neglects any additional load-carrying mechanism that may be generated through shear in the SG interlayer. The series I beams therefore reach an average post-breakage strength of 17.5 kN, whereas the analytical model describes a maximum post-breakage strength level of 14.4 kN, see Figure 8.16. This means that the observed post-breakage strength of the series I beams amounts to about 120% of the analytically modelled post-breakage strength. However, for the type III beams, which demonstrated a post-breakage strength of 36.4 kN and have an analytically predicted post-breakage strength of 34.3 kN, the observed post-breakage strength amounts only to about 106 % of the predicted strength. This reduced percentage for the series III beams indicates that the additional load-carrying mechanism generated by crack-bridging glass fragments is less effective, or largely absent, in the series III beams. Whether this is a specific effect of size or related to a difference in the density of the cracks in the glass could not be derived from this research.

6.5.3. Lateral stability aspects

The series III beams (3.2 m) have been tested in a lateral torsional buckling test setup to explore their lateral stability performance. Figure 6.5 shows a plot of the load versus the horizontal displacements of an exemplary lateral torsional buckling beam test performed on a series III beam. The full results are provided in Appendix I.

The diagram in Figure 6.5 demonstrates that lateral displacement of the beams only occurs at the post-breakage stage and not at the linear elastic stage. At the post-breakage stage the lateral stiffness of the beams is gradually decreased due to cracking of the glass. However, the observed lateral displacement amounted to 47.2 mm at maximum, which is only about 1.4 times the width of the beam laminate. The observed horizontal movement did not cause the final failure of the beam specimen. Final collapse of the beam was caused by failure of the beam laminate along a diagonal shear crack, see Figure 6.6, which had gradually enlarged during the post-breakage stage.
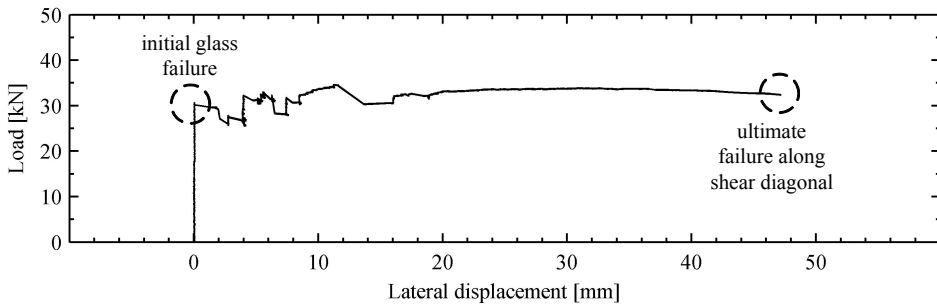
Figure 6.5: Plot of the load versus the horizontal displacements of an exemplary 3.2 m series III beam tested in a lateral torsional buckling test setup.
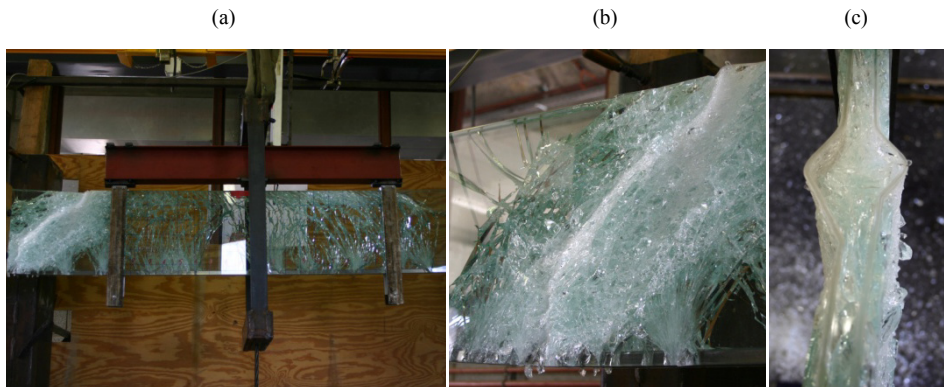
Figure 6.6: Photographs of a series III beam in the test setup, with buckled zone along a diagonal shear crack; (a) side view; (b) Close-up of the diagonal shear crack; (c) Top view of the buckled zone.

6.6.   Conclusions

From the comparison of the results of the series I beams (1.5 m, with hollow section reinforcement) and series II beams (1.5 m, with solid section reinforcement) it is concluded that varying the reinforcement percentage – while maintaining the bond area between the glass and the reinforcement the same – does influence the structural performance of the beams. Increasing the amount of reinforcement at the lower (tensile) edge of the beam, lowers its neutral axis. The lowering of the neutral axis results in a reduced height of the (initial) cracks in the glass. Furthermore, increasing the amount of reinforcement in the section effectively increases the post-breakage strength and stiffness of the beams, due to an increase in total tensile capacity of the reinforcement.

From the comparison of the results of the series I beams (1.5 m) and series III beams (3.2 m) it is concluded that beam size has only a limited effect on the post-breakage behaviour. Apart from a reduction in effectiveness of the additional load-carrying mechanism – which is generated by crack-bridging glass fragments that transfer bending induced forced through shear in the SG interlayer – the series III beams demonstrate similar post-breakage behaviour as the series I beams.

Chapter 7
Experimental investigations into the structural response of SG-laminated glass beams with embedded glass fiber reinforcement

Chapters 5 and 6 showed promising results for the SG interlayer acting as a bond between the glass and the metal reinforcement. To further exploit these profitable bonding properties and to enhance the transparency of the reinforced glass beams, the current chapter investigates the possibilities of embedding semi-transparent GFRP (Glass Fiber Reinforced Polymer) rods in the SG interlayer of glass beams. The findings from this investigation will be implemented in the integrated discussion of the research results, presented in Chapter 9 and Chapter 10.

Abstract

This chapter investigates the structural response of SG-laminated glass beams with semi-transparent GFRP (Glass Fiber Reinforced Polymer) reinforcement rods embedded in the interlayer. To do so, two test series have been performed. Firstly, a series of pull-out specimens has been tested at -20, +23 and +60°C to investigate the pull-out resistance of the GFRP rods. Secondly, a series of SG-laminated double-layer glass beams with GFRP rods embedded in the interlayer have been tested in four-point bending to investigate their structural behaviour. Both test series have been conducted for round (Ø 2 mm) GFRP rods made of E-glass fiber filaments embedded in a polyester resin, and flat (0.8*6 mm) GFRP rods made of S-glass fiber filaments embedded in an epoxy resin. The results of the pull-out tests showed superior pull-out strength of the specimens with the flat rods, due to the larger bond area of the flat rods compared to the round rods. The results of the bending tests demonstrated a superior post-breakage performance of the beams with the flat rods, due to a higher strength and stiffness of the S-glass filaments compared to the E-glass filaments. Furthermore, the bending tests demonstrated that despite the absence of any yield mechanism in the GFRP rods, the beams were able to develop semi-ductile post-breakage behaviour. From the tests it is concluded that the application of GFRP rods as embedded reinforcement in the SG interlayer of glass beams is a very promising concept. The combination of highly redundant structural performance and high transparency make the beams appealing for architectural and structural applications.

Background information

Material support and assistance

- Van Noordenne Groep,
  Hardinxveld Giessendam, The Netherlands

- Dupont de Nemours, Glass Laminating Solutions,
  Mechelen, Belgium

- Van Dijk Pultrusions & Saint Gobain,
  The Netherlands

Technical support and assistance

- Kees Baardolf,
  Building Technology Laboratory,
  Faculty of Architecture, TU Delft, The Netherlands

- Lerobel,
  Hasselt, Belgium

Test facilities

Pull-out tests

- Materials Laboratory,
  Faculty of Mechanical, Maritime and Materials Engineering,
  TU Delft, The Netherlands

Bending tests

- Materials Laboratory,
  Faculty Mechanical, Maritime and Materials Engineering,
  TU Delft, The Netherlands

- Stevin Laboratory,
  Faculty of Civil Engineering and Geosciences,
  TU Delft, The Netherlands

Research partly conducted in collaboration with

- Calvin Leung, Martien Rademakers,
  Faculty of Civil Engineering and Geosciences, TU Delft, The Netherlands

7.1. Introduction

The SG-laminated reinforced glass beams tested in Chapter 5 and 6 have demonstrated that the polymer interlayer SentryGlas® (SG) is an excellent candidate for bonding metal reinforcement to a glass beam. Due to its high bond strength and shear stiffness the SG interlayer effectively activates the reinforcement. Furthermore, the SG interlayer shows low viscosity during the lamination process. Due to this low viscosity, the SG interlayer easily adapts to different shapes and geometrical tolerances.

Based on these promising results and favourable properties of the SG interlayer, it is expected that the SG interlayer can be exploited for a novel concept of embedded reinforcement. This concept, which has been developed within this study, embodies the embedment of GFRP (Glass Fiber Reinforced Polymer) rods in the interlayer of structural glass beams, see Figure 7.1. Instead of bonding the reinforcement at the recessed edge, as has been done for the metal reinforced glass beams studied in Chapter 5 and 6, the reinforcement sections are now embedded ('molten') into the SG interlayer between the glass layers.
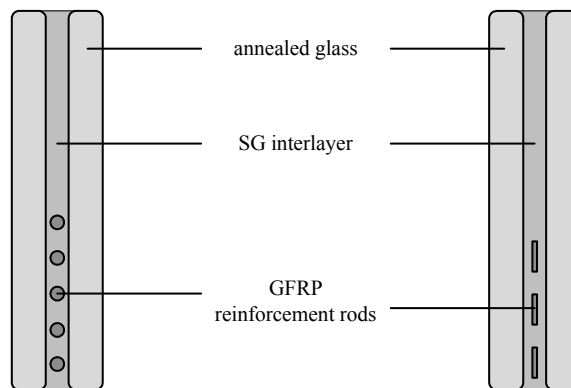
Figure 7.1: Schematic representation of the concept of glass beams with GFRP (Glass Fiber Reinforced Polymer) reinforcement rods embedded in the SentryGlas® interlayer.

A similar concept of embedded reinforcement has been studied by Feirabend and Sobek [Feirabend, 2010; Feirabend & Sobek, 2008; Feirabend &Sobek, 2009], who reported promising results for laminated glass panes with a metal wire-mesh and metal perforated sheet embedded in a PVB (poly-vinyl-butyral) or SG (SentryGlas®) interlayer, see Chapter 3. However, different from the concept presented in this chapter, the study of Feirabend focuses on glass panes loaded out-of-plane which are essentially intended for window and overhead glazing. The concept of embedded reinforcement for structural glass beams which are loaded in-plane has – to the author's knowledge – not been studied before.

It is assumed that structural glass beams with GFRP reinforcement rods embedded in the interlayer provide some advantages over metal-reinforced glass beams. Firstly, due to the high tensile strength and semi-transparent appearance of the GFRP rods, the amount and visual impact of the reinforcement will be limited, which enhances the transparency of the beam. Secondly, the reinforcement can be positioned anywhere within the beam laminate, which enables an intensification of reinforcement at highly stressed zones. Finally, the GFRP reinforcement rods are embedded within the beam laminate and not exposed at the beam edge, which protects the GFRP rods from direct impact and might shield them from humidity effects.

However, since the GFRP rods lack any yield mechanism, the GFRP reinforced glass beams might respond totally different from the metal-reinforced glass beams investigated in Chapter 5 and 6. For the latter beams, a high post-breakage strength and a ductile post-breakage response was obtained due to the high tensile strength and the plastic deformation capacity of the stainless steel reinforcement. Whether the GFRP reinforced glass beams provide a similar safe post-breakage response is yet unknown.

This chapter therefore investigates the structural response of glass beams with GFRP rods embedded in the SG interlayer. To do so, two test series have been conducted. Firstly, a pull-out test series has been performed at -20, +23 and +60°C on small scale glass laminates with GFRP rods embedded in the SG interlayer. These tests focused on the pull-out strength of the GFRP rods at different temperature levels. Secondly, a series of four-point bending tests has been performed on 1.5 m double-layer SG-laminated glass beams with GFRP rods embedded in the interlayer. These bending tests focused on the post-breakage response of the beams at +23°C. Both test series have been conducted for round (Ø 2 mm) and flat (0.8*6 mm) GFRP rods.

Section 7.2 presents the layout and geometry of the beam specimens. Subsequently, section 7.3 describes the test setup and the test method. Thereafter, the results are presented and discussed in sections 7.4, 7.5 and 7.6. Finally, the conclusions from this research are provided in section 7.7.

7.2.   Test specimens

Table 7.1 provides the number of specimens that was made and tested for both the pull-out and bending tests. The applied materials and the geometries of the specimens are briefly presented in the following sub-sections.

Table 7.1: Number of specimens per test type and test condition.

Test condition	Pre-conditioning	Pull-out specimens		Beam specimens	
		round rods	flat rods	round rods	flat rods
-20°C	1 week at -23°C	2	2	-	-
+23°C	1 week at +23°C	2	3	2	2
+60°C	24 hours at +63°C	2	3	-	-
Total		6	8	2	2

7.2.1.   Materials

The pull-out and beam specimens were made of annealed glass, GFRP reinforcement rods and SG interlayer sheets.

For the glass ordinary annealed float glass was used, which was cut and ground by a commercial supplier. The material properties of the glass are described in Chapter 4.

For the GFRP reinforcement either round (Ø 2 mm) or flat (0.8*6 mm) rods were applied. The round rods consisted of *E-glass* fiber filaments embedded in a *polyester* matrix. Their estimated tensile load capacity amounts to 5.0 kN per rod. The flat rods consisted of *S-glass* fiber filaments embedded in an *epoxy* resin. Their estimated tensile load capacity amounts to 10.8 kN per rod. More detailed material properties of the GFRP rods are provided in Chapter 4.

The SG interlayer was applied in sheet thicknesses of $t = 0.89$ and $t = 1.52$ mm. The material properties of the SG interlayer are described in Chapter 4.

The applied assembly and production process is described in Chapter 10.

7.2.2.   Pull-out specimens

The pull-out specimens consisted of two small double-layered glass laminates with either a round or a flat GFRP rod embedded in the SG interlayer, see Figure 7.2. The glass laminates consisted of two 100*100 mm glass plates with a thickness of 10 mm. For the specimens with the round GFRP rod three SG interlayer sheets were applied of which the middle sheet was cut to host the GFRP rod, see Figure 7.2 (a). The middle SG interlayer sheet was applied to assure a full adhesion along the perimeter of the GFRP rod and to prevent lateral movement of the round rod during the manufacturing process. For the specimens with the flat GFRP rod two SG interlayer sheets were applied, see Figure 7.2 (b).
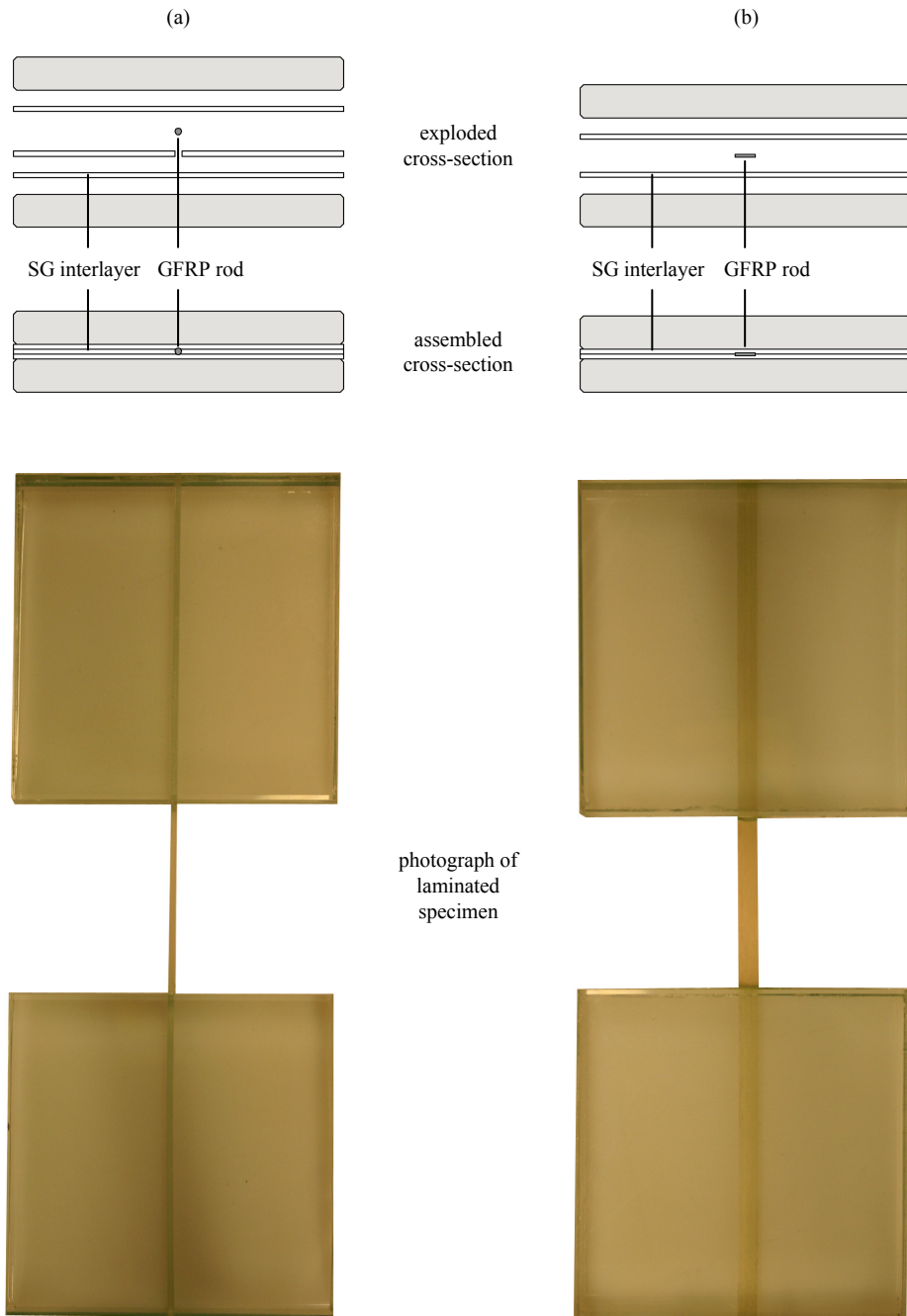
Figure 7.2: Exploded cross-section, assembled cross-section and photograph of the GFRP pull-out specimens; (a) Pull-out specimens with the round GFRP rods; (b) Pull-out specimens with flat GFRP rods.

7.2.3. *Beam specimens*

The beam specimens, with a length of 1.5 m, consisted of a double-layer glass laminate with either 5 round or 3 flat GFRP reinforcement rods embedded in the SG interlayer, see Figure 7.3. For each beam specimen three SG interlayer sheets were applied. The middle sheet was cut to host the GFRP rods and to keep the GFRP rods at the correct position during the lamination process. Any differences in thickness between the rods and the SG interlayer were levelled due to the low viscosity of the SG interlayer during the lamination process.
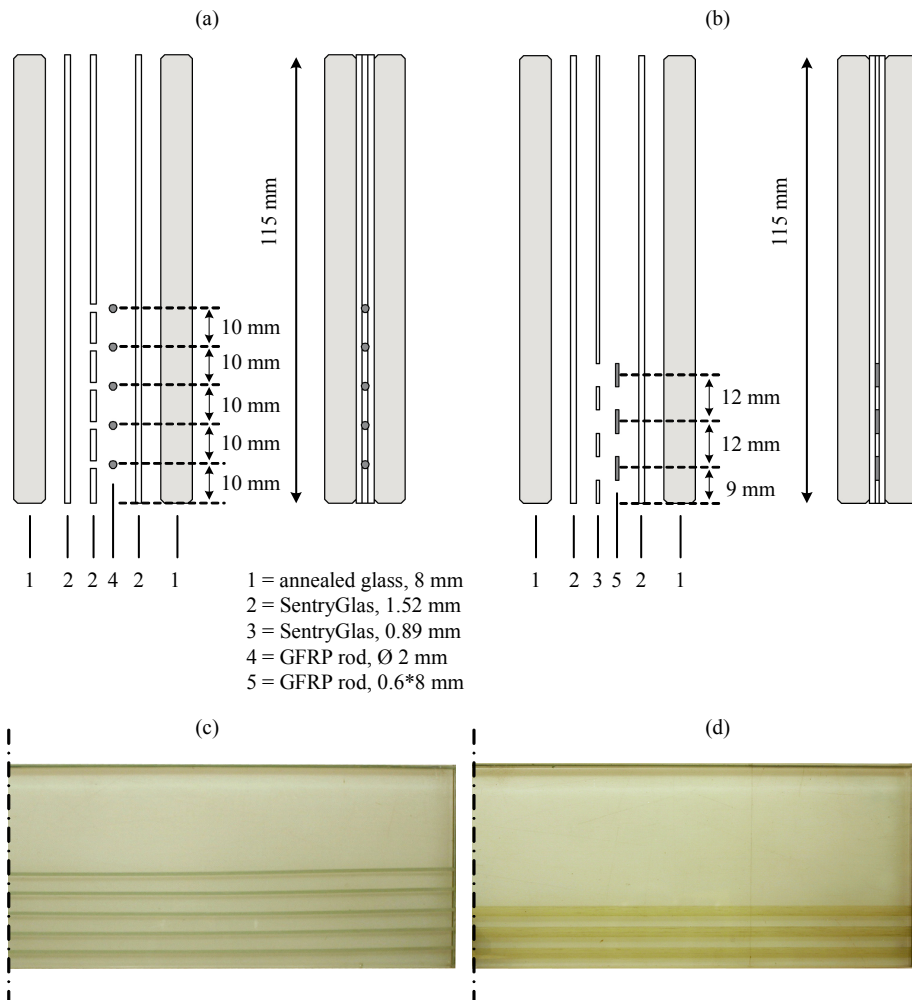
Figure 7.3: Beam specimens with round or flat GFRP rods embedded in the SG interlayer; (a) & (b) exploded and assembled cross-section; (c) & (d) Close-up photograph of the laminated specimens (side view).

7.3.   Test setups

The test setup of the pull-out and bending tests are separately described in the following sub-sections[i].

7.3.1.   Pull-out test setup

The pull-out tests at -20, +23 and +60°C were performed on a standard Zwick Z100 universal testing machine, which was provided with custom-made steel brackets to host the pull-out specimens, see Figure 7.4. One part of the pull-out specimens was placed in the upper bracket and the other part in the lower bracket. The upper bracket was moved upwards at a constant displacement rate of 2 mm/minute, whereas the lower bracket was fixed. This way the GFRP rod was loaded in tension thereby pulling it out of the glass laminate. During the tests the load and the displacement of the crosshead were measured at an interval of 0.01 seconds.

For the pull-out tests at -20 and +60°C an insulated climate box was put around the test setup. This climate box was either cooled with vaporized liquid nitrogen or heated with an electric heating element. A fan at the back side of the climatic box generated an air flow throughout the climate box which ensured a relatively even temperature level throughout the climate box. During the tests the temperature was measured and automatically set at a constant level of either -20 or +60°C (±3°C).
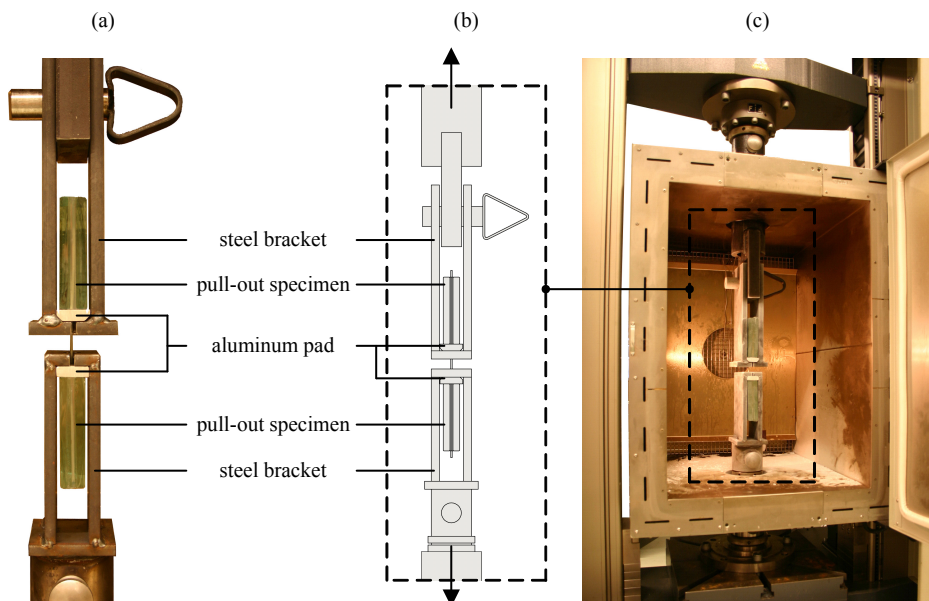
Figure 7.4: Pull-out test setup for the GFRP pull-out specimens.

---

[i] For the full results and exemplary photo sequences of the bending tests is referred to Appendix I

Prior to the pull-out tests the specimens were conditioned for several days, see Table 7.1. The specimens tested at room temperature were conditioned for 1 week at +23°C (±1°C) in the same room as the test setup. The specimens tested at -20°C were conditioned for 1 week at -23°C (±1°C) in an ordinary refrigerator. The conditioning temperature was selected 3 degrees lower than the testing temperature to compensate for any heat gain during the mounting of the specimens in the test setup, which took about 2 minutes per specimen. The specimens tested at +60°C were conditioned for 24 hours in an oven at +63°C (±1°C); again with an additional 3 degrees to compensate for any heat loss during the mounting of the specimens in the test setup.

7.3.2. Bending test setup

The beam specimens were tested in four-point bending on either a Zwick Z100 or Instron universal test machine which were provided with a custom-made support frame. The support, load and lateral support span corresponded to the values depicted in Figure 7.5. The beams were loaded at a vertical displacement rate of 1 mm/min until initial failure occurred. Thereafter the test speed was stepwise increased to 2 and 5 mm/minute respectively, to limit the test duration. During all bending test the inflicted load and the vertical displacement of the cross head were measured. The bending tests were conducted at room temperature (+23°C).
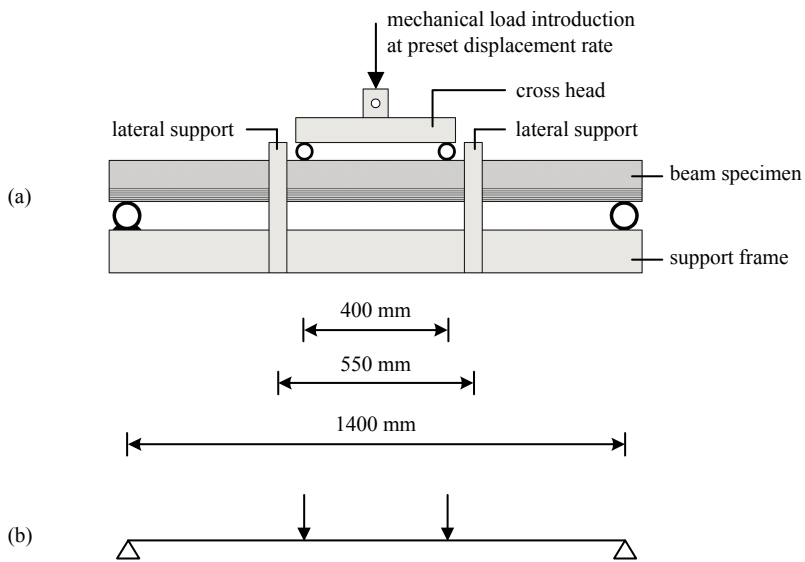
Figure 7.5: Load and support spans applied for the bending tests on the GFRP-reinforced glass beams; (a) schematic representation of the applied custom-made support frame; (b) loading scheme.

7.4. Results

The results of the pull-out and bending tests are separately presented in the following sections.

7.4.1. Pull-out test results

The results of the pull-out tests at -20, +23 and +60°C are presented in Table 7.2. Additionally, Figure 7.6 shows the load-displacement diagrams of the pull-out tests.

The pull-out specimens showed a capacity of carrying increasing loads until bond failure occurred, which caused a drop in load. For some pull-out specimens a residual pull-out resistance remained, which either gradually dropped or caused a hysteresis effect in the load-displacement diagram, see e.g. Figure 7.6 (a), (c) and (d).

Before reaching the ultimate pull-out load, some pull-out specimens showed partial failure of the GFRP rods. Some of the glass-fiber filaments within the resin matrix broke, while the majority remained intact. This partial failure of the GFRP rods caused disruptions in the load-displacement diagrams, see Figure 7.6.

Table 7.2: Overview of the experimental results of the GFRP pull-out tests.

Maximum load		Round			Flat		
		-20°C	+23°C	+60°C	-20°C	+23°C	+60°C
Specimen #I	[kN]	2.9	3.3	2.4	10.7	8.4	9.0
Specimen #II	[kN]	3.1	3.2	2.2	10.7	9.4	8.5
Specimen #III	[kN]	n/a	n/a	n/a	n/a	9.4	6.4
mean	[kN]	3.0	3.2	2.3	10.7	9.1	8.0
st.dev	[kN]	0.1	0.0	0.1	0.0	0.6	1.4
rel.st.dev.	[%]	4.4	1.5	4.9	0.0	6.6	17.3

Pull-out test results of the specimens
with the *round* GFRP rods

(a)

Pull-out test results of the specimens
with the *flat* GFRP rods

(b)

-20°C

(c)

(d)

+23°C

(e)

(f)

+60°C
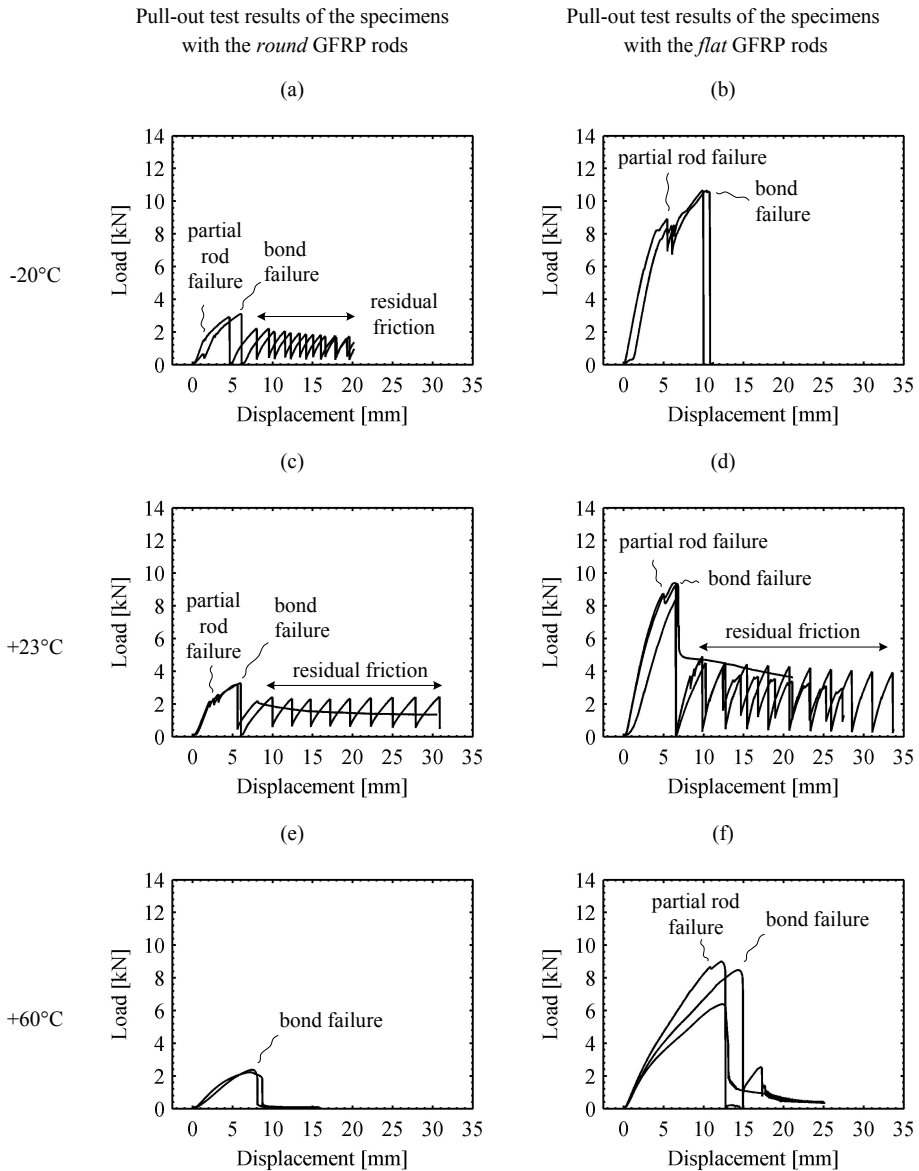
Figure 7.6: Load-displacement diagrams of the pull-out tests on the specimens with the GFRP rods.

7.4.2.   Bending test results

The results of the bending tests are presented in Table 7.3. Additionally, Figure 7.7 provides the load-displacement diagrams and a schematic representation of the cracking sequence of the beam specimens. This cracking sequence is numbered 1-3 which correlates to the letters in the load-displacement diagrams.

The beams showed linear elastic response until initial glass failure occurred. A V-shaped crack occurred in the glass, see Figure 7.7 (1), which ran in only one of the two glass sheets. After a drop in load, the load increased again and additional cracks occurred in the glass beams, see Figure 7.7 (2). As loading was continued the cracks gradually started to propagate and additional cracking occurred. Between the loading and support points typical diagonal shear cracks occurred, see Figure 7.7 (3). At the end of the loading procedure the cracks in the beams were more or less evenly divided along the beam.

For the beams with the round GFRP reinforcement rods the tests had to be stopped at a displacement level of about 60 to 70 mm. At this stage the ultimate displacement capacity of the test setup had been reached. For the beams with the flat GFRP reinforcement rods, the test setup had been adapted to enlarge the displacement range. One beam with flat GFRP rods ultimately failed due to explosive glass failure at the tensile zone, whereas the other failed due to explosive glass failure at both the compression and tensile zone.

Table 7.3: Experimental results of the bending tests on the GFRP reinforced glass beams.

		Beams with round rods	Beams with flat rods
Initial failure load			
Specimen #I	[kN]	5.7	5.0
Specimen #II	[kN]	7.8	6.0
mean	[kN]	6.8	5.5
st. dev.	[kN]	1.5	0.8
rel. st .dev.	[%]	22.2	13.8
Maximum post breakage load			
Specimen #I	[kN]	7.9	11.9
Specimen #II	[kN]	7.7	11.3
mean	[kN]	7.8	11.6
st. dev.	[kN]	0.1	0.5
rel. st .dev.	[%]	1.4	4.0
Max.post-breakage load / initial load			
Specimen #I	[%]	138.6	239.5
Specimen #II	[%]	98.9	186.1
mean	[%]	118.8	212.8
st. dev.	[%]	28.1	37.7
rel. st .dev.	[%]	23.6	17.7
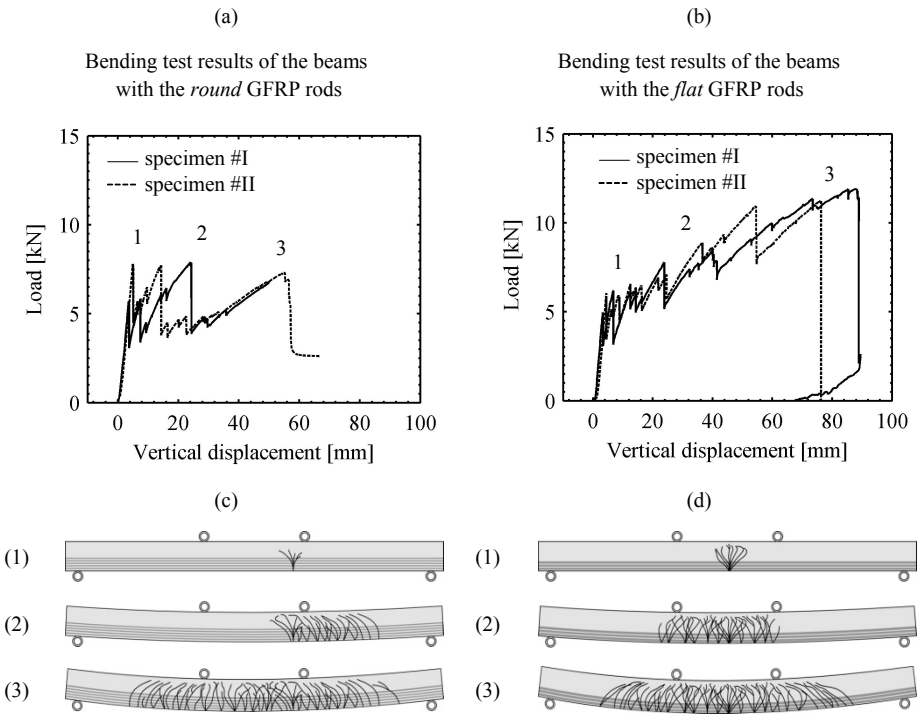
Figure 7.7: Results of the bending tests on the GFRP-reinforced glass beams.

7.5.   Discussion pull-out tests

The performance of the pull-out specimens and the influence of the test temperature on this performance are discussed in the following sub-sections.

7.5.1.   *Pull-out performance*

The results of the pull-out tests demonstrate that bonding a GFRP reinforcement rod to glass, using the SG interlayer, is a feasible concept. Both the specimens with the round and the specimens with the flat GFRP rods showed relatively high pull-out strength levels. This indicates that GFRP rods could both be feasible as embedded reinforcement in SG-laminated glass beams.

The pull-out specimens demonstrated differences in strength performance between the specimens with the round and with the flat GFRP rods. The pull-out strength of the specimens with the flat GFRP rods was larger than the pull-out strength of the specimens with the round GFRP rods. At all temperature levels the specimens with the flat rods reached higher pull-out strength levels than the specimens with the round rods.

This difference in pull-out strength strength is directly related to the difference in bond area between the round and flat GFRP rods. Whereas the circumference of the round rods amounts to $\pi*1^2 = 6.3$ mm, it amounts to $0.8 + 0.8 + 6 + 6 = 13.6$ for the flat specimens. This means that the bond area between the SG interlayer and the glass fiber rods is about twice as large for the flat rods than for the round rods. Although for both the round and flat GFRP rods not the full circumference of the rods will be contributing as significant to the shear transfer, their difference in shear transferring area remains significant. As a result of the large shear transfer area, the flat rods show a high shear transfer capacity and consequently high pull-out strength.

Additionally, the difference in pull-out strength performance of the specimens with the round and flat GFRP rods might have, to some extent, also been caused by a difference in resin matrix. Whereas the round rods have been made with a polyester resin, the flat rods have been made with an epoxy resin. There might be a difference in the adhesion of the SG interlayer to the cured polyester and epoxy resin. However, this possible difference in bond strength cannot be derived from the tests performed within this research and requires additional testing.

7.5.2. Influence of test temperature

Similar to the pull-out test results presented in Chapter 5, the GFRP pull-out specimens demonstrated differences in pull-out strength at the different test temperatures. This difference is illustrated in Figure 7.8, which shows a bar graph of the average pull-out strength per specimen geometry (round or flat GFRP rod) and per test temperature (-20, +23 and +60°C).
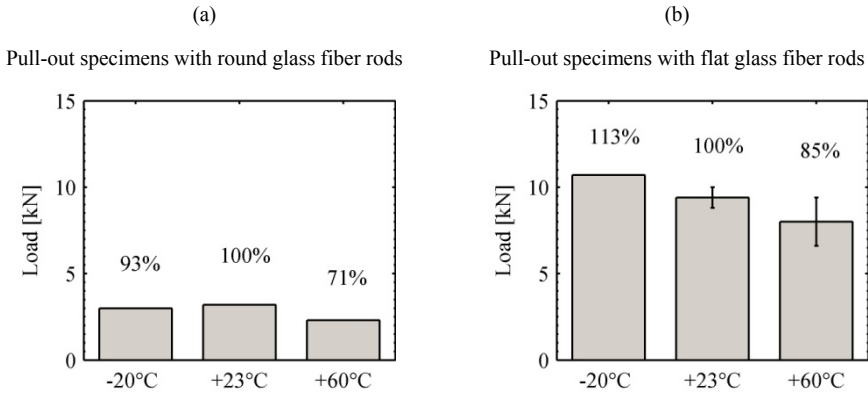
Figure 7.8: Bar graph of the mean pull-out strength values per specimen type and temperature level. Room temperature (+23°C) has been set as a reference temperature (100%). It should be noted that the error bars are only plotted for the series that consist of 3 specimens.

At +23°C the pull-out strength of the specimens – both the specimens with the round and the flat rods – was relatively high. Due to a high shear stiffness of the SG interlayer at this temperature level the shear transfer capacity of the specimens and related pull-out strength was large.

At +60°C the pull-out strength and stiffness of both the specimens with the round rods and the specimens with the flat rods was smallest. This reduced pull-out strength and stiffness is explained by the reduced shear stiffness of the SG interlayer at and above its glass transition temperature of ~ +55°C, see Chapter 4. Due to this reduced shear stiffness the shear transfer capacity of the SG interlayer is limited, which limits the pull-out strength performance of the specimens. However, it should be noted that the scatter in the results of the specimens with the flat rods tested at +60°C is relatively large. Some of them almost reached pull-out strength values similar to the pull-out strength values at +23°C. It seems that for those specimens the relatively large bond area of the flat glass fiber rods, as has been showed in the previous section, largely compensates for the loss in shear stiffness of the SG interlayer.

At -20°C the pull-out strength of the specimens with the flat rods increased compared to +23°C, whereas it slightly decreased for the specimens with the round rods. For the specimens with the flat rods, the increased pull-out strength was even sufficient to cause full failure of the GFRP rods, see Figure 7.9 (d). The tendency of increasing pull-out strength at lower temperature levels, which has also been observed in Chapter 5 for metal inserted pull-out specimens, is in line with an increased shear stiffness of the SG interlayer at lower temperatures. The decrease in pull-out strength of the specimens with the round rods tested at -20°C does not fit this line of reasoning and might have been caused by a geometrical effect of the round rods or by the polyester matrix. However, no specific explanation for this decrease in pull-out strength of the round specimens at -20°C has been found. Furthermore, it should be noted that the number of specimens was very small. Additional testing will be necessary to confirm the decrease in pull-out strength of the specimens with the round rods at -20°C.

tested specimens with round GFRP rods   tested specimens with flat GFRP rods

(a)   (b)   (c)   (d)   (e)   (f)

-20°C   +23°C   +60°C   -20°C   +23°C   +60°C
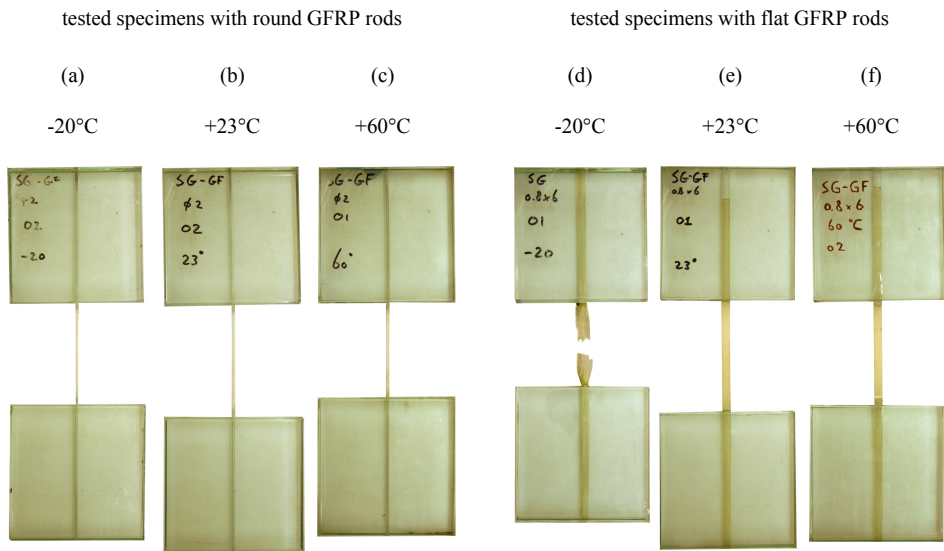
Figure 7.9: Photographs of exemplary GFRP pull-out specimens after the pull-out test.

7.6. Discussion bending tests

The results of the bending tests demonstrate that embedding a GFRP reinforcement rod in the SG interlayer of the beam can be a feasible concept. The beams displayed significant post-breakage strength and stiffness. Despite the absence of a plastic deformation capacity of the GFRP rods, the beams even showed a semi-ductile post-breakage response. This semi-ductility originated from repetitive cracking of the glass and local elongation of the GFRP rods, which gradually reduced the post-breakage stiffness of the beam. Possibly the gradual reduction in post-breakage stiffness was further stimulated by local debonding of the GFRP rods, which allows for an enlarged elongation of the GFRP rods and consequently larger crack opening displacement. However, whether the latter mechanism occurred during the tests could not be observed nor derived from the results.

Overall, the beams with the flat GFRP rods reached higher post-breakage strength levels than the beams with the round GFRP rods. This difference is mainly caused by a difference in strength of the applied reinforcement in the beams. Whereas the total tensile load capacity of the five round rods amounts to 25.2 kN (5*5.0 kN), the total tensile load capacity of the three flat rods amounts to 32.3 kN (3*10.8 kN). The higher total tensile load capacity of the flat GFRP effectively enhances the post-breakage strength of the beams. Furthermore, the flat GFRP rods are located more towards the tensile edge of the beam, than the round GFRP rods, see Figure 7.3. This increases the internal lever arm between the compressive force in the glass and the tensile force in the reinforcement, which effectively increases the total moment capacity of the beams.

Although not all beam specimens have been tested to full destruction, some noteworthy 'failure' modes occurred.

Firstly, one beam with round GFRP reinforcement rods (beam #II) developed a kind of plastic hinge. This plastic hinge drastically limited its bending stiffness, as can be seen at the very end of its load displacement diagram in Figure 7.7 (a), and caused the beam to crack in two parts, as can be seen in Figure 7.11 (b). Similar plastic hinges have been observed for the metal-reinforced beams, described in Chapter 5, and are the result of local delamination of reinforcement and concentrated crack growth through all sheets of the beam laminate. For the metal-reinforced beams the moment capacity of the plastic hinge is governed by yielding of the metal reinforcement, which causes a reduction in stiffness of the overall beam response. Since the GFRP rods do not show any plastic deformation, the reduction in bending stiffness, as is observed in Figure 7.7 (a), is probably the result of local debonding of the glass fiber rods and progressive glass cracking towards the compression zone. This allows for larger crack opening displacements and consequently a reduction of the overall bending stiffness.

Secondly, the beams with the flat GFRP reinforcement rods showed explosive final failure. For beam #I with flat rods the glass suddenly detached at the tensile zone, see Figure 7.10 (c), causing collapse of the beam. For beam #II with flat rods the glass detached both at the tensile and the compression zone, see Figure 7.10 (d). As locally no compression zone remained, the beam buckled within the test setup, see Figure 7.11 (b). Although explosive glass failure has been observed before at the compression zone of reinforced glass beams, see Chapter 6, it has not been observed before at the tensile zone. The explosive detachment of glass at the tensile zone is most likely the result of a combined action of high stress within the glass and a very large deformation of the beam laminate. The beams with the flat GFRP reinforcement rods reached significant post-breakage strength levels, while simultaneously reaching a deformation displacement of about 65 to 80% of the beam height. It is expected that this combined action of high stress and large deformation, caused the glass to be catapulted from the beam laminate. However, further study will be necessary to understand this phenomena.
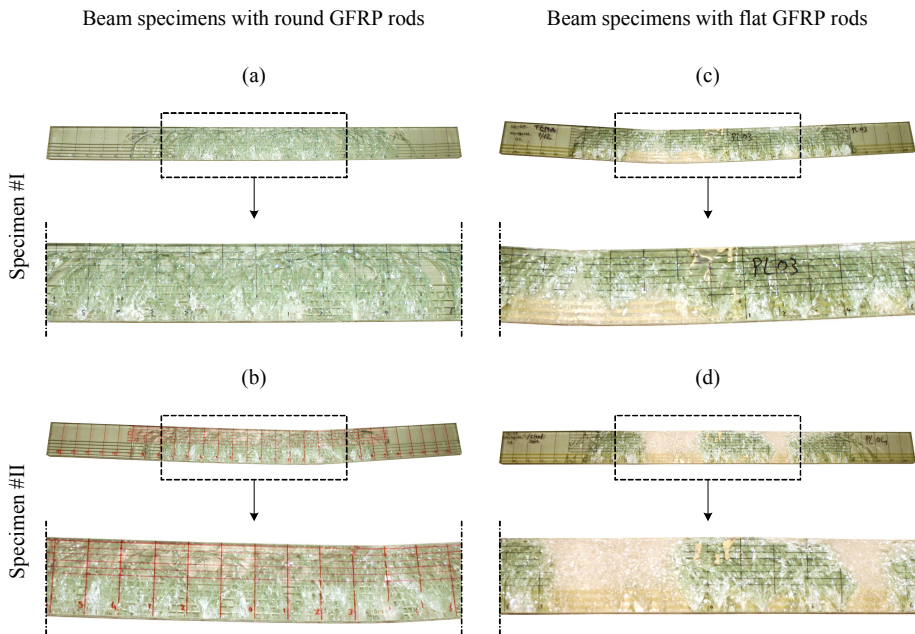
Figure 7.10: Photographs of tested GFRP-reinforced glass beam specimens.
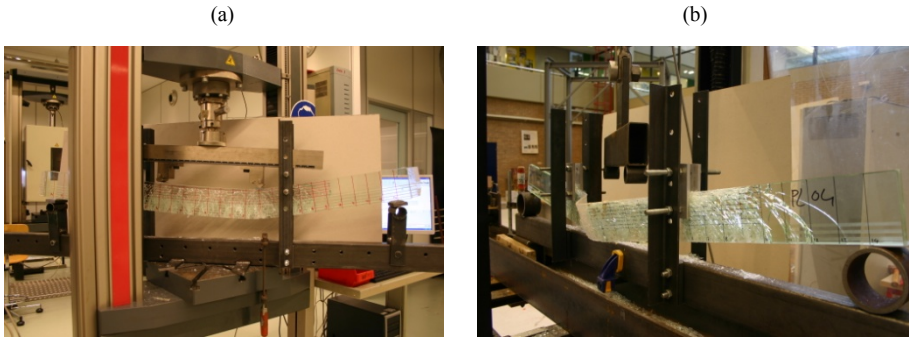
Figure 7.11: Photographs of GFRP-reinforced glass beams at the end of the bending tests;
(a) beam #II with round rods cracks open in two parts; a 'plastic hinge' forms.
(b) beam #II with flat rods buckles due to explosive glass failure.

7.7.   Conclusions

From the pull-out tests it is concluded that it is feasible to bond a GFRP reinforcement rod to glass with significant bond strength, using the SG interlayer. Both the specimens with the round and the specimens with the flat GFRP rods showed relatively high pull-out strength levels. However, the pull-out strength of the specimens with the flat rods is superior to the pull-out strength of the specimens with the round rods. At all test temperatures (-20, +23 and +60°C) the specimens with the flat rods showed higher pull-out strength levels. This superior performance is mainly the result of the larger bond area of the flat specimens compared to the round specimens.

From the bending tests it is concluded that embedding a GFRP reinforcement rod in the SG interlayer of the beam can be a feasible concept, which provides the beam significant post-breakage strength and stiffness. Despite the absence of a plastic deformation capacity in the GFRP rods, the beams showed semi-ductile post-breakage response, which mainly originated from repetitive cracking of the glass and local elongation of the GFRP rods.

Overall, it is concluded that embedding semi-transparent GFRP reinforcement rods in SG-laminated glass beams is a very promising concept, which provides redundant post-breakage beam response. Their excellent structural performance combined with their transparent appearance make the beams highly appealing for structural and architectural applications.

Chapter 8
Analytical and numerical modelling of the structural response

This chapter focuses on the analytical and numerical modelling of the structural response of reinforced glass beams. The experimental results of Chapters 5 and 6 are used as a reference to validate the models. The findings from the analytical and numerical investigations are implemented in the integrated discussion of the structural response of reinforced glass beams, which is presented in Chapter 9.

Abstract

An analytical and a numerical model to describe the structural response of reinforced glass beams are investigated in this chapter. The analytical model has been developed in this research in analogy with reinforced concrete. The 2D numerical model makes use of DIANA Finite Element Analysis software and a novel user-defined subroutine to perform a sequence of linear elastic analyses in which cracking of the glass and plastic deformation of the reinforcement is simulated by means of saw-tooth reduction diagrams. Both models are validated by comparing their results to the experimental results of three different GB-bonded and SG-laminated beam geometries that have been tested at room temperature in Chapters 5 and 6. This comparison demonstrates that the results of the models, in terms of load-displacement diagrams, correspond fairly well to the experimental results of the GB-bonded beams. For the SG-laminated beams, however, the models tend to underestimate the post-breakage strength. This difference is caused by an additional load-carrying mechanism which is generated by crack-bridging glass fragments that transfer forces over the crack through shear in SG interlayer. Since the models neglect any layering of the glass, this mechanism is not accounted for. Furthermore, the comparison of the model results with the experimental results demonstrates that the numerically obtained cracking sequences are mainly indicative and insufficiently consistent with the experimental results. Moreover, the geometry and number of cracks resulting from the numerical model are dependent on model parameters such as mesh size, mesh geometry and shear retention factor. Overall, it is concluded that both the analytical and numerical model provide a promising method for describing the post-breakage strength of reinforced glass beams. However, both models currently neglect the layering of the glass and the bond between the glass and the reinforcement. Further studies should focus on incorporating bond-slip and layering of the glass, to further increase the accuracy of the model results.

Background information

Research done in collaboration with

Analytical model:

- Gerrie Hobbelman,
  Faculty of Architecture, TU Delft, The Netherlands

Numerical model:

- Anne van de Graaf, Max Hendriks,
  Faculty of Civil Engineering and Geosciences, TU Delft, The Netherlands

- Daniele Trovato,
  Politecnico di Torino, Italy

8.1. Introduction

This chapter focuses on the analytical and numerical modelling of the structural response of reinforced glass beams. The analytical model has been developed in this research in analogy with the reinforced concrete theory. The numerical model makes use of a novel user-defined subroutine in the DIANA Finite Element Analysis software. Both models are briefly introduced below.

The analytical model has been developed in this study based on the analytical models used for describing the structural response of reinforced concrete [Braam & Lagendijk, 2008; Walraven, 2006]. Since reinforced glass shows – especially at the post-breakage stage – large similarities with reinforced concrete, it is expected that this analogy is valid. Based on the reinforced concrete theory, equations have been derived in this study which can be used to construct either an M-κ (moment-curvature) diagram or an F-δ (force-displacement) diagram for reinforced glass beams. The latter can be used for a direct comparison with load-displacement diagrams obtained from experiments.

The numerical model makes use of the DIANA Finite Element Analysis software. Firstly, a 2D numerical model is built using plane stress elements for the glass and truss elements for the reinforcement. Secondly, a novel user-defined subroutine, which is currently under development at Delft University of Technology [Van de Graaf, Hendriks & Rots, 2009; Van de Graaf, Hendriks & Rots, 2010], is applied to run a sequence of linear elastic analyses. This Sequentially Linear Analysis (SLA) technique, which was introduced by Rots and further developed by Rots, Belletti & Invernizzi, De Jong et al. and Van de Graaf [DeJong, Hendriks & Rots, 2008; Rots, 2001; Rots, Belletti & Invernizzi, 2008; Van de Graaf, 2008], is especially suited to address the problems associated with the numerical modelling of brittle materials. As a result of brittle material response 'standard' non-linear analysis techniques often run into convergence problems. The SLA technique avoids these problems by replacing the 'standard' incremental-iterative analysis scheme by a series of scaled linear analyses. Furthermore, the nonlinear stress-strain law is replaced by a saw-tooth reduction diagram. In the current research this SLA technique and the associated saw-tooth reduction diagrams are used to simulate both cracking of the glass and yielding of the reinforcement. The numerical model describes the structural response of reinforced glass beams in terms of load-displacement diagram and cracking sequence.

To validate both the analytical and the numerical model, they have been applied to describe the structural response of three different beam types. These beam types have been experimentally investigated in Chapter 5 and 6. By comparing the model results with the experimental results, the models have been validated. Additionally, the consistency of the numerical model has been investigated by varying the mesh size, mesh geometry and other model parameters.

Section 8.2 presents the three different beam types that are analyzed in this chapter. Subsequently, sections 8.3 and 8.4 describe the analytical and numerical models in more detail. Thereafter, the results of the analytical and numerical models and a comparison of the model results with the experimental results is provided and discussed in sections 8.5 and 8.6. Additionally, the effects of several parameters of the numerical model on its results are described. Finally, section 8.7 provides the conclusions from the study presented in this chapter.

8.2.   Beam types

The three different beam types that are analyzed in this chapter are presented in Figure 8.1, 8.2 and 8.3. Beam type I, see Figure 8.1, refers to the 1.5 m GB-bonded and SG-laminated reinforced glass beams with a hollow section stainless steel reinforcement, investigated in Chapter 5. Beam type II, see Figure 8.2, refers to the 1.5 m SG-laminated beams with a solid section stainless steel reinforcement, investigated in Chapter 6. Beam type III, see Figure 8.3, refers to the 3.2 m SG-laminated stainless steel reinforced glass beams investigated in Chapter 6.

Physically, all beam types consist of a triple-layer glass laminate with a square reinforcement section bonded at the inner recessed edge. For the analytical and numerical models, the beams have been translated to solid section beams. The adhesive or interlayer bond between the individual glass sheets and between the glass and the reinforcement has not been incorporated. It is assumed that the glass is rigidly interconnected and that the reinforcement is also rigidly connected to the glass without the possibility of any bond-slip. A schematic representation of the assumed cross-sections for the analytical and numerical models is displayed in Figures 8.1(b), (c), 8.2 (b), (c) and 8.3 (b), (c).

			(a) Physical		(b) Analytical	(c) Numerical
			GB	SG		
Section dimensions outer glass layers	$b*h$	[mm]	6*125 [i]	6*125 [i]	-	-
Section dimensions inner glass layer	$b*h$	[mm]	10*115 [i]	10*115 [i]	-	-
Section dimensions reinforcement	$b*h*t$	[mm]	10*10*1 [i]	10*10*1 [i]	-	-
Thickness bondline	t_{bond}	[mm]	≈ 0.1 [i] (GB)	1.52 [i] (SG)	-	-
Beam width	b_{beam}	[mm]	22.2 [ii]	25.04 [iii]	22 [iv]	22 [iv]
Beam height	h_{beam}	[mm]	125 [i]	125 [i]	125	120 [v]
Beam length	l_{beam}	[mm]	1500 [i]	1500 [i]	1500	1500
Reinforcement area	A_{re}	[mm^2]	36 [i]	36 [i]	36	36
Glass area	A_{gl}	[mm^2]	2650 [i]	2650 [i]	2650	2530
Initial bending stiffness [vi]	$EI_{composite}$	[Nmm^2]	2.51*10^{11}	2.51*10^{11}	2.51*10^{11}	2.46*10^{11}

[i]   Nominal values

[ii]   Nominal width, including 2 bond lines with a nominal thickness of $t ≈ 0.1$ mm each.

[iii]   Nominal width, including 2 interlayers with a nominal thickness of $t = 1.52$ mm each (before lamination).

[iv]   Only the nominal width of the glass is accounted for in the models; $2*6$ mm $+ 1*10$ mm $= 22$ mm. Adhesive layers or foil interlayers are disregarded in the models.

[v]   In order to obtain a similar moment of inertia as the physical beam, the section height of the numerical model has been based on the distance between the upper beam edge and the axis of the reinforcement.

[vi]   Calculated according to Equation 8.2; for the physical beam based on the nominal dimensions.

Figure 8.1: Physical, analytical and numerical cross section of beam type I.

		(a)	(b)	(c)
		Physical	Analytical	Numerical

Beam type II

			Physical	Analytical	Numerical
Section dimensions outer glass layers	$b*h$	[mm]	$6*125$ [i]	-	-
Section dimensions inner glass layer	$b*h$	[mm]	$10*115$ [i]	-	-
Section dimensions reinforcement	$b*h*t$	[mm]	$10*10*1$ [i]	-	-
Thickness bond line	t_{bond}	[mm]	1.52 [i] (SG)	-	-
Total beam width	b_{beam}	[mm]	25.04 [ii]	22 [iii]	22 [iii]
Total beam height	h_{beam}	[mm]	125 [i]	125	120 [iv]
Beam length	l_{beam}	[mm]	1500 [i]	1500	1500
Reinforcement area	A_{re}	[mm^2]	100 [i]	100	100
Glass area	A_{gl}	[mm^2]	2650 [b]	2650	2530
Initial bending stiffness [v]	$EI_{composite}$	[Nmm^2]	$2.91*10^{11}$	$2.91*10^{11}$	$2.87*10^{11}$

[i]   Nominal values

[ii]   Nominal width, including 2 interlayers with a nominal thickness of $t = 1.52$ mm each (before lamination).

[iii]   Only the nominal width of the glass is accounted for in the models; $2*6$ mm + $1*10$ mm = 22 mm. The foil interlayers are disregarded in the models.

[iv]   In order to obtain a similar moment of inertia as the physical beam, the section height of the numerical model has been based on the distance between the upper beam edge and the axis of the reinforcement.

[v]   Calculated according to Equation 8.2; for the physical beam based on the nominal dimensions.

Figure 8.2: Physical, analytical and numerical cross section of beam type II.

			(a)	(b)	(c)
			Physical	Analytical	Numerical

Beam type III

			Physical	Analytical	Numerical
Section dimensions outer glass layers	$b*h$	[mm]	8*285 [i]	-	-
Section dimensions inner glass layer	$b*h$	[mm]	15*270 [i]	-	-
Section dimensions reinforcement	$b*h*t$	[mm]	15*15*1.5 [i]	-	-
Thickness bond line	t_{bond}	[mm]	1.52 [i] (SG)	-	-
Beam width	b_{beam}	[mm]	34.04 [ii]	31 [iii]	31 [iii]
Beam height	h_{beam}	[mm]	285 [i]	285	277.5 [iv]
Beam length	l_{beam}	[mm]	3200 [i]	3200	3200
Reinforcement area	A_{re}	[mm^2]	81 [i]	81	81
Glass area	A_{gl}	[mm^2]	8610 [i]	8610	8602.5
Initial bending stiffness [v]	$EI_{composite}$	[Nmm^2]	4.18*10^{12}	4.18*10^{12}	4.16*10^{12}

[i]   Nominal values

[ii]   Nominal width, including 2 interlayers with a nominal thickness of t = 1.52 mm each (before lamination).

[iii]   Only the nominal width of the glass is accounted for in the models; 2*8 mm + 1*15 mm = 31 mm. The foil interlayers are disregarded in the models.

[iv]   In order to obtain a similar moment of inertia as the physical beam, the section height of the numerical model has been based on the distance between the upper beam edge and the axis of the reinforcement.

[v]   Calculated according to Equation 8.2; for the physical beam based on the nominal dimensions.

Figure 8.2: Physical, analytical and numerical cross section of beam type III.

8.3.   Analytical model

The analytical model has been developed in this research in analogy with reinforced concrete[i]. Similar to reinforced concrete, the post-breakage load-carrying mechanism in reinforced glass beams is generated by a tensile force in the reinforcement and a compressive force in the (un-cracked) compression zone. However, whereas reinforced concrete demonstrates non-linear behaviour of the compression zone, this is not the case for reinforced glass. Glass responds linear elastically both in tension and compression.

Based on the reinforced concrete theory, equations have been derived which can be used to describe either the M-κ (moment-curvature) relation or the F-δ (force-displacement) relation for reinforced glass beams, see Figures 8.6 and 8.7. For the derivation of these equations it is assumed that the glass responds perfectly linear elastic and that the reinforcement material (i.e. steel) responds elastic-perfectly-plastic, see Figure 8.4. Thus no strain-hardening of the reinforcement material is taken into account. Furthermore, it is assumed that the reinforcement is rigidly connected to the glass. No material parameters for the intermediary bond have been defined. Moreover, the *hypothesis of Bernoulli* (plane sections remain plane after bending) is applied and it is assumed that the strains in the glass and the reinforcement are distributed according to Figure 8.5. For the comparison of the analytical results with the experimental results the material parameters as listed in Table 8.1 are applied.
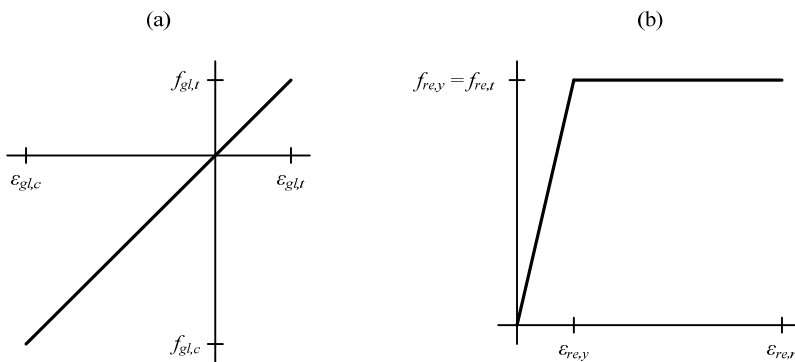
Figure 8.4: Schematic representation of the stress-strain diagrams adopted for the analytical prediction method; (a) stress-strain diagram for the glass; a perfectly linear elastic response both in tension and compression has been assumed; (b) stress-strain diagram for the stainless steel reinforcement; no strain-hardening has been considered, an elastic-perfectly-plastic response has been assumed, and thus $f_{re,y} = f_{re,t}$.

[i] A similar approach has been used by Ølgaard, Nielsen & Olesen [Ølgaard, Nielsen & Olesen, 2009].
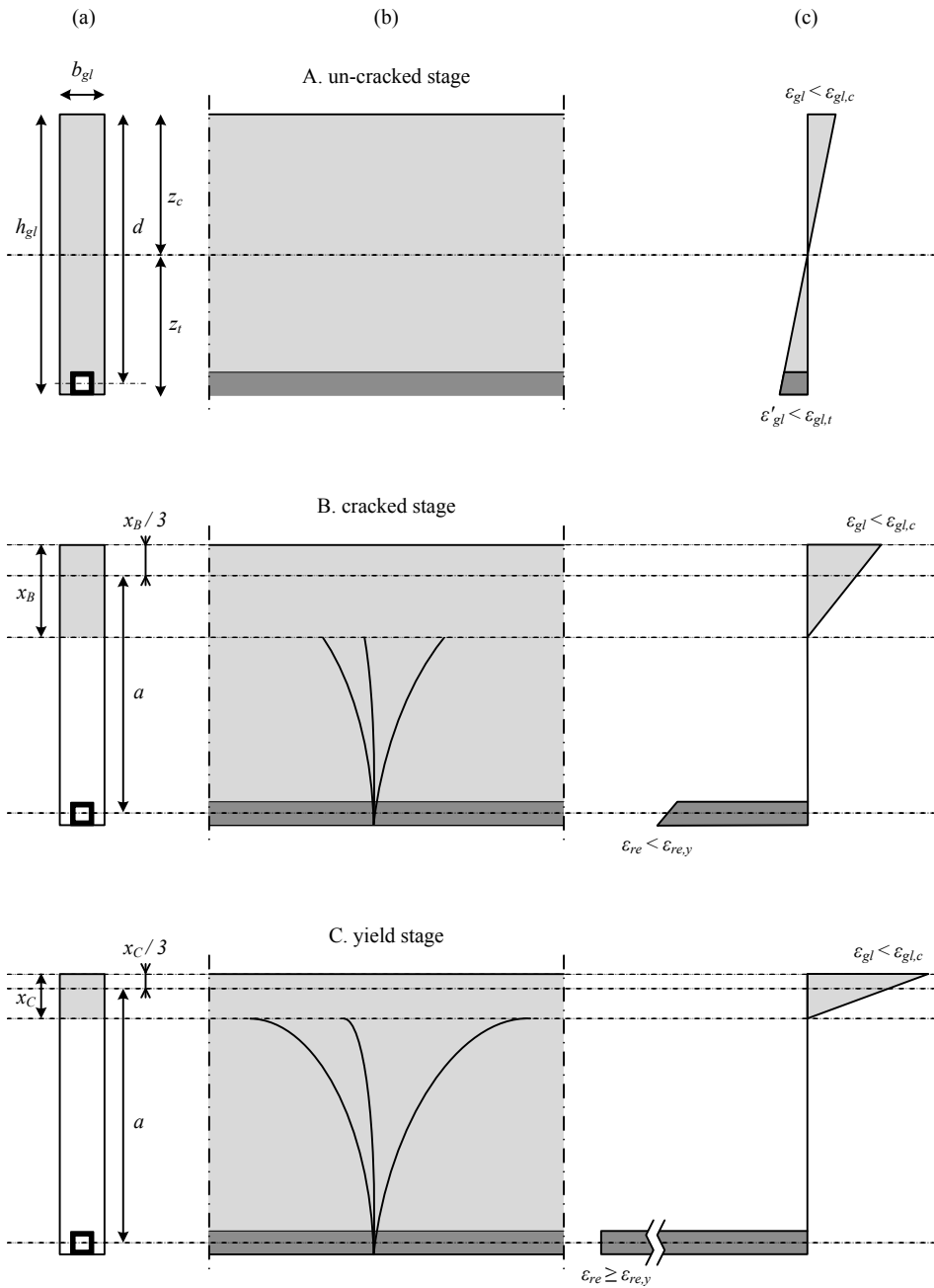
Figure 8.5: Schematic representation of the strain distribution in reinforced glass beams.

Table 8.1: Material parameters adopted for the analytical model.

			Annealed glass			Stainless steel	
Young's modulus	E_{gl}	N/mm^2	70 x10^3	E_{re}	N/mm^2	190 x10^3	
Tensile strength	$f_{gl,t}$	N/mm^2	45 [a]	$f_{re,t} = f_{re,y}$	N/mm^2	853 [b]	
Strain at rupture	-	-	-	$\varepsilon_{re,r}$	%	30 [c]	
Compressive strength	$f_{gl,c}$	N/mm^2	350 [d]	-	-	-	

[a]   taken from [EN 572-2:2004];

[b]   derived from uni-axial tensile tests on stainless steel reinforcement sections, see Figures 8.12 and 8.13.

[c]   derived from uni-axial tensile tests on stainless steel reinforcement sections, see Figures 8.12 and 8.13.

[d]   estimated value.

8.3.1.   Constructing the M-κ diagram

The M-κ diagram shows three different stages, see Figure 8.6. For each stage a different M-κ relation, thus a different equation, applies. The different stages are described and the different equations are provided below. For a full derivation of the equations is referred to Appendix II.
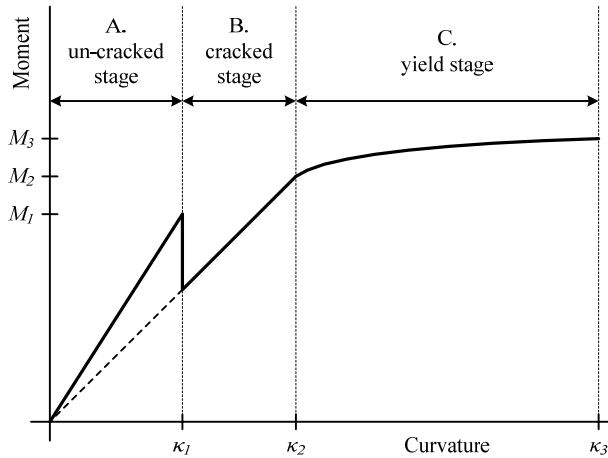
Figure 8.6: Schematic M-κ diagram of a normal-reinforced glass beam
loaded in displacement controlled bending

A)   Un-cracked stage.

At stage A, 'the un-cracked stage', both the glass and reinforcement respond linear elastically, see Figure 8.5. No cracks occur in the glass. The *M-κ* relation at stage A is given by Equation 8.1:

$$\kappa_A = \frac{M}{EI_{composite}} \tag{8.1}$$

with the bending stiffness of the composite beam ($EI_{composite}$) according to Equation 8.2:

$$EI_{composite} = E_{gl} \sum_{i=n}^{n} \left(I_{yy,i} \frac{E_i}{E_{gl}} + z_i^2 A_i \left(\frac{E_i}{E_{gl}} \right) \right) \tag{8.2}$$

with:

i = considered component in the section (either glass or reinforcement)

n = total number of components in the section

z_i = distance between the axis of the considered component and the neutral axis of the beam section

A_i = cross-sectional area of the considered element

E_{gl} = Young's modulus of glass (the main component in the section)

E_i = Young's modulus of the considered component in the section.

$I_{yy,i}$ = moment of inertia of the considered component

The full derivation of Equation 8.2 is provided in Appendix II.

B)   Cracked stage

At stage B, 'the cracked stage', the tensile strength of the glass is exceeded and cracks occur in the glass. The reinforcement bridges the cracks and is loaded in tension within its linear elastic trajectory, see Figure 8.5. The moment capacity of the beam is generated by a compressive force in the glass and a tensile force in the reinforcement. The stiffness of the beam is decreased compared to the linear elastic stage. The *M-κ* relation at stage B is given by Equation 8.3:

$$\kappa_B = \frac{M}{(d - x_B) \cdot (A_{re} \cdot E_{re})\left(d - \frac{x_B}{3}\right)}$$

(8.3)

with the height of the compression zone at stage B (x_B), see Figure 8.5, according to Equation 8.4:

$$x_B = -\left(\frac{A_{re} \cdot E_{re}}{b_{gl} \cdot E_{gl}}\right) + \sqrt{2 \cdot d \cdot \left(\frac{A_{re} \cdot E_{re}}{b_{gl} \cdot E_{gl}}\right) + \left(\frac{A_{re} \cdot E_{re}}{b_{gl} \cdot E_{gl}}\right)^2}$$

(8.4)

and with:

b_{gl} =   width of the glass, see Figure 8.5

d =   distance between top of section and axis of the reinforcement, see Figure 8.5

A_{re} =   cross-sectional area of the reinforcement

E_{gl} =   Young's modulus of glass

E_{re} =   Young's modulus of the reinforcement material

The full derivation of Equations 8.3 and 8.4 is provided in Appendix II.

C)   Yield stage

At stage C, 'the yield stage', the reinforcement starts to yield, see Figure 8.6. Although the tensile force in the reinforcement cannot increase anymore, the moment capacity of the beam can still increase. The cracks in the glass propagate into the initial compression zone, thereby decreasing the height of the compression zone, thus increasing the internal leverarm (*a*) between the compressive and tensile force, see Figure 8.5. This enlarges the moment capacity of the beam. The *M-κ* relation at stage C is given by Equation 8.5:

$$\kappa_C = \frac{2 \cdot A_{re} \cdot f_{re,y}}{9 \cdot b_{gl} \cdot E_{gl} \left(d - \frac{M}{A_{re} \cdot f_{re,y}} \right)^2} \tag{8.5}$$

with:

b_{gl} = width of the glass, see Figure 8.5

d = distance between top of section and axis of the reinforcement, see Figure 8.5.

$f_{re,y}$ = yield strength of the reinforcement

A_{re} = cross-sectional area of the reinforcement

E_{gl} = Young's modulus of glass

E_{re} = Young's modulus of the reinforcement material

The full derivations of Equation 8.5 are provided in Appendix II.

8.3.2.   Constructing the F-δ diagram

Alternative to the M-κ diagram an F-δ (force-displacement) diagram can be constructed, see Figure 8.7. This F-δ diagram is similar to the M-κ diagram, but eases a comparison of the analytical results with the experimental results.
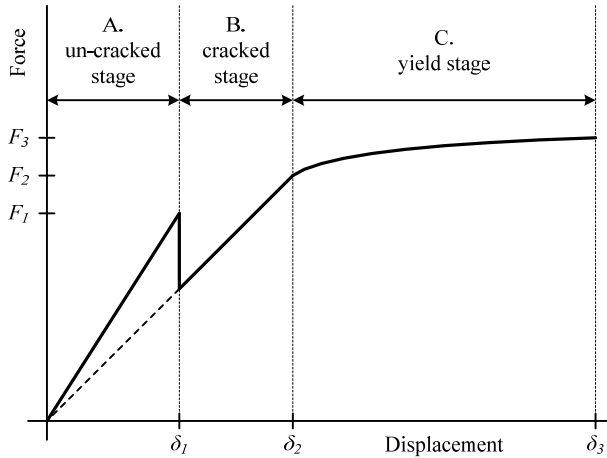
Figure 8.7: Schematic F-δ diagram of a normal-reinforced glass beam
loaded in displacement controlled bending

For the construction of this F-δ diagram Equation 8.6 can be used, which relates the applied force F to the deformation of the beam at mid-span ($\delta_{midspan}$) for beams loaded in four-point bending[i]:

$$\delta_{midspan} = \frac{\frac{F}{2} \cdot a_{setup}}{24 \cdot EI} \cdot \left(3 \cdot l_{setup}^2 - 4 \cdot a_{setup}^2\right) \tag{8.6}$$

with:

$$F = \frac{2 \cdot M}{a_{setup}} \tag{8.7}$$

and with:

a_{setup} = distance between the loading point and the support point, see Figure 8.8

l_{setup} = distance between the beam supports, see Figure 8.8

---

[i] More specifically, Equation 8.6 is a general beam formula that can be used to calculate the deformation at mid-span for a simple beam loaded by two equal and symmetrically placed concentrated loads; i.e. four-point bending loading.

EI = bending stiffness, according to either Equation 8.2, 8.9 or 8.10

F = applied force, see Figure 8.8

M = bending moment at mid-span

Alternatively, Equation 8.8, which relates the applied force F to the deformation underneath the loading points ($\delta_{loadpoint}$), can be used:

$$\delta_{loadpoint} = \frac{\frac{F}{2} \cdot a_{setup}}{6 \cdot EI} \cdot \left(3 \cdot l_{setup} \cdot a_{setup} - 4 \cdot a_{setup}^2\right) \tag{8.8}$$

The latter equation is especially useful for the comparison of the analytical results with the results of the experiments in which the deformation of the beam specimens has been measured by means of the displacement of the cross-head, see Chapters 5 and 6.
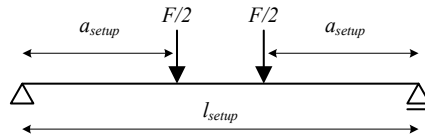
Figure 8.8: Schematic representation of a four-point bending test setup.

The bending stiffness (EI) varies between the different stages. For stage A, the 'uncracked stage', the bending stiffness (EI) can be calculated according to Equation 8.2. At stage B, the 'cracked stage', the bending stiffness is reduced and follows Equation 8.9:

$$EI_B = (d - x_B) \cdot (A_{re} \cdot E_{re}) \cdot \left(d - \frac{x_B}{3}\right) \tag{8.9}$$

with:

d = distance between top of section and axis of the reinforcement, see Figure 8.5.

x_B = height of the compression zone at stage B, according to Equation 8.4

A_{re} = cross-sectional area of the reinforcement

E_{re} = Young's modulus of the reinforcement material

For stage C, the 'yield stage', the bending stiffness follows Equation 8.10:

$$EI_C = \frac{9 \cdot b_{gl} \cdot E_{gl} \cdot \left(\frac{F}{2} \cdot a_{setup}\right) \cdot \left(d - \frac{\left(\frac{F}{2} \cdot a_{setup}\right)}{A_{re} \cdot f_{re,y}}\right)^2}{2 \cdot A_{re} \cdot f_{re,y}} \tag{8.10}$$

with:

a_{setup} = distance between the loading point and the support point, see Figure 8.8

b_{gl} = width of the glass, see Figure 8.5

$f_{re,y}$ = yield strength of the reinforcement

A_{re} = cross-sectional area of the reinforcement

E_{gl} = Young's modulus of glass

F = applied force, see Figure 8.8

8.4.   Numerical model

The numerical method makes use of a 2D model that is built using the DIANA Finite Element Analysis software. Additionally, a novel user-defined subroutine is applied to run a sequence of linear elastic analyses on the 2D model. The main concept of this Sequentially Linear Analysis (SLA) technique is to prevent a negative tangential stiffness for brittle materials, by replacing the 'standard' incremental-iterative analysis scheme by a series of scaled linear analyses, while at the same time replacing the nonlinear softening stress-strain diagram of negative slope by a saw-tooth reduction diagram of positive slopes, see Figure 8.9. In the current study saw-tooth reduction diagrams are applied to simulate both cracking of the glass and yielding of the reinforcement, which implies the use of a smeared crack model.

The following subsections successively describe the setup of the 2D numerical model, the SLA procedure, the smeared crack model, the applied saw-tooth reduction diagrams and a number of model parameters that have been varied in this study to investigate their effects on the numerical results. All the model files, command files and saw-tooth reduction files that have been used in this research are provided in Appendix III.
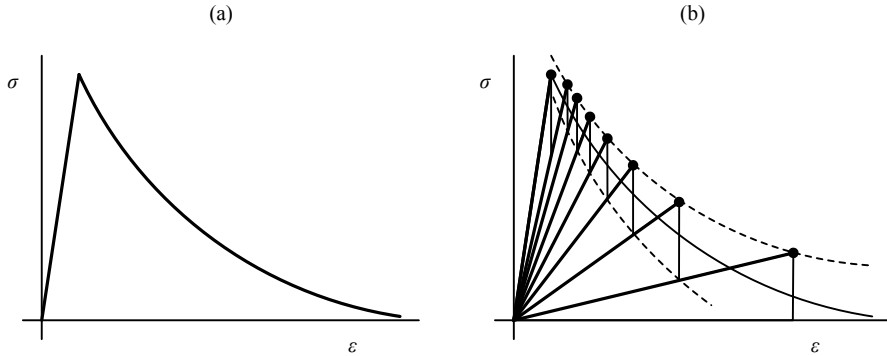
Figure 8.9: Stress-strain diagrams; (a) stress-strain diagram with non-linear softening curve, with negative slope; (b) alternative saw-tooth diagram, with only positive slopes.

8.4.1. Setup 2D model

For the numerical model the beams have been modelled in 2D using DIANA, see Figure 8.10. In this 2D model the glass of the beam has been discretized using either eight-node quadrilateral, or six-node triangular plane stress elements. The reinforcement has been built from quadratic truss elements. The specific element types are presented in Appendix III.

In the 2D model the glass has been modelled as one full section, instead of individual glass layers bonded together, see Figure 8.10. Furthermore, no adhesive or foil interlayers between the glass and the reinforcement have been incorporated in the 2D model. The reinforcement truss elements are directly connected to the quadratic glass elements, thus no bond-slip is incorporated in the model and no bond parameters are defined.
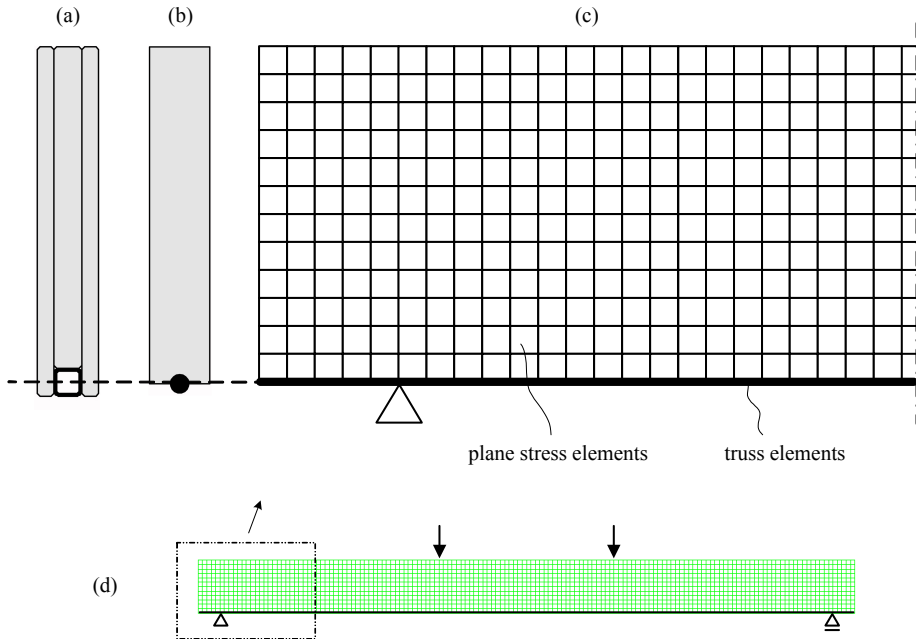
Figure 8.10: Setup of the numerical model; (a) physical cross-section; (b) numerical cross section;
(c) fragment of the applied rectangular mesh; (d) full view of the mesh.

8.4.2.   SLA procedure

During the SLA procedure, the following steps are performed [Van de Graaf, 2008]:

a) A linear-elastic analysis with a representative (unit) load is performed.

b) The element with the largest maximum stress over tensile strength ratio (the critical element) is determined.

c) The representative load is scaled such that a critical stress state is obtained.

d) The stiffness and strength properties of the critical element are updated according to a user-defined saw-tooth reduction diagram (to simulate cracking or plastic deformation of that element).

e) Steps (a) to (d) are repeated until a user-defined number of loops has been reached. This number of loops is selected such that the damage in the beam has spread to the desired level.

For a more extensive description of the SLA procedure is referred to the publications of Van de Graaf [Van de Graaf, 2008; Van de Graaf, Hendriks & Rots, 2009; Van de Graaf, Hendriks & Rots, 2010].

8.4.3.   Smeared crack model

For the numerical procedure a smeared crack model has been applied. The glass and the reinforcement have been modelled as homogeneous isotropic materials with initial material parameters as provided in Table 8.2, see section 8.4.4. When the maximum principal tensile stress exceeds the initial tensile strength of the glass or the reinforcement, a smeared crack is initiated perpendicular to the direction of this principle stress. The initial isotropic constitutive matrix of that 'cracked' or 'plastically deformed' element is replaced by an orthotropic matrix.

In a smeared crack model the true discrete crack with a certain crack opening w is conceived to be a continuum with a crack strain smeared out over the element size, see Figure 8.10. The fracture energy (G_f) is defined as the amount of energy required to create one unit of area of fracture surface. For a discrete crack this energy consumption is equal to the area underneath the stress (σ) versus crack opening (w) diagram, see Figure 8.10(a); i.e. the integral of (σ) versus (w). For a smeared crack, the crack opening is transferred to a crack strain (ε) according to Equation 8.11:

$$\varepsilon = \frac{w}{h_{cbw}} \tag{8.11}$$

with:

h_{cbw} =   crack band width, see Figure 8.10 and Equation 8.12.

w =   crack opening

The crack band width (h_{cbw}) is related to the size of the considered element. Here, it is assumed as the square root of the element area ($A_{element}$) [Rots, 1988], following Equation 8.12:

$$h_{cbw} = \sqrt{A_{element}} \tag{8.12}$$

In this way, smeared crack analyses can be made mesh size objective.

(a)   (b)
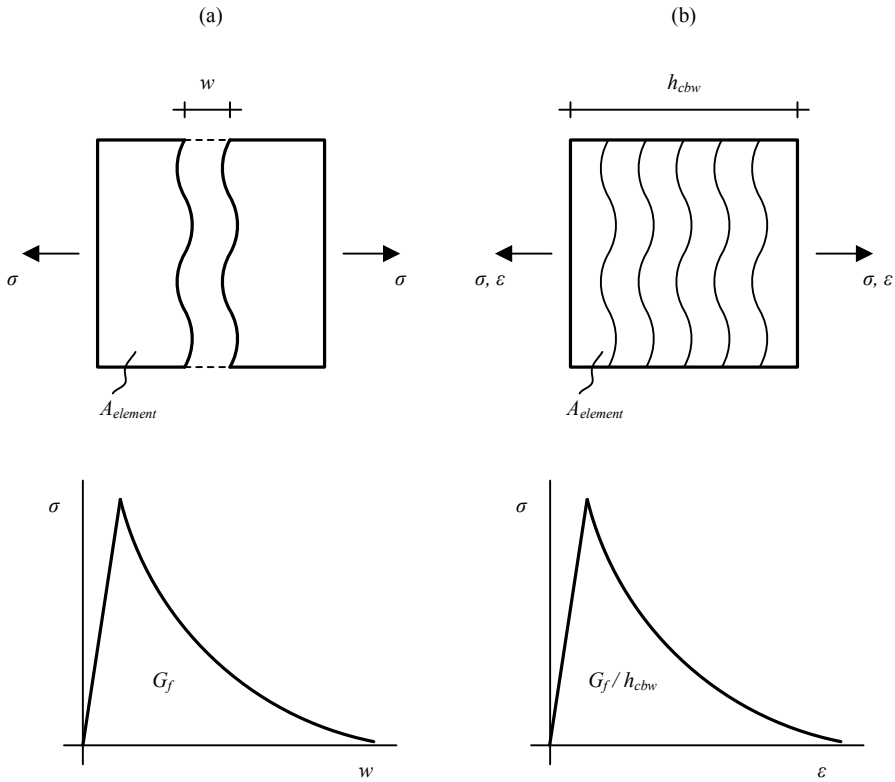
Figure 8.10: Schematic representation of a crack, and schematic representation of the constitutive law for a (a) discrete crack and; (b) smeared crack.

8.4.4. Saw-tooth reduction diagrams

To simulate cracking of the glass or plastic deformation of the reinforcement, the properties of a 'cracked' or 'plastically deformed' element are updated according to user-defined saw-tooth reduction diagrams. These saw-tooth diagrams are separately defined for the glass and the reinforcement.

For the glass, the saw-tooth reduction diagrams have been constructed based on an adopted stress-strain law for glass, which is referred to as 'mother curve', see Figure 8.11. The initial trajectory of this 'mother curve' is constructed based on the adopted initial material parameters (Young's modulus and tensile strength) provided in Table 8.2. The second trajectory of the 'mother curve' is constructed based on the condition that the area underneath the curve should meet G_f/h_{cbw}, see also Figure 8.10. Glass is extremely brittle (i.e. G_f is very small), which implies that for typical values of h_{cbw} the stress-strain diagram shows a negative tangential stiffness or so-called 'snap-back'. For non-linear analyses this snap-back response generally causes severe problems and

divergence of the analysis results. The currently applied SLA technique avoids this snap-back response by defining the saw-tooth reduction diagram, which consists of multiple linear-elastic curves with only positive slopes. Since the linear saw-tooth stiffness is always positive, the analysis always 'converges'.

Table 8.2: Initial material parameters adopted for the numerical model [i].

			Annealed glass	Stainless steel
Initial Young's modulus	E	N/mm^2	$70*10^3$	$190*10^3$
Poisson's ratio	υ	-	0.23	0.265
Initial tensile strength [a]	f_t	N/mm^2	45 [b]	550 [c]
Fracture Energy	G_f	J/m^2	3 [d]	n/a

[a]   After reaching the initial tensile strength the strength and stiffness of the critical element has been updated according to the saw-tooth reduction curves, given in Figure 8.13; see also Figures 8.11 and 8.12;

[b]   Taken from [EN 572-2:2004];

[c]   Derived from uni-axial tensile tests on stainless steel reinforcement sections;

[d]   Taken from [Haldimann, Luible & Overend, 2008];
       However, also other values are available in the literature.

To construct the saw-tooth diagram for the glass, the construction technique as proposed by Trovato [Trovato, 2009] has been applied in the current study. Basically, this construction technique implies the definition of an upper and a lower band along the negative tangent of the mother curve, see Figure 8.11. The total width of the band is related to the desired number of teeth (or: reduction steps). Between the upper and lower band the saw-tooth curve is defined, such that the area underneath the saw-tooth curve equals the area underneath the initial mother curve. This guarantees that the fracture energy associated with the saw-tooth diagram equals the fracture energy associated with the mother curve. For a more detailed description of the construction techniques for saw-tooth diagrams is referred to [Rots, Belletti & Invernizzi, 2008].

---

[i] In the current exploratory study fixed values for the tensile strength and the fracture energy (as provided in Table 8.2) have been applied. Future study may focus on the effect of different values for the tensile strength and the fracture energy (that can be found in the literature) on the numerical results.
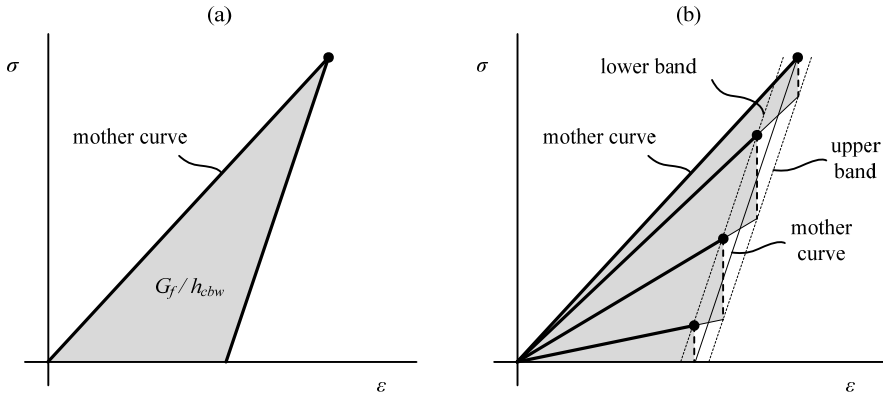
Figure 8.11: Schematic representation of (a) the adopted stress-strain law for glass, 'mother curve'; and (b) the saw-tooth reduction diagram based on the mother curve.

For the stainless steel a similar saw-tooth reduction diagram has been constructed to simulate plastic deformation of the reinforcement section. This saw-tooth diagram has been constructed based on a uni-axial tensile test on the metal reinforcement section, see Figure 8.12. The saw-tooth diagram basically consists of several linear-elastic curves aimed at the uni-axial tensile test curve. The number of teeth (or: reduction curves) defines how well the tensile behaviour of the reinforcement is followed.

It should be noted that Figures 8.11 and 8.12 only provide a schematic representation of the applied saw-tooth reduction diagrams. The actual diagrams that are applied in this research are given in Figure 8.13.
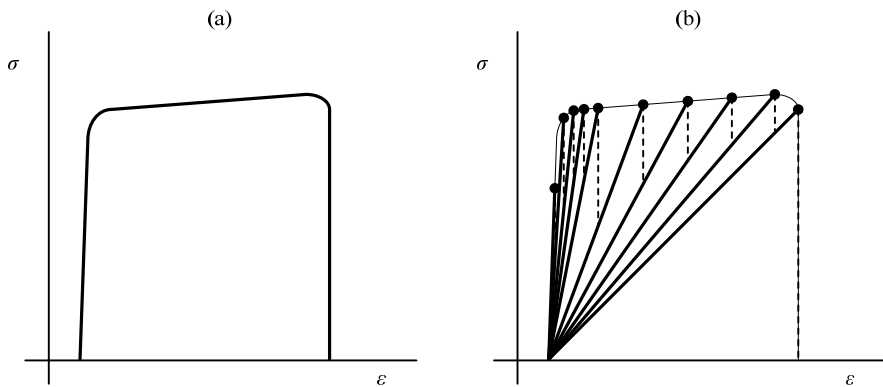
Figure 8.12: Schematic representation of (a) the experimental result of an uni-axial tensile test on a stainless steel reinforcement section; and (b) the saw-tooth reduction diagram based on the uni-axial tensile test result.

8.4.5.   *Variation of model parameters*

To investigate their effect on the numerical results, some model parameters have been varied. This has been done for beam model I, see Table 8.3. For the other beam models (II and III) no variation of model parameters has been applied. The model parameters that have been varied in beam model I are briefly discussed below.

Firstly, the shear retention factor (β) has been varied between 0.001, 0.01, 0.1 and 1 for beam type I models I-1, I-2, I-3 and I-4, see Table 8.3. This shear retention factor defines the reduction in shear stiffness for a 'cracked' element. More specifically, upon cracking the linearly elastic shear modulus (G) of the cracked element is reduced according to the shear retention factor (β). The value of the factor should meet $0 \leq \beta \leq 1.0$, in which 0 represents no shear retention thus full reduction in shear modulus, whereas 1.0 represents full shear retention thus no reduction in shear modulus.

Secondly, the number of reduction steps (rs) in the saw-tooth reduction diagrams of both the glass and reinforcement has been varied between 5 and 10, see Figure 8.13. This has been done for beam type I, models I-1, I-5, I-6 and I-7, see Table 8.3.

Thirdly, the size of the rectangular elements has been altered between 5 and 10 mm square, see Figure 8.14(a), (b). Due to the variation in element size and thus element area ($A_{element}$), the crack band width (h_{cbw}) alters, see Equation 8.12. This variation has been done for beam type I models I-1 and I-8, see Table 8.3.

Finally, the geometry of the elements[i] has been varied between rectangular (r) and triangular (tr), see Figure 8.14(a), (c). This has been done for beam type I models I-1 and I-9, see Table 8.3.

---

[i] The applied element types are described in Appendix III.

Table 8.3: Overview of the numerical models per beam type.

Beam type							I					II	III

		ref.	variation β			variation rs_{gl} & rs_{re}			var. h_{cbw}	var. mg		
modelnr.		I-1	I-2	I-3	I-4	I-5	I-6	I-7	I-8	I-9	II	III
mesh geometry	mg	r	r	r	r	r	r	r	r	tr	r	r
crack band width	h_{cbw}	10	10	10	10	10	10	10	5	7	10	23
shear retention factor	β	0.01	0.001	0.1	1	0.01	0.01	0.01	0.01	0.01	0.01	0.01
reduction steps glass	rs_{gl}	5	5	5	5	5	10	10	5	5	5	5
reduction steps reinforcement	rs_{re}	10	10	10	10	5	5	10	10	10	10	10

mg	=	mesh geometry
r	=	rectangular
tr	=	triangular
β	=	shear retention factor
h_{cbw}	=	crack band width
rs_{gl}	=	reduction steps glass
rs_{re}	=	reduction steps reinforcement
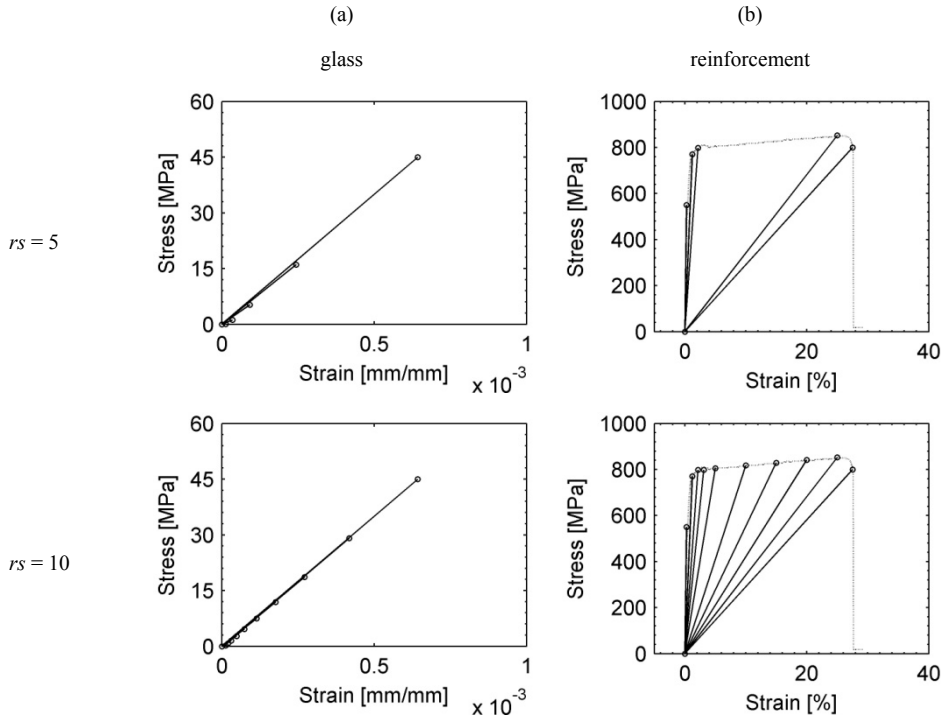
Figure 8.13: Variation of reduction steps (*rs*) for glass and reinforcement for crack band width $h_{cbw} = 10$.

10 mm

Rectangular ($mg = r$)

(a) $A_{element} = 10*10$ mm $= 100$ mm^2

$h_{cbw} = \sqrt{100} = 10$

10 mm

5 mm

Rectangular ($mg = r$)

(b) $A_{element} = 5*5$ mm $= 25$ mm^2

$h_{cbw} = \sqrt{25} = 5$

5 mm

10 mm

Triangular ($mg = tr$)

(c) $A_{element} = 0.5*10*10$ mm $= 50$ mm^2

$h_{cbw} = \sqrt{50} \approx 7$

10 mm
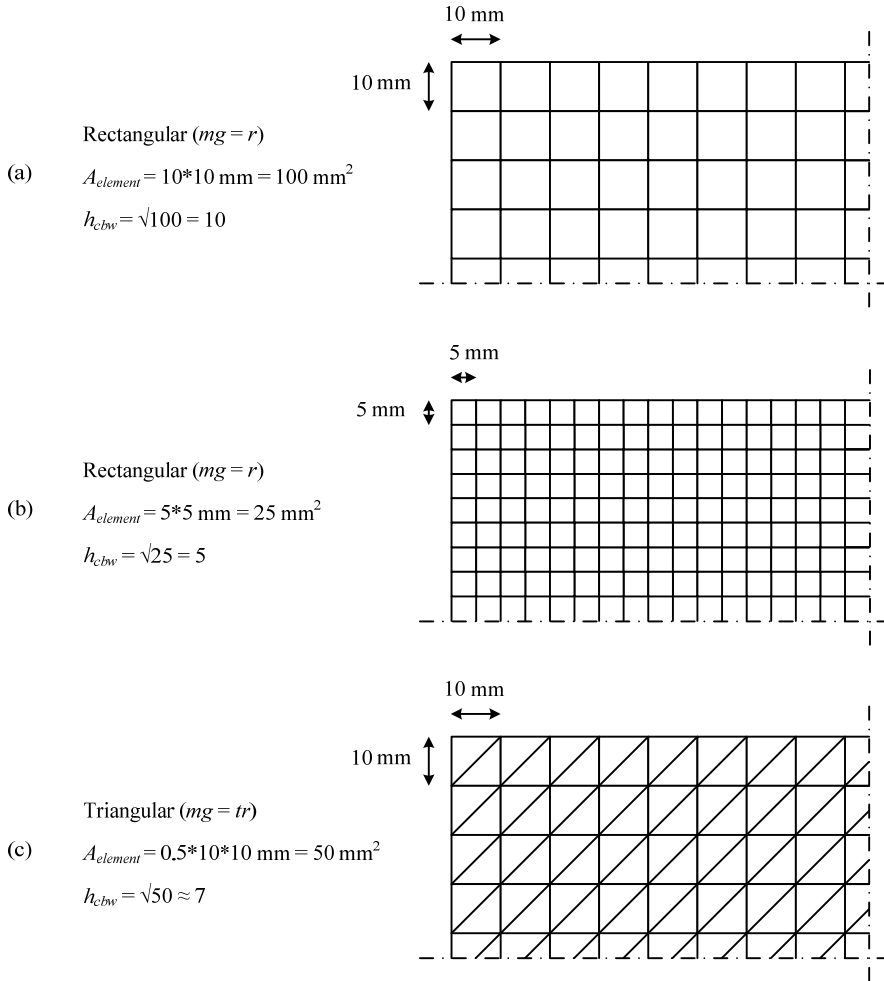
Figure 8.14: Variation of mesh size and mesh geometry for beam type I;
The applied element types are presented in detail in Appendix III.

8.5.   Results

Figure 8.15 displays the results from the analytical and numerical models for the three different beam types. It shows a combined plot per beam type of the analytically generated load-displacement diagram and the numerically generated load-displacement diagram for the numerical models I-1, II and III. Furthermore, Figure 8.15 contains contour plots displaying the reduction in E-modulus of the model elements, which indicates cracking or plastic deformation of that specific model element.

Load-displacement diagrams
resulting from the analytical
and numerical models

Deformed contour plots of the reduced
E-modulus (crack pattern) resulting
from the numerical model.
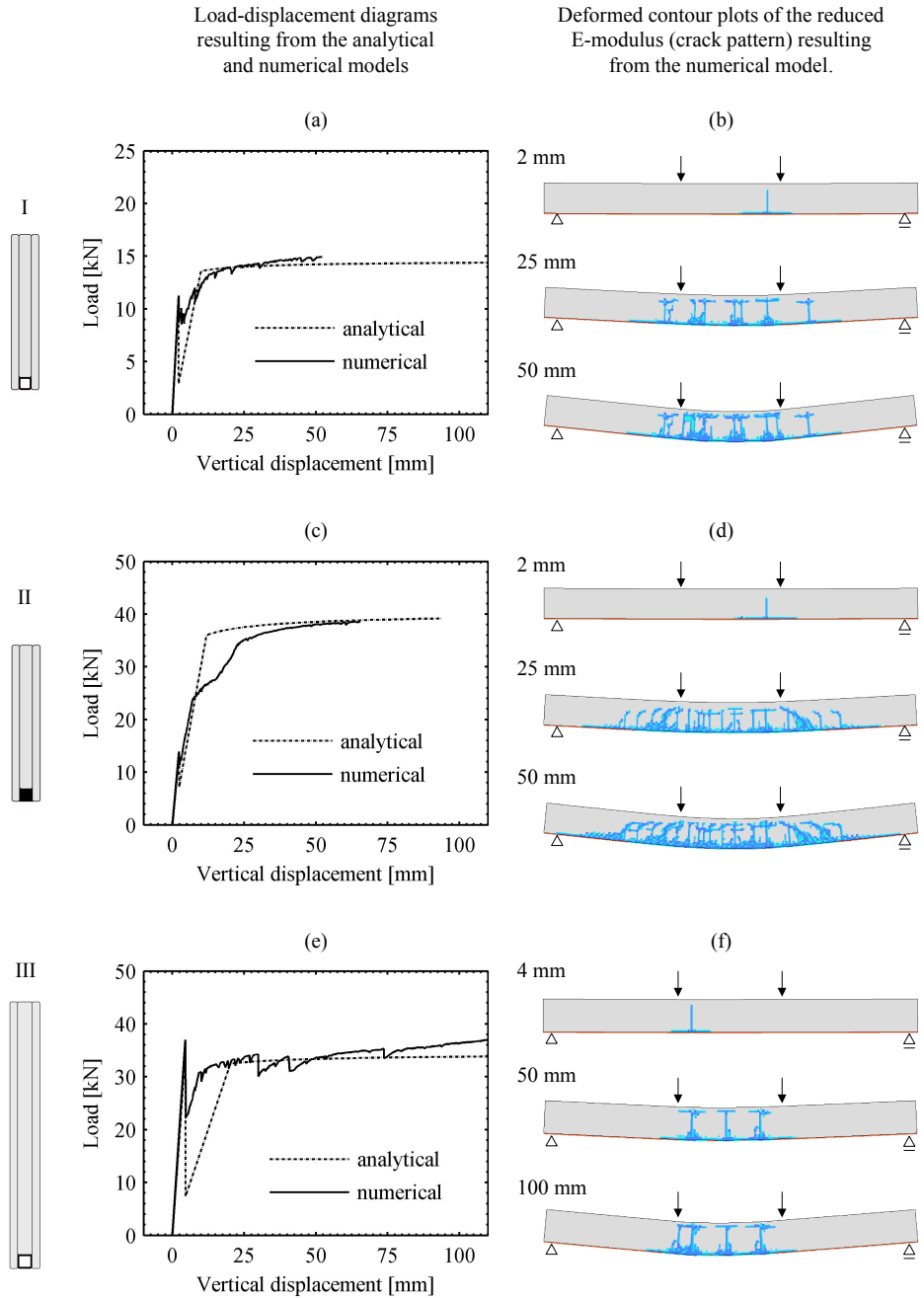
Figure 8.15: Analytical and numerical results for beam type I, II and III.

8.6.   Discussion

In the following subsections a comparison of the analytical, numerical and experimental results is provided. Furthermore, the effects of the variation of model parameters on the numerical results are discussed.

8.6.1.   *Comparison analytical, numerical and experimental results*

From Figure 8.15 it can be seen that the analytical and numerical results are in good agreement with each other in terms of load-displacement diagrams. Compared to the numerical model, the analytical model demonstrates only a small 'undershoot' immediately after initial glass failure (i.e. after the initial peak in the curve). This undershoot is caused by the rather coarse reduction in bending stiffness that is implemented in the analytical model upon initial glass failure. However, despite this initial undershoot, the analytical and numerical model reach similar post-breakage strength values.

From Figures 8.16, 8.17 and 8.18 it can be seen that the analytical and numerical results are in fairly good agreement with the experimental results. Especially the repetitive peaks in the post-breakage response are well simulated by the numerical model, without running into convergence problems. This is due to the fact that the numerical model runs a series of positive-defined linear-elastic analyses by which any divergence of the analysis results is prevented. Although the repetitive peaks in the post-breakage response are not simulated by the analytical model, it generally demonstrates similar post-breakage levels as is observed in the experimental results.

In terms of cracking it should be noted that the numerical model generally predicts the occurrence of only one crack upon initial glass failure, which is similar to what has been observed in the experiments. Whereas in standard non-linear analyses multiple integration points may crack simultaneously due to the use of finite load increment steps, the currently applied SLA technique uses a load scaling technique which allows for only a single integration point to change status (i.e. to crack) at a time. Although at the linear elastic stage the bending stresses between the loading points will be approximately similar for all glass elements along the tensile beam edge, only one element will initiate initial glass fracture. Due to computer accuracy, solver accuracy, node numbering and ordering of the system of equations, the peak stress in one element will differ a fraction (e.g. 10^{-20} N/mm^2) from the stress in the other elements. That critical element will then cause initial glass failure and its material properties will be adjusted according to the next reduction curve in the saw-tooth reduction diagram [Rots et al., 2009].

However, apart from the similarities between the model results and the experimental results, also some striking differences between them occurred. These differences are discussed below.

Firstly, for beam type I and II the predicted initial bending stiffness at the linear elastic stage differs slightly from the experimental results, see Figure 8.16 (e) and Figure 8.17 (c). This difference originates from the method that has been used to determine the vertical displacement of the beams during the experiments. For the type I and II beams only the displacement of the loading mechanism (or: 'the cross-head') instead of the actual deformation of the beam at mid-span has been recorded during the tests, see Chapters 5 and 6. Besides the displacement of the beams, the recorded displacement of the cross-head includes all other deformations within the test setup[i]. Consequently, the initial bending stiffness obtained from the experiments is lower than the initial bending stiffness resulting from the models.

Secondly, the analytically and numerically generated load-displacement diagrams of beam type I largely correspond to the load-displacement diagrams resulting from the experiments on the GB-bonded beams, but they differ from the load-displacement diagrams resulting from the experiments on the SG-laminated beams, see Figure 8.16. The analytical and numerical models both underestimate the post-breakage strength of the SG-laminated beams. This difference stems from an additional load-carrying mechanism in the SG-laminated beams. As is explained in Chapter 5, this additional load-carrying mechanism is generated by crack-bridging glass fragments that transfer forces over the crack through shear in the SG interlayer. In the analytical and numerical models the bond system – in this case the SG interlayer – has not been incorporated. Therefore, the analytical and numerical models do not incorporate the additional load-carrying mechanism that is generated in the SG-laminated beams, and thus underestimate the post-breakage strength of the SG-laminated beams. Since the additional load-carrying mechanism is absent in the GB-bonded beams[ii], as will be explained in Chapter 9, the model results are largely in agreement with the experimental results of the GB-bonded beams. It is expected that for the SG-laminated beams the numerical results can be improved by incorporating layering of the glass by which the additional load-carrying mechanism can be simulated. However, this requires the use of interface elements between the individual glass layers and the use of a 3D model, which are both currently not yet applicable for the SLA technique. It is therefore recommended to further develop the SLA technique for interface elements and for 3D modelling.

---

[i] Attempts to correct the experimental displacement values by subtracting the expected displacements within the test setup by means of post-calculation did not give the desired result.
[ii] In the GB-bonded beams the cracks in the glass generally run through the full width of the laminate, whereas they are blocked by the interlayer in the SG-laminated beams. For a more in depth explanation see Chapter 9.

Thirdly, the numerical model demonstrates mainly orthogonal T-shaped cracks in the glass, whereas the experiments show mainly V-shaped cracks (between the loading points), see Figures 8.16, 8.17 and 8.18. This difference is largely explained by the regular and square mesh geometry that has been applied for the numerical models I-1, II and III. As will be further explained in section 8.6.5, a triangular mesh geometry and a rotating crack model will facilitate cracks to run also diagonally instead of only orthogonally.

Fourthly, the number of cracks in the numerical model does not always correlate to the number of cracks in the experimental results. As will be explained in sections 8.6.2 and 8.6.4, the number of cracks in the numerical model partly depends on the applied shear retention factor and the mesh density. Assumedly, these parameters could be further tuned to approach the experimental result more closely.

Finally, the analytical and numerical model do not describe local or full debonding (or: bond-slip) of reinforcement, whereas this does occur in the experiments. The models assume a rigid and infinitively strong bond between the glass and the reinforcement. No material parameters for the bond are defined. Bond failure, and thus debonding of reinforcement, cannot occur in the models and its effects on the overall structural response of reinforced glass beams are therefore not described by the models. It is expected that incorporating the bond between the glass and the reinforcement in the models could improve their results. It will for instance enable the models to describe collapse of the beams as a consequence of full debonding of reinforcement. For the analytical model it is expected that the bond could be incorporated by extending the current model with an additional set of equations by which the shear distribution in the bond can be calculated. From this calculation bond failure can be determined. Possibly, the studies performed by Ølgaard, Nielsen & Olesen [Ølgaard, Nielsen & Olesen, 2009], who developed a basic model for calculating the shear stress in the adhesive bond of reinforced glass beams by means of a modified Volkersen analysis, can be used for a further development of the analytical model. For the numerical model, the bond between the glass and the reinforcement could be incorporated by inserting interface elements between the glass and the reinforcement. By means of these interface elements, bond-slip of reinforcement could be simulated. However, as has been mentioned before, the SLA technique is currently not suited for the application of interface elements. Therefore, further development of the SLA technique is required.

Beam type I
1.5 m, hollow section reinforcement

(a)

(b)

(c)

(b)

(e)

(f)
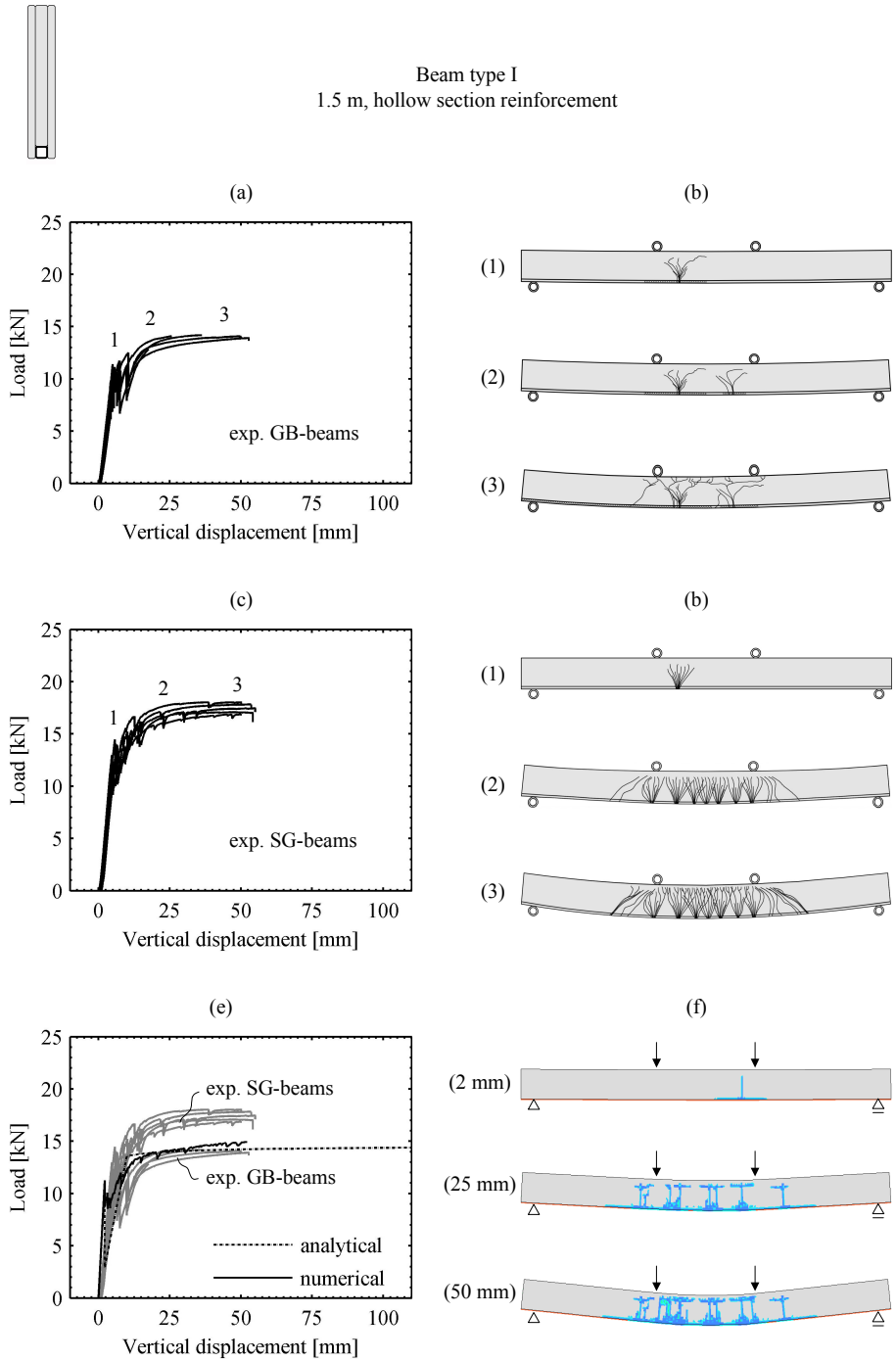
Figure 8.16: Experimental, analytical and numerical (model I-1) results for beam type I.

Beam type II
1.5 m, full section reinforcement
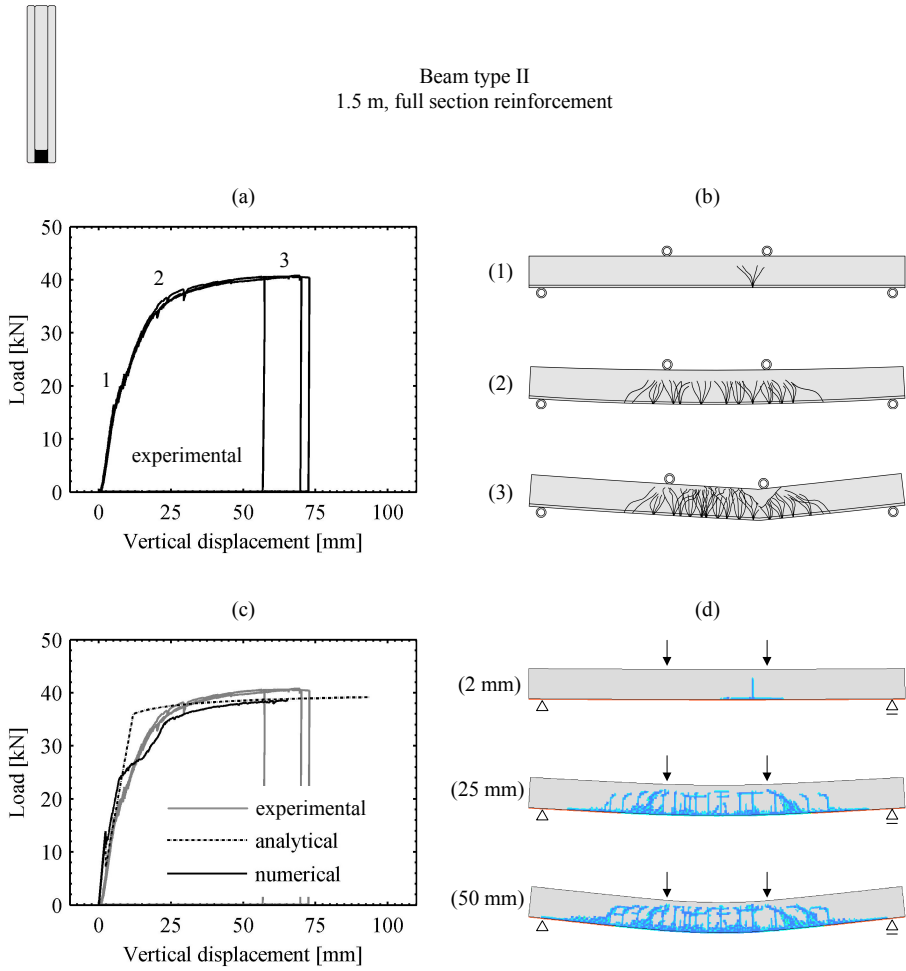
Figure 8.17: Experimental, analytical and numerical (model II) results for beam type II.

Beam type III
3.2 m, hollow section reinforcement

(a)

(b)

(c)

(d)
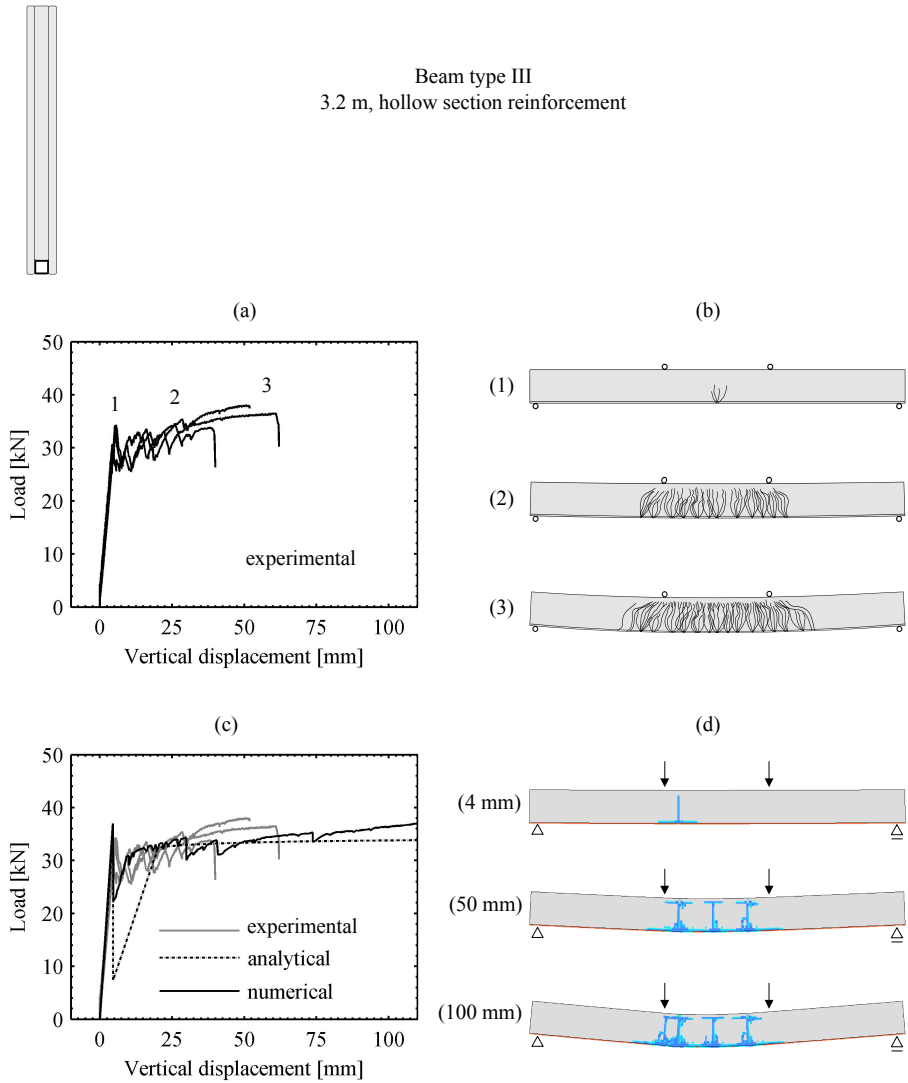
Figure 8.18: Experimental, analytical and numerical (model III) results for beam type III.

8.6.2.   Effect of the shear retention factor on the numerical results

Varying the shear retention factor (β) in the numerical models leads to only a small variation in the numerically predicted load-displacement curves, see Figure 8.19(a). However, it does significantly alter the results of the predicted crack behaviour of the beams, see Figure 8.19(b), (c). Whereas model I-2 with a very low value of $\beta = 0.001$ (i.e. almost full reduction of the shear modulus of the 'cracked' element) shows a relatively limited number of cracks, model I-4 with the highest possible value of $\beta = 1$ (i.e. no reduction of the shear modulus of the 'cracked' element) shows highly extensive cracking. Due to the high shear retention factor in model I-4 the level of shear force transferred by the 'cracked' elements is not reduced. This causes more extensive stressing of the surrounding elements, which in turn start to crack. However, this more extensive cracking is generally not in line with the experimental results. From the current study it is observed that a relatively low shear retention factor of $\beta = 0.01$ generally yields a cracking sequence which is in reasonable agreement with the experimental results.
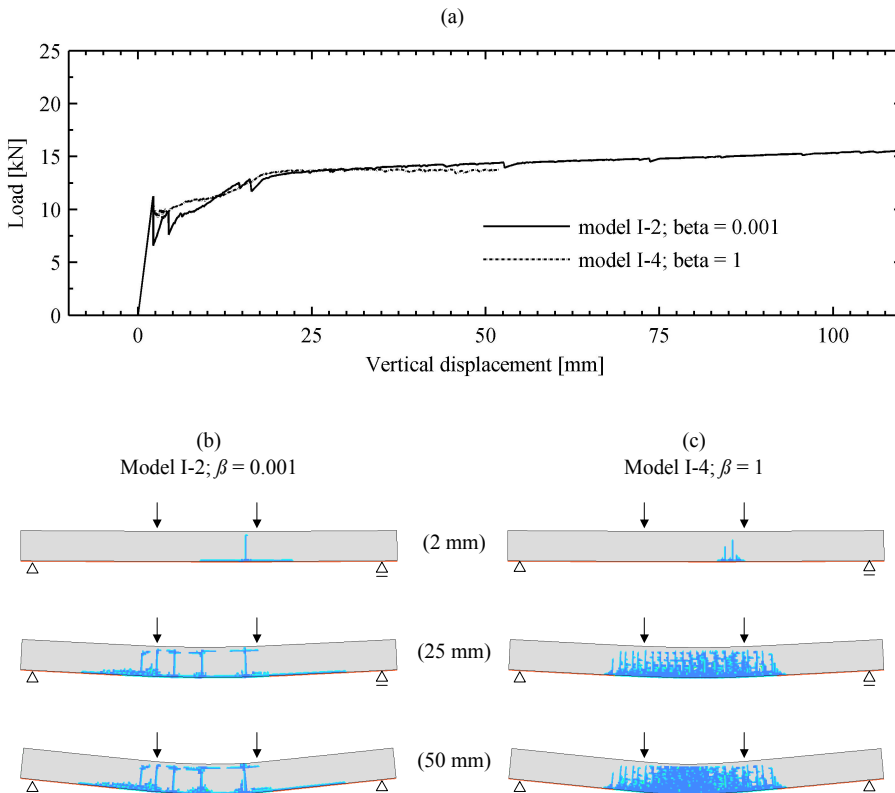
Figure 8.19: Effect of variation in shear retention factor β on the numerical results.

8.6.3.   Effect of the number of reduction steps on the numerical results

Varying the number of saw-tooth reduction steps for the glass stress-strain response does not alter the numerical results. Although the number of reduction steps for the glass between model I-5 and I-6 and between model I-1 and I-7 has been varied between 5 and 10 respectively (rs_{gl} = 5 or 10), they yield identical results, see Figure 8.20 (a). Both in load-displacement and in cracking behaviour the results of these models are perfectly similar. From this observation it is concluded that the material behaviour of the glass can be rather accurately captured in the numerical model using only a relatively limited number of saw-tooth reduction steps.

(a)

(b)
Model I-5 and I-6; rs_{gl} = 5 or 10; rs_{re} = 5

(c)
Model I-1 and I-7; rs_{gl} = 5 or 10; rs_{re} = 10
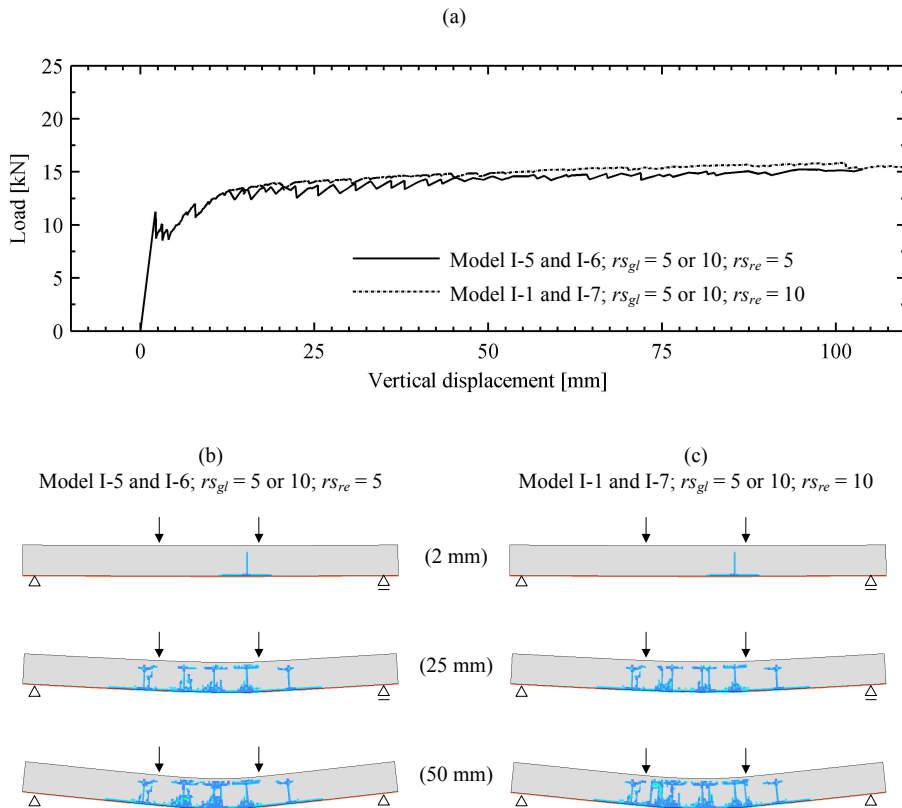
Figure 8.20: Effect of reduction steps on the numerical results; (a) load-displacement plot of model I-5, I-6, I-1 and I-7; (b) cracking sequence of model I-5 and I-6; (c) cracking sequence of model I-1 and I-7; It should be noted that model I-5 and I-6 demonstrate perfectly similar results, which is also the case for model I-1 and model I-7.

Varying the number of saw-tooth reduction steps for the steel reinforcement, however, does alter the numerical results. Whereas the load-displacement curves of models I-5 and I-6 (both with a number of reduction steps for the reinforcement of $rs_{re} = 5$) show frequent drops at the post-breakage stage, the load-displacement curves of models I-1 and I-7 (both with a number of reduction steps for the reinforcement of $rs_{re} = 10$) show a smooth trajectory at the post-breakage stage, see Figure 8.20(a)[i]. Due to the increased number of saw-tooth reduction steps, the plastic deformation of the steel reinforcement is more accurately followed in the numerical model. This leads to smoother post-breakage curves which are more in line with the experimental results.

8.6.4. *Effect of mesh size on the numerical results*

Mesh refinement, as has been done for model I-8 ($h_{cbw} = 5$) compared to model I-1 ($h_{cbw} = 10$), leads to only small differences in the load-displacement diagrams resulting from the numerical models, see Figure 8.21(a).

However, mesh refinement does significantly alter the cracking behaviour of the numerical models, see Figure 8.21(b), (c). Whereas model I-1 with a rather coarse mesh ($h_{cbw} = 10$) shows a relatively limited number of cracks, model I-8 with a refined mesh ($h_{cbw} = 5$) demonstrates more extensive cracking. It is assumed that this more extensive cracking originates from the increased number of possible crack instances offered by the increased number of model elements. Since the cracking behaviour resulting from the numerical model is preferably independent of mesh size, it is recommended to study the cause of the mesh dependency in more detail in future research[ii].

Additionally, mesh refinement seems to facilitate diagonal cracking. Whereas model I-1 with a rather coarse mesh ($h_{cbw} = 10$) shows mainly orthogonal cracks, model I-8 with a refined mesh ($h_{cbw} = 5$) shows a tendency for diagonal shear cracks, see Figure 8.21. These diagonal shear cracks have also been observed for the experimental results, see Figure 8.16. A specific reason for this increased tendency for diagonal cracking has not been found and needs more in depth study of the numerical procedure.

---

[i] It should be noted that model I-5 and I-6 demonstrate perfectly similar results, which is also the case for model I-1 and model I-7, see Figure 8.20.
[ii] Here, also the inclusion of bond-slip of the reinforcement and interlayers between the glass sheets in the model, is considered to be important as it is expected to influence the crack spacing.
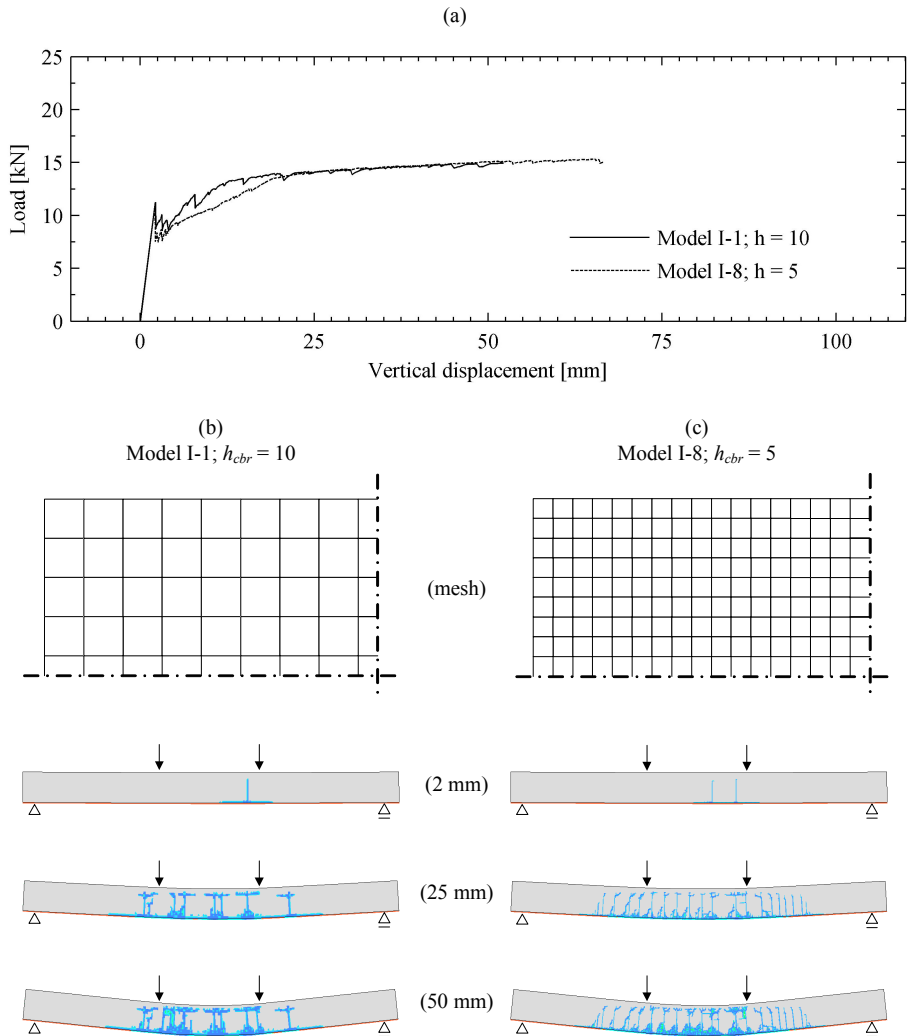
Figure 8.21: Effect of mesh size on the numerical results; .(a) load-displacement plot of model I-1 and I-8;
(b) cracking sequence of model I-1; (c) cracking sequence of model I-8.

8.6.5.   Effect of mesh geometry on the numerical results

Changing the mesh geometry from rectangular to triangular alters the numerical results both in terms of load-displacement diagram and cracking sequence, see Figure 8.23.

Firstly, compared to model I-1 with a rectangular mesh, model I-9 with a triangular mesh tends to overestimates the post-breakage strength, see Figure 8.23 (a). As has been observed in preceding research [Van de Graaf, 2008] it is assumed that this overestimation originates from an interlocking effect of the triangular mesh geometry, which causes an increased shear stiffness of the 'cracked' elements.

Secondly, the cracking sequence resulting from the numerical model I-9 with the triangular mesh shows a tendency for V-shaped cracks, whereas the numerical model I-1 with the rectangular mesh shows mainly T-shaped cracks. Although both the rectangular and the triangular mesh make use of a fixed crack model, which does not allow for any crack rotation within the elements, the triangular mesh geometry facilitates a diagonal cracking possibility which is absent for the rectangular mesh. This diagonal cracking possibility allows for the occurrence of the V-shaped cracks which have also been observed in the experiments, see Figure 8.16. It is assumed that a cross-diagonal mesh, instead of the currently applied 'single-diagonal' mesh could even further facilitate the occurrence of V-shaped cracks as the crack can propagate along the mesh in both directions, see Figure 8.22. Alternatively, sophisticated meshing algorithms, such as the *Delaunay* triangulation algorithm, can be applied to obtain a suitable triangular mesh. Furthermore, it is assumed that the application of a rotating crack model instead of the currently applied fixed crack model can even further improve the path of the V-shaped cracks. However, at the time of writing the SLA technique is not suited for the application of a rotating crack model. It is therefore recommended to implement a rotating crack model for the SLA technique in future research.
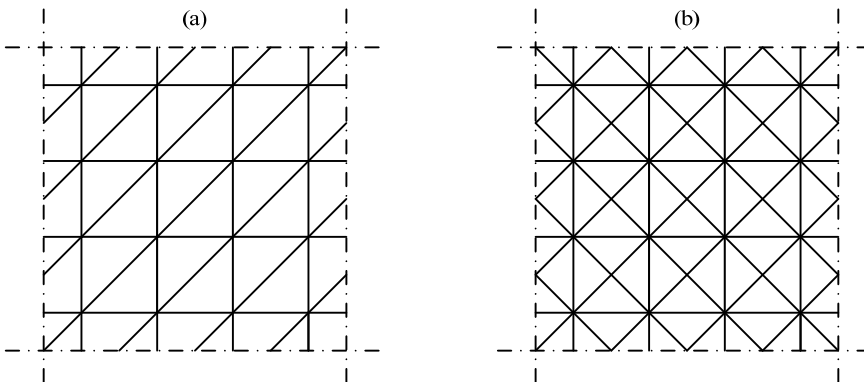
Figure 8.22: (a) Currently applied 'single-diagonal' mesh; (b) alternative 'cross-diagonal' mesh.

(a)

(b)
Model I-1; rectangular mesh

(c)
Model I-9; triangular mesh

(mesh)

(2 mm)

(25 mm)

(50 mm)
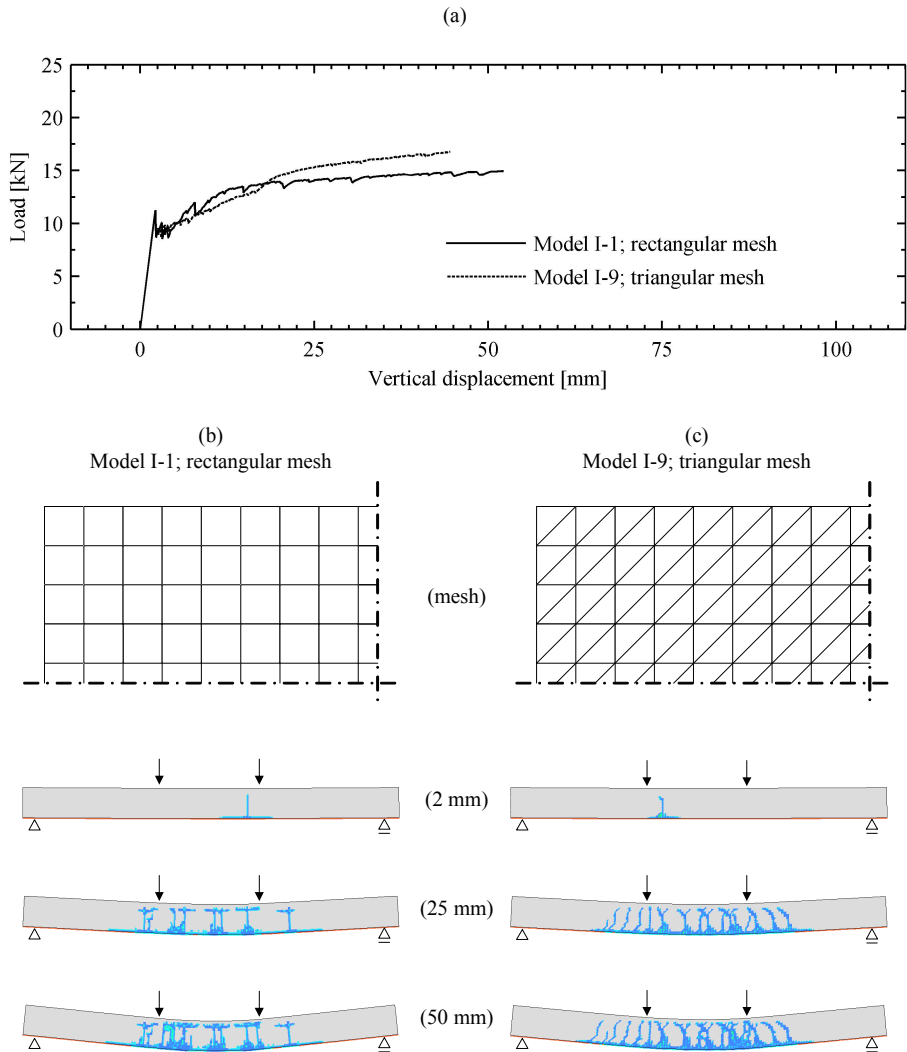
Figure 8.23: Effect of mesh geometry on the numerical results;
(a) load-displacement plot of model I-1 (rectangular mesh) and I-9 (triangular mesh);
(b) cracking sequence of model I-1; (c) cracking sequence of model I-9.

8.7.   Conclusions

From the analytical results, and the comparison with the experimental results, it concluded that the analogy with reinforced concrete is valid. The analytical model, which has been developed in analogy with reinforced concrete, provides rather accurate results in terms of load-displacement diagrams. Especially for the GB-bonded beams the analytical results are in good agreement with the experimental results. For the SG-laminated beams, however, the analytical model tends to underestimate the post-breakage strength. This difference in post-breakage strength is caused by an additional load-carrying mechanism which is generated by crack-bridging glass fragments that transfer forces over the crack through shear in the SG interlayer. Since the analytical model assumes a solid cross section of the glass, without any interlayer sheets, this additional load-carrying mechanism is absent in the analytical results. Furthermore, the analytical model does not take the bond between the glass and the reinforcement into account. Bond failure, and thus debonding of reinforcement, is not described by the model. The effects of debonding of reinforcement on the overall structural response of reinforced glass beams are therefore not given by the analytical model.

From the numerical results, and the comparison with the experimental results, it is concluded that the numerical model – which makes use of the novel sequentially linear elastic analysis (SLA) technique and the associated saw-tooth reduction diagrams to simulate cracking of the glass and/or plastic deformation of the reinforcement – provides fairly accurate results in terms of load-displacement diagrams. The numerical model simulates the repetitive peaks in the post-breakage response of the reinforced glass beams rather well, without running into convergence problems. However, similar to the analytical model, no layering of the glass and thus no interlayer sheets between the glass layers have been incorporated in the numerical model, which again causes an underestimation of the post-breakage strength of the SG-laminated beams. Furthermore, similar to the analytical model, the numerical model does not take the bond between the glass and the reinforcement into account. Bond-slip of the reinforcement and its effects on the structural response of reinforced glass beams are therefore not described by the numerical model. Moreover, the cracking sequences resulting from the numerical model are only indicative and insufficiently consistent with the experimental results.

Overall, it is concluded that both the analytical and the numerical model provide a promising method for describing the structural response of reinforced glass beams. Although rather coarse assumptions have been made in the models, such as disregarding the interlayer between the individual glass layers and disregarding any bond-slip of reinforcement, they overall yield similar beam response as has been observed in the experiments.

It is expected that the accuracy of the analytical model could be further enhanced by incorporating the bond between the glass and the reinforcement to be able to describe debonding of reinforcement. Furthermore, in addition to the current model, it could be explored whether strut-and-tie modelling [Schlaich, Schäfer & Jennewein, 1987] can be used to describe internal beam forces and to determine load and crack paths in reinforced glass beams.

It is expected that the numerical model could be enhanced by incorporating interface elements to simulate layering of the glass and bond-slip of the reinforcement. However, this requires a further development of the SLA technique, as interface elements are currently not applicable with the SLA procedure. Furthermore, the numerical model could be enhanced by the application of more sophisticated meshing alternatives and rotating crack formulations to more accurately simulate the crack paths in the glass.

PART IV

Integrated discussion
of the
research results

Part I

Introduction

Chapter 1

Introduction to
the research

Part II

Theoretical
framework

| **Chapter 2** | **Chapter 3** | **Chapter 4** |
| Structural glass beams | The reinforced glass beam concept | Materials applied in this research |

Part III

Experimental,
analytical and
numerical
investigations

| **Chapter 5** | **Chapter 6** | **Chapter 7** | **Chapter 8** |
| Experimental investigations into the effects of bond type, temperature, thermal cycling, humidity and load duration on the structural response | Experimental investigations into the effects of reinforcement percentage and beam size on the structural response | Experimental investigations into the structural response of SG-laminated glass beams with embedded glass fibre reinforcement | Analytical and numerical modelling of the structural response |

Part IV

Integrated
discussion of
the research
results

| **Chapter 9** | **Chapter 10** |
| Integrated discussion on the structural aspects of reinforced glass beams | Integrated discussion on the production and design aspects of reinforced glass beams |

Part V

Retrospect
and
prospect

| **Chapter 11** | **Chapter 12** |
| Conclusions | Recommendations |

Chapter 9
Integrated discussion on
the structural aspects of reinforced glass beams

This chapter provides an integrated discussion on the structural aspects of reinforced glass beams. This discussion is based on the experimental, analytical and numerical results that are presented in Chapters 5, 6, 7 and 8. Similarly, the following Chapter 10 provides an integrated discussion on the production and design aspects of reinforced glass beams. The key issues that are brought forward in these integrated discussions are incorporated in the Conclusions and Recommendations that are presented in Chapter 11 and Chapter 12 respectively.

Abstract

Based on the experimental, analytical and numerical investigations an integrated discussion on the structural response of reinforced glass beams is provided in this chapter. Three different structural stages – the un-cracked stage, the cracked stage and the yield stage – and three different failure mechanisms – bond failure, glass failure and reinforcement failure – are characterized. From the experimental investigations into the effects of the parameters *bond system, temperature, thermal cycling* and *humidity* it is observed that they have a specific effect on the extent of bond failure that occurs at the cracked and the yield stage. More excessive bond failure, and thus more excessive debonding of reinforcement, results in lower post-breakage strength of the reinforced glass beams. From the investigations into the effects of the parameter *load duration* it is observed that long-duration loading of cracked reinforced glass beams results in creep of the beams. However, despite the observed creep, the beams could still carry 80% of the predicted ultimate failure load for more than 15 months. From the investigations into the effects of the parameter *reinforcement material* it is observed that despite any yield capacity of the reinforcement, the reinforced glass beams can still show semi-ductile post-breakage response. From the investigations into the effects of the parameter *reinforcement percentage* it is observed that it has a specific effect on the height of the initial cracks in the glass and on the post-breakage strength and stiffness of the beams. From the investigations into the effects of the parameter *beam size* it is observed that it has only a limited effect on the structural performance of reinforced glass beams. From the analytical and numerical investigations into the modelling of the structural response of reinforced glass beams, it is observed that both the analytical and the numerical models describe similar beam response as is seen in the experiments. However, it is expected that the accuracy of their results can be enhanced by incorporating the bond system (i.e. bond-slip of the reinforcement and layering of the glass) in the models.

9.1.   Introduction

This Chapter provides, based on the results of the experimental, analytical and numerical investigations done in Chapter 5, 6, 7 and 8, an integrated discussion on the structural aspects of reinforced glass beams.

Firstly, the structural response of reinforced glass beams is characterized in section 9.2.

Secondly, the effects of the parameters *bond system*, *temperature*, *thermal cycling*, *humidity*, *load duration*, *reinforcement material*, *reinforcement percentage* and *beam size* on the structural response are explained and evaluated in section 9.3.

Thirdly, the analytical and numerical models that have been investigated in this research are discussed and evaluated in Section 9.4.

Finally, an overall evaluation is provided.

9.2.   Characterization of the structural response

The characteristic structural response of a normal-reinforced glass beam loaded in bending is schematized in Figure 9.1. Basically, three stages A) un-cracked stage, B) cracked stage and C) yield stage are distinguished. Furthermore, three ultimate failure causes 1) bond failure, 2) glass failure and 3) reinforcement failure are distinguished. These stages and failure causes are discussed in the following sub-sections.
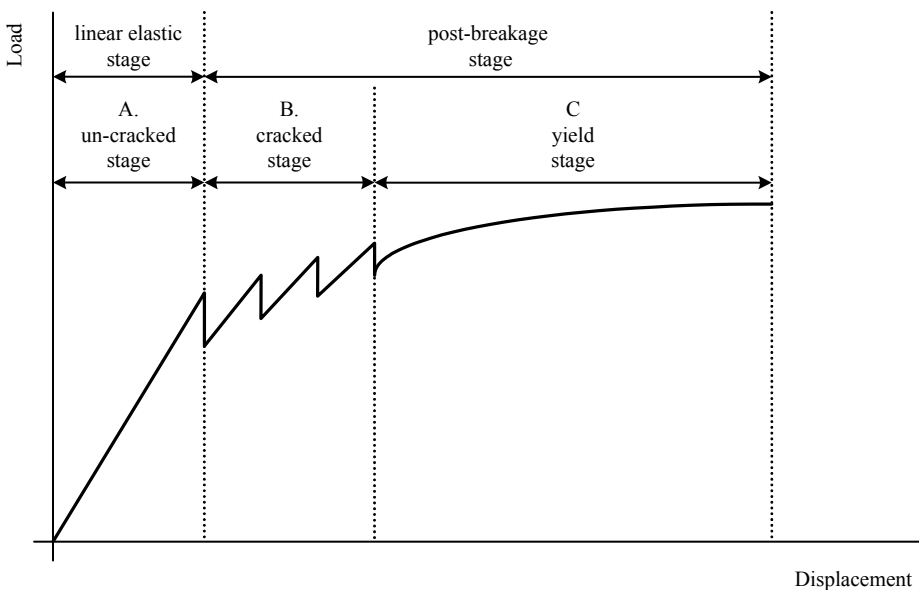
Figure 9.1: Schematic representation of a characteristic force-displacement diagram of a reinforced glass beam loaded in displacement controlled bending.

A. un-cracked stage

B. cracked stage

un-cracked
compression zone

N_{gl}

a = internal leverarm

N_{re}

local de-bonding

C. yield stage

diminishing height
compression zone

N_{gl}

a = internal leverarm

cracks
extending into
compression
zone

N_{re}

progressive
de-bonding
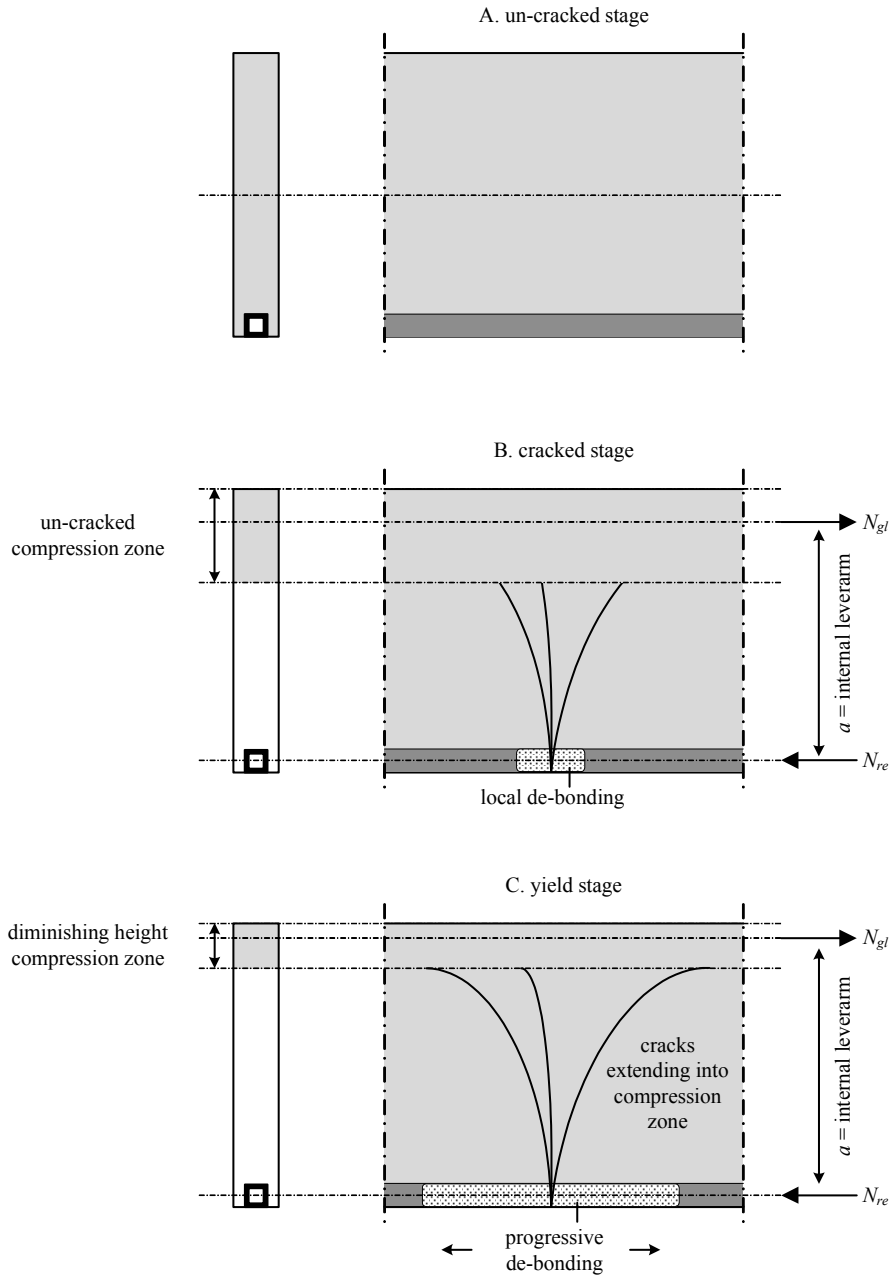
Figure 9.2: Schematic representation of the behaviour of a reinforced glass beam
at the different loading stages.

9.2.1. Stages

A)   un-cracked stage

At this stage the beam is un-cracked and both the glass and the reinforcement are loaded within their linear elastic range, see Figures 9.1 and 9.2. The main load-carrying material is the glass. Additionally, the reinforcement, which is semi-rigidly connected to the glass, contributes to the overall resistance of the composite beam.

B)   cracked stage

At this stage cracks develop in the glass, and the reinforcement is activated in tension, see Figures 9.1 and 9.2. The compressed part of the glass remains un-cracked, and a load-carrying mechanism is generated by a compressive force in the glass and a tensile force in the reinforcement. Cracks successively appear in the glass, causing the frequent disruptions in the load-displacement diagram, see Figure 9.1.

Typical V-shaped cracks appear in the glass, see Figure 9.2. These bending induced cracks originate from the tensile zone and branch towards the compression zone. Additionally, diagonal shear cracks might appear in the glass. Depending on the crack blocking properties of the bond between the glass layers, see section 9.3.1, the cracks run in only one or propagate instantly through multiple glass layers of the beam. Despite the occurrence of the cracks, the compression zone remains un-cracked as the crack propagation is halted by the reinforcement located at the tensile edge of the beam.

Along with the appearance of the cracks in the glass, typically some local debonding of reinforcement occurs, see Figure 9.2. Upon glass failure the reinforcement is activated and the bond between the glass and reinforcement is locally highly stressed. It is assumed that due to the energy release upon glass fracture and the sudden change in stress state the bond is shock loaded. This combined effect of high stress and shock load causes failure of the bond along a certain distance on either side of the crack origin in the glass.

C)   yield stage

At this stage the glass is extensively cracked and the reinforcement starts to plastically deform, which provides a ductile post-breakage response, see Figure 9.1. The existing cracks start to branch into the (initial) compression zone thereby diminishing the height of the compression zone, see Figure 9.2. Due to the diminishing height of the compression zone the load-axis of the compressive force in the glass moves upwards. This upward shift of the compressive load-axis enlarges the internal lever arm between the compressive force in the glass and the tensile force in the reinforcement. This gradually enlarging lever arm increases the moment capacity of the cracked beam, which explains the slight increase in load capacity observed in the load-displacement diagram, see Figure 9.1.

During the yield stage generally progressive debonding of reinforcement occurs. The bond that has already locally failed upon glass fracture progressively fails outwards along the reinforcement towards the beam ends, see Figure 9.2. In case this progressive debonding leads to full debonding of reinforcement, the beam collapses.

9.2.2.   *Failure causes*

Three ultimate failure causes are distinguished. Collapse of the reinforced glass beams can occur due to either 1) bond failure[i], 2) glass failure or 3) reinforcement failure. These three failure causes are discussed below.

1)   Bond failure

All forces between the glass and the reinforcement are transferred through the intermediary bond. In case of (local) failure of the bond, the forces can (locally) not be transferred anymore, which will affect the structural response of the beam. Bond failure, and thus debonding of reinforcement, can occur to different extents, see Figure 9.3. The effects of different extents of bond failure on the structural response of reinforced glass beams are discussed below.

1a)   *local bond failure.*

As already indicated in section 9.2.1, some local bond failure, thus local debonding of reinforcement, generally occurs upon failure of the glass[ii]. On either side of the crack origin in the glass, the reinforcement debonds along a certain distance, see Figure 9.3(a). As a result of this debonding of reinforcement, the reinforcement elongates over a greater length, which causes the crack to open up further. Due to this larger crack opening displacement the cracks in the glass are less effectively halted upon glass failure. The cracks can travel greater distances, which causes a more severe weakening of the beam.

1b)   *progressive bond failure*

As loading of the reinforced glass beams is continued after initial glass failure, progressive bond failure and debonding of reinforcement can occur. The local debonded zones start to extend outwards, towards the beam ends, see Figure 9.3 (b). Due to this increased debonding of reinforcement, the (existing) cracks in the glass can open up further, which stimulates the occurrence of local weak spots. At these spots, where the glass laminate is cracked through the full width of the beam laminate[iii], the beams open up and plastic hinges develop. At these plastic hinges the moment capacity is governed by plastic deformation of the reinforcement.

---

[i] Mixed mode (combined cohesive and adhesive) bond failure was most commonly observed in this research.
[ii] The extent of local bond failure depends on various parameters, such as temperature and the bond strength and fracture toughness of the bond system, as is explained in the following sections.
[iii] Whether a glass laminate will crack through the full width of the laminate is largely dependent on the applied bond system and its crack blocking properties, as is explained in section 9.3.1.

1c)   full bond failure

When the debonded zone reaches one beam end, the reinforcement is fully detached[i], see Figure 9.3(c). Since the tensile force in the reinforcement cannot be transferred anymore, the beam collapses. This collapse can occur abruptly or more gradually. The latter occurs when a residual friction between the reinforcement and the glass is generated by failed adhesive remainders. This has for instance been observed for the GB-bonded beams tested at high temperature, see Chapter 5.
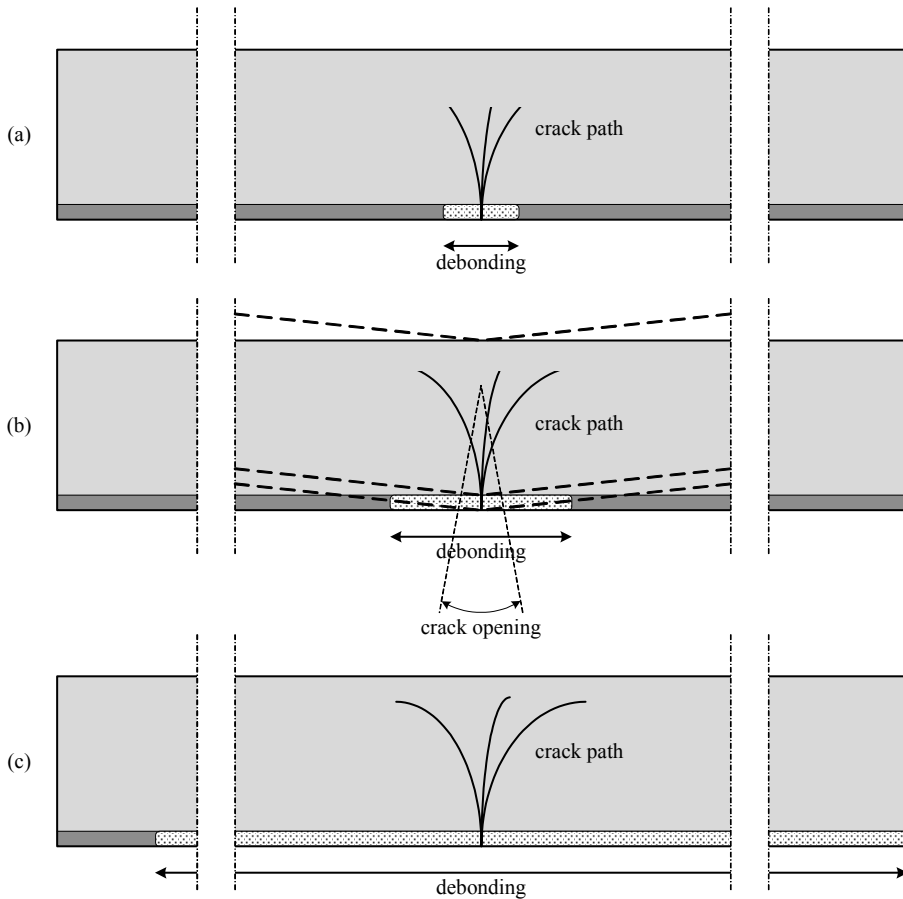
Figure 9.3: Schematic representation of the debonding of reinforcement as a result of bond failure.
(a) local bond failure and debonding of reinforcement;
(b) progressive bond failure and debonding of reinforcement; a plastic hinge is developed;
(c) full bond failure and debonding of reinforcement towards one beam end.

---

[i] Full debonding of reinforcement has not been observed for the SG-laminated reinforced glass beams.

2)   Glass failure

Failure of the glass can eventually also lead to collapse of the reinforced glass beam. Different failure modes which are related to the failure of the glass are discussed below.

2a)   failure of the compression zone

This failure mode might occur at the yield stage. Due to crack branching into the compression zone, the height of the compression zone gradually reduces. This causes increased stressing of the glass at the compression zone. When the strength of the compression zone is exceeded sudden and explosive glass failure occurs. The compressive force cannot be transferred anymore and the beam collapses.

2b)   buckling

Lateral torsional buckling might occur due to extensive cracking of the glass combined with increased stressing of the compression zone. This failure mode is highly dependent on the geometry of the beam. For the rather thick/stocky beams tested in Chapter 8 in a lateral torsional buckling test setup this failure mode did not occur. However, for slender reinforced glass beams tested in associated research by Louter [Louter, 2006a] this failure mode did occur.

2c)   shear failure

Due to excessive shear cracking of the glass, the beam might be locally severely weakened. This might cause local failure and collapse of the beam. This failure mode has been observed for the 3.2 m beam investigated in Chapter 6.

3)   Reinforcement failure.

This failure mode might occur at the yield stage. Upon reaching the ultimate strain limit of the reinforcement, the reinforcement will fail. The tensile force cannot be transferred anymore and the beam collapses. It should be noted, however, that this failure mode has not been encountered during this research[i].

---

[i] The strain at break of the stainless steel reinforcement is rather high and amounts to 30%, which makes reinforcement failure an unlikely cause for the stainless steel reinforced glass beams. For the GFRP rods the strain at break is much smaller, which makes reinforcement failure somewhat more likely for the GFRP-reinforced glass beams. However, this failure cause did not occur in this research.

9.3.   Parameter effects on the structural response

The structural response of reinforced glass beams, as it is characterized in section 9.2, is influenced by different parameters such as *bond system*, *temperature*, *thermal cycling*, *humidity*, *load duration*, *reinforcement material*, *reinforcement percentage* and *beam size*. The effects of these parameters have been experimentally investigated in Chapters 5, 6 and 7 and are discussed in the following sub-sections.

9.3.1.   Effects of the bond system on the structural response

The effects of the bond system on the structural response of reinforced glass beams have been investigated in Chapter 5. The pull-out tests (at -20, +23, +60 and 80°C, after thermal cycling and after humidity exposure) and the bending tests (at -20, +23 and +60°C and after thermal cycling) conducted in that chapter have been performed both for GB-bonded and SG-laminated specimens. From the test results it is observed that the applied bond system has a significant effect on the structural response of reinforced glass beams.

From the results of the pull-out tests it is observed that the performance of the SG-laminated pull-out specimens was – apart from the thermal cycling tests – superior to the performance of the GB-bonded pull-out specimens. Due to the higher bond strength of the SG interlayer compared to the GB adhesive, the SG-laminated pull-out specimens reached higher pull-out loads.

The observed higher bond strength of the SG interlayer is also reflected in the results of the bending tests. Due to the higher bond strength (and assumedly higher fracture toughness) of the SG interlayer compared to the GB adhesive, the extent of bond failure, thus the extent of debonding of reinforcement, was significantly smaller in the SG-laminated beams than in the GB-bonded beams. The cracks in the SG-laminated beams were therefore more effectively arrested, which enhanced the post-breakage performance of the SG-laminated beams compared to the GB-bonded beams. Furthermore, due to the relatively high bond strength of the SG interlayer, none of the SG-laminated beam specimens showed full debonding of reinforcement. Apart from some local debonding, the reinforcement remained largely attached, which enabled the SG-laminated beams to fully exploit the strength and plastic deformation capacity of the reinforcement and to develop a ductile post-breakage response. On the contrary, most GB-bonded beams finally collapsed due to full debonding of reinforcement.

Additionally, the SG-laminated beams profited – at least at room temperature – from the SG interlayer acting as a crack barrier between the glass layers of the laminate. Due to this crack barrier, the cracks in the SG-laminated beams were localized to one glass layer only and did not run through the full width of the laminate, see Figure 9.4. Although the SG-laminated beams were cracked at various locations, a crack in one layer was therefore often locally bridged by glass fragments in the other layer(s). These bridging glass fragments were able to transfer (tensile) forces over the crack through

shear in the SG interlayer. This provided the SG-laminated beams, apart from the reinforcement, with an additional tensile force transferring mechanism[i] which enhanced the residual resistance of the beams [Bos, 2009]. As a result of this additional load-carrying mechanism the SG-laminated beams reached higher post-breakage loads than the GB-bonded beams. Due to the absence of a crack blocking mechanism in the GB-bonded beams, the cracks in the GB bonded beams generally propagated through the full width of the beam, see Figure 9.4. This eliminates the possibility of crack bridging glass fragments and an additional load-carrying mechanism. However, it should be noted that the SG-laminated beams largely loose the additional load-carrying mechanism at -20 and +60°C. At -20°C the toughness of SG interlayer reduces, which causes local rupture of the SG interlayer. This causes cracks to run through the full width of the laminate which eliminates the possibility of crack-bridging glass fragments. At +60°C the strength and stiffness of the SG interlayer is reduced, which causes more extensive debonding and thus plastic hinges to occur, see section 9.2. These plastic hinges counteract on the additional load-carrying mechanism.

(a)
GB-bonded

(b)
SG-laminated
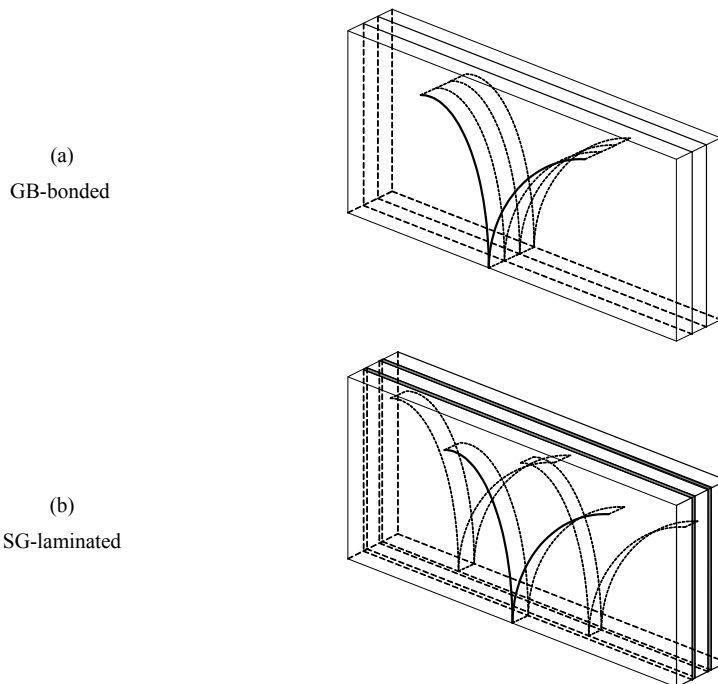
Figure 9.4: Cracking behaviour of GB-bonded and SG-laminated beams; (a) GB-bonded beams. The cracks generally run through the full width of the laminate; (b) SG-laminated beams. The crack runs in only one layer, due to the crack blocking properties of the SG interlayer.

---

[i] A similar effect has been observed by Veer [Veer, Riemslag & Ting. 2001] for polycarbonate laminated glass beams.

9.3.2.   Temperature effects on the structural response

Temperature has a significant effect on the structural response of both GB-bonded and SG-laminated reinforced glass beams, see Figure 9.5. Especially at the post-breakage stage the structural response of reinforced glass beams changes with temperature. This change in structural response originates from the change in strength and stiffness of the applied bond system with temperature. The effects of temperature on the structural response have been investigated in Chapter 5 by means of pull-out and bending tests on GB-bonded and SG-laminated specimens. The results are summarized below.

The GB-bonded beams demonstrated highly ductile post-breakage response at +23˚C, whereas this post-breakage response significantly changed at +60˚C. Due to decreased strength of the GB adhesive bond at +60˚C – as demonstrated by the pull-out tests – the GB-bonded beams showed full debonding of reinforcement early in the post-breakage stage[i]. This full debonding of reinforcement caused collapse of the beam. However, due to the residual friction between the reinforcement and the glass, which was generated by failed adhesive remainders, the beams showed gradual instead of instant collapse, see Figure 9.5.

The response of the GB-bonded beams also changed at -20°C compared to +23°C. Due to reduced fracture toughness and bond strength of the GB adhesive at -20°C – as demonstrated by the pull-out tests – the GB beams almost instantly showed full debonding of reinforcement at the post-breakage stage. This caused brittle collapse of the GB-bonded beams at -20°C at much lower post-breakage loading levels than had been observed at +23°C, see Figure 9.5.
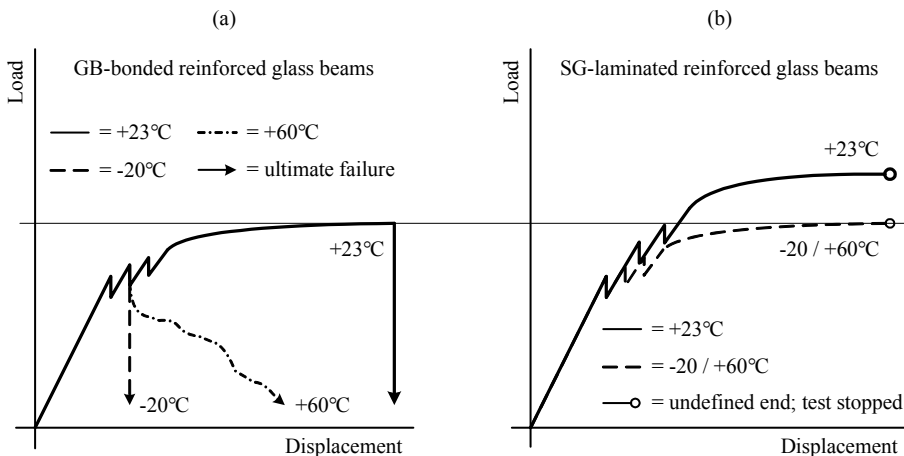
Figure 9.5: Schematic representation of the effect of temperature on the structural response of the beams.

---

[i] These findings are supported by similar results obtained by Louter in associated research [Louter, Veer & Belis, 2008], on similar GB-bonded reinforced glass beams.

The SG-laminated beams, investigated in Chapter 5, also demonstrated a difference in structural response between +23 and +60°C. At +23°C the SG-laminated beams profited from an (additional) load-carrying mechanism, which was – as is explained in the previous section – generated by crack-bridging glass fragments that transferred forces over the cracks through shear in the SG interlayer. At +60°C, however, the SG-laminated beams largely lost this additional load-carrying mechanism. Due to a reduced bond strength and stiffness of the SG interlayer at +60°C more excessive debonding of reinforcement occurred, which stimulated the occurrence of plastic hinges in the beam. These plastic hinges counteracted on the additional load-carrying mechanism that had been observed at +23°C. Additionally, it is assumed that the efficiency of the additional load-carrying (or: crack-bridging) mechanism decreased at +60°C due to reduced shear stiffness of the SG interlayer at +60°C. This caused a reduction in residual resistance of the SG-laminated beams at +60˚C compared to +23°C, see Figure 9.5. However, it should be noted that despite the more excessive debonding of reinforcement, the reinforcement remained largely attached, which enabled the SG-laminated reinforced glass beams to develop ductile post-breakage response. Their post-breakage strength level was similar to the post-breakage strength level of the GB-bonded beams tested at +23°C, see Figure 9.5.

The SG-laminated beams also showed differences in structural response between +23 and -20˚C. Due to decreased fracture toughness of the SG interlayer at -20˚C, the SG-laminated beams showed more excessive bond failure, thus debonding of reinforcement, which stimulated the occurrence of plastic hinges. These plastic hinges again counteracted on the additional load-carrying mechanism of the crack bridging glass fragments. Furthermore, this additional load-carrying mechanism was eliminated upon local rupture of the SG interlayer which occurred due to reduced toughness of the SG interlayer at -20˚C. Due to the absence of the additional load-carrying mechanism at -20°C, the post-breakage strength of the SG-laminated beams was reduced compared to +23°C, see Figure 9.5. However, it should again be noted that despite the more excessive debonding of reinforcement, the reinforcement remained largely attached to the glass, which enabled the beams to develop a ductile post-breakage response.

9.3.3.   *Thermal cycling effects on the structural response*

Thermal cycling has a significant negative effect on the GB-bonded reinforced glass beams, whereas it has only a limited effect on the SG-laminated metal-reinforced glass beams, see Figure 9.6. The effect of thermal cycling on the structural response of GB-bonded and SG-laminated stainless steel reinforced glass beams has been investigated in Chapter 5. The beams have been exposed to 150 cycles between -20 and +30°C and tested in four-point bending afterwards. The results are summarized below.

The GB-bonded reinforced glass beams demonstrated a significant effect of thermal cycling on their structural response. The non-exposed GB-bonded reinforced glass beams showed ductile post-breakage response. However, after the thermal cycling

procedure the GB-bonded reinforced glass beams demonstrated brittle post-breakage response. Due to excessive bond failure, the reinforcement rapidly debonded at the post-breakage stage. It is assumed that this excessive bond failure is caused by an accumulation of damage in the GB adhesive bond during the thermal cycling procedure. Due to a difference in thermal expansion between the glass and the stainless steel reinforcement, the intermediary bond was (repetitively) strained during the thermal cycling procedure. It is assumed that this (repetitive) straining caused damage in the bond, which resulted in excessive bond failure and full debonding of reinforcement, early at the post-breakage stage. Consequently, the beams collapsed.

The SG-laminated beams showed, contrary to the GB-bonded beams, almost no effect of the thermal cycling procedure on the structural response. Apart from a small decrease in post-breakage strength, due to somewhat more excessive debonding of reinforcement, the post-breakage response was not significantly affected by the thermal cycling procedure. The overall structural response of the thermal cycling exposed SG-laminated beams was similar to the non-exposed SG-laminated beams, see Figure 9.6.

It is assumed that this difference in thermal cycling effect on the GB-bonded and SG-laminated beams originates from a difference in thickness and stiffness of the bond. The relative large thickness of the SG interlayer ($t = 1.52$ mm) assumedly results in a more flexible bond which allows for relatively large shear deformation. On the contrary, the small thickness of the GB adhesive bond ($t \approx 0.1$ mm) assumedly results in a rigid bond which does not allow for large shear deformation. The SG interlayer is therefore better capable of taking up shear deformation, that is imposed by the difference in thermal expansion of the glass and the reinforcement, than the GB adhesive bond.
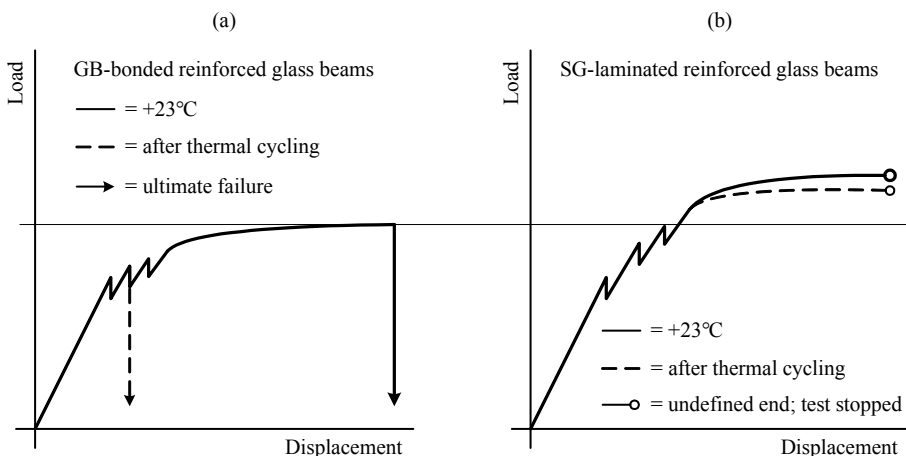
Figure 9.6: Schematic representation of the effect of thermal cycling on the structural response of the beams.

9.3.4. *Humidity effects on the structural response*

Humidity has an inconsistent but predominantly negative effect on the structural response of SG-laminated reinforced glass beams, see Figure 9.7. The effect of humidity on the structural response of SG-laminated reinforced glass beams has been investigated in Chapter 5. This has been done by means of pull-out and bending tests that have been performed on specimens that had been pre-exposed to 100% relative humidity at 50°C for 4 weeks. The results are summarized below.

The pull-out tests clearly demonstrated a negative effect of humidity on the bond strength of the SG interlayer. Compared to non-exposed specimens, the pull-out strength of the humidity-exposed specimens was reduced by 45%. It is assumed that during the humidity-exposure procedure, water has permeated between the glass and the SG interlayer, thereby breaking the physical bond between them.

At first instance this negative effect of humidity seemed absent for the SG-laminated reinforced glass beams. The humidity-exposed SG-laminated reinforced glass beams responded similarly to non-exposed beams, and demonstrated ductile post-breakage response, see Figure 9.7. However, for one (out of three) SG-laminated beam specimen, sudden and brittle collapse occurred at the post-breakage stage, due to full delamination of the SG-laminate at mid-span. Although the laminate did not show any visual defects such as local delamination or 'haze' directly after the humidity exposure procedure, the SG-laminate displayed sudden delamination during the bending test. It is assumed that this delamination was a result of the humidity pre-exposure, which has caused a weakening of the SG bond due to the permeation of water, similar as has been observed at the pull-out tests. Why the delamination of the SG-laminate only occurred for one beam specimen is unclear. Possibly the delamination was not caused by the humidity exposure, but by an error during the manufacturing process. However, this could not be traced and seems less probable. It is therefore recommended to investigate the effects of humidity on the structural performance of reinforced glass beams in more detail and to take caution in the application of the beams in highly humid environments.
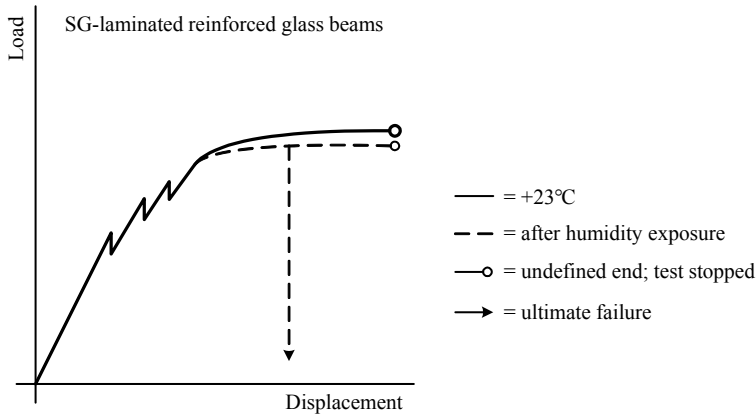
Figure 9.7: Schematic representation of the effect of humidity on the structural response of the beams.

9.3.5. *Long-duration post-breakage loading response*

For long-duration post-breakage loading the SG-laminated reinforced glass beams demonstrate a vertical creep deformation. However, this vertical creep deformation does not endanger the safety performance of the beams. They can still carry the required load for a significant and sufficient period of time. The long-duration loading response of SG-laminated reinforced glass beams has been investigated in Chapter 5. This has been done by means of long-duration pull-out and bending tests. Their results are summarized below.

From the results of the long-duration post-breakage bending tests performed on SG-laminated reinforced glass beams, it is observed that the cracked beams show creep under constant loading. This creep originates from creep deformation of the SG interlayer between the glass and the reinforcement, which has also been observed at the long-duration pull-out tests. Due to creep of the SG interlayer the reinforcement displayed creep movement, which caused a vertical deformation of the beam. Additionally, the creep movement of the reinforcement caused the cracks in the glass to open up further, which stimulated a further propagation of the cracks. This crack propagation caused a further reduction in bending stiffness of the beams and a consequent increase in vertical deformation of the beam. Moreover, the increase in vertical deformation of the beam was further increased by additional cracking of the glass, which caused a further reduction in bending stiffness thus an increase in vertical deformation of the beams.

Despite the observed creep, however, the cracked SG-laminated reinforced glass beams could still carry load for significant periods of time. All beam specimens reached post-breakage loading times of more than 3 months. For one specimen the test was stopped after this time frame. For the two other specimens the tests were continued and they are,

at the time of writing, loaded for more than 11 and 15 months respectively at 80% of the predicted ultimate failure load. Although they still show a vertical creep deformation, they did not collapse. This significant redundancy of the SG-laminated reinforced glass beams indicate that the beams provide sufficient post-breakage safety even for long-duration post-breakage loading.

9.3.6.   *Effects of reinforcement material on the structural response.*

The effects of reinforcement material on the structural response can be derived from a comparison of the structural performance of the SG-laminated stainless steel reinforced glass beams investigated in Chapter 5 and 6, and the SG-laminated GFRP (Glass Fiber Reinforced Polymer) reinforced glass beams investigated in Chapter 7. The stainless steel reinforced beams consist of triple-layer glass laminates with a square reinforcement section bonded at the recessed inner edge, whereas the GFRP reinforced glass beams consist of double-layer glass laminates with reinforcement rods embedded in the SG interlayer. Their structural response is characterized in Figure 9.8.

The stainless steel reinforced glass beams demonstrate ductile post-breakage response. This ductility originates from plastic deformation of the stainless steel reinforcement. Furthermore, due to the high ultimate strain of stainless steel, tensile failure of the reinforcement did not occur for the beams tested in this research. Before reaching the ultimate strain of the reinforcement, the beams had either already collapsed due to a different failure cause (see section 9.2.2) or the tests had to be stopped upon reaching the displacement limit of the test setup.

The GFRP-reinforced glass beams demonstrate semi-ductile post-breakage response. Although the GFRP rods lack any plastic deformation capacity, the beams still demonstrate semi-ductile post-breakage response. This semi-ductility does not originate from the reinforcement, but from repetitive cracking of the glass, which gradually reduces the stiffness of the beam. Additionally, it is assumed that the semi-ductility originates from local debonding of the GFRP reinforcement rods which allows the cracks to open up further thereby gradually reducing the bending stiffness.
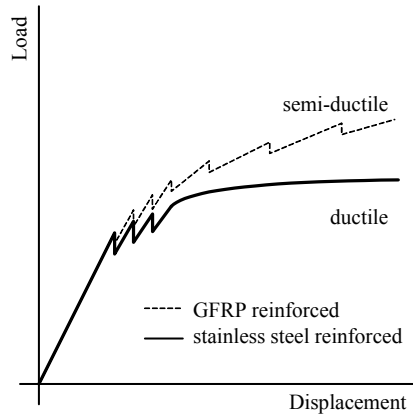
Figure 9.8: Schematic representation of the difference in structural response
between stainless steel reinforced and the GFRP reinforced glass beams.

9.3.7.   Effects of reinforcement percentage on the structural response.

The reinforcement percentage, and thus the amount of reinforcement in the cross-section of a reinforced glass beam, has a direct influence on the stiffness of the beam at the cracked stage and on its post-breakage strength, see Figure 9.9. The characterization provided in Figure 9.9 is based on the results of the bending tests performed in Chapter 6 on two series of SG-laminated reinforced glass beams with identical cross-section dimensions, but with either a hollow or solid reinforcement section. Increasing the reinforcement percentage, and thus increasing the total tensile stiffness and strength of the reinforcement, results in an increase in post-breakage stiffness and strength of the beam. Furthermore, increasing the reinforcement percentage causes a lowering of the neutral beam axis and thereby a reduction of the height of the (initial) cracks in the glass. This argumentation is also valid in reverse.
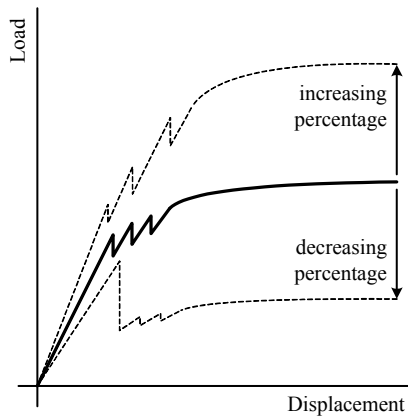
Figure 9.9: Schematic representation of the effect of reinforcement percentage
on the structural response of reinforced glass beams.

9.3.8.   Beam size effects

Beam size has – at least for the beam dimensions and beam assemblies investigated in this research – only a small effect on the structural response of reinforced glass beams. The effects of beam size have been investigated in Chapter 6. This has been done through bending tests on small (1.5 m) and large (3.2 m) SG-laminated reinforced glass beams.

Apart from their obvious size-related difference in load-carrying capacity, the investigated beams showed only small differences in structural response. The main difference between the small and the large beams was that the additional load-carrying mechanism, which is generated by glass fragments that locally bridge cracks in neighbouring glass layers, was less efficient for the large beams than for the small beams. This slightly limited the residual resistance of the large beams. However, the large beams still reached significant post-breakage levels, which were in line with the analytically predicted post-breakage levels.

9.4.   Analytical and numerical modelling

The investigations done in Chapter 8 have focused on two methods to describe the structural response of reinforced glass beams. Firstly, an analytical model has been developed based on the reinforced concrete theory. Secondly, a numerical model, which makes use of a novel SLA technique and saw-tooth reduction diagrams to simulate cracking of the glass and plastic deformation of the reinforcement, has been investigated for its ability to describe the structural response of reinforced glass beams.

From the analytical and numerical investigations, it is observed that both models provide a promising method for describing the structural response of reinforced glass beams. Even though rather coarse assumptions have been made in the models, such as disregarding the bond between the glass and the reinforcement and the layering of the glass, they overall yield similar beam response as has been observed in the experiments. However, also some distinct differences occur between the modelled results and the experimental results, which are directly related to the assumptions made in the models. Two important differences are indicated below.

Firstly, debonding of reinforcement is not taken into account in the models. Both the analytical and the numerical model assume a rigid and infinitively strong bond between the glass and the reinforcement. Therefore bond failure and thus debonding of reinforcement is not described by the models. The effects of local debonding – as are described in section 9.2.2 – and collapse due to full debonding of reinforcement are thus not incorporated in the model results.

Secondly, the layering of the glass is not taken into account in the models. A solid cross-section is assumed in the models, and thus no effects of the GB adhesive or the SG-interlayer on the structural beam response are described by the models. Especially for the SG-laminated beams, which generate an additional load-carrying mechanism by means of shear transfer in the SG interlayer, see section 9.3, the model results deviate from the experimental results. More specifically, the models underestimate the post-breakage strength of the SG-laminated beams.

It is expected that the accuracy of the models could be enhanced by incorporating the bond between the glass and the reinforcement and by incorporating layering of the glass.

For the analytical model this could be done by extending the current model with an additional set of equations by which the shear distribution in the bond can be calculated and from which bond failure can be determined. Incorporating the layering of the glass in the analytical model may be complex, and no suggestion is given here.

For the numerical model the bond between the glass and the reinforcement could be incorporated by means of interface elements. These interface elements could be used to simulate local or full debonding (i.e. bond-slip) of the reinforcement. Similarly, the

layering of the glass could be simulated by means of interface elements positioned between the individual glass layers. However, this would require an update of the currently applied 2D model to a 3D model. Currently, the SLA is not suited for 3D modelling, and thus further development is required to be able to apply the SLA technique for the layering of glass. Furthermore, the SLA technique is currently not suited for the application of interface elements. This should thus also be further developed before the bond between the reinforcement and the glass and between the individual glass layers can be simulated.

9.5. Evaluation

From the integrated discussion on the structural aspects of reinforced glass beams, provided in the current chapter, it is observed that the reinforced glass beam concept is a feasible concept, which provides high redundancy for structural glass beams. Both for the stainless steel reinforced and GFRP-reinforced glass beams investigated in this research, high residual strength and (semi-)ductility have been observed at the post-breakage stage.

Furthermore, some key issues regarding the GB-bonded beams, the SG-laminated beams and the analytical and numerical model follow from the integrated discussion presented in the current chapter. These are discussed in the following sub-sections.

9.5.1. GB-bonded reinforced glass beams

The GB-bonded metal-reinforced glass beams investigated in Chapter 5 showed ductile post-breakage combined with a significant post-breakage strength. However, the GB-bonded beams demonstrated this response only at room temperature. For the other test conditions such as low temperature, high temperature and after thermal cycling the residual resistance dropped and/or the post-breakage ductility was absent[i]. These significant negative effects of temperature and thermal cycling on their post-breakage strength drastically limit their field of application.

However, it should be noted that the performance of the GB-bonded beams could possibly be improved by the application of a different manufacturing process. Currently, the applied manufacturing technique, which has been developed in this research, allows only for a more or less fixed adhesive thickness of $t \approx 0.1$ mm. A change in bond thickness might enhance the performance of the GB-bonded beams.

---

[i] Associated research indicates that the GB-bonded beams still show good structural performance after humidity exposure.

9.5.2. SG-laminated reinforced glass beams

The SG-laminated reinforced glass beams showed promising results. At all investigated conditions (at -20, +23 and +60˚C, after thermal cycling, after humidity exposure and for long-duration post-breakage loading) the SG-laminated beams showed high residual resistance and post-breakage ductility. The SG interlayer provides some specific structural advantages[i]; (1) it provides high bond strength, which limits the extent of debonding of reinforcement; (2) it acts as a crack barrier, which prevents cracks to run through the full width of the laminate; and (3) it prevents from glass fragments falling from cracked reinforced glass beams.

However, the observed delamination of one SG-laminated beam specimen after the humidity exposure procedure urges for caution. Additional research into the effects of humidity on the SG-laminate is required.

9.5.3. Analytical and numerical modelling

From the experimental investigations it is observed that the parameter *bond system* has some specific effects on the structural response of reinforced glass beams, see section 9.3.1. However, the bond system – both between the glass and the reinforcement and between the individual glass layers – is currently not incorporated in the analytical and numerical model. It is expected that incorporating the bond system in the models will further increase their accuracy in describing the structural response of reinforced glass beams. Future research should therefore focus on this issue.

---

[i] Additionally, the SG interlayer provides some advantages from a production and design point of view. These are discussed in Chapter 10.

Chapter 10
Integrated discussion on the production
and design aspects of reinforced glass beams

This chapter provides an integrated discussion on the production and design aspects of reinforced glass beams, based on the experiences and knowledge gained from the experimental research presented in Chapters 5, 6 and 7. It forms an addition to Chapter 9 which provides an integrated discussion on the structural aspects of reinforced glass beams. The key issues that are brought forward in these integrated discussions are incorporated in the Conclusions and Recommendations that are presented in Chapter 11 and Chapter 12 respectively.

Abstract

For the production of the specimens in this research, two different production techniques have been applied. For the production of the GB-bonded specimens, a semi-automated adhesive bonding process, which has been developed in this research, has been applied. The main advantage of this technique is that the length of the final beam product is not bound by the production process. For the production of the SG-laminated specimens, a vacuum-bag autoclave lamination process has been applied. The main advantage of this technique is that it is a known and proven technique for laminating glass. Using these techniques, two different beam geometries have been made in this research. Firstly, the semi-automated bonding process and the vacuum bag lamination process have been applied to produce the GB-bonded and SG-laminated triple-layer glass beams with a stainless steel reinforcement section bonded at the inner recessed edge. Specific attention point for this beam geometry is that the size of the reinforcement matches the size of the inner glass layer. Any deviation in size needs otherwise to be compensated for by the intermediary bond. Secondly, the vacuum-bag lamination technique has been applied for the production of the double-layer SG-laminated glass beams with GFRP reinforcement rods embedded in the SG interlayer. A specific attention point for this beam geometry is that the width of the reinforcement should be limited to be able to integrate it in the interlayer. From the experiences and knowledge gained from the production of the specimens needed for the experiments, it is observed that the two beam designs that have been investigated in this research are feasible both from a design and a production point of view.

10.1.   Introduction

This Chapter discusses the production and design aspects of reinforced glass beams. This discussion is based on the practical experiences and knowledge gained from the experimental investigations done in this research.

Firstly, section 10.2 discusses the two production processes that have been applied in this research to manufacture the specimens. These are a semi-automated adhesive bonding process that has been developed in this research for the production of the GB-bonded beam specimens and a vacuum-bag autoclave lamination process that has been applied for the production of the SG-laminated beam specimens. Additionally, a manual adhesive bonding process which could be applied for the production of special beam geometries is briefly discussed.

Secondly, section 10.3 discusses the design aspects of the two beam geometries that have been studied in this research. These are the triple-layer GB-bonded and SG-laminated beams with a stainless steel reinforcement section bonded at the inner recessed edge, and the SG-laminated double-layer glass beams with the GFRP reinforcement rods embedded in the SG interlayer. In addition to these investigated beam geometries, alternative beam designs are proposed. Furthermore, issues concerning the thermal expansion differences between the glass and the reinforcement, issues concerning oversized reinforced glass beams and issues concerning multifunctional use of the reinforcement are briefly discussed.

Finally, an evaluation of the production and design aspects of reinforced glass beams is provided.

10.2.   Production processes

The two production processes that have been applied in this research for the production of the GB-bonded and SG-laminated reinforced glass beams are discussed in the following subsections. Additionally, a manual adhesive bonding process for special beam geometries is briefly discussed.

10.2.1.   *Semi-automated adhesive bonding process for GB-bonded beams*

For the production of the GB-bonded reinforced glass beams a semi-automated adhesive bonding process has been developed within this research. Since the UV-curing acrylate GB adhesive is originally intended to bond small surfaces, such as hinges or knobs to glass doors, no process for bonding large surfaces existed at the beginning of this research project. To be able to bond the relatively large glass surfaces of the reinforced glass beams, a new bonding process had to be developed. The main challenge of bonding large surfaces is to prevent air inclusions in the cured adhesive bond which might weaken the bond and which affect the visual quality of the beam. The semi-automated adhesive bonding process developed in this research, therefore makes use of a compression roller mechanism which drives the air out of the adhesive before the adhesive is polymerized by UV-illumination, see Figure 10.1 and 10.2.

The procedure of the semi-automated adhesive bonding process is as follows. Firstly, the individual glass sheets and the reinforcement section are cleaned with 2-propanol. Secondly, the glass sheets and reinforcement section are provided with the uncured intermediary adhesive liquid, which is manually applied by means of an ordinary paint roller. Thirdly the glass sheets and the reinforcement section are assembled in flat position in a wooden mold. The wooden mold prevents any undesired movement of the glass layers due to possible 'floating' of the glass layers on the uncured adhesive liquid. Fourthly, the assembled beam is transported in a compression roller mechanism by means of transport rollers. Subsequently, the assembled beam is compressed by the compression roller mechanism while the transport rollers move the uncured beam laminate forward. This way the air in the adhesive is driven out and air inclusions are avoided. Finally, the beam is illuminated by UV-light to polymerize the adhesive. By adjusting the speed of the transport rollers the illumination time is altered, which should be targeted between about 30 seconds and 2 minutes. The precise curing time depends on the applied intensity of the UV-light and on the applied glass thicknesses in the beam laminate.

(a)

wooden mold   glass beam   compression rollers   UV-lamps   transport rollers

(b)
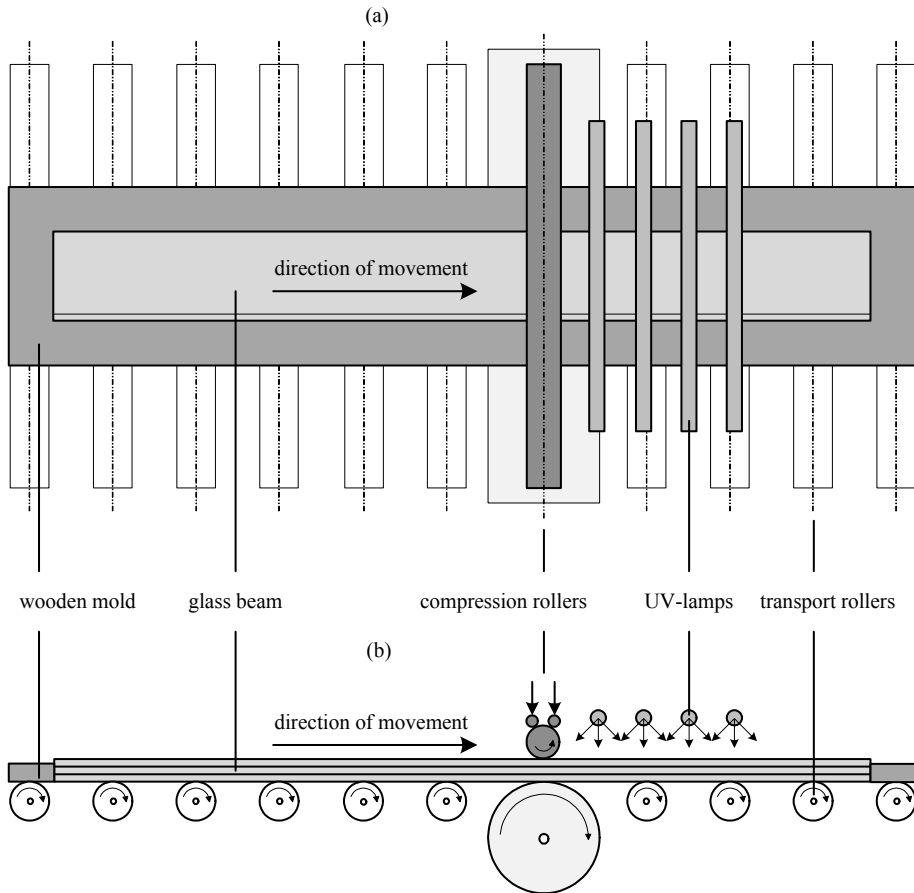
Figure 10.1: Schematic representation of the semi-automated adhesive bonding process;
(a) top view; (b) side view.

(a)   (b)
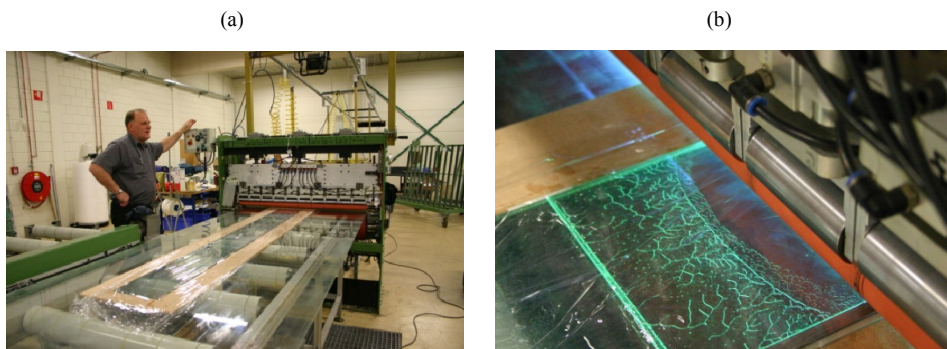
Figure 10.2: Semi-automated adhesive bonding process;
(a) Overview of the process with un-cured reinforced glass beam assembled in a wooden mold;
(b) A compression roller mechanism drives the air out of the un-cured adhesive between the glass layers.

An advantage of the GB adhesive and the associated semi-automated adhesive bonding process is that the beam assembly is rapidly cured. Polymerization of the GB adhesive is realized within 30 seconds to 2 minutes by illumination of UV-light. This effectively speeds up the production process.

A second advantage of this production technique is that the length of the final beam product is not restricted by the production process. In theory, infinite beam lengths can be made with this semi-continuous bonding process[i]. However, the height of the beam assembly is limited to the width of the pressure rollers, which currently is about 1.2 m. Furthermore, the thickness of the final beam assembly is limited to about 60 to 80 mm. For larger thicknesses the stiffness of the uncured beam assembly becomes too high, which frustrates the compression rollers to effectively drive the air out of the adhesive.

A disadvantage of the semi-automated bonding process is that it requires a high pressure of the roller mechanism to drive the air out of the adhesive. The consequence is that the adhesive thickness automatically results from the pressure needed to drive the air out the adhesive. Larger adhesive thicknesses, which could compensate for tolerances on the glass and reinforcement, are therefore difficult to realize. Furthermore, due to the pressure of the roller mechanism there is a significant risk of glass breakage during the manufacturing process.

10.2.2.   Vacuum-bag autoclave lamination process for SG-laminated beams

For the manufacturing of the SG-laminated reinforced glass beams a vacuum bag autoclave lamination process has been applied. With this autoclave process heat and atmospheric pressure is applied to the pre-assembled beam laminate which is placed in a vacuum-bag. The process and equipment is similar to the process applied for producing PVB-laminated glass. However, the processing of the SG interlayer and the required settings for temperature, atmospheric pressure and cycle time are different.

The vacuum bag autoclave lamination process of the SG-laminated reinforced glass beams is as follows. Firstly, the glass sheets and reinforcement section(s) are cleaned using 2-propanol. Secondly, the SG interlayer sheets are cut to the required size using a simple cutter, e.g. a Stanley knife, or a mechanized sheet cutter. Thirdly, the beam laminate is assembled and temporary fixed with heat resistant tape. Subsequently, the beam composite is put in a sealed plastic bag which is vacuumized afterwards and put in the autoclave, see Figure 10.3. During the autoclave lamination process the initially translucent/opaque SG interlayer turns transparent. Furthermore, due to the high temperature involved with the autoclave lamination process, the SG interlayer becomes semi-liquid and starts to flow. The SG interlayer bonds all components and after a cool down process the finished laminate is removed from the autoclave.

---

[i] However, it should be noted that above a certain span the material efficiency of a (reinforced) glass beam decreases. Schetters [Schetters, 2007] has estimated this span at 18.5 m for reinforced annealed float glass beams.

(a)   (b)

Figure 10.3: (a) The assembled reinforced glass beam in a vacuum bag, prior to lamination;
(b) two 1.5 m beam specimens in vacuum bags ready to enter the autoclave (in the back).

An advantage of the SG interlayer and the associated autoclave lamination process is the low viscosity of the SG interlayer during the lamination cycle. Due to this low viscosity, the SG easily conforms to tolerances on the glass and the reinforcement. This adaptability to dimensional tolerances is further enhanced by the relatively large thickness ($t = 0.89$, 1.52 or 2.28 mm) of the SG interlayer.

A disadvantage of the autoclave lamination process is that the length of the beams is restricted by the size of the autoclave. Oversized autoclaves which are suitable for the production of large span glass beams, are not yet widely available in the glass industry. However, the glass industry is currently rapidly advancing towards oversized glass products[i]. As a result, the number of oversized autoclaves available in the glass industry is rapidly increasing.

A second disadvantage of this production technique is the possibility of glass fracture during the process due to a difference in thermal expansion between the glass and the reinforcement. During the heating process the, for instance, metal reinforcement expands more than the glass. As the SG interlayer solidifies during the cooling process the reversed expansion of the reinforcement will stress the SG interlayer bond and thereby the glass, which might cause glass breakage. Although this problem did not occur for the beams manufactured in the current research, it requires specific attention.

---

[i] The advancements in the field of oversized glass products is illustrated by the 21 m spliced laminated glass beam and the 18 m insulated glass panel that were presented at the latest Glasstec fair in 2010 in Düsseldorf.

10.2.3.   Manual adhesive bonding

Special beam geometries, such as T-section, I-section or box-section beams, see Figures 10.9, 10.10 and 10.11, are difficult to produce with either the semi-automated adhesive bonding process or the vacuum bag autoclave lamination method. They require an additional manual adhesive bonding process. The web(s) and flange(s) of the beam can be separately manufactured using the semi-automated adhesive bonding process or the vacuum bag autoclave lamination process and can subsequently be joined using a manual adhesive bonding process to compose the T-section, I-section or box-section glass beam. However, the quality of this manually made adhesive bond might be less consistent than the quality that results from a semi-automated bonding process.

10.3.   Beam designs

In this research two different beam geometries have been studied, see Figure 10.4. Firstly, triple-layer GB-bonded or SG-laminated full-section annealed float glass beams with a stainless steel reinforcement section bonded at the inner recessed edge have been investigated. Secondly, double-layer SG-laminated full-section annealed float glass beams with GFRP reinforcement rods embedded in the SG interlayer have been investigated. The following subsections discuss the design aspects of these beam geometries. Furthermore, alternative beam designs are suggested.
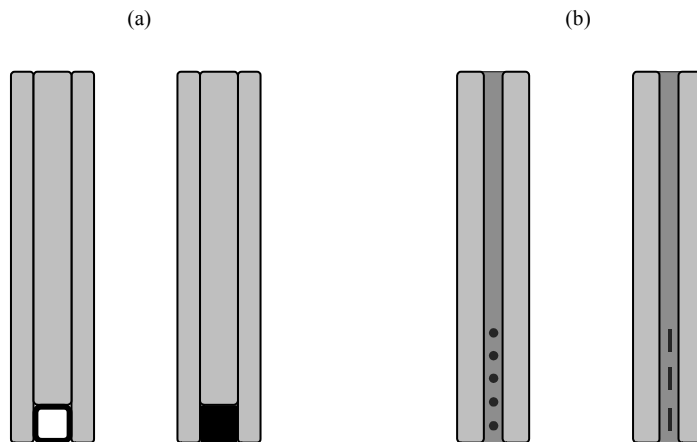
Figure 10.4: (a) Cross-section of triple-layer annealed float glass beams with a stainless steel reinforcement section bonded at the inner recessed edge; (b) Cross-section of double-layer annealed float glass beams with GFRP reinforcement rods embedded in the interlayer.

10.3.1. *Glass beams with reinforcement bonded at the inner recessed edge*

The first beam geometry that has been investigated in this research consists of three layers of annealed float with a square stainless steel section bonded at the inner recessed edge, see Figure 10.4 (a). Either hollow section or full section reinforcement has been applied. The beam assembly has been either bonded with the GB adhesive or laminated with the SG interlayer.

For this beam geometry an important aspect in terms of beam design and production is that the nominal width of the reinforcement section is the same as the nominal thickness of the inner glass layer(s)[i]. If the reinforcement and the glass are not of the same size, gaps will occur which have to be filled by the bond system, see Figure 10.5. Especially for the GB adhesive, which is preferably cured in a relatively small thickness range of $t \approx 0.1$ mm, filling these gaps will be problematic. For the SG interlayer, which has a relatively large sheet thickness of $t = 0.89$, 1.52 or 2.28 mm and which shows low viscosity during the production process (see section 10.2), filling these gaps will be less problematic. However, if the resulting SG bond thickness is too large, the shear strength and stiffness of the SG bond will probably be reduced, which will negatively affect the overall performance of the final beam product.

In this respect, it should be noted that there is not a matching reinforcement width for all glass thicknesses. The most commonly used nominal glass thicknesses in structural glass beams are 8, 10, 12 and 15 mm[ii], whereas the standard width of e.g. stainless steel square hollow sections amount to 10, 15, 20, 25 and 30 mm[iii]. For some beam designs it might therefore be a puzzle to find a good match between the dimensions of the inner glass layer(s) and the reinforcement.

Furthermore, specific attention should be given to the dimensional tolerances on the glass and the reinforcement. Although the tolerances on the thickness of the glass and the width of e.g. stainless steel hollow sections are relatively small, see Table 10.1, they should be compensated for by the bond system. As is explained above, compensating for these dimensional tolerances is problematic for the GB adhesive, due to the absence of a 'gap-filling' capacity.

---

[i] In this research the inner layer of the beams consisted of only one glass layer. However, the inner layer may also consists of multiple glass layers [Louter, 2008], as long as the total nominal width of the inner glass layers is the same as the width of the reinforcement section.
[ii] Full range is 2, 3, 4, 5, 6, 8, 10, 12, 15, 19 and 25 mm. The practical thicknesses (for building applications) range from 4 to 19 mm.
[iii] Larger widths are possible, but are not relevant for this application

(a)   (b)
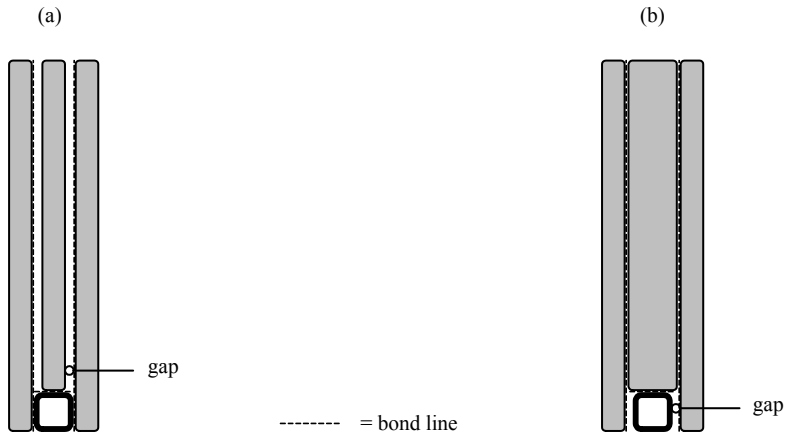
Figure 10.5: Gaps might occur due to dimensional differences between the thickness of the inner glass layer and the width of the reinforcement; (a) inner glass < reinforcement; (b) inner glass > reinforcement.

Table 10.1: Dimensional tolerances on glass according to [EN 572-2: 2004] and bright steel according to [EN 10278: 1999]. [i]

Glass		Stainless steel box section, H11	
Nominal thickness	Tolerance	Nominal dimensions	Tolerance class to ISO 286-2
[mm]	[mm]	[mm]	[mm]
2-3-4-5-6	± 0.2	> 6 to ≤ 10	+0 / -0.090
8 – 10 – 12	± 0.3	> 10 to ≤ 18	+0 / -0.110
15	± 0.5	> 18 to ≤ 30	+0 / -0.130
19 - 25	± 1.0	> 30 to ≤ 50	+0 / -0.160

---

[i] The tolerances on the thickness of the glass are provided in Table 10.1. It should be noted that for economical reasons glass is commonly produced at the low range of the indicated tolerance range. More specifically, glass is generally produced in the smallest allowable thickness. A nominal glass thickness of e.g. 10 mm will therefore most commonly result in an actual thickness of about 9.7 mm.

10.3.2.   Glass beams with GFRP rods embedded in the interlayer

The second beam geometry that has been investigated in this research consists of two layers of annealed float glass with semi-transparent GFRP (Glass Fiber Reinforced Polymer) reinforcement rods embedded in the interlayer. For the GFRP reinforcement either round or flat rods have been applied. This beam geometry has been laminated using the SG interlayer.

For this beam geometry an important aspect in terms of beam production and design is that the width of the reinforcement should be limited – approximate range 0.1 to 3 mm – to be able to integrate it in the interlayer. Due to this rather limited thickness of the reinforcement, it is probable that multiple reinforcement sections have to be integrated to reach a sufficient reinforcement percentage. If the thickness of the reinforcement is 0.89 mm[i] or more, it is possible and recommended to place 'spacer' interlayer strips between the individual reinforcement sections, see Figure 10.6. The purpose of these spacers is twofold. Firstly, they avoid any movement of the reinforcement rods during the manufacturing process. Secondly, they limit the probability of any air inclusions between the individual reinforcement rods in the final beam product.
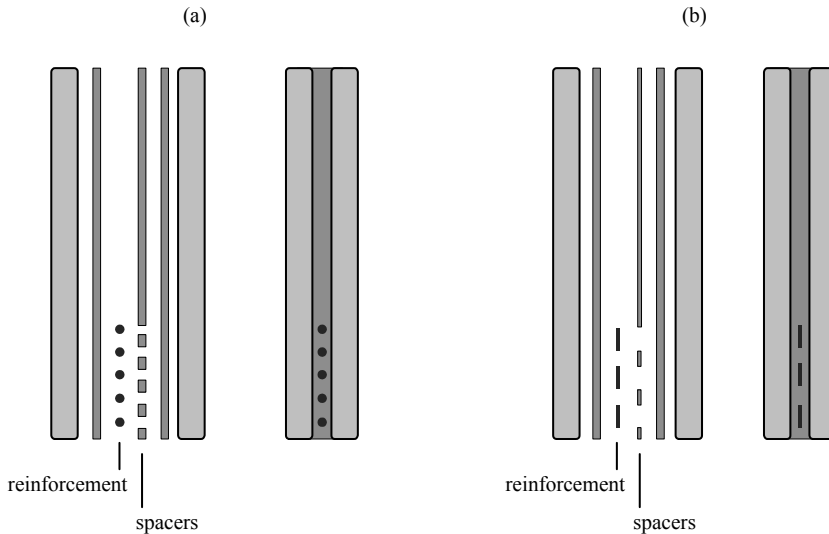
Figure 10.6: Exploded and assembled view of double-layer annealed float glass beams with (a) round and (b) flat reinforcement rods embedded in the interlayer. Interlayer spacers are applied to prevent movement of the reinforcement during the production and to prevent from air inclusions in the final beam product.

---

[i] 0.89 mm is currently the smallest available thickness of the SG interlayer.

An advantage of the embedment of reinforcement in the interlayer between the glass sheets is that the reinforcement can be positioned anywhere in the web of the beam. This enables the intensification of reinforcement at the most intensive stress field(s) [Leung, 2010]. Extra reinforcement could for instance be applied at mid span where the bending moment is highest, see Figure 10.7 (c)

Another advantage of the embedment of reinforcement is that the reinforcement sections are positioned in the 'core' of the beam and fully surrounded by the interlayer and the glass layers. Instead of being exposed at the edge, the reinforcement sections are protected from direct impact by means of the glass sheets on either side of the reinforcement sections. Especially for impact sensitive reinforcement materials such as glass fiber this is an advantage. Moreover, instead of being exposed at the edge, the reinforcement sections are encapsulated by the interlayer and shielded from direct exposure to humidity or corrosive environments.

Finally, embedment of reinforcement provides the possibility of influencing the architectural expression of the beams, see Figure 10.7. As the reinforcement sections are positioned in the web of the beam, the reinforcement rods are clearly exposed. When optimal transparency is desired the reinforcement sections could be (semi-)transparent, such as the glass fiber reinforcement rods applied in this research. When a pronounced architectural expression is desired, specific non-transparent reinforcement materials, reinforcement geometries (e.g. wire-mesh, or perforated sheets) or reinforcement shapes (e.g. curved) could be applied in the web of the beam, see Figure 10.7.
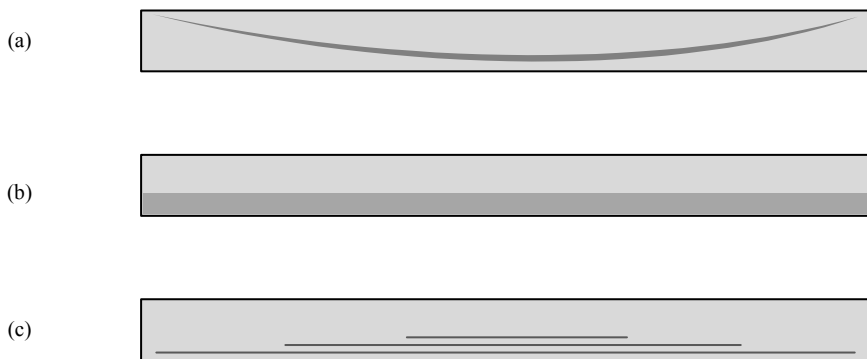
Figure 10.7: Reinforcement possibilities for glass beams with reinforcement embedded in the interlayer; (a) curved reinforcement embedded in the interlayer; (b) wire mesh reinforcement embedded in the interlayer; (c) intensification of reinforcement at the highly stressed mid-zone of the beam.

10.3.3. *Alternative beam designs*

Besides the two beam designs discussed in the previous sections, the reinforced glass beam concept is applicable to a variety of beam designs.

Figure 10.8 shows some suggestions for full-section beam designs. Besides integrating the reinforcement at the inner recessed edge or in the interlayer of the glass beams, as has been done in this research, the reinforcement can also be bonded directly to the edge of the beam or integrated at recessed side edges of the beam, see Figure 10.8(a) and (b).

Furthermore, when improved lateral stability of a reinforced glass beam is desired, alternative beam geometries such as T-section, I-section or box-section[i] beam geometries can be composed, see Figures 10.9, 10.10 and 10.11. An important aspect of T-section, I-section or box-section glass beams – in terms of beam production and design – is the joint between the web and the flange(s). This joint, cannot easily be realized with the production methods applied in this research, see section 10.2.1 and 10.2.2. Whereas the individual web(s) and flange(s) of the beam can be produced with the semi-automated adhesive bonding process or with the (vacuum-bag) autoclave lamination process, the joints between the web(s) and flange(s) require a manual adhesive bonding process, see section 10.2.3. These beam geometries are therefore somewhat more difficult to realize.
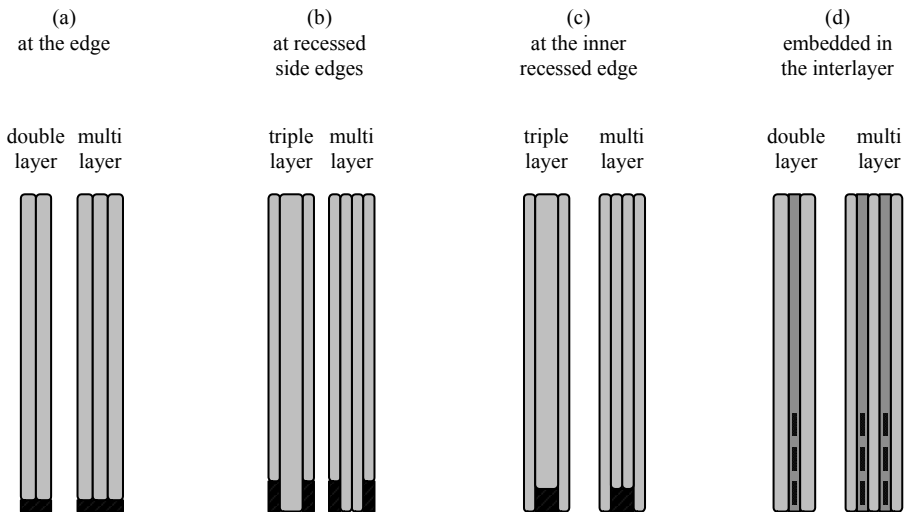
Figure 10.8: Alternative full section reinforced glass beam designs.

---

[i] Specific difficulty of a box-section glass beam is possible occurrence of dust and water condensation in the inaccessible inside of the beam. This issue, however, is not further addressed here.
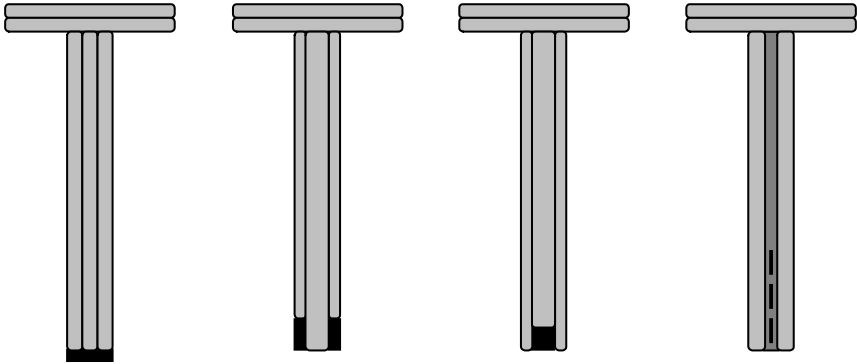
Figure 10.9: Suggestions for T-section reinforced glass beams. [*]
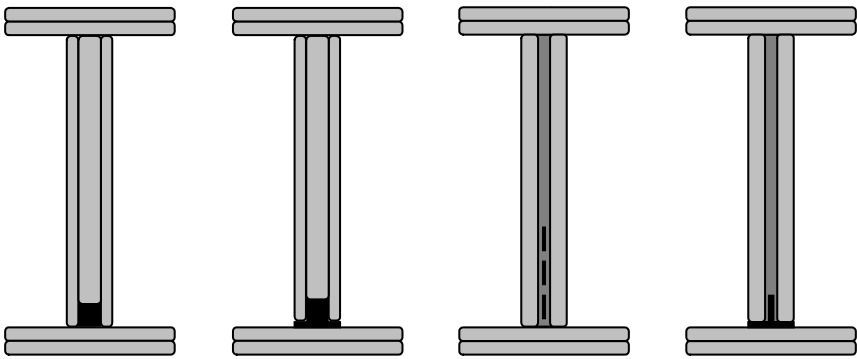
Figure 10.10: Suggestions for I-section reinforced glass beams. [*]
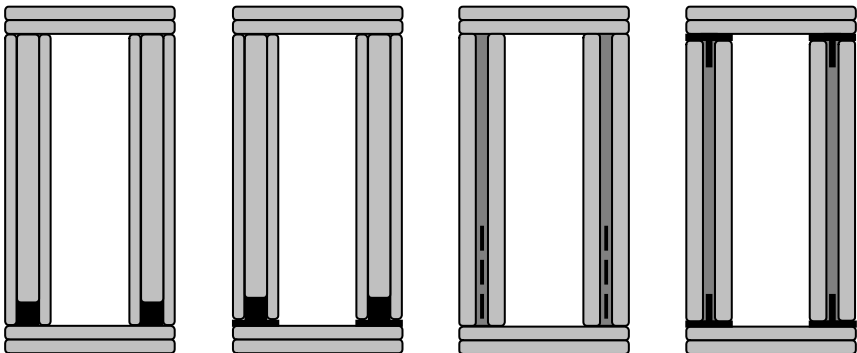
Figure 10.11: Suggestions for box-section reinforced glass beams. [*]

[*] The (right-angled) connections between the web(s) and flange(s) of the beam designs proposed in Figures 10.9, 10.10 and 10.11 cannot easily – or even not at all – be realized with the semi-automated adhesive bonding process or the autoclave lamination process discussed in sections 10.2.1 and 10.2.3. It is proposed to realize these connections with a manual adhesive bonding technique, which is briefly discussed in section 10.2.3. This implies, however, that the proposed beam geometries are more difficult to realize than the full section beam geometries presented in Figure 10.8.

10.3.4. Thermal expansion difference between glass and reinforcement

An issue that should be addressed for reinforced glass beams is the difference in thermal expansion between the glass and the reinforcement. Due to this difference in thermal expansion a difference in linear expansion between the glass and the reinforcement will occur when the temperature deviates from the ambient temperature. This difference in elongation between the glass and the reinforcement imposes a shear deformation upon the bond system.

To avoid debonding of reinforcement as a result of the imposed shear deformation, the bond system should be capable of undergoing this shear deformation without failure. In this respect, the SG interlayer seems better suited than the GB adhesive. Due to its relatively large thickness (t = 0.89, 1.52 or 2.28 mm), the SG interlayer has a larger shear deformation capacity than the GB adhesive, which has a rather limited thickness ($t \approx 0.1$ mm).

The issue of thermal expansion becomes more important with increasing beam sizes. For the relatively small 1.5 m stainless steel reinforced glass beams investigated in this research, the absolute difference in linear expansion between the stainless steel (AISI 304) reinforcement and the glass amounts to 0.007 mm/m·°C, which results in a difference of 0.42 mm within a temperature range of 20±40°C. This difference is still relatively small. However, for larger span glass beams of e.g. 18 m this difference increases to 5.04 mm, which might become more problematic for the bond system to deal with. To limit the difference in thermal expansion between the reinforcement and the glass in stainless steel reinforced glass beams, a different type of stainless steel, with a thermal expansion coefficient more close to that of glass, could be applied. The thermal expansion coefficient of, for instance, ferritic stainless steel type AISI 430 is much closer to the thermal expansion coefficient of glass, see Table 10.2. However, this type of stainless steel is not widely available in a variety of section geometries and dimensions. Finding a suitable reinforcement section which can be integrated in a glass beam might therefore be difficult, though, probably not impossible. Alternatively, titanium might be applied as reinforcement, since it has an identical thermal expansion coefficient as glass, see Table 10.2. However, titanium has some practical limitations in terms of machining and economical costs.

Table 10.2: Thermal expansion coefficient of glass and stainless steel.

		Glass	Stainless steel		Titanium
			304	430	-
Thermal expansion coefficient	x 10^{-6}	9.0	16.0	10.0	8.5

10.3.5. Oversized reinforced glass beams

Oversized reinforced glass beams – i.e. beams exceeding the standard 6 m length of glass sheets – can be made by applying multiple layers of glass which are ordered according to a certain segmentation scheme (spliced beam), see Chapter 2, together with a continuous reinforcement section. The segmentation scheme for the glass can be either symmetric, with coinciding seams, or asymmetric, with staggered seams, see Figure 10.12. These segmentation schemes have been applied for reinforced glass beam specimens investigated in associated research [Louter et al., 2005; Louter, 2007; Schetters, 2007; Veer, Riemslag & Ting, 2001]. Special attention should be given to the calculation of the stresses in the beams. At the seams the stresses will be higher due to a reduction of the cross-section.

Alternatively, oversized beams can be made by applying oversized glass sheets. This eliminates the use of a segmentation scheme, and thus continuous glass beams can be made. However, the use of oversized glass sheets is currently still rather exceptional.

It should be noted, however, that above a certain span the material efficiency of a (reinforced) glass beam decreases. From exploratory calculations done by Schetters [Schetters, 2007] it is estimated that above a span of 18.5 m the dead load (own weight) of a segmented reinforced annealed float glass beam becomes too large compared to the allowable live load. It is expected that above that span it becomes inefficient to apply (segmented) reinforced glass beams and that other solutions should be sought.
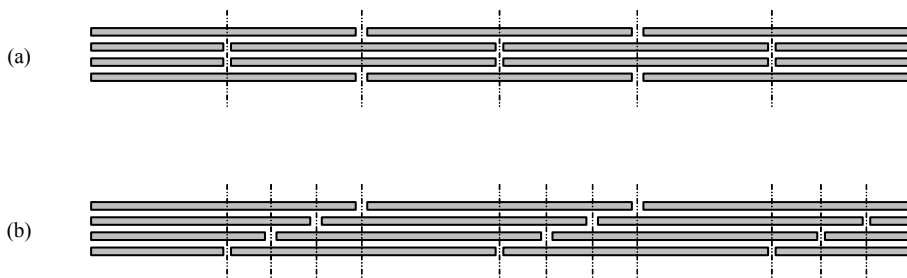
Figure 10.12: Segmentation scheme of (splice-laminated) oversized reinforced glass beams; top view;
(a) Symmetric segmentation scheme; (b) Asymmetric segmentation scheme.

10.3.6. *Multifunctional use of reinforcement*

The reinforced glass concept offers some specific opportunities for a multifunctional use of the reinforcement. This is especially the case for the stainless steel reinforced glass beams with the reinforcement bonded at the inner recessed edge. Besides its primary function as reinforcement, the stainless steel which is exposed at the edge can simultaneously be used as a backing for façade or roof cladding fixations, see Figure 10.13. For this purpose the reinforcement section can be applied in a large variety of geometries to conform to the specific connection needed. A similar concept of multifunctional use of the reinforcement has recently been presented by Weller, Weimar & Meier [Weller, Weimar & Meier, 2010], who developed glass fins with a stainless steel reinforcement that simultaneously functions as a connector to a facade cladding system. For this concept a similar GB adhesive as is studied in the current research has been applied to bond the reinforcement to the edge of the glass.

(a)   (b)
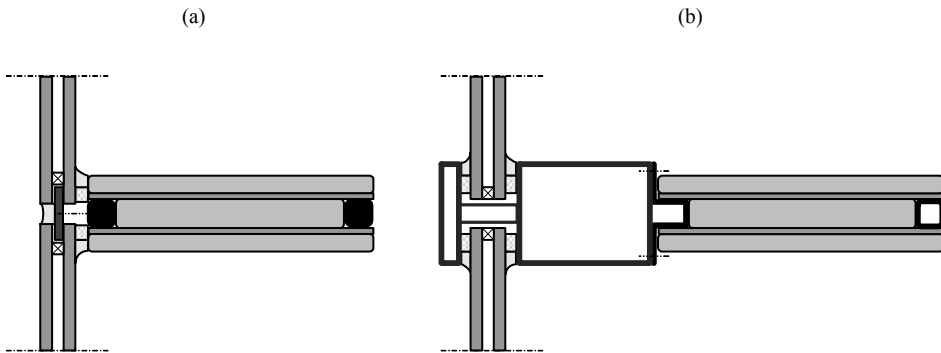
Figure 10.13: Suggestions for multi-functional use of metal reinforcement section integrated at the inner recessed edge of the glass beams; (a) two-sided reinforced glass façade fin with solid section reinforcement acting as a backing for the fixing of the glass façade sheets; (b) two-sided reinforced glass façade fin with reinforcement functioning as a connector to a façade cladding system.

10.4.   Evaluation

From the integrated discussion on the production and design aspects of reinforced glass beams, provided in the Chapter, the following key issues follow.

Firstly, it is observed that the two beam designs that have been investigated in this research are feasible both from a design and a production point of view.

Secondly, it is observed that the SG interlayer and the associated vacuum bag autoclave lamination process offers the most promising production technique for reinforced glass beams. Due to its relatively large thickness and its low viscosity when heated during the lamination process, the SG interlayer easily conforms to any dimensional inaccuracies on the glass and/or reinforcement. Furthermore, due to its low viscosity during the lamination process the SG interlayer easily flows around reinforcement sections embedded in the interlayer.

Thirdly, it is observed that the beams with the reinforcement embedded in the interlayer allow for a large variety of reinforcement geometries (e.g. full sections, strips or meshes), reinforcement materials (e.g. glass fiber, carbon fiber, stainless steel, etc.) reinforcement shapes (e.g. straight or curved) or reinforcement quantity (e.g. extra reinforcement at specific highly stressed zones) to be integrated in the beam design. This provides some specific possibilities to influence the architectural expression of the beams.

Finally, it is observed that the beams with the reinforcement bonded at the inner recessed edge provide specific possibilities for a multifunctional use of the reinforcement section. Since the (metal) reinforcement is exposed at the edge, it can be used for instance for fixing façade or roof cladding.

PART V

Retrospect and Prospect

Part I

Introduction

Chapter 1

Introduction to the research

Part II

Theoretical framework

Chapter 2

Structural glass beams

Chapter 3

The reinforced glass beam concept

Chapter 4

Materials applied in this research

Part III

Experimental, analytical and numerical investigations

Chapter 5

Experimental investigations into the effects of bond type, temperature, thermal cycling, humidity and load duration on the structural response

Chapter 6

Experimental investigations into the effects of reinforcement percentage and beam size on the structural response

Chapter 7

Experimental investigations into the structural response of SG-laminated glass beams with embedded glass fibre reinforcement

Chapter 8

Analytical and numerical modelling of the structural response

Part IV

Integrated discussion of the research results

Chapter 9

Integrated discussion on the structural aspects of reinforced glass beams

Chapter 10

Integrated discussion on the production and design aspects of reinforced glass beams

Part V

Retrospect and prospect

Chapter 11

Conclusions

Chapter 12

Recommendations

Chapter 11
Conclusions

This chapter provides the conclusions from the research presented in the preceding chapters. The following chapter, Chapter 12, presents the recommendations for future research.

Abstract

From the experimental investigations performed in this research it is concluded that reinforcing an annealed float glass beam, in order to obtain safe post-breakage behaviour, is a feasible and safe concept. The experiments demonstrated that significant post-breakage strength and stiffness can be obtained through the addition of a reinforcement section at the tensile zone of the glass beam. Furthermore, it is concluded that the SG-laminated beams performed best. The SG-laminated beams showed only limited debonding of reinforcement at the post-breakage stage, whereas the GB-bonded beams often show full debonding of reinforcement and consequent collapse. Moreover, it is concluded that the SG-laminated reinforced glass beams are feasible to be applied in practice. Even at high and low service temperatures, after thermal cycling and for long-duration loading, the SG-laminated reinforced glass beams show redundant post-breakage performance. However, it should be noted that the effect of humidity on the structural response is not yet sufficiently understood to be able to apply the SG-laminated reinforced glass beams in (highly) humid environments. Additionally, it is concluded that the SG interlayer is well-suited for the production of reinforced glass beams. Due to the low viscosity of the hot SG during the autoclave process, the SG easily adjusts to its surroundings, which allows it to adapt to dimensional tolerances and which allows for the embedment of reinforcement in the SG interlayer. From the analytical investigations performed in this research it is concluded that the analogy with reinforced concrete is valid. Furthermore, it is concluded that the analytical model offers a basic, but fairly accurate tool to describe the overall structural response of reinforced glass beams. From the numerical investigations it is concluded that the sequentially linear elastic analysis (SLA) method and the associated saw-tooth diagrams offer a suitable technique for the simulation of glass fracture and plastic deformation of reinforcement. Furthermore, it is concluded that the numerical model rather accurately describes the structural response of reinforced glass beams in terms of load-displacement diagrams. However, it should be noted that both the analytical and the numerical model currently neglect any layering of the glass and do not incorporate an intermediary bond between the glass and the reinforcement.

11.1.   Introduction

This chapter provides the conclusions from the current study into the structural aspects of reinforced glass beams. Firstly, the conclusions from the experimental investigations are provided in section 11.2. Subsequently, the conclusions from the analytical and numerical investigations are provided in section 11.3.

11.2.   Conclusions from the experimental investigations

The experimental investigations done in this research focused on the effects of the parameters *bond system*, *temperature*, *thermal cycling*, *humidity*, *load duration*, *reinforcement material*, *reinforcement percentage* and *beam size* on the structural response of reinforced glass beams. This was done by means of pull-out tests to investigate the pull-out strength of the reinforcement, and by means of bending tests to investigate the structural response of reinforced glass beams.

Two specific bond systems were investigated, namely the UV-curing acrylate adhesive GB368 (GB) and the ionomer SentryGlas® (SG) interlayer. Furthermore, two specific beam geometries were investigated, namely triple-layer annealed float glass beams with a stainless steel reinforcement section bonded (with the GB adhesive or the SG interlayer) at the inner recessed tensile edge, and double-layer annealed float glass beams with GFRP (Glass Fiber Reinforced Polymer) reinforcement rods embedded in the SG interlayer.

The following subsections provide the conclusions from the experimental investigations.

11.2.1. Bond system

From the results of the pull-out tests and bending tests performed on GB-bonded and SG-laminated specimens it is concluded that the SG-laminated specimens demonstrate better performance[i]. In the pull-out tests series the SG-laminated specimens consistently showed the highest bond strength. Furthermore, in the bending test series the SG-laminated beams consistently reached higher post-breakage strength levels.

Due to the high bond strength of the SG interlayer, the SG-laminated beams demonstrated only limited debonding of reinforcement at the post-breakage stage. This effectively enhanced their post-breakage performance. None of the SG-laminated reinforced glass beams failed due to full debonding of reinforcement. For all the SG-laminated beams the reinforcement remained largely attached to the glass, whereas full debonding of reinforcement was often observed for the GB-bonded beams.

---

[i] The in this research observed performance levels of the investigated bond systems should not be interpreted for applications outside the scope of this research. For applications outside the scope of this research, different conditions may apply – such as a different bond geometry, loading condition, manufacturing technique, etc. – which may lead to a different performance of the bond system than is observed in this research.

However, it should be noted that the performance of the GB-bonded beams could possibly be enhanced by the application of an improved manufacturing process. Currently, the applied manufacturing technique, which was developed in this research, allows only for a more or less fixed adhesive thickness of $t \approx 0.1$ mm. A change in bond thickness might enhance the performance of the GB-bonded specimens.

Furthermore, it is concluded that the SG-laminated reinforced glass beams are the most feasible to be applied in practice. The SG-laminated beams demonstrated redundant response even at high and low service temperatures (within the range of -20 to +60°C) and after cyclic temperature loads (150 cycles between -20 to +30°C, for 1.5 m beams). Despite a negative change in post-breakage performance at high and low temperatures and after thermal cycling, the beams showed high post-breakage strength and ductile post-breakage response. Additionally, the SG-laminated beams performed very well in the long-duration loading tests, and did not even collapse after being loaded for 3 to 15 months at 80% of the predicted ultimate failure load.

However, it should be noted that the effects of humidity on the structural response are not yet sufficiently understood to be able to apply the SG-laminated reinforced glass beams in (highly) humid environments. The observed delamination of an SG-laminated beam after the humidity exposure procedure urges for caution and requires additional studies into the effect of humidity on the SG laminate.

Additionally, it is concluded that the SG interlayer is well-suited for the production of reinforced glass beams and can be applied for various beam geometries. Due to the low viscosity of the SG interlayer during the autoclave process, the SG interlayer easily adapts to the geometry of the glass and the reinforcement and easily conforms to dimensional tolerances. This low viscosity of the SG interlayer during the lamination process allows for the embedment of reinforcement in the SG interlayer, as has been done in this research for the GFRP-reinforced glass beams. These beams with embedded reinforcement are attractive in multiple respects. From a structural point of view they offer the possibility of applying additional reinforcement at highly stressed zones. From a durability point of view the embedded reinforcement sections are well shielded from direct impact and from direct humidity exposure. Finally, from an architectural point of view the embedded reinforcement offers the possibility to give the beam a specific architectural expression through the application of specific reinforcement materials and/or geometries.

11.2.2. Temperature

From the results of the pull-out tests conducted at -20, +23, +60 and +80°C and the bending tests performed at -20, +23 and +60°C it is concluded that increased and decreased temperature levels both negatively affect the post-breakage response of reinforced glass beams. However, for the GB-bonded beams this effect was more significant than for the SG-laminated beams.

At increased temperatures the strength and stiffness of the GB adhesive bond and the SG interlayer bond decreased, which caused more excessive debonding of reinforcement at the post-breakage stage. This reduced the efficiency of the reinforcement in halting crack growth in the glass and stimulated the occurrence of plastic-hinges in the beam. For the GB-bonded beams the more excessive debonding or reinforcement even led to full debonding and bond-slip of the reinforcement, which resulted in collapse of the beams. For the SG-laminated beams the more excessive debonding led to the occurrence of plastic hinges, but the beams did not collapse.

At decreased temperatures the strength, stiffness and toughness of the bond between the glass and reinforcement altered, which again causes more excessive debonding of reinforcement thus less efficient crack halting by the reinforcement. For the GB-bonded beams the more excessive debonding was caused by a decrease in bond strength of the GB adhesive at decreased temperatures. This decreased bond strength caused full debonding of reinforcement, thus collapse of the beams, shortly after initial glass failure. For the SG-laminated beams it is assumed that the more excessive debonding resulted from a decrease in toughness of the SG bond at decreased temperature levels. However, despite the more excessive debonding in the SG-laminated beams, the reinforcement remained largely attached and the beams could still develop ductile post-breakage response without showing collapse.

11.2.3. *Thermal cycling*

From the results of the pull-out and bending tests performed after thermal cycling it is concluded that thermal cycling has a significant negative effect on the post-breakage response of the GB-bonded beams, whereas it has only a limited effect on the SG-laminated glass beams[i].

It is assumed that this difference in thermal cycling effect on the structural response of the reinforced glass beams originated from a difference in thickness and stiffness of the bond systems. The relatively large thickness of the SG interlayer ($t = 1.52$ mm) resulted in a more flexible bond, which allowed for more shear deformation than the relatively thin and rigid GB adhesive bond ($t \approx 0.1$ mm). Assumedly, the SG interlayer was therefore better able to conform to the shear deformation that was imposed by a difference in thermal expansion of the glass and the reinforcement.

11.2.4. *Humidity*

From the results of the pull-out and bending tests performed after a humidity exposure procedure, it is concluded that humidity can negatively affect the post-breakage performance of SG-laminated reinforced glass beams.

---

[i] It should be noted, however, that both the GB-bonded and SG-laminated pull-out specimens showed a significant decrease in strength after the thermal cycling procedure.

The pull-out tests indicated a significant reduction in bond strength of the SG bond after the humidity exposure procedure. At first instance this reduced bond strength was not reflected in the performance of the humidity exposed beam specimens. The humidity exposed SG-laminated reinforced glass beams showed similar (ductile) response as has been observed for non-exposed specimens. However, one (out of three) beam specimens displayed excessive delamination of the SG laminate at the post-breakage stage. It is assumed that this delamination was caused by the humidity exposure procedure. Since it only occurred for one specimen, though, it may also be the result of an incidental manufacturing error. However, this could not be traced and further research is needed.

11.2.5. Load duration

From the results of the long-duration pull-out and bending tests, it is concluded that the SG-laminated reinforced glass beams provide excellent post-breakage resistance for significant periods of time.

Although the long-duration pull-out tests indicated creep of the SG interlayer bond, this was not a critical parameter for the long-duration performance of the SG-laminated beam specimens. Despite some creep deformation, due to creep of the SG interlayer and additional cracking of the glass, the SG-laminated beams were able to withstand the applied load for a significant period of time. More specifically, they were able to carry up to 80% of the predicted ultimate failure load for more than 3 and even up to 15 months in the cracked stage without showing collapse. This indicates that there will be sufficient time to detect failure and to take measures in case of fracture of a SG-laminated reinforced glass beam applied in a building structure.

11.2.6. Reinforcement material

From the bending tests performed on both stainless steel reinforced and GFRP (Glass Fiber Reinforced Polymer) reinforced glass beams it is concluded that both materials perform well as reinforcement in annealed float glass beams. Furthermore, it is concluded that semi-ductile post-breakage response can be obtained without any plastic deformation capacity of the reinforcement.

The stainless steel reinforced glass beams demonstrated, due to the plastic deformation capacity of the stainless steel reinforcement, ductile post-breakage response. Furthermore, due the high tensile strength of the stainless steel reinforcement, the beams reached significant post-breakage strength levels.

The GFRP reinforced glass beams showed, despite the absence of any yield capacity of the GFRP reinforcement rods, semi-ductile post-breakage response. This semi-ductility originated from progressive cracking of the glass, which gradually reduced the bending stiffness of the beams. Additionally, it is assumed that the semi-ductility originated from local debonding of the GFRP reinforcement rods which allowed the cracks to open up further thereby gradually reducing the bending stiffness.

11.2.7. Reinforcement percentage

From the results of the bending tests on beams with varying reinforcement percentages is concluded that varying the reinforcement percentage influences the height of the initial cracks in the glass and influences the post-breakage strength of the reinforced glass beams.

Increasing the reinforcement percentage caused a lowering of the neutral beam axis and thereby a reduction of the height of the (initial) cracks in the glass. Furthermore, due to the higher total strength and stiffness of the reinforcement the beams demonstrated higher strength and stiffness at the post-breakage strength.

11.2.8. Beam size

From the results of the bending tests on the 1.5 m and 3.2 m triple-layer SG-laminated glass beams with a stainless steel reinforcement section bonded at the inner recessed edge, it is concluded that the effects of beam size on the structural response are limited.

The 1.5 m and 3.2 m beams demonstrated similar cracking response and post-breakage ductility. Only a small difference in post-breakage response between the 1.5 m and 3.2m beams occurred. The 1.5 m SG-laminated beams profited from an additional load-carrying mechanism, which was generated by glass fragments that locally bridged cracks in neighbouring glass layers. These crack-bridging glass fragments were able to transfer (tensile) forces over the crack through shear in the SG interlayer. This provided the 1.5 m SG-laminated beams, apart from to the reinforcement, with an additional tensile force transferring mechanism which enhanced the residual resistance of the beams. For the 3.2 m SG-laminated beams this mechanism seemed largely absent. No specific explanation for this difference was found.

11.3.   Conclusions from the analytical and numerical investigations

An analytical and a numerical model to describe the structural response of reinforced glass beams were investigated in this research, see Chapter 8. The model results were compared with the experimental results.

The analytical model was developed in this research in analogy with reinforced concrete. Equations were derived from the reinforced concrete theory which were then applied to describe the structural response of reinforced glass beams in terms of M-κ (moment-curvature) or F-δ (force-displacement) diagrams.

The 2D numerical model made use of DIANA Finite Element Analysis software and a novel user-defined sequentially linear analysis (SLA) technique in which cracking of the glass and plastic deformation of the reinforcement was simulated by means of saw-tooth reduction diagrams. This numerical model was used to describe the structural response of reinforced glass beams in terms of F-δ (force-displacement) curves and to generate cracking sequences of the glass.

The following sub-sections provide the conclusions from the analytical and numerical investigations.

11.3.1.   Analytical model

From the analytical investigations it is concluded that the analogy of reinforced glass with reinforced concrete is valid. The analytical model described the post-breakage response of – especially GB-bonded – reinforced glass beams fairly well and provided a basic tool to describe the linear elastic and the post-breakage response of reinforced glass beams in terms of load-displacement relation.

However, the specific influence of the bond system applied in the reinforced glass beams was not incorporated in the analytical model. The analytical model assumed a solid cross-section without any layering of the glass. The additional load-carrying mechanism generated by crack-bridging glass fragments in the SG-laminated glass beam through shear in the SG interlayer was therefore not predicted by the model. Furthermore, the analytical model did not take the bond between the glass and the reinforcement into account. Any effects of bond failure and thus debonding of reinforcement on the structural response of reinforced glass beams were therefore not described by the model.

11.3.2.   Numerical model

From the numerical investigations it is concluded that the sequentially linear elastic analysis (SLA) method and the associated saw-tooth diagrams offer a suitable technique for simulating cracking of the glass and plastic deformation of the reinforcement. The numerical model rather accurately described the structural response of the reinforced glass beams in terms of load-displacement diagrams. Furthermore, the numerical model was able to simulate the frequent peaks in the post-breakage curve without running into convergence problems.

However, similar to the analytical model, no layering of the glass and thus no interlayer sheets between the glass layers was incorporated in the numerical model. This caused, similar to the analytical model, an underestimation of the post-breakage strength of the SG-laminated beams. Furthermore, the bond between the glass and the reinforcement was, again similar to the analytical model, not incorporated in the model. Bond-slip of the reinforcement and its effects on the structural response of reinforced glass beams were therefore not described by the numerical model. Moreover, the cracking sequences resulting from the numerical model were only indicative and insufficiently consistent with the experimental results. The number and shape of the cracks in the glass were not sufficiently accurate described by the numerical model.

Chapter 12
Recommendations

This final chapter closes this research on the structural aspects of reinforced glass beams and provides recommendations for future research.

Abstract

A number of topics are recommended to investigate in future research. Firstly, it is recommended to further investigate the effects of specific parameters on the structural response of reinforced glass beams, such as humidity, beam size and glass type. Especially the effect of humidity on the SG-laminated reinforced glass beams should be investigated in more detail. Secondly, it is recommended to further develop the analytical and the numerical model to enhance their results. Especially the incorporation of the bond between the glass and the reinforcement in the models could enhance their results. Furthermore, the implementation of layering of the glass in the numerical model could enhance its results. Thirdly, it is recommended to investigate the possibilities of embedded reinforcement in more detail. The current research showed that embedding reinforcement is promising both from a structural and an architectural point of view. Fourthly, it is recommended to further investigate the post-breakage lateral stability of reinforced glass beams. Especially for laterally unsupported components that are both axially loaded and in bending, such as load-bearing facade fins/columns, the post-breakage stability might become crucial. Finally, it is recommended to also investigate an alternative beam concept which makes use of post-tensioning tendons to apply a compressive pre-load on the beam. It is expected that through this activation of the tension components the structural performance of glass beams can even be enhanced further.

12.1.   Introduction

From this research various recommendations for further studies follow.

Firstly, section 12.2 provides recommendations concerning further investigations into various (combined) parameters on the structural response of reinforced glass beams. Secondly, section 12.3 provides recommendations for further studies into the analytical and numerical modelling. Thirdly, section 12.4 describes recommendations for further studies into embedded reinforcement. Fourthly, section 12.5 provides recommendations for further studies into the lateral stability of reinforced glass beams. Finally, section 12.6 provides recommendations for an alternative concept of post-tensioned glass beams.

12.2.   Parameter studies

12.2.1. Effect of humidity

The current research has revealed an inconsistent – though probably negative – effect of humidity on the structural response of SG-laminated reinforced glass beams. During the bending tests that have been performed after humidity exposure, one out of the three SG-laminated beam specimens demonstrated delamination of the SG-laminate at the post-breakage stage. It is assumed that this delamination originates from the humidity exposure which has decreased the bond strength of the SG interlayer. This reduction in bond strength was also observed in the pull-out tests. However, two out of the three beam specimens did not reveal any sign of being affected by the humidity exposure. This may indicate that the observed delamination is related to an incidental manufacturing error. However, this could not be traced.

It is therefore recommended to investigate the effects of humidity on the bond strength of the SG interlayer in more detail. Specific attention could be given to whether the humidity affects only the perimeter of the SG-laminate or whether the humidity permeates further into the laminate. This will provide valuable information for the design of reinforced glass beams. If the humidity pre-dominantly affects the perimeter of the SG-laminate, it would be recommended to design the beams such that the reinforcement is not positioned directly at the edge of the laminate, but somewhat away from the edge as has been done for the SG-laminated beams with embedded reinforcement investigated in Chapter 7. It is expected that this will limit or even eliminate any negative effects of humidity on the structural functioning of the system at the post-breakage stage.

Furthermore, it is – in case humidity turns out to have a significant negative effect on the SG bond strength – recommended to investigate humidity blocking measures. Possibly the permeation of water between the glass and SG interlayer can be avoided through the application of an edge seal along the perimeter of the SG-laminate. Perhaps an ordinary silicone seal can be applied, or similar sealing measures as are used for insulated glass can be applied. However, specific attention should be given to avoid a chemical mismatch between the edge seal and the SG-interlayer, to avoid any degradation of the SG interlayer due to the edge seal.

12.2.2. Beam size effect

The effects of beam size on the structural response of SG-laminated reinforced glass beams have been investigated in Chapter 6. From this investigation it was concluded that beam size only has a limited effect on the structural response of SG-laminated reinforced glass beams. In this research two different beam sizes, namely 1.5 m and 3.2 m beams, have been investigated. However, compared to the oversized glass beams that are increasingly applied in contemporary architecture, see Chapter 2, the latter beam size is still rather small.

It is therefore recommended to further investigate the effects of beam size by a further scaling of the beams. Complementary to the studies performed in this research, future research should focus on larger beam sizes of e.g. 6, 12 and possibly 18 m. These studies should confirm whether or not the effects of beam size are still rather limited for large and oversized SG-laminated reinforced glass beams. It should, however, be noted that the production of the 12 and 18 m laminated glass beams is not yet common practice, which might complicate the study in terms of budget.

12.2.3. Effect of heat-strengthened and tempered glass

This research has focused on the structural aspects of reinforced *annealed float glass* beams. Annealed float glass has been selected because of its favorable fracture pattern. Upon failure, this glass type shows rather localized fracture instead of full fragmentation. For reinforced glass beams this localized fracture prevents from full disintegration of the beam upon glass failure. The current research has demonstrated that the reinforced annealed float glass beams provide a significant post-breakage resistance. However, due to the use of annealed float glass, their design strength is rather low, which results in rather large cross-sectional dimensions.

It is recommended to also investigate the use of heat-strengthened and fully tempered glass in reinforced glass beams. The main advantage of heat-strengthened or fully tempered glass is that these glass types have a higher (design) tensile strength, which could reduce the cross-section dimensions of the beams. Furthermore, due to the higher strength of heat-strengthened and fully tempered glass, connections to the surrounding members will be easier to realize.

However, it should be noted that, as indicated by the research of Kreher [Kreher, 2004] on timber reinforced glass beams, the application of heat-strengthened or fully tempered glass might lead to a reduction in residual resistance of the reinforced glass beams. It was observed in the research of Kreher that due to the more extensive fracture pattern of heat-strengthened and fully tempered glass, the post-breakage integrity of the heat-strengthened and fully tempered timber-reinforced glass beams was less compared to the annealed timber-reinforced float glass beams. However, the research of Kreher has only focused on single-layer reinforced glass beams. The application of laminated glass (i.e. SG-laminated glass) might give different results due to an interaction between the glass layers through the (SG) interlayer. Furthermore, since the crack pattern of heat-strengthened glass is largely similar to annealed float glass, it is expected that the loss of integrity at the post-breakage stage will be limited and that heat-strengthened glass beams will still reach significant post-breakage strength levels.

Additionally, it should be noted that the application of heat-strengthened or fully tempered glass in reinforced glass beams might require a thorough quality control of the pre-stress level in the glass. The level of pre-stress in heat-strengthened and fully tempered glass might vary significantly between manufacturers or between different production batches. It is expected that this variation in pre-stress level will influence the structural response of the reinforced glass beams. For instance, if the heat-strengthened glass is at the lower end of the pre-stress range it will crack similar to annealed float glass. However, when it is at the high end of the pre-stress range its cracking pattern will be more similar to fully tempered glass. Due to this possible large variation in pre-stress level, the cracking pattern, thus the post-breakage integrity of the reinforced glass beams, will differ significantly. To be able to guarantee a proper functioning of the reinforced glass beams it will therefore be necessary to have a high level quality control of the pre-stress level in the glass, before it is applied in reinforced glass beams.

12.2.4.   *Strengthening effect of the reinforcement*

This research has mainly focused on the *post-breakage* response of reinforced glass beams and no specific attention has been given to the *un-cracked* stage. For the calculation of the moment of inertia (I_y) of the beam composite at the un-cracked stage, see Chapter 8, it was assumed that the reinforcement fully contributes to the overall beam resistance. However, whether this assumption is correct has not been investigated in this research. Furthermore, to what extent this 'strengthening' effect of the reinforcement changes with temperature – due to a change in stiffness of the intermediary bond – or with time – due to possible creep of the intermediary bond – is yet unknown.

It is therefore recommended to investigate this strengthening effect of the reinforcement on the beam resistance at the *un-cracked* stage. In this respect, various topics could be addressed. These topics are briefly described below.

Firstly, it should be investigated whether the reinforcement has any effect on the initial bending stiffness at all. This could be done by simply comparing the initial bending stiffness of un-reinforced with reinforced glass beams. Apart from the presence or absence of the reinforcement, the un-reinforced and reinforced glass beams should have equal section dimensions.

Secondly, it could be investigated to what extent the strengthening effect of the reinforcement is affected by temperature. Temperature influences the stiffness of the intermediary bond between the glass and the reinforcement, and might thus influence the strengthening effect of the reinforcement. This line of reasoning seems to be supported by the temperature tests performed in Chapter 5. From these tests it is observed that the initial failure strength of the reinforced glass beams changes with temperature. The reinforced glass beams tested at -20°C showed higher initial failure strength levels than at room temperature. Reversibly, reinforced glass beams tested at +60°C demonstrated lower initial failure strength levels than at room temperature. To what extent this change in initial beam resistance is related to a change in stiffness of the intermediary bond and a consequent change in reinforcement activation could not be derived from this research. Possibly other effects might have played a role in the difference in initial failure strength, such as differences in sub-critical crack growth due to variations in test temperature, relative humidity and loading rate between the different test series.

Thirdly, it should be investigated whether the strengthening of the reinforcement on the initial beam resistance changes in time. Due to creep of the intermediary bond, the strengthening effect of the reinforcement might decrease in time. However, since the stress in the intermediary bond is assumed to be rather small, the extent of creep is probably insignificant.

Finally, future research could focus on determining whether the reinforcement has any effect on the tensile strength of the glass itself. Besides its contribution to the overall stiffness of reinforced glass beams, the reinforcement might also contribute to the local strength of the glass. As the reinforcement bridges flaws in the glass the tensile stresses at the flaw tip might be reduced (tension-release). This same favourable flaw-bridging effect of reinforcement is suggested by Bos [Bos, 2009] who encountered increased glass failure stress levels of reinforced annealed float glass beams compared to non-reinforced annealed float glass beams. Furthermore, the level of strength enhancement by flaw-bridging of the reinforcement might again be dependent on temperature and time, due to a change in shear stiffness of the intermediary bond.

12.2.5. Combined parameters

This research has focused on the separate effects of bond system, temperature, thermal cycling, humidity, load duration, reinforcement material, reinforcement percentage, beam size and lateral stability on the structural response of reinforced glass beams. However, the combined effect of these parameters on the structural response of reinforced glass beams has not been studied. For specific applications this might be interesting to study.

It is recommended to further investigate the combined effect of a selected number of parameters on the structural response of reinforced glass beams. This should be done for relevant parameter combinations. This will provide more insight in the safety performance of reinforced glass beams.

12.3.   Analytical and numerical model

It is recommended to further develop the analytical and the numerical model that have been investigated in this research.

Firstly, it is recommended to incorporate the bond between the glass and the reinforcement in the models. This will enable the models to describe the effects of bond failure, and thus debonding of reinforcement, on the overall structural response of the reinforced glass beams.

For the analytical model this can possibly be done by extending the model with a set of equations that can be used to determine the shear stress in the bond between the glass and the reinforcement. The studies performed by Ølgaard, Nielsen & Olesen [Ølgaard, Nielsen & Olesen, 2009], who developed a basic model for calculating the shear stress in the adhesive bond of reinforced glass beams by means of a modified Volkersen analysis, can possibly be used for this further development of the analytical model.

For the numerical models this incorporation of the bond between the glass and the reinforcement could be done by means of interface elements that are inserted between the glass and the reinforcement. These interface elements could then be used to simulate bond-slip of the reinforcement. However, the sequentially linear analysis (SLA) technique that has been applied in the current research, is not yet suited for the application of interface elements. Further development of SLA technique is therefore required.

Secondly, it is recommended to incorporate layering of the glass in the models. This enables the models to simulate the effects of the bond system (i.e. the layer between the glass layers) on the overall structural response of the beams. For example, this enables the simulation of the additional load-carrying mechanism that is generated in the SG-laminated beams.

For the numerical model the layering of the glass could be accomplished by means of interface elements positioned between the individual glass layers. However, as mentioned before, the SLA technique is currently not yet suited for the application of interface elements and thus further development is required. Furthermore, layering of the glass probably requires an update of the currently applied 2D model to a 3D model. However, the SLA technique is currently not applicable for 3D modelling and thus further development is required.

Additionally, it is recommended to explore the applicability of strut-and-tie modelling for reinforced glass beams. Possibly this modelling technique can be used in addition or alternatively to the currently developed analytical model, to describe internal beam forces and to determine load and crack paths in the beams.

Finally, it is recommended to extend the SLA technique for rotating crack models. Currently the SLA technique only allows for fixed cracks models, which do not allow for any crack rotation within the model elements. It is expected that the application of a rotating crack model will enhance the shape of the predicted crack pattern to conform to the V-shaped cracks generally observed in the experiments.

12.4.   Embedded reinforcement

This research has demonstrated that embedding reinforcement in the SG-interlayer of laminated glass beams is a feasible and very promising concept. In multiple respects, such as structural performance, architectural expression and manufacturing possibilities, the concept of embedding reinforcement is successful. It offers possibilities for the development of highly transparent beams (in case of e.g. (semi-) transparent GFRP reinforcement rods) and beams with a specific architectonic expression.

It is therefore recommended to further investigate the possibilities of the concept of embedded reinforcement in SG-laminated glass beams. Future research could focus on various topics. These topics are briefly described below.

Firstly, future research could focus on a further increase of the transparency of glass beams with reinforcement embedded in the interlayer. Currently, the GFRP rods still have a translucent appearance, which results from the resin matrix take surrounds the glass fiber filaments. Possibly the transparency of this resin matrix can be enhanced in order to increase the transparency of the full GFRP rod.

Secondly, in addition to the double-layer glass beams investigated in this research, future research should focus on the structural response of triple-(or more)layer glass beams with embedded glass fiber reinforcement. This will increase the available space for incorporating reinforcement, which will effectively enhance the post-breakage performance of the beams. Furthermore, it provides the opportunity to diversify over the different interlayers, e.g. in terms of reinforcement geometry, amount and position.

Finally, future research could explore the possibilities of other reinforcement materials than glass fiber. The application of more pronounced reinforcement materials or geometries, such as perforated metal sheet or wire mesh, could be attractive from an architectural point of view and might give the beam a specific architectonic expression

12.5.   Lateral stability

The lateral stability of reinforced glass beams has been explored in Chapter 6. The 3.2 m SG-laminated stainless steel reinforced glass beams tested in that chapter showed only limited lateral deflection at the post-breakage stage. Probably due to their rather large width and rather stiff SG interlayer sheets, lateral buckling was largely prevented. However, lateral buckling at the post-breakage stage has been observed for more slender reinforced glass beams studied in associated research [Louter et al., 2006a]. Even despite the presence of (a limited number of) lateral supports during the four-point bending procedure, these rather slender beams buckled at mid-span. Due to excessive cracking of the glass at the post-breakage stage, the lateral stability of the beam was much affected.

It is therefore recommended to investigate the lateral stability of reinforced glass beams in more detail. Especially for applications in which the compressed edge of a reinforced glass beam is laterally un-supported, it is essential to know the lateral stability performance of the beam. Too much lateral deformation, either at the linear-elastic stage or at the post-breakage stage, might endanger the integrity of the structure. At the linear elastic stage the lateral stability of the beam could be predicted using lateral torsional buckling prediction methods for glass beams, as are for instance presented by Belis, Blaauwendraad and Luible [Belis, 2005; Blaauwendraad, 2007; Luible, 2004]. However, at the post-breakage stage these lateral buckling predictions do not apply anymore. Due to cracking of the glass the lateral stability of the beams changes and might significantly decrease.

12.6.   Post-tensioned glass beams

As an alternative to reinforced glass beams, the structural response of post-tensioned glass beams has been explored in associated research. These post-tensioned glass beams contain one or two un-bonded steel tendons that are positioned at the long edge of the beam and tensioned at the beam ends. The purpose of these post-tensioning tendons is twofold. Firstly, the tendons apply a compressive pre-stress to the glass, which enhances the tensile (bending) resistance of the glass. Secondly, the pre-stressing steel tendons provide – similar to the reinforcement in reinforced glass beams – the beam significant post-breakage resistance and ductile post-breakage response.

The main difference between the reinforced glass beams and the post-tensioned glass beams is the level of activation of the tension components. The reinforcement in reinforced glass beams is a rather passive tension component which is mainly activated after glass failure, whereas the tendons in post-tensioned glass beams are pre-tensioned and actively contribute to overall beam resistance both at the un-cracked and the cracked stage.

It is recommended to further investigate the potential of post-tensioned glass beams. The exploratory investigations into post-tensioned glass beams, see Appendix IV, have demonstrated that post-tensioning a glass beam is a feasible and promising concept. The investigated post-tensioned glass beams showed, as a result of the post-tensioning tendons, high initial failure strength and high post-breakage strength. Furthermore, the post-tensioned showed, compared to the reinforced glass beams, more controlled initial glass cracking. However, due to the persisting pre-stress of the post-tensioning tendons, the post-tensioned beams showed a rather explosive ultimate glass failure. This aspect should be further investigated in future research.

Appendices

Appendix I: Experimental results

I.1 Experimental results Chapter 5

I.1.1 Pull-out test results at -20, +23, +60 and +80°C, after TC, after HE

The results of the pull-out tests performed at -20, +23, +60 and +80°C, after thermal cycling and after humidity exposure done in Chapter 5, are listed in Table I.1.

Table I.1: Experimental results of the pull-out tests, performed in Chapter 5.

Test name		GB-bonded pull-out test results						SG-laminated pull-out test results					
		-20 °C	+23 °C	+60 °C	+80 °C	TC	HE	-20 °C	+23 °C	+60 °C	+80 °C	TC	HE
Maximum load													
spec. #1		10.8	16.6	4.7	2.5	1.6	6.8	27.2	20.6	10.5	3.2	6.0	11.3
spec. #2		11.4	16.7	4.9	2.7	8.6	6.4	26.2	22.9	12.2	3.1	6.6	10.7
spec. #3		9.5	16.9	4.6	2.5	11.1	6.1	19.3	21.8	10.7	3.4	6.0	14.2
mean	[kN]	10.5	16.7	4.7	2.6	7.1	6.4	24.2	21.8	11.1	3.2	6.2	12.1
st.dev.	[kN]	1.0	0.2	0.2	0.1	4.9	0.3	4.3	1.2	0.9	0.2	0.3	1.8
rel.st.dev.	[%]	9.3	1.1	3.3	3.4	68.9	5.1	17.8	5.3	8.1	4.9	5.1	15.2

I.1.2   *Pull-out test results for long-duration loading*

The results of the long-duration pull-out tests performed in Chapter 5 are presented in Table I.2 and Figure I.1.

Table I.2: Experimental results of the pull-out tests for long-duration loading on
SG-laminated pull-out specimens, performed in Chapter 5.

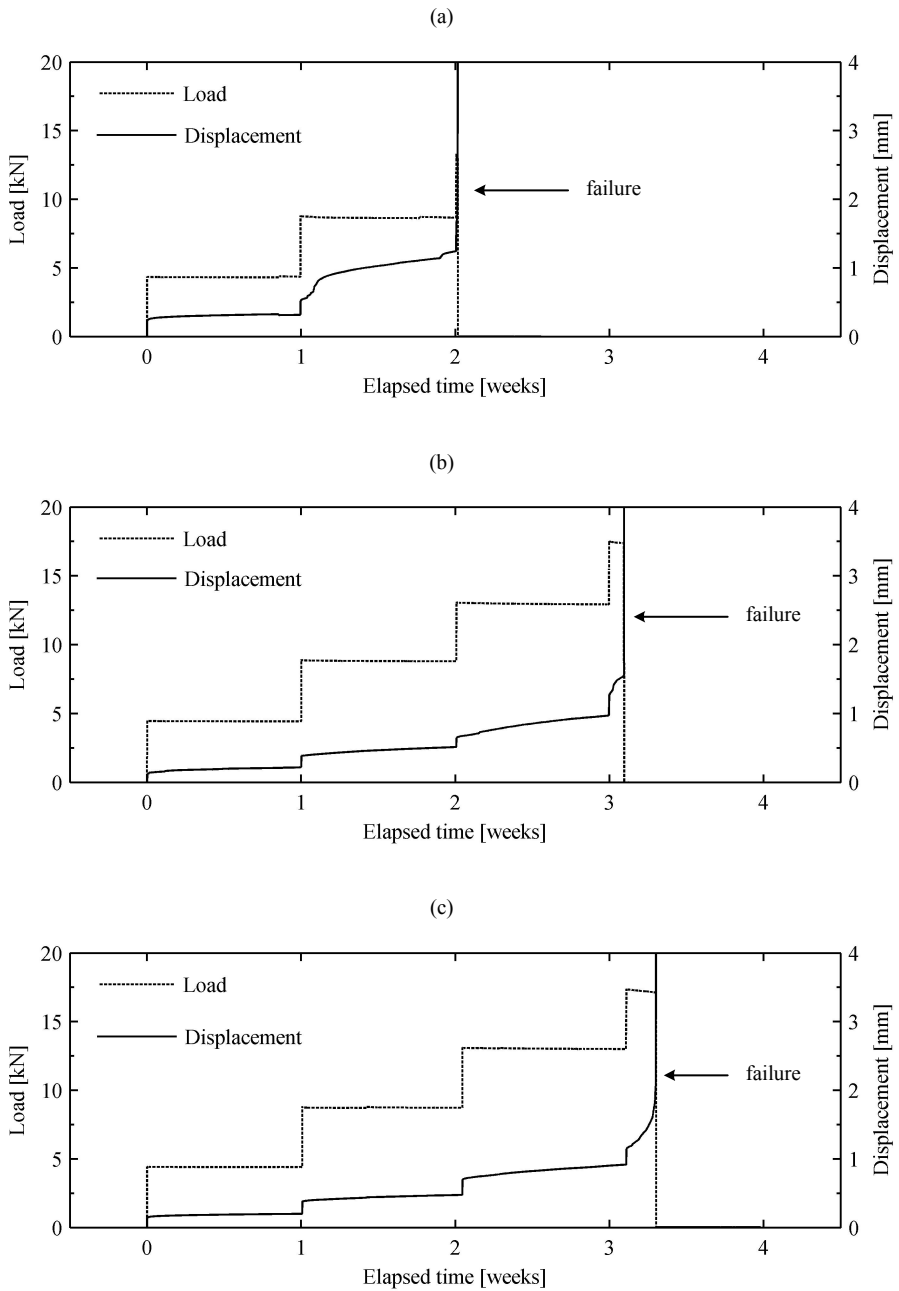| Pull-out specimen name	Maximum load level		Maximum time span
	kN	% of mean at +23˚C	weeks
SG #01	13.3	61.2	2.0
SG #02	17.6	80.5	3.1
SG #03	17.4	79.8	3.3

(a)

(b)

(c)

Figure I.1: Result of the long-duration pull-out tests on SG-laminated pull-out specimens;
(a) specimen #01; (b) specimen #02, (c) specimen #03.

I.1.3   Bending test results at -20, +23, +60 and +80°C, after TC, after HE

The results of the bending tests performed in Chapter 5 at -20, +23 and +60°C, after thermal cycling and after humidity exposure are listed in Table I.3.

Table I.3: Experimental results of the bending tests performed in Chapter 5.

Test name		GB-bonded beam specimens					SG-laminated beam specimens				
		-20 °C	+23 °C	+60 °C	TC	HE	-20 °C	+23 °C	+60 °C	TC	HE
Number of spec.		5	5	5	3	0	5	5	5	3	3
Maximum load											
spec. #1		13.9	11.4	10.1	10.5	-	15.3	11.4	8.7	9.3	11.7
spec. #2		14.6	10.9	9.6	10.7	-	18.1	10.7	11.0	12.0	12.2
spec. #3		12.9	9.3	8.4	10.8	-	15.5	10.8	9.4	9.0	15.0
spec. #4		11.4	9.8	10.3	-	-	17.8	12.8	9.0	-	-
spec. #5		14.5	9.9	10.2	-	-	13.9	13.0	7.4	-	-
Mean	[kN]	13.4	10.3	9.7	10.7	-	16.1	11.7	9.1	10.1	13.0
st.dev	[kN]	1.3	0.9	0.8	0.1	-	1.8	1.1	1.3	1.7	1.8
rel.st.dev.	[%]	9.9	8.4	8.3	1.3	-	11.2	9.5	14.4	16.5	13.7
Post-breakage load											
spec. #1		7.7	14.1	9.6	11.6	-	15.1	16.9	14.1	16.1	15.9
spec. #2		10.7	12.8	9.8	17.1	-	16.1	17.5	14.9	17.1	16.3
spec. #3		9.8	14.2	9.1	9.3	-	16.2	17.1	13.5	16.4	17.9
spec. #4		10.3	13.9	9.8	-	-	15.7	17.8	14.6	-	-
spec. #5		10.1	14.1	9.2	-	-	14.1	18.0	14.3	-	-
mean	[kN]	9.7	13.8	9.5	12.7	-	15.4	17.5	14.3	16.5	16.7
st.dev.	[kN]	1.2	0.6	0.3	4.0	-	0.9	0.5	0.5	0.5	1.0
rel.st.dev.	[%]	12.0	4.1	3.6	31.6	-	5.6	2.8	3.7	3.2	6.1
Post-/ini.- fail. load											
spec. #1		55.3	123.7	95.2	110.2	-	98.9	148.7	161.7	173.5	136.1
spec. #2		73.6	117.7	102.4	159.6	-	88.7	164.6	135.1	143.0	133.5
spec. #3		76.2	152.8	109.3	86.6	-	104.8	158.3	142.7	183.2	119.0
spec. #4		90.5	141.6	95.4	-	-	88.0	138.9	162.1	-	-
spec. #5		69.6	142.5	89.8	-	-	101.8	138.8	193.7	-	-
mean	[%]	73.1	135.7	98.4	118.8	-	96.4	149.9	159.1	166.6	129.5
st.dev.	[%]	12.6	14.5	7.6	37.2	-	7.7	11.6	22.7	21.0	9.2
rel.st.dev.	[%]	17.3	10.7	7.7	31.4	-	7.9	7.7	14.2	12.6	7.1

I.1.4   Bending test results for long-duration loading

The results of the long-duration bending tests performed in Chapter 5 are presented in Figure I.2.
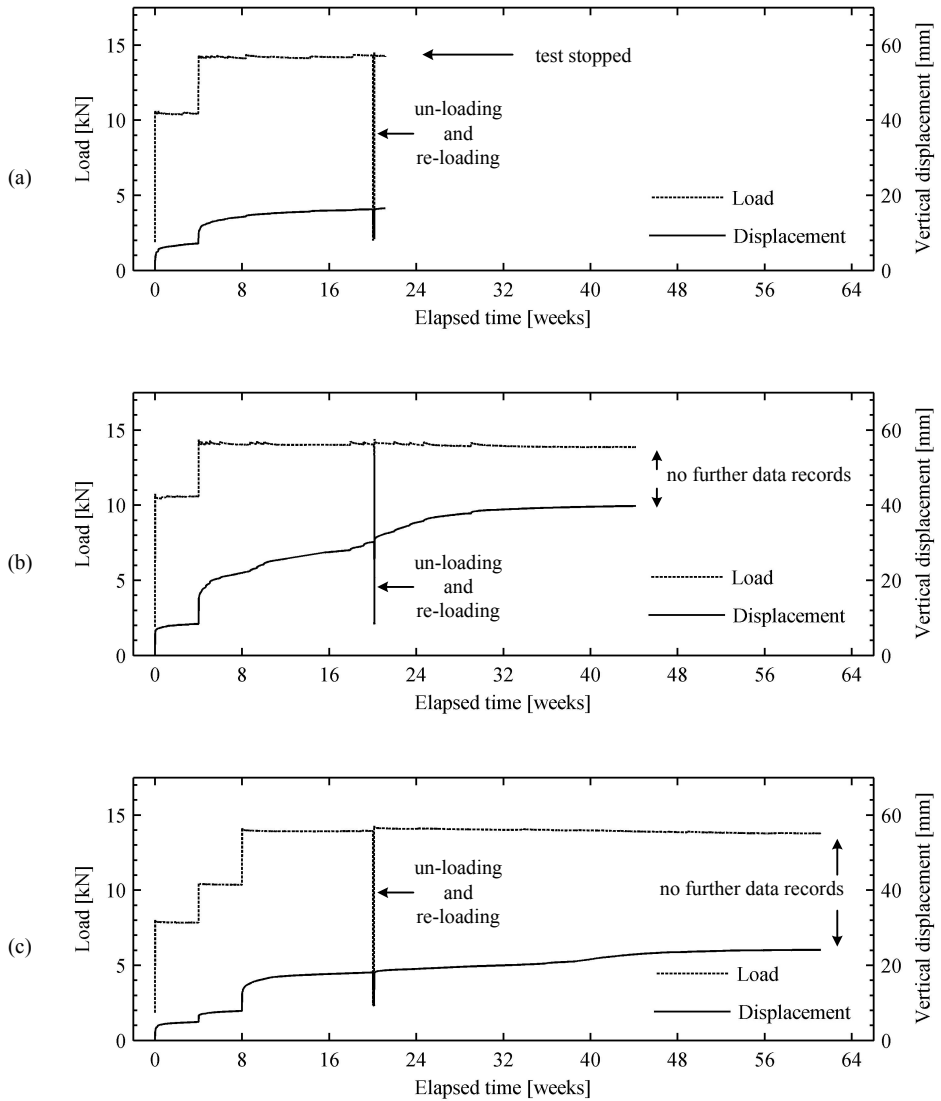
Figure I.2: Results of the long-duration bending tests on SG-laminated reinforced glass beams; (a) specimen #01; (b) specimen#02; (c) specimen #03.

I.2   Experimental results Chapter 6

I.2.1   *Bending test results of the series I, II and III beams.*

The results of the bending tests performed in Chapter 6 are provided in Table I.4.

Table A.1.4: Experimental results of the bending tests performed in Chapter 6.

		Beam series I	Beam series II	Beam series III
Initial failure load				
spec. #1	[kN]	11.4	16.5	30.6
spec. #2	[kN]	10.7	17.6	33.8
spec. #3	[kN]	10.8	16.5	34.3
spec. #4	[kN]	12.8	-	-
spec. #5	[kN]	13.0	-	-
mean	[kN]	11.7	16.9	32.9
st.dev.	[kN]	1.1	0.7	2.0
rel.st.dev.	[%]	9.5	3.9	6.1
Maximum post-breakage load				
spec. #1	[kN]	16.9	40.8	34.6
spec. #2	[kN]	17.5	40.6	36.5
spec. #3	[kN]	17.1	40.5	38.0
spec. #4	[kN]	17.8	-	-
spec. #5	[kN]	18.0	-	-
mean	[kN]	17.5	40.6	36.4
st.dev.	[kN]	0.5	0.1	1.7
rel.st.dev.	[%]	2.8	0.4	4.8
Post-breakage/initial load ratio				
spec. #1	[%]	148.7	247.3	113.0
spec. #2	[%]	164.6	230.2	108.1
spec. #3	[%]	158.3	244.6	111.1
spec. #4	[%]	138.9	-	-
spec. #5	[%]	138.8	-	-
mean	[%]	149.9	240.7	110.7
st.dev.	[%]	11.7	9.2	2.5
rel.st.dev.	[%]	7.7	3.8	2.3

I.2.2   Lateral torsional buckling test results of the series III beams.

The results of the lateral torsional buckling tests on the 3.2 m SG-laminated stainless steel reinforced series III beams performed in Chapter 6 are provided in Figure I.3.
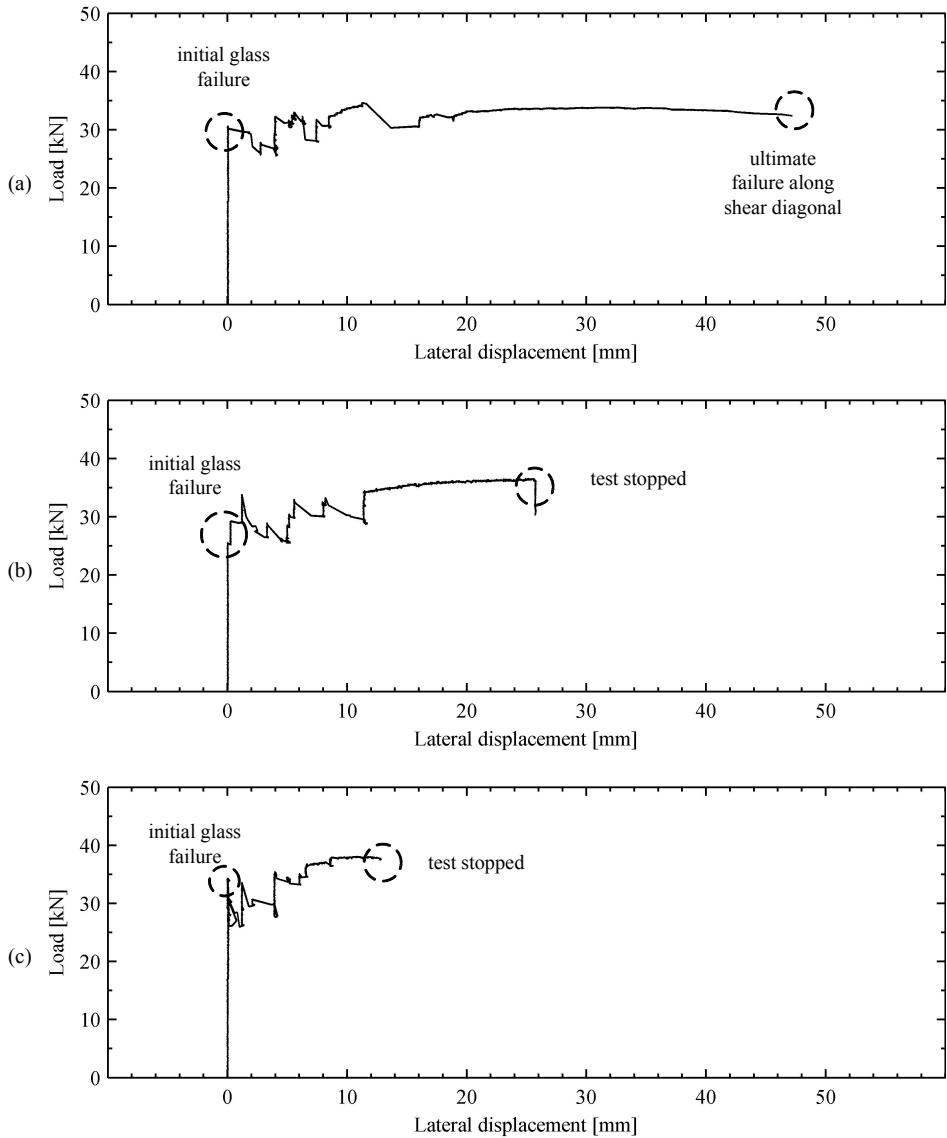
Figure I.3: Results of the lateral torsional buckling tests performed in Chapter 6 on the series III beams;
(a) specimen #01; (b) specimen #02; (c) specimen #03.

I.3   Photo sequences of the bending tests

Figures I.4 to I.9 provide photo-sequences of some exemplary bending tests performed in this research. The specific layout of the specimens is indicated in the Figures, along with a reference to the associated chapter.

GB-bonded, 1.5 m, stainless steel reinforced, hollow section reinforcement; room temperature
(Chapter 5)

(a)   (b)

(c)   (d)

(e)   (f)

Figure I.4: Photo sequence of an exemplary bending test on a 1.5 m GB-bonded reinforced glass beam, with hollow section reinforcement

SG-laminated, 1.5 m, stainless steel reinforced, hollow section reinforcement; room temperature
(Chapter 5+6, series I)

(a)   (b)

(c)   (d)

(e)   (f)
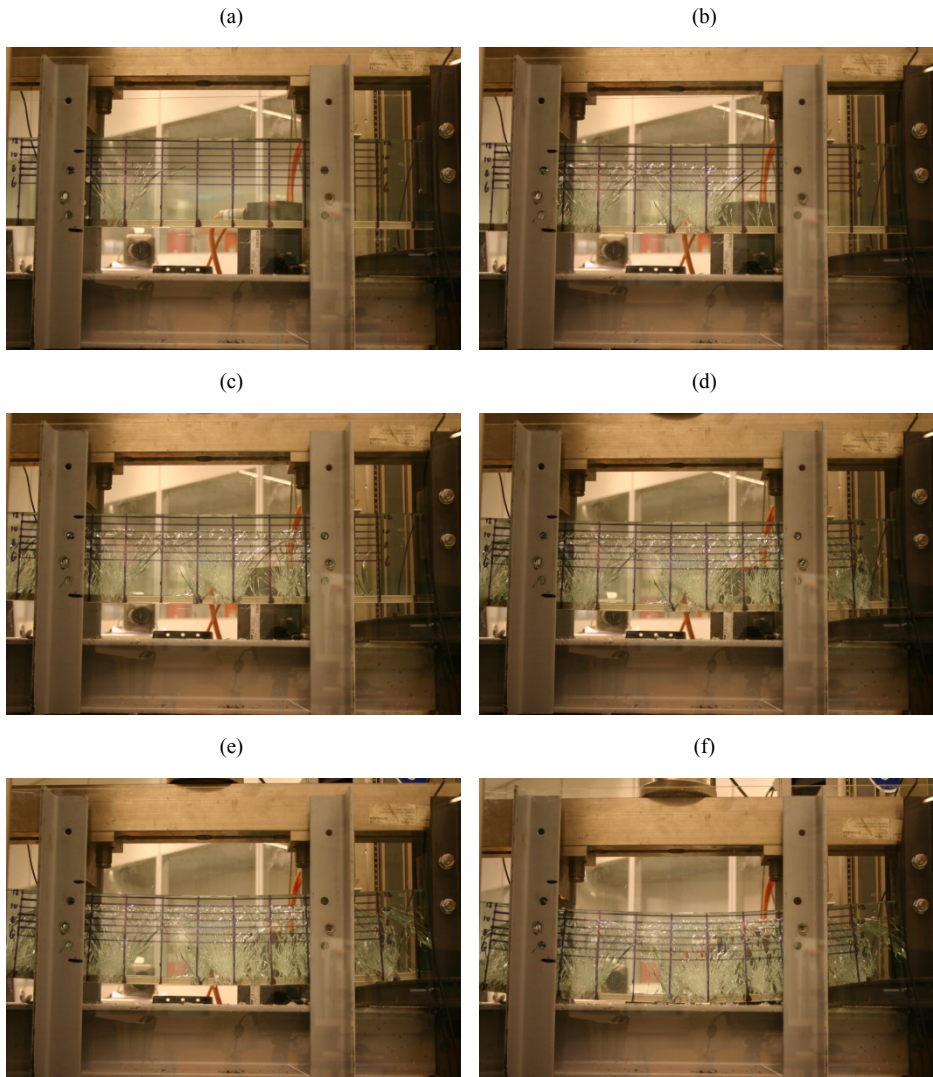
Figure I.5: Photo sequence of an exemplary bending test on a 1.5 m SG-laminated reinforced glass beam,
with hollow section reinforcement.

SG-laminated, 1.5 m, stainless steel reinforced, full section reinforcement; room temperature
(Chapter 6, series II)

(a)

(b)

(c)

(d)

(e)

(f)

Figure I.6: Photo sequence of an exemplary bending test on a 1.5 m SG-laminated reinforced glass beam, with full section reinforcement.

SG-laminated, 3.2 m, stainless steel reinforced, hollow section reinforcement; room temperature
(Chapter 6, series III)

(a)

(b)

(c)

(d)

(e)

(f)

Figure I.7: Photo sequence of an exemplary bending test on a 3.2 m SG-laminated reinforced glass beam, with hollow section reinforcement; lateral torsional buckling test.

SG-laminated, 1.5 m, GFRP reinforced, round reinforcement rods; room temperature
(Chapter 7)

(a)

(b)

(c)

(d)

(e)

(f)
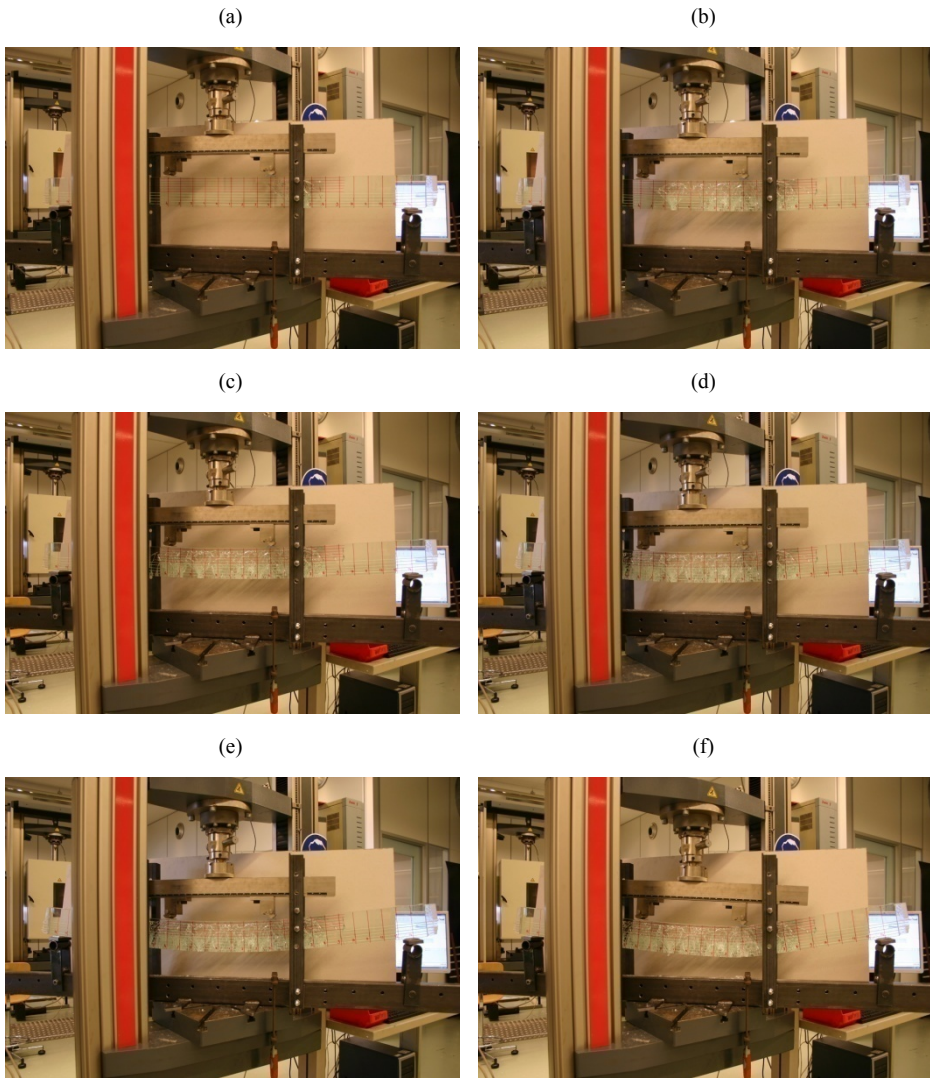
Figure I.8: Photo sequence of an exemplary bending test on a 1.5 m SG-laminated
GFRP-reinforced glass beam, with round reinforcement rods.

SG-laminated, 1.5 m, GFRP reinforced, flat reinforcement rods; room temperature
(Chapter 7)

(a)   (b)

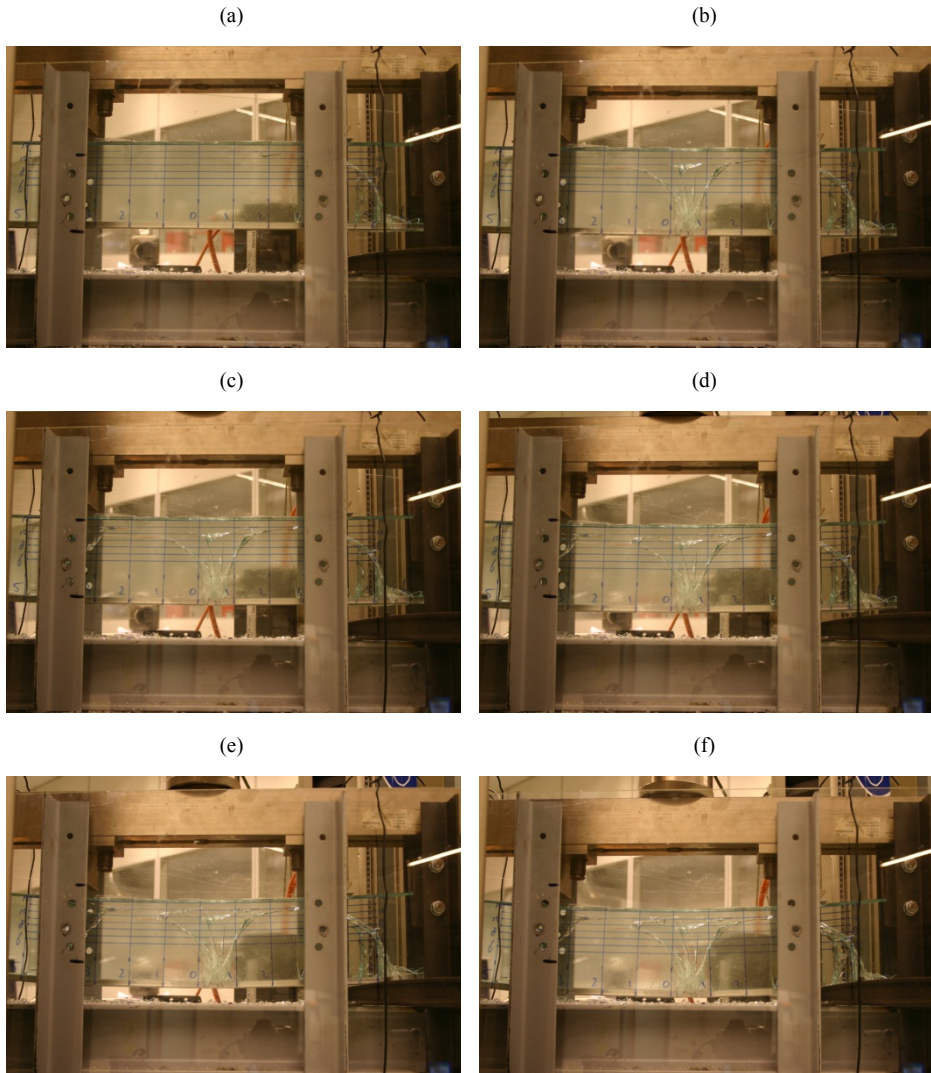(c)   (d)


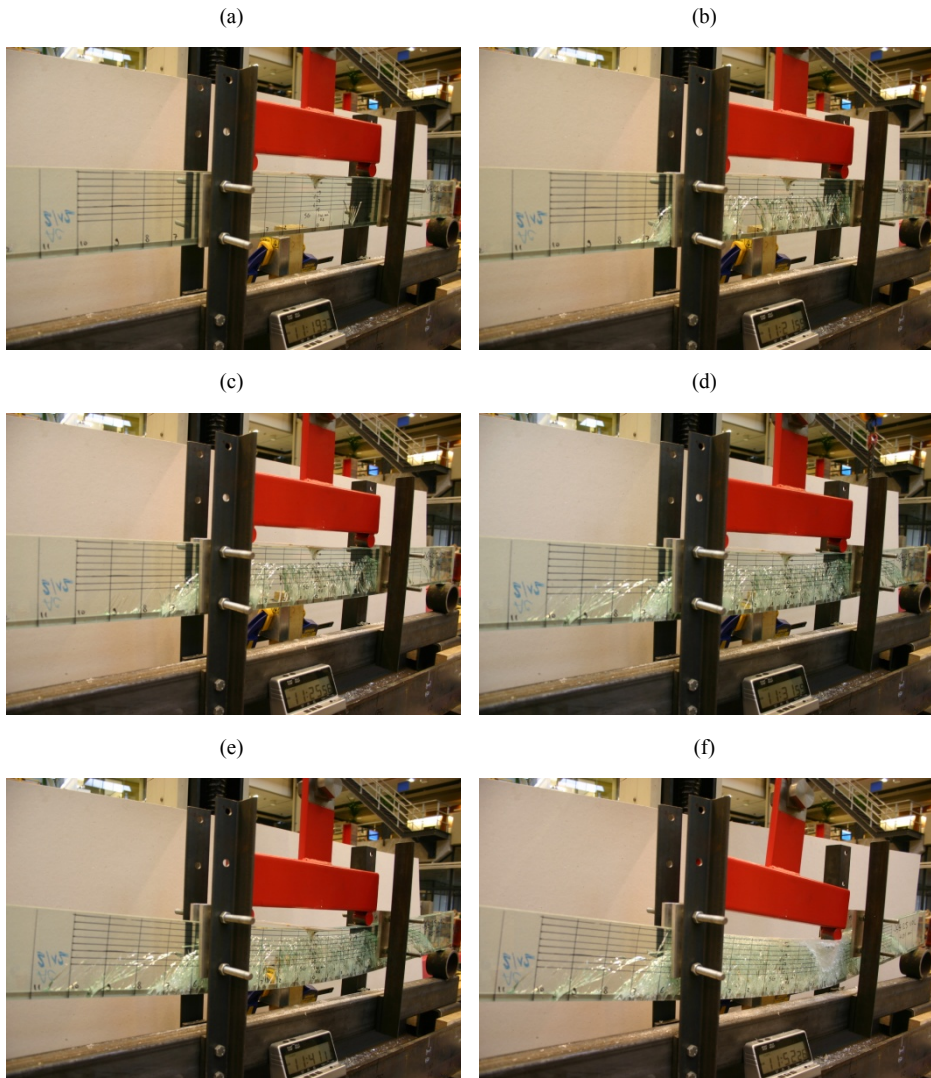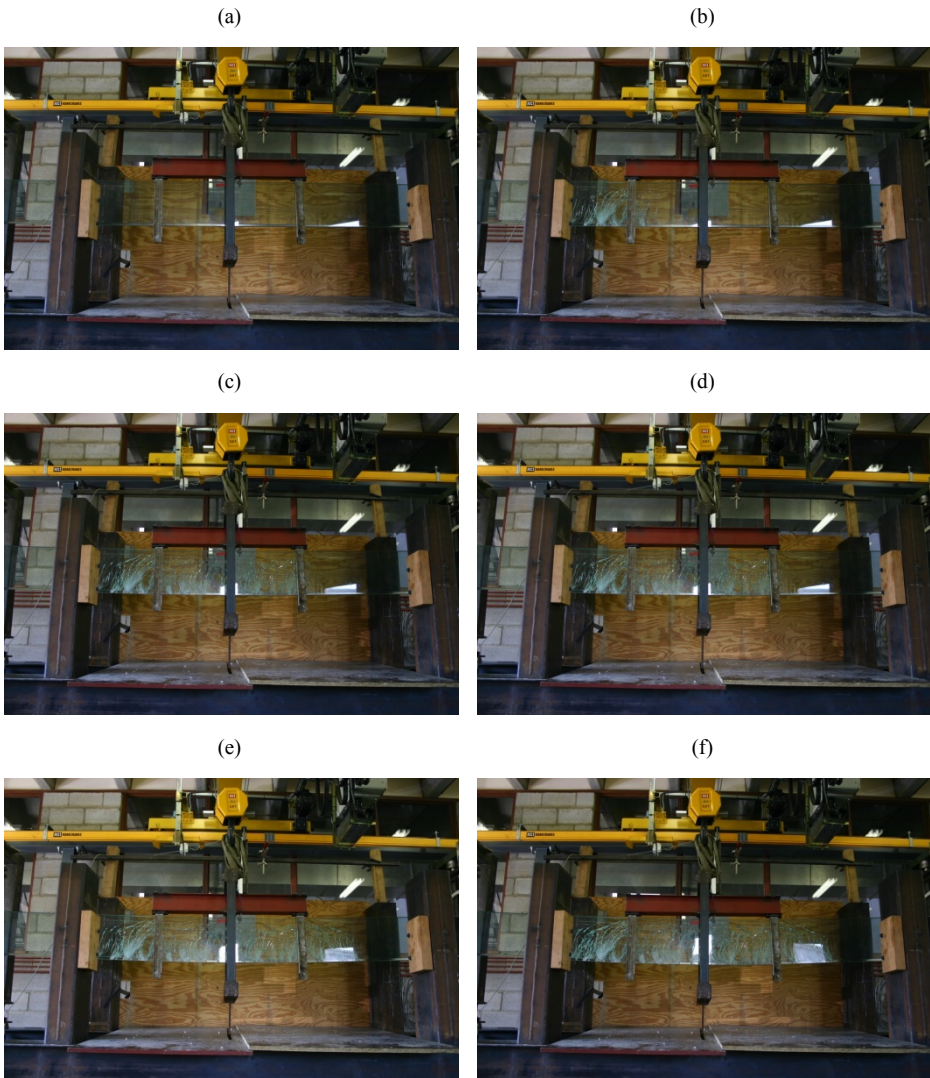(e)   (f)
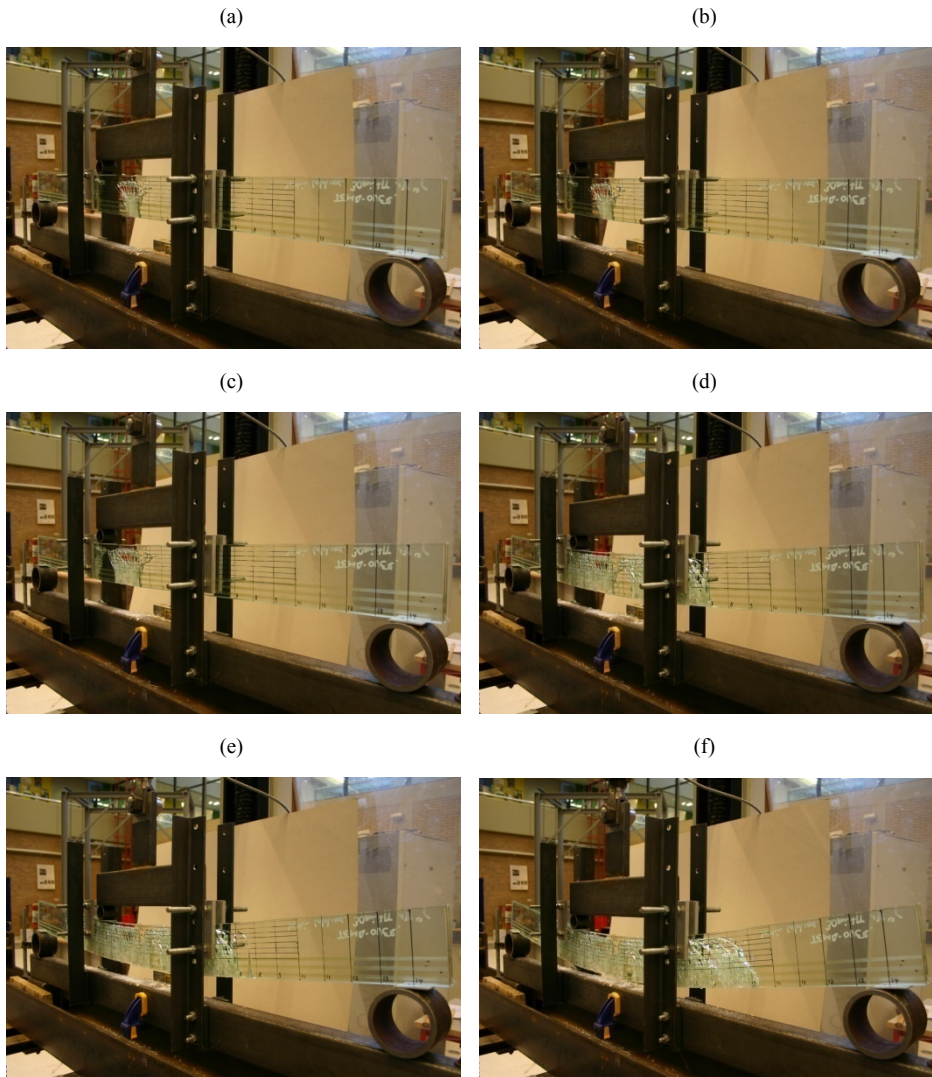
Figure I.9: Photo sequence of an exemplary bending test on a 1.5 m SG-laminated
GFRP-reinforced glass beam, with flat reinforcement rods.

Appendix II: Analytical model; derivation of equations

II.1   Introduction

The typical structural response of a reinforced glass beam loaded in displacement-controlled bending is schematized in the moment-curvature (M-κ) diagram shown in Figure II.1. Basically, three stages are distinguished, which are:

A) *Un-cracked stage.*

B) *Cracked stage*

C) *Yield stage*

The following sections describe how the *M-κ* diagram is constructed. For this it is assumed that the strains in the glass and the reinforcement are distributed according to Figure II.2. Furthermore, it is assumed that the glass responds perfectly linear elastic and that the reinforcement material (i.e. steel) responds elastic-perfectly-plastic, see Figure II.3. Additionally, it is assumed that the reinforcement is rigidly connected to the glass. No material parameters for the intermediary bond have been defined. Finally, it is assumed that the curvature *κ* of the beam follows Figure II.4 and is expressed by the equation provided in that figure. For the symbols applied in the formulas in this appendix is referred to Figures II.1 to II.4, to Chapter 8 and to the list of symbols and abbreviations given at the beginning of this dissertation.
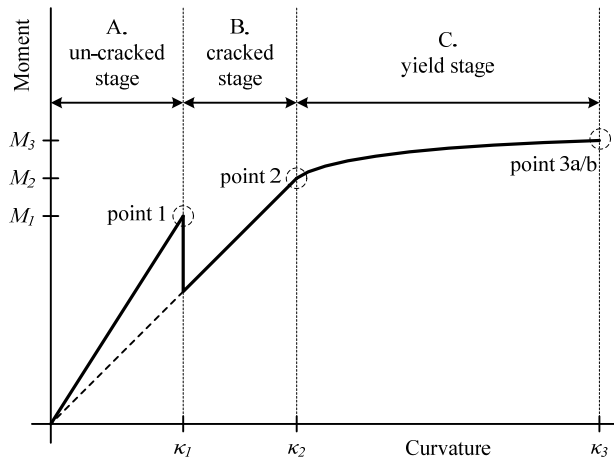
Figure II.1: *M-κ* diagram of a reinforced glass beam loaded in bending
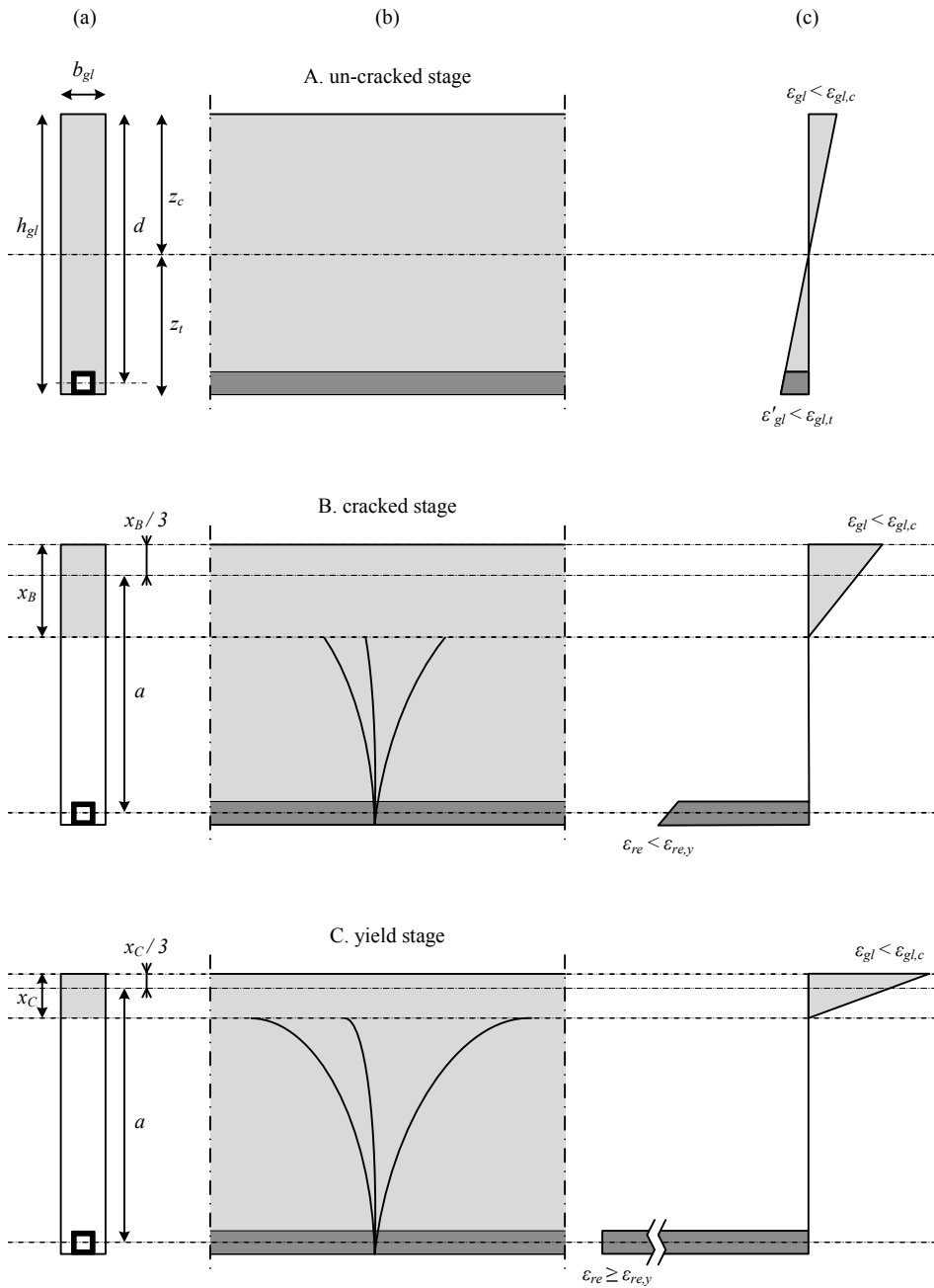
Figure II.2 (re-print of Figure 8.5): Schematic representation of the strain distribution
in reinforced glass beams.

(a)   (b)
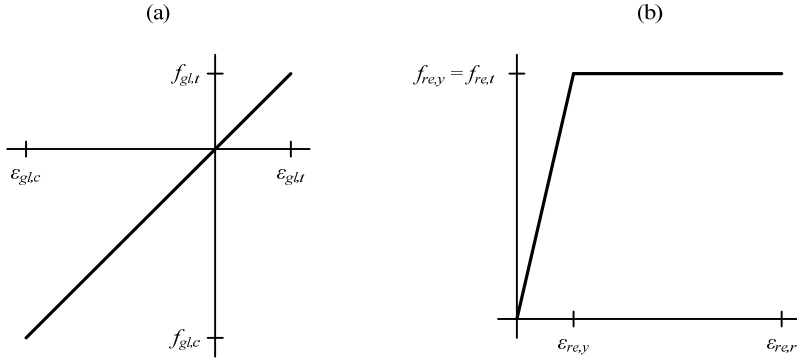
Figure II.3 (re-print of Figure 8.4):: Schematic representation of the stress-strain diagrams adopted for the analytical prediction method; (a) stress-strain diagram for the glass; a perfectly linear elastic response both in tension and compression has been assumed; (b) stress-strain diagram for the reinforcement; no strain-hardening has been considered, a elastic-perfectly-plastic response has been assumed, and thus $f_{re,y} = f_{re,t}$.

$$\kappa = \frac{\Delta\varphi}{\Delta x} = \frac{\varepsilon_1 + \varepsilon_2}{h}$$
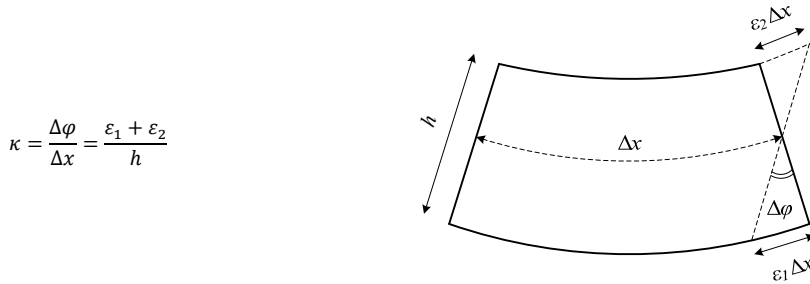
Figure II.4: Definition of the curvature of a beam.

II.1   Stage A: Un-cracked stage

At the un-cracked stage the reinforced glass beam shows no glass failure. Both the glass and reinforcement are at their linear elastic range. The stresses within the beam are distributed according to Figure II.2(a). The curvature κ of the beam is directly related to the bending moment M and the bending stiffness EI of the beam according to Equation II.1:

$$\kappa = \frac{M}{EI} \qquad\qquad\qquad (II.1)$$

To be able to construct the M-κ curve at the un-cracked stage it is therefore necessary to know the initial bending stiffness EI of the reinforced glass beam composite. Since the glass and the reinforcement within in the beam composite have different E-moduli, this has to be taken into account in the calculation of the overall stiffness EI of the beam. It

is suggested to compensate for this difference in E-moduli in the calculation of an equivalent second moment of area $I_{yy,eq}$ of the beam composite. Following the *Rules of Steiner*, the equivalent second moment of area $I_{yy,eq}$ around the central y-axis, see Figure II.2(a), can then be calculated according to Equation II.2:

$$I_{yy,eq} = \sum_{i=n}^{n} \left(I_{yy,i} \cdot f_i + z_i^2 \cdot A_i \cdot f_i \right) \tag{II.2}$$

In this equation the second moment area $I_{yy,i}$ of the individual components within the cross-section and the product of their area A_i and the squared distance z_i of their central axis to the overall central axis y are summed. Furthermore, the aspect ratio f_i between the E-modulus E_i of the considered component in the cross-section and the E-modulus E_{gl} of glass, which is the dominant material within the cross-section, is taken into account through Equation II.3:

$$f_i = \frac{E_i}{E_{gl}} \tag{II.3}$$

Now that the equivalent second moment of area $I_{yy,eq}$ around the central y-axis is known, the overall bending stiffness (EI_A) of the beam composite at stage A is expressed by Equation II.4:

$$EI_A = EI_{composite} = E_{gl} \cdot I_{yy,eq} \tag{II.4}$$

The curvature κ_A at the un-cracked stage is now expressed by Equation II.5:

$$\kappa_A = \frac{M}{EI_A} \tag{II.5}$$

The initial part of the *M-κ* diagram can now be constructed based on Equation II.5. However, this equation is only valid up until initial glass failure at point 1 is reached, see Figure II.1.

II.2 Point 1: Initial glass failure

At point 1 initial glass failure occurs, see Figures II.1 and II.2. At this point the tensile strain ε'_{gl} at the tensile edge of the glass exceeds the ultimate tensile strain $\varepsilon_{gl,t}$ of the glass. The bending moment at initial glass failure is expressed by Equation II.6:

$$M_1 = \frac{\varepsilon_{gl,t} \cdot EI_A}{z_t} \tag{II.6}$$

The curvature κ_1 at initial glass failure is subsequently derived from Equation II.1, II.4 and II.6, and follows Equation II.7:

$$\kappa_1 = \frac{M_1}{EI_A} = \frac{\varepsilon_{gl,t}}{z_t} \tag{II.7}$$

II.3 Stage B: Cracked stage

Upon initial glass failure a crack will occur in the glass. The crack originates from the tensile edge and travels up to the compression zone, leaving the compression zone over a height x un-cracked, see Figure II.2. The reinforcement bridges the cracks and transfers the tensile forces. The stress state instantly changes from Figure II.2(b) to Figure II.2(c).

The curvature κ at the cracked stage is expressed by Equation II.8 (see Figure II.4):

$$\kappa_1 = \frac{|\varepsilon_{gl}| + \varepsilon_{re}}{d} \tag{II.8}$$

To be able to calculate the strain ε'_{gl} in the glass and the strain ε_{re} in the reinforcement and subsequently the curvature κ_B at stage B, it is necessary to know the height x_B of the compression zone at stage B. This height can be derived from the equilibrium statement that the compressive force in the glass should equal the tensile force in the reinforcement. Equation II.9 therefore applies:

$$N_{gl} = N_{re} \tag{II.9}$$

from which Equation II.10 follows (see Figure II.2):

$$\frac{1}{2} \cdot b_{gl} \cdot x_B \cdot \varepsilon_{gl} \cdot E_{gl} = A_{re} \cdot E_{re} \cdot \varepsilon_{re} \tag{II.10}$$

which yields:

$$\varepsilon_{gl} = \frac{2 \cdot A_{re} \cdot E_{re} \cdot \varepsilon_{re}}{b_{gl} \cdot x_B \cdot E_{gl}} \tag{II.11}$$

Furthermore, concerning the strain in the glass and reinforcement Equation II.12 is valid:

$$\frac{\varepsilon_{gl}}{\varepsilon_{re}} = \frac{x_B}{d - x_B}$$

(II.12)

which yields:

$$\varepsilon_{re} = \varepsilon_{gl} \cdot \left(\frac{d - x_B}{x_B} \right)$$

(II.13)

Combining Equation II.11 and Equation II.13 yields Equation II.14:

$$\varepsilon_{re} = \left(\frac{2 \cdot A_{re} \cdot E_{re} \cdot \varepsilon_{re}}{b_{gl} \cdot x_B \cdot E_{gl}} \right) \cdot \left(\frac{d - x_B}{x_B} \right)$$

$$= 2 \cdot \left(\frac{A_{re} \cdot E_{re} \cdot \varepsilon_{re}}{b_{gl} \cdot E_{gl}} \right) \cdot \left(\frac{d - x_B}{x_B} \right)$$

$$= 2 \cdot \left(\frac{A_{re} \cdot E_{re} \cdot \varepsilon_{re}}{b_{gl} \cdot E_{gl}} \right) \cdot (d - x_B) \cdot \frac{1}{x_B^2}$$

(II.14)

From which it is derived that:

$$x_B^2 = 2 \cdot (r) \cdot (d - x_B)$$

(II.15)

with:

$$r = \left(\frac{A_{re} \cdot E_{re}}{b_{gl} \cdot E_{gl}} \right)$$

(II.16)

From this the height x_B of the compression zone at stage B is derived:

$$x_B^2 = 2 \cdot r \cdot (d - x_B)$$

$$x_B^2 = 2 \cdot r \cdot d - 2 \cdot r \cdot x_B$$

$$x_B^2 + 2 \cdot r \cdot x_B = 2 \cdot r \cdot d$$

$$x_B^2 + 2 \cdot r \cdot x_B + r^2 = r \cdot d + r^2$$

$$(x_B + r)^2 = 2 \cdot r \cdot d + (r)^2$$

$$x_B + r = \pm \sqrt{2 \cdot r \cdot d + (r)^2}$$

$$x_B = -r \pm \sqrt{2 \cdot r \cdot d + (r)^2}$$

(II.17)

Because the height of the compression zone x should be positive, it is derived that x_B is expressed by Equation II.18:

$$x_B = -\left(\frac{A_{re} \cdot E_{re}}{b_{gl} \cdot E_{gl}}\right) + \sqrt{2 \cdot \left(\frac{A_{re} \cdot E_{re}}{b_{gl} \cdot E_{gl}}\right) \cdot d + \left(\frac{A_{re} \cdot E_{re}}{b_{gl} \cdot E_{gl}}\right)^2} \tag{II.18}$$

Additionally, to reach equilibrium at the cracked stage the bending moment M at stage B should equal the internal bending moment, according to Equation II.19:

$$M = N_{re} \cdot a = A_{re} \cdot E_{re} \cdot \varepsilon_{re} \cdot \frac{x_B}{3} \tag{II.19}$$

From which it is derived that the strain ε_{re} in the reinforcement at stage B can be expressed as a function of M, following Equation II.20:

$$\varepsilon_{re} = \frac{M}{A_{re} \cdot E_{re} \cdot \left(d - \frac{x_B}{3}\right)} \tag{II.20}$$

Combining Equation II.8 and Equation II.20 yields the curvature κ_B at stage B as expressed by Equation II.21:

$$\kappa_B = \frac{\left|\varepsilon_{gl}\right| + \varepsilon_{re}}{d}$$

$$= \frac{\varepsilon_{re} \cdot \left(\frac{x_B}{d - x_B}\right) + \varepsilon_{re}}{d}$$

$$= \frac{\varepsilon_{re}}{(d - x_B)}$$

$$= \frac{M}{(d - x_B) \cdot (A_{re} \cdot E_{re}) \cdot \left(d - \frac{x_B}{3}\right)} \tag{II.21}$$

The second part of the M-κ diagram can now be constructed according to Equation II.22, up to point 2 where the reinforcement starts to yield, see Figure II.1.

II.4   Point 2, yielding of reinforcement

At point 2 the reinforcement starts to yield as the tensile strain ε_{re} in the reinforcement reaches the yield strain $\varepsilon_{re,y}$ of the reinforcement. The bending moment M_2 at this point is expressed by Equation II.22:

$$M_2 = A_{re} \cdot \varepsilon_{re,y} \cdot E_{re} \cdot \left(d - \frac{x_B}{3}\right) = A_{re} \cdot f_{re,y} \cdot \left(d - \frac{x_B}{3}\right) \tag{II.22}$$

Subsequently, the curvature κ_2 at point 2 can be calculated following Equation II.21, which results in Equation II.23:

$$\kappa_2 = \frac{M_2}{(d - x_B) \cdot (A_{re} \cdot E_{re}) \cdot \left(d - \frac{x_B}{3}\right)} \tag{II.23}$$

II.5   Stage C, yield stage

At stage C the reinforcement is yielding (or: plastically deforming) and the cracks in the glass propagate further into the compression zone, thereby gradually reducing the height x_C of the value of compression zone. Due to this decrease in height x_C of the compression zone, the internal lever-arm z increases and the moment capacity of the beam shows, despite yielding of the reinforcement, a slight increase.

The height of the compression zone (x_C) at stage C can be derived from Equation II.24 which is valid to reach equilibrium at stage C:

$$M = N_{re,y} \cdot a$$

$$= A_{re} \cdot \varepsilon_{re,y} \cdot E_{re} \cdot \left(d - \frac{x_C}{3}\right)$$

$$= A_{re} \cdot f_{re,y} \cdot \left(d - \frac{x_C}{3}\right) \tag{II.24}$$

From this equation it is derived that the (varying) height x_C of the compression zone at stage C is expressed by:

$$x_C = 3 \cdot \left(d - \frac{M}{\left(A_{re} \cdot f_{re,y}\right)}\right) \tag{II.25}$$

Additionally, to reach equilibrium Equation II-26 applies, see Figure II.2:

$$N_{gl} = N_{re,y} \tag{II.26}$$

which yields:

$$\frac{1}{2} b_{gl} \cdot x_C \cdot \varepsilon_{gl} \cdot E_{gl} = A_{re} \cdot f_{re,y} \tag{II.27}$$

From which it is derived that the compressive strain ε_{gl} in the glass follows Equation II-28:

$$\varepsilon_{gl} = \frac{2 \cdot A_{re} \cdot \varepsilon_{re,y} \cdot E_{re}}{b_{gl} \cdot x_C \cdot E_{gl}} \tag{II.28}$$

Similar to Equation II-13 the strain in the reinforcement is expressed by Equation II.29:

$$\varepsilon_{re} = \varepsilon_{gl} \cdot \left(\frac{d - x_C}{x_C}\right) \tag{II.29}$$

The curvature κ_C of the beam at stage C is subsequently related to the bending moment M, by combining Equations II.8, II.25 and II.29 into Equation II.30:

$$\kappa_C = \frac{|\varepsilon_{gl}| + \varepsilon_{re}}{d} = \frac{\varepsilon_{gl} + \varepsilon_{gl} \cdot \left(\dfrac{d - x_C}{x_C}\right)}{d} = \frac{\varepsilon_{gl}}{x_C} = \frac{2 \cdot A_{re} \cdot f_{re,y}}{b_{gl} \cdot E_{gl} \cdot x_C^2}$$
$$= \frac{2 \cdot A_{re} \cdot f_{re,y}}{9 \cdot b_{gl} \cdot E_{gl} \cdot \left(d - \dfrac{M}{A_{re} \cdot f_{re,y}}\right)^2} \tag{II.30}$$

The third part of the M-κ diagram can now be constructed according to Equation II.30, up to point 3 where either compressive glass failure (point 3a) or tensile failure of the reinforcement (point 3b) occurs.

II.6 Point 3a: compressive failure glass

At compressive glass failure the compressive strain ε_{gl} in the glass exceeds the ultimate compressive strain $\varepsilon_{gl,ult}$ in the glass. The bending moment M_{3a} at the point of glass failure is expressed by Equation II.31:

$$M_{3a} = A_{re} \cdot f_{re,y} \cdot \left(d - \frac{x_{3a}}{3}\right) = A_{re} \cdot \varepsilon_{re,y} \cdot E_{re} \cdot \left(d - \frac{x_{3a}}{3}\right) \tag{II.31}$$

The minimum height x_{3a} of the compression zone at which the ultimate compressive strain $\varepsilon_{gl,c}$ in the glass is reached is expressed by Equation II.32:

$$x_{3a} = \frac{b_{gl} \cdot \varepsilon_{gl,c} \cdot E_{gl}}{2} \tag{II.32}$$

Subsequently, the curvature κ_{3a} at point 3a is calculated following Equation II.30, which yields Equation II.33:

$$\kappa_{3a} = \frac{2 \cdot A_{re} \cdot f_{re,y}}{9 \cdot b_{gl} \cdot E_{gl} \cdot \left(d - \dfrac{M_{3a}}{A_{re} \cdot f_{re,y}}\right)} \tag{II.33}$$

II.7 Point 3b: tensile failure reinforcement

At point 3b the tensile strain ε_{re} of the reinforcement exceeds the ultimate tensile strain $\varepsilon_{re,r}$ of the reinforcement. From Equation II.24 it is derived that the strain ε_{gl} in the glass at point 3b is expressed by Equation II.34:

$$\varepsilon_{gl,3b} = \frac{2 \cdot A_{re} \cdot f_{re,t}}{b_{gl} \cdot x_{3b} \cdot E_{gl}} = \frac{2 \cdot A_{re} \cdot \varepsilon_{re,r} \cdot E_{re}}{b_{gl} \cdot x_{3b} \cdot E_{gl}} \tag{II.34}$$

Additionally, it is derived from Equation II.13, that the ultimate tensile strain $\varepsilon_{re,r}$ in the reinforcement follows Equation II.35:

$$\varepsilon_{re,r} = \varepsilon_{gl,3b} \cdot \left(\frac{d - x_{3b}}{x_{3b}}\right) = \left(\frac{2 \cdot A_{re} \cdot f_{re,t}}{b_{gl} \cdot x_{3b} \cdot E_{gl}}\right) \cdot \left(\frac{d - x_{3b}}{x_{3b}}\right)$$

$$= 2 \cdot \left(\frac{A_{re} \cdot f_{re,t}}{b_{gl} \cdot E_{gl}}\right) \cdot (d - x_{3b}) \cdot \frac{1}{x_{3b}^2} \tag{II.35}$$

From which it is derived that:

$$x_{3b}^2 = 2 \cdot (p) \cdot (d - x_{3b})$$ (II.36)

with:

$$p = \frac{A_{re} \cdot f_{re,t}}{b_{gl} \cdot E_{gl} \cdot \varepsilon_{re,r}}$$ (II.37)

From this, the height x_{3b} of the compression zone at point 3b is derived:

$$x_{3b}^2 = 2 \cdot p \cdot (d - x_{3b})$$

$$x_{3b}^2 = 2 \cdot p \cdot d - 2 \cdot p \cdot x_{3b}$$

$$x_{3b}^2 + 2 \cdot p \cdot x_{3b} = 2 \cdot p \cdot d$$

$$x_{3b}^2 + 2 \cdot (p) x_{3b} + (p)^2 = 2 \cdot p \cdot d + (p)^2$$

$$(x_{3b} + p)^2 = 2 \cdot p \cdot d + (p)^2$$

$$x_{3b} + p = \pm\sqrt{2 \cdot p \cdot d + (p)^2}$$

$$x_{3b} = -p \pm \sqrt{2 \cdot p \cdot d + (p)^2}$$ (II.38)

Because x should be positive, it is derived that x_B is expressed by Equation II.39:

$$x_{3b} = \left(\frac{A_{re} \cdot f_{re,t}}{b_{gl} \cdot E_{gl} \cdot \varepsilon_{re,r}}\right) + \sqrt{2 \cdot \left(\frac{A_{re} \cdot f_{re,t}}{b_{gl} \cdot E_{gl} \cdot \varepsilon_{re,r}}\right) \cdot d + \left(\frac{A_{re} \cdot f_{re,t}}{b_{gl} \cdot E_{gl} \cdot \varepsilon_{re,r}}\right)^2}$$ (II.39)

The bending moment M_{3b} at the point of reinforcement failure (point 3b) is expressed by Equation II.40:

$$M_{3b} = A_{re} \cdot \varepsilon_{re,r} \cdot E_{re} \cdot \left(d - \frac{x_{3b}}{3}\right)$$ (II.40)

Similar to Equation II.30, the curvature κ_{3b} at point 3b subsequently follows Equation II.41:

$$\kappa_{3b} = \frac{2 \cdot A_{re} \cdot f_{re,t}}{9 \cdot b_{gl} \cdot E_{gl} \cdot \left(d - \dfrac{M_{3b}}{A_{re} \cdot f_{re,t}}\right)}$$ (II.41)

Appendix III: Numerical model; elements and files

III.1 Element types

For the numerical prediction method the reinforced glass beams have been modeled in 2D model using DIANA, see Chapter 8. In this 2D model the glass of the beam has been discretized using either eight-node quadrilateral, see Figure III.1(a), or six-node triangular plane stress elements, see Figure III.1(b). The reinforcement has been built up from quadratic truss elements, see Figure III.1(c).
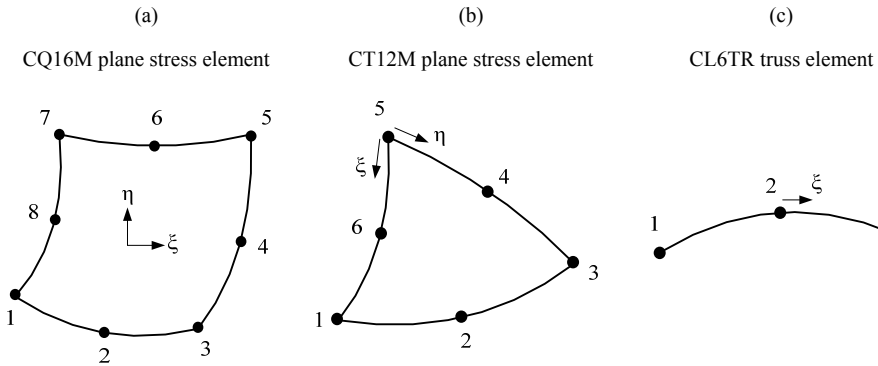
Figure III.1: Element types applied for the numerical calculation in Diana [De Witte & Kikstra, 2002].

A more detailed description, as given in the Diana user's manual [De Witte & Kikstra, 2002], of the element types presented in Figure III.1 is provided below.

The CQ16M element, see Figure III.1(a), is an eight-node quadrilateral isoparametric plane stress element. It is based on quadratic interpolation and Gauss integration. The polynomial for the displacement u_x and u_y can be expressed as:

$$u_i\,(\xi, \eta) = a_0 + a_1\xi + a_2\eta + a_3\xi\eta + a_4\xi^2 + a_5\eta^2 + a_6\xi^2\eta + a_7\xi\eta^2$$

Typically, this polynomial yields a strain ε_{xx} which varies linearly in x direction and quadratically in y direction. The strain ε_{yy} varies linearly in y direction and quadratically in x direction. The shear strain γ_{xy} varies quadratically in both directions. By default Diana applies 2x2 integration which yields optimal stress points, 3x3 is suitable option. Schemes higher than 3x3 are unsuitable [De Witte & Kikstra, 2002].

The *CT12M element*, see Figure III.1(b), is a six-node triangular isoparametric plane stress element. It is based on quadratic interpolation and area integration. The polynomial for the displacement u_x and u_y can be expressed as:

$$u_i\,(\xi, \eta) = a_0 + a_1\xi + a_2\eta + a_3\xi\eta + a_4\xi^2 + a_5\eta^2$$

Typically, this polynomial yields an approximately linear strain variation in x and y direction. By default Diana applies 3-point integration [De Witte & Kikstra, 2002].

The *CL6TR element*, see Figure III.1(c), is a three-node numerically integrated truss element with two displacement u_x and u_y in each node. This element can be used in two-dimensional dynamic and nonlinear analysis of cables. The interpolation polynomial for the displacement u_x and u_y can be expressed as:

$$u_i\,(\xi) = a_0 + a_1\xi + a_2\xi^2$$

Typically, this polynomial yields a strain which varies linearly along the bar axis. Strain and stress are purely axial. By default Diana applies a 2-point Gauss integration scheme.

III.2   Model files

III.2.1.   Model file for model I-1 to I-7

```
FEMGEN MODEL      : 1500
ANALYSIS TYPE     : Structural 2D
MODEL DESCRIPTION : 1500, 1500x120mm, 36 mm2 reinforcement, h=10
'UNITS'
LENGTH    MM
TIME      SEC
TEMPER    KELVIN
FORCE     N
'COORDINATES' DI=2
    1      0.000000E+00     0.000000E+00
    2      5.000000E+00     0.000000E+00
[…]
 5724      1.500000E+03     1.500000E+01
 5725      1.500000E+03     5.000000E+00
'ELEMENTS'
CONNECTIVITY
    1 CL6TR  1 2 3
    2 CL6TR  3 4 5
[…]
  149 CL6TR  297 298 299
  150 CL6TR  299 300 301
  151 CQ16M  302 374 303 387 315 398 314 386
  152 CQ16M  303 375 304 388 316 399 315 387
[…]
1949 CQ16M  5592 5700 5593 5713 5605 5724 5604 5712
 1950 CQ16M  5593 5701 299 300 301 5725 5605 5713
MATERIALS
/ 151-1950 /  1
```

```
/ 1-150 /  2
GEOMETRY
/ 151-1950 /  1
/ 1-150 /  2
DATA
/ 151-1950 /  1
/ 1-150 /  2
'MATERIALS'
   1 YOUNG     7.000000E+04
     POISON    2.300000E-01
     TAUCRI    1
     BETA      [0.001 or 0.01 or 0.1 or 1]
   2 YOUNG     1.900000E+05
     POISON    2.700000E-01
'FILOS'
/materi(1)/RDSCHM   HARDIA
/materi(2)/RDSCHM   HARDIA
'GEOMETRY'
   1 THICK     2.200000E+01
   2 CROSSE    3.600000E+01
'DATA'
    1 LINEAR
    2 LINEAR
'GROUPS'
ELEMEN
   1 GL / 1-1950 /
NODES
   2 GL_N / 1-5725 /
ELEMEN
   3 RE / 1-150 /
NODES
   4 RE_N / 1-301 /
'SUPPORTS'
 / 11 /   TR    1
 / 11 291 /   TR    2
'LOADS'
CASE 1
NODAL
 1 FORCE 2   0.0
CASE 2
NODAL
 1814 FORCE 2 -0.100000E+05
 3254 FORCE 2 -0.100000E+05
'DIRECTIONS'
    1   1.000000E+00   0.000000E+00   0.000000E+00
    2   0.000000E+00   1.000000E+00   0.000000E+00
    3   0.000000E+00   0.000000E+00   1.000000E+00
'END'
```

1.1.2.   Model file for model I-8

```
FEMGEN MODEL        : 1500
ANALYSIS TYPE       : Structural 2D
MODEL DESCRIPTION : 1500, 1500x120mm, 36 mm2 reinforcement, h=5
'UNITS'
LENGTH    MM
TIME      SEC
TEMPER    KELVIN
FORCE     N
'COORDINATES' DI=2
    1     0.000000E+00    0.000000E+00
    2     2.500000E+00    0.000000E+00
[…]
22248     1.447500E+03    1.000000E+01
22249     1.447500E+03    5.000000E+00
'ELEMENTS'
CONNECTIVITY
    1 CL6TR  1 2 3
    2 CL6TR  3 4 5
[…]
  299 CL6TR  598 599 600
  300 CL6TR  600 601 343
  301 CQ16M  602 866 603 891 627 914 626 890
  302 CQ16M  603 867 604 892 628 915 627 891
[…]
 7499 CQ16M  21312 22224 21313 22249 12961 13224 12960 22248
 7500 CQ16M  21313 22225 600 601 343 13225 12961 22249
MATERIALS
/ 301-7500 /  1
/ 1-300 /  2
GEOMETRY
/ 301-7500 /  1
/ 1-300 /  2
DATA
/ 301-7500 /  1
/ 1-300 /  2
'MATERIALS'
   1 YOUNG     7.000000E+04
     POISON    2.300000E-01
     TAUCRI    1
     BETA      0.01
   2 YOUNG     1.900000E+05
     POISON    2.700000E-01
'FILOS'
/materi(1)/RDSCHM   HARDIA
/materi(2)/RDSCHM   HARDIA
'GEOMETRY'
   1 THICK     2.200000E+01
   2 CROSSE    3.600000E+01
'DATA'
    1 LINEAR
    2 LINEAR
```

```
'GROUPS'
ELEMEN
   1 GL / 1-7500 /
NODES
   2 GL_N / 1-22249 /
ELEMEN
   3 RE / 1-300 /
NODES
   4 RE_N / 1-601 /
'SUPPORTS'
 / 21 /   TR     1
 / 21 343 /   TR     2
'LOADS'
CASE 1
NODAL
 1 FORCE 2   0.0
CASE 2
NODAL
 2330 FORCE 2 -0.100000E+05
 8114 FORCE 2 -0.100000E+05
'DIRECTIONS'
    1   1.000000E+00   0.000000E+00   0.000000E+00
    2   0.000000E+00   1.000000E+00   0.000000E+00
    3   0.000000E+00   0.000000E+00   1.000000E+00
'END'
```

III.2.3.   Model file for model I-9

```
FEMGEN MODEL     : 1500_CT12M_01
ANALYSIS TYPE    : Structural 2D
MODEL DESCRIPTION : 1500, 1500x120mm, 36 mm2 reinforcement, mg=t, h=7
'UNITS'
LENGTH   MM
TIME     SEC
TEMPER   KELVIN
FORCE    N
'COORDINATES' DI=2
    1      0.000000E+00      0.000000E+00
    2      5.000000E+00      0.000000E+00
[…]
7524     1.500000E+03     1.500000E+01
 7525     1.500000E+03     5.000000E+00
'ELEMENTS'
CONNECTIVITY
    1 CL6TR  1 2 3
    2 CL6TR  3 4 5
[…]
  149 CL6TR  297 298 299
  150 CL6TR  299 300 301
  151 CT12M  302 374 303 387 314 386
  152 CT12M  303 388 315 410 314 387
[…]
 3749 CT12M  7333 7489 299 7513 7345 7512
```

```
 3750 CT12M  299 300 301 7525 7345 7513
MATERIALS
/ 151-3750 /  1
/ 1-150 /  2
GEOMETRY
/ 151-3750 /  1
/ 1-150 /  2
DATA
/ 151-3750 /  1
/ 1-150 /  2
'MATERIALS'
   1 YOUNG    7.000000E+04
     POISON   2.300000E-01
     TAUCRI   1
     BETA     0.01
   2 YOUNG    1.900000E+05
     POISON   2.700000E-01
'FILOS'
/materi(1)/RDSCHM   HARDIA
/materi(2)/RDSCHM   HARDIA
'GEOMETRY'
   1 THICK    2.200000E+01
   2 CROSSE   3.600000E+01
'DATA'
    1 LINEAR
    2 LINEAR
'GROUPS'
ELEMEN
   1 GL / 1-3750 /
NODES
   2 GL_N / 1-7525 /
ELEMEN
   3 RE / 1-150 /
NODES
   4 RE_N / 1-301 /
'SUPPORTS'
 / 11 /   TR     1
 / 11 291 /   TR    2
'LOADS'
CASE 1
NODAL
 1 FORCE 2   0.0
CASE 2
NODAL
 2234 FORCE 2 -0.100000E+05
 4154 FORCE 2 -0.100000E+05
'DIRECTIONS'
    1   1.000000E+00   0.000000E+00   0.000000E+00
    2   0.000000E+00   1.000000E+00   0.000000E+00
    3   0.000000E+00   0.000000E+00   1.000000E+00
'END'
```

III.2.4.   Model file for model II

```
FEMGEN MODEL       : 1500
ANALYSIS TYPE      : Structural 2D
MODEL DESCRIPTION : 1500 1500x120mm 100 mm2 reinforcement
'UNITS'
LENGTH    MM
TIME      SEC
TEMPER    KELVIN
FORCE     N
'COORDINATES' DI=2
     1      0.000000E+00     0.000000E+00
     2      5.000000E+00     0.000000E+00
[…]
 5724      1.500000E+03     1.500000E+01
 5725      1.500000E+03     5.000000E+00
'ELEMENTS'
CONNECTIVITY
     1 CL6TR  1 2 3
     2 CL6TR  3 4 5
[…]
  149 CL6TR  297 298 299
  150 CL6TR  299 300 301
  151 CQ16M  302 374 303 387 315 398 314 386
  152 CQ16M  303 375 304 388 316 399 315 387
[…]
 1949 CQ16M  5592 5700 5593 5713 5605 5724 5604 5712
 1950 CQ16M  5593 5701 299  300  301  5725 5605 5713
MATERIALS
/ 151-1950 /  1
/ 1-150 /  2
GEOMETRY
/ 151-1950 /  1
/ 1-150 /  2
DATA
/ 151-1950 /  1
/ 1-150 /  2
'MATERIALS'
   1 YOUNG    7.000000E+04
     POISON   2.300000E-01
     TAUCRI   1
     BETA     0.01
   2 YOUNG    1.900000E+05
     POISON   2.700000E-01
'FILOS'
/materi(1)/RDSCHM   HARDIA
/materi(2)/RDSCHM   HARDIA
'GEOMETRY'
   1 THICK    2.200000E+01
   2 CROSSE   1.000000E+02
'DATA'
   1 LINEAR
   2 LINEAR
```

```
'GROUPS'
ELEMEN
   1 GL / 1-1950 /
NODES
   2 GL_N / 1-5725 /
ELEMEN
   3 RE / 1-150 /
NODES
   4 RE_N / 1-301 /
'SUPPORTS'
 / 11 /   TR     1
 / 11 291 /   TR     2
'LOADS'
CASE 1
NODAL
 1 FORCE 2   0.0
CASE 2
NODAL
 1814 FORCE 2 -0.100000E+05
 3254 FORCE 2 -0.100000E+05
'DIRECTIONS'
    1   1.000000E+00   0.000000E+00   0.000000E+00
    2   0.000000E+00   1.000000E+00   0.000000E+00
    3   0.000000E+00   0.000000E+00   1.000000E+00
'END'
```

III.2.5.   Model file for model III

```
FEMGEN MODEL       : 3200
ANALYSIS TYPE      : Structural 2D
MODEL DESCRIPTION : 3200_feb
'UNITS'
LENGTH    MM
TIME      SEC
TEMPER    KELVIN
FORCE     N
'COORDINATES' DI=2
    1      0.000000E+00      0.000000E+00
    2      1.250000E+01      0.000000E+00
[…]
5496      3.200000E+03      3.468750E+01
 5497      3.200000E+03      1.156250E+01
'ELEMENTS'
CONNECTIVITY
    1 CL6TR  1 2 3
    2 CL6TR  3 4 5
[…]
  143 CL6TR  285 286 287
  144 CL6TR  287 288 289
  145 CQ16M  1 2 3 327 291 329 290 326
  146 CQ16M  3 4 5 328 292 330 291 327
[…]
1871 CQ16M  5436 5472 5437 5485 5449 5496 5448 5484
```

```
 1872 CQ16M  5437 5473 287 288 289 5497 5449 5485
MATERIALS
/ 145-1872 /  1
/ 1-144 /  2
GEOMETRY
/ 145-1872 /  1
/ 1-144 /  2
DATA
/ 145-1872 /  1
/ 1-144 /  2
'MATERIALS'
   1 YOUNG     7.000000E+04
     POISON    2.300000E-01
     TAUCRI    1
     BETA      0.01
   2 YOUNG     1.900000E+05
     POISON    2.70000E-01
'FILOS'
/materi(1)/RDSCHM   HARDIA
/materi(2)/RDSCHM   HARDIA
'GEOMETRY'
   1 THICK     3.100000E+01
   2 CROSSE    8.100000E+01
'DATA'
    1 LINEAR
    2 LINEAR
'GROUPS'
ELEMEN
   1 GL / 1-1872 /
NODES
   2 GL_N / 1-5497 /
ELEMEN
   3 RE / 1-144 /
NODES
   4 RE_N / 1-289 /
'SUPPORTS'
 / 5 /   TR     1
 / 5 285 /   TR     2
'LOADS'
CASE 1
NODAL
 1 FORCE 2   0.0
CASE 2
NODAL
 1694 FORCE 2 -0.200000E+05
 3134 FORCE 2 -0.200000E+05
'DIRECTIONS'
    1   1.000000E+00   0.000000E+00   0.000000E+00
    2   0.000000E+00   1.000000E+00   0.000000E+00
    3   0.000000E+00   0.000000E+00   1.000000E+00
'END'
```

III.3.   Command file

Command file applied for all numerical models.

```
*FILOS
 INITIA
*INPUT
*INPUT
 READ APPEND FILE="[reduction file.dat]"
*NONLIN
!SEGMENT sl01
   TYPE PHYSIC OFF
    BEGIN OUTPUT
      TABULA
       BEGIN SELECT
         NODES  [load introduction points] 11 1814
       END SELECT
       DISPLA  TOTAL  TRANSL  GLOBAL
       FORCE  REACTI  TRANSL  GLOBAL
     END OUTPUT
     BEGIN OUTPUT FEMVIE
       STATUS  USER   ITEM01
       DISPLA
     END OUTPUT
 BEGIN EXECUT
   BEGIN LOAD
     STEPS EXPLIC SIZES 1.0(10000)
   END LOAD
  BEGIN ITERAT
     METHOD NEWTON REGULA
     MAXITE=10
     BEGIN CONVER
      ENERGY OFF
      FORCE CONTIN TOLCON=1.0E-06
      DISPLA OFF
     END CONVER
  END ITERAT
 END EXECUT
*END
```

III.4. Saw-tooth reduction files

III.4.1. Saw-tooth reduction file for models I-1 to I-4

```
'materials'
1      hardia 7.00000E+04  4.50000E+01
              6.93331E+04  1.69150E+01
              6.58187E+04  6.09396E+00
              5.65583E+04  1.98730E+00
              3.21568E+04  4.28805E-01
              1.00000E-05  0.00000E+00
2      hardia 1.90000E+05  5.50000E+02
              6.25214E+04  7.70000E+02
              3.63438E+04  7.90000E+02
              2.56115E+04  7.98000E+02
              1.97147E+04  8.00000E+02
              1.61200E+04  8.06000E+02
              8.17750E+03  8.17750E+02
              5.53000E+03  8.29500E+02
              4.20625E+03  8.41250E+02
              3.41200E+03  8.53000E+02
              2.90909E+03  8.00000E+02
```

III.4.2. Saw-tooth reduction file for model I-5

```
'materials'
1      hardia 7.00000E+04  4.50000E+01
              6.93331E+04  1.69150E+01
              6.58187E+04  6.09396E+00
              5.65583E+04  1.98730E+00
              3.21568E+04  4.28805E-01
              1.00000E-05  0.00000E+00
2      hardia 1.90000E+05  5.50000E+02
              6.25214E+04  7.70000E+02
              3.63438E+04  7.90000E+02
              3.41200E+03  8.53000E+02
              2.90909E+03  8.00000E+02
```

III.4.3.   Saw-tooth reduction file for model I-6

```
'materials'
1       hardia 7.00000E+04   4.50000E+01
               6.96857E+04   2.91263E+01
               6.87188E+04   1.86743E+01
               6.72318E+04   1.18787E+01
               6.49446E+04   7.46044E+00
               6.14268E+04   4.58782E+00
               5.60161E+04   2.72012E+00
               4.76942E+04   1.50580E+00
               3.48946E+04   7.16288E-01
               1.52081E+04   2.02970E-01
               1.00000E-05   0.00000E+00
2       hardia 1.90000E+05   5.50000E+02
               6.25214E+04   7.70000E+02
               3.63438E+04   7.90000E+02
               3.41200E+03   8.53000E+02
               2.90909E+03   8.00000E+02
```

III.4.4.   Saw-tooth reduction file for model I-7

```
'materials'
1       hardia 7.00000E+04   4.50000E+01
               6.96857E+04   2.91263E+01
               6.87188E+04   1.86743E+01
               6.72318E+04   1.18787E+01
               6.49446E+04   7.46044E+00
               6.14268E+04   4.58782E+00
               5.60161E+04   2.72012E+00
               4.76942E+04   1.50580E+00
               3.48946E+04   7.16288E-01
               1.52081E+04   2.02970E-01
               1.00000E-05   0.00000E+00
2       hardia 1.90000E+05   5.50000E+02
               6.25214E+04   7.70000E+02
               3.63438E+04   7.90000E+02
               2.56115E+04   7.98000E+02
               1.97147E+04   8.00000E+02
               1.61200E+04   8.06000E+02
               8.17750E+03   8.17750E+02
               5.53000E+03   8.29500E+02
               4.20625E+03   8.41250E+02
               3.41200E+03   8.53000E+02
               2.90909E+03   8.00000E+02
```

III.4.5. Saw-tooth reduction file for model I-8

```
'materials'
1      hardia 7.00000E+04  4.50000E+01
              6.88547E+04  1.99762E+01
              6.37790E+04  8.35064E+00
              5.25321E+04  3.10407E+00
              2.76109E+04  7.36293E-01
              1.00000E-05  0.00000E+00
2      hardia 1.90000E+05  5.50000E+02
              6.25214E+04  7.70000E+02
              3.63438E+04  7.90000E+02
              2.56115E+04  7.98000E+02
              1.97147E+04  8.00000E+02
              1.61200E+04  8.06000E+02
              8.17750E+03  8.17750E+02
              5.53000E+03  8.29500E+02
              4.20625E+03  8.41250E+02
              3.41200E+03  8.53000E+02
              2.90909E+03  8.00000E+02
```

III.4.6. Saw-tooth reduction file for model I-9

```
'materials'
1      hardia 7.00000E+04  4.50000E+01
              6.91231E+04  1.83900E+01
              6.48851E+04  7.14414E+00
              5.46449E+04  2.49000E+00
              2.99012E+04  5.63875E-01
              1.00000E-05  0.00000E+00
2      hardia 1.90000E+05  5.50000E+02
              6.25214E+04  7.70000E+02
              3.63438E+04  7.90000E+02
              2.56115E+04  7.98000E+02
              1.97147E+04  8.00000E+02
              1.61200E+04  8.06000E+02
              8.17750E+03  8.17750E+02
              5.53000E+03  8.29500E+02
              4.20625E+03  8.41250E+02
              3.41200E+03  8.53000E+02
              2.90909E+03  8.00000E+02
```

III.4.7.   Saw-tooth reduction file for model II

```
'materials'
1       hardia 7.00000E+04  4.50000E+01
               6.93331E+04  1.69150E+01
               6.58187E+04  6.09396E+00
               5.65583E+04  1.98730E+00
               3.21568E+04  4.28805E-01
               1.00000E-05  0.00000E+00
2       hardia 1.90000E+05  5.50000E+02
               6.25214E+04  7.70000E+02
               3.63438E+04  7.90000E+02
               2.56115E+04  7.98000E+02
               1.97147E+04  8.00000E+02
               1.61200E+04  8.06000E+02
               8.17750E+03  8.17750E+02
               5.53000E+03  8.29500E+02
               4.20625E+03  8.41250E+02
               3.41200E+03  8.53000E+02
               2.90909E+03  8.00000E+02
```

III.4.8.   Saw-tooth reduction file for model III

```
'materials'
1       hardia 7.00000E+04  4.50000E+01
               6.96608E+04  1.38293E+01
               6.74639E+04  4.13600E+00
               6.03500E+04  1.14257E+00
               3.73137E+04  2.18158E-01
               1.00000E-05  0.00000E+00
2       hardia 1.90000E+05  5.50000E+02
               6.25214E+04  7.70000E+02
               3.63438E+04  7.90000E+02
               2.56115E+04  7.98000E+02
               1.97147E+04  8.00000E+02
               1.61200E+04  8.06000E+02
               8.17750E+03  8.17750E+02
               5.53000E+03  8.29500E+02
               4.20625E+03  8.41250E+02
               3.41200E+03  8.53000E+02
               2.90909E+03  8.00000E+02
```

Appendix IV: Post-tensioned glass beams

IV.1   Introduction

As an alternative to the reinforced glass beams investigated in this research, post-tensioned glass beams have been studied in associated research. The main difference between both beam types is the activation of the tension components. The reinforcement in reinforced glass beams is a rather passive tension component which is mainly activated after glass failure. However, the tendons in post-tensioned glass beams are pre-tensioned and contribute actively to overall beam resistance.

The following sections discuss the post-tensioned glass beam concept and related aspects in more detail. Subsequently, an evaluation of the concept and a brief comparison with the reinforced glass beam concept is provided.

IV.2   Post-tensioned glass beam concept

The post-tensioned glass beam concept makes use of steel tendons which are fed through a cavity in annealed float glass beams and tensioned at the beam ends. This way a compressive force is introduced at the beam ends. The concept does not make use of any adhesive connection between the tendons and the glass.

The goal/purpose of the post-tensioned glass beam concept is twofold. Firstly, the steel tendons apply a compressive pre-stress to the glass, which enhances the tensile resistance of the glass. Secondly, the pre-stressing steel tendons provide the glass beam a significant post-breakage resistance and ductile post-breakage response.

Two post-tensioned beam prototypes have been built and tested by Louter in associated research. The following subsections provide a description of these prototypes. Furthermore, the results of the bending tests performed on the prototypes are briefly discussed.

IV.2.2   Post-tensioned T-section beam

In 2004, a T-section post-tensioned glass beam prototype has been built and tested by Louter [Bos et al., 2004; Louter, 2004], see Figure IV.1, IV.2 and IV.3. This prototype consisted of a segmented triple-layer glass web (2 outer layers of 8 mm and an inner layer of 10 mm) and a segmented double-layer glass flange (2*8 mm), which have been bonded using the GB acrylate adhesive. Annealed float glass has been applied and the edges of both the web and the flange have been cut and ground in a curve, see Figure IV.1. The length of the beam was 3 m, while the height of the beam varied from 110 to 210 mm and the width of the beam from 60 to 90 mm. A curved stainless steel hollow section (10*10*1 mm) has been integrated in the web of the beam, see Figure IV.1.

Through this hollow section a Ø 7 mm high strength (σ_y = 1670 MPa) steel tendon was fed and tensioned at the beam ends. For this tensioning, steel heads and an intermediary layer of neoprene were positioned at the beam ends. The pre-stressing effect of the curved steel tendon is twofold. Firstly, it exerts a compressive pre-stress at the beam ends. Secondly, due to its curvature it provides an upwards lift and additional resistance to the beam.

By means of a hydraulic jack the prototype was post-tensioned with a force of 20 kN and was subsequently tested in four-point bending, see Figure IV.2. After the linear elastic stage the beam showed an initial V-shaped crack, similar to the ones observed in reinforced glass beams. As loading was continued, the beam showed some additional cracking and a significant increase in post-breakage resistance (until 117 % of its initial failure load). Finally, explosive glass failure occurred at the compression zone, which locally pulverized the glass. Due to the increased stressing of the glass and the already present compressive pre-stress, the ultimate compressive strength of the glass was exceeded and the glass failed causing collapse of the beam, see Figure IV.3. However, due to the persisting upward lift of curved post-tensioning tendon, the beam was catapulted upwards upon removing the loading mechanism.

The results of the bending test on the post-tensioned T-section glass beam showed that the concept of post-tensioning an annealed glass beam is feasible. The beam showed high residual resistance after initial glass failure. However, the explosive final failure, see Figure IV.3, and the persisting pre-load after glass failure poses possible risks for building applications.
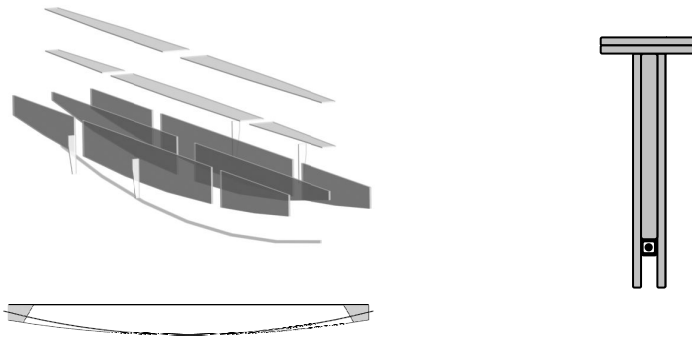

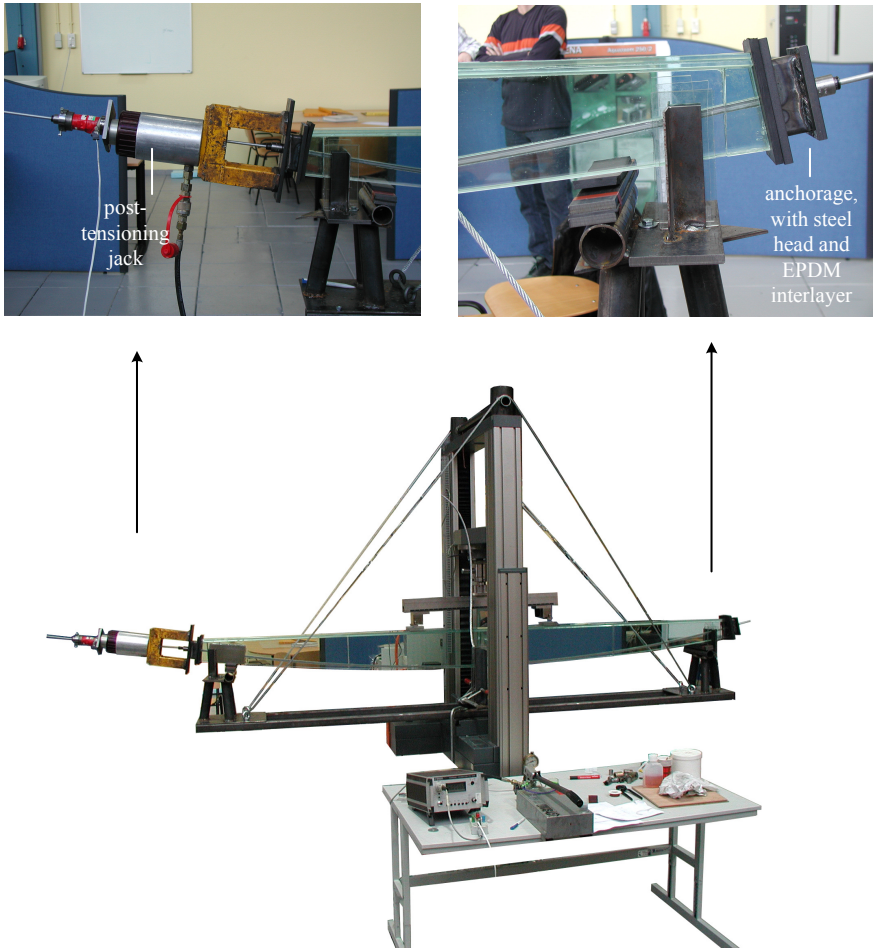Figure IV.1: Layout of the post-tensioned T-section beam [Louter, 2004].

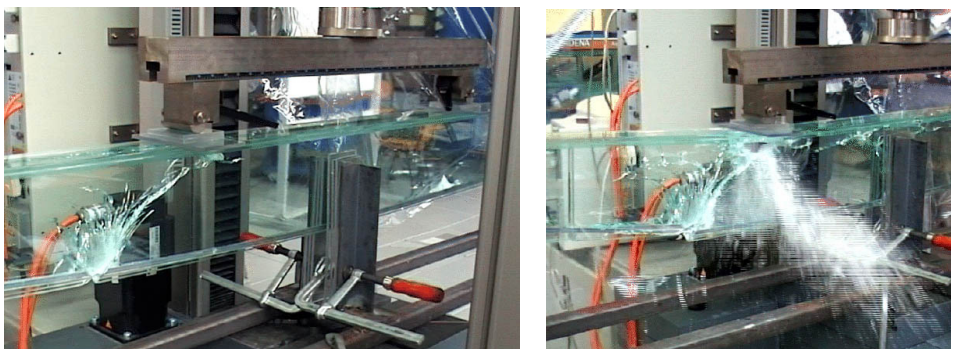Figure IV.2: Post-tensioned T-section beam in bending test setup [Louter, 2004].

Figure IV.3 Post-tensioned T-section beam during the bending test [Louter, 2004].

IV.2.3   Post-tensioned hollow section glass beam

In 2007 a post-tensioned hollow section glass beam has been built and tested by Louter & Veer [Louter & Veer, 2007b], see Figures IV.4, IV.5 and IV.6. The beam consisted of PVB laminated (4.4.1) outer panels with a stainless steel hollow section (10*10*1 mm) bonded in between both at the bottom and the top edge, see Figure IV.4. Annealed float glass has been applied and all components were bonded with the GB acrylate adhesive. Both at the bottom and the top edge of the beam a Ø 7 mm high strength σ_y = 1670 MPa) steel tendon was fed through the stainless steel box section and tensioned at the beam ends. To tension the tendons, U-shaped steel coverings have been slit over the beam ends. Prior to the tensioning of the tendons the cavity between the U-shaped steel coverings and the glass beam end has been filled with aluminum epoxy putty, to even out any irregularities and to guarantee an equalized load introduction.
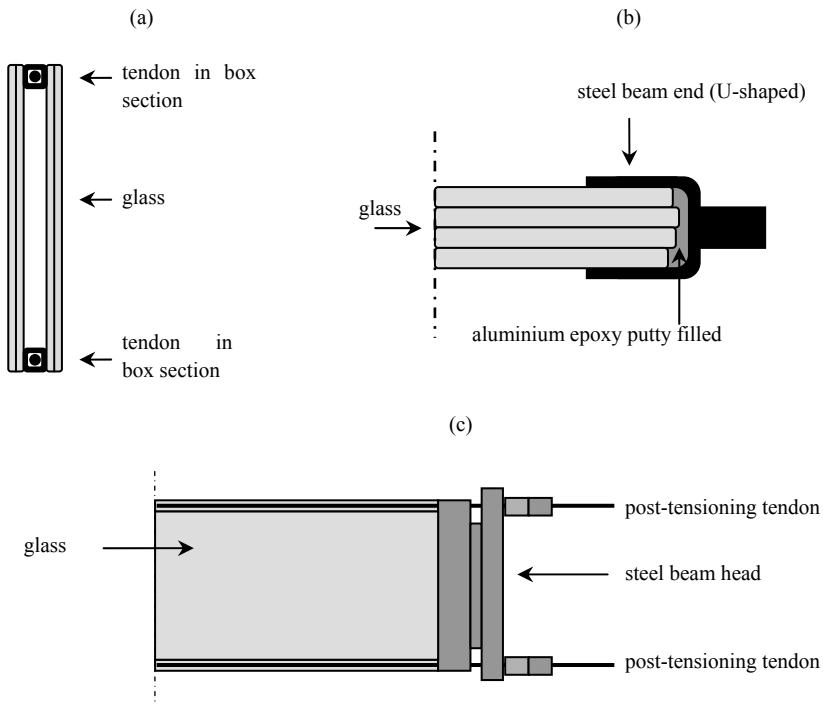

Figure IV.4: Post-tensioned hollow-section glass beam [Louter & Veer, 2007b];
(a) cross section; (b) top view beam end; (c) side view of beam end.

By means of synchronized hydraulic jacks – one for the upper and one for the lower tendon – the beam has been post-tensioned and subsequently tested in four-point bending. After the linear elastic stage the beam showed an initial dense V-shaped crack, see Figure IV.5 (a). As loading was continued, additional cracking and horizontal crack propagation occurred, see Figure IV.5 (b). The beam showed an increase in post-breakage strength (until 110 % of its initial failure load) and a (semi-)ductile post-breakage response, until the beam explosively buckled at one beam end, see Figure IV.6. At this beam end the PVB laminated glass outer panes had detached from the stainless steel box sections. Due to the applied compressive load from the post-tensioning tendons the beam locally buckled.

Compared to the response of a reinforced glass beam of an equal size – though with a different layout – the post-tensioned beam showed some striking differences, see Figure IV.5. Due to the compressive pre-stress the cracks in the post-tensioned glass beam – especially the initial cracks – were much earlier halted than in the reinforced glass beam. Therefore a larger compressive zone remained for the post-tensioned glass beam. However, the fracture pattern of the initial crack(s) in the post-tensioned beam was much more dense than in the reinforced glass beam. This difference in crack density is related to the higher energy release in the post-tensioned glass beam, which showed an about 1.8 times higher initial failure load than the reinforced glass beam. Finally, as a result of the post-tensioning force, the post-tensioned glass beam reached an about 1.7 times higher post-breakage strength than the reinforced glass beam.

From the result of the bending test on the post-tensioned glass beam and the comparison with the reinforced glass beam result it is observed that post-tensioning a glass beam offers a great potential. The compressive force applied by the steel post-tensioning tendons effectively enhances both the initial resistance load and the post-breakage resistance. However, despite the more controlled initial cracking behaviour – the cracks in the post-tensioned glass beam travelled less high than in the reinforced glass beam – the explosive final failure behaviour of the post-tensioned glass beam as a result of the applied pre-stress urges for caution. Additional research into the structural response of post-tensioned glass beams is therefore recommended.
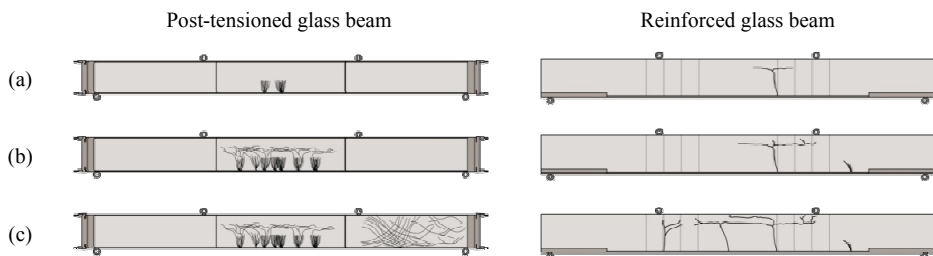

Figure IV.5: crack development in a post-tensioned glass beam and a reinforced glass beam [Louter & Veer, 2007b];.

Figure IV.6: Post-tensioned glass beam buckled at right beam end.

IV.3   Example of post-tensioned glass beams applied in practice

The feasibility of post-tensioned glass beams is demonstrated by a practical application of post-tensioned glass beams which is presented by Schober et al. [Schober, Gerber & Schneider, 2004; Schober, Gerber & Schneider, 2007], see Figure IV.7. The post-tensioned glass beams have been applied in a newly built glass roof covering spanning between two existing buildings. The triple-layer (10.15.10 mm) laminated and tempered glass beams span 6.2 m. The beams are curved along the lower edge and have a height of 396 mm at mid-span. The middle layer of the beam has been recessed to create a slot in which a small aluminum U-section and a stainless steel post-tensioning tendon of Ø 10 mm have been incorporated. The tendon is tensioned at the beam ends by means of stainless steel end pieces. The gap/space between the steel and the glass is filled with two-component mortar. The purpose of the steel tendon is to reduce the tensile stresses in the glass and to increase the residual resistance of the beams. To what extent the post-tensioning tendon has been pre-tensioned is not stated in the publication of Schober.

(a)   (b)

(c)   (d)
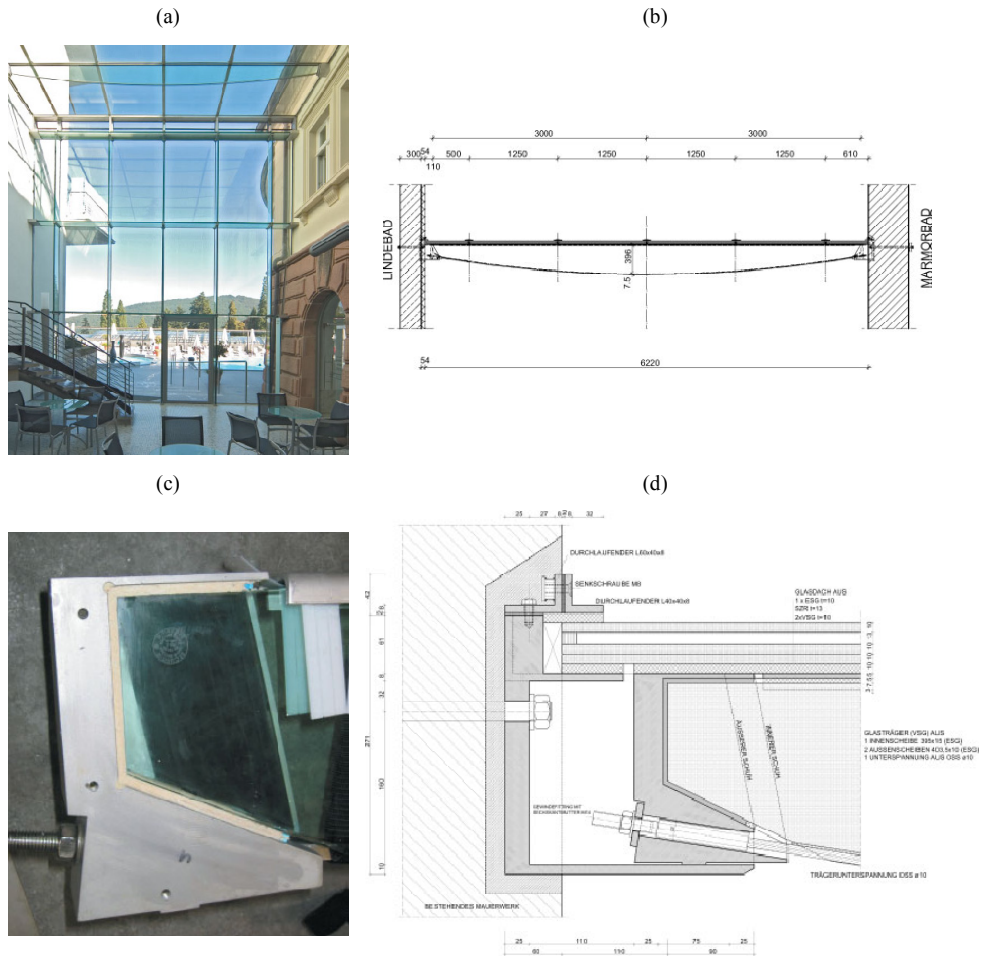
Figure IV.7: Post-tensioned glass beams applied in a glass roof covering, Badenweiler [Schober, Gerber & Schneider, 2004]; (a) photograph of the structure; (b) overview of the post-tensioned beam; (c) post-tensioned heads/shoes at the beam ends; (d) cross section at support, including the post-tensioning beam ends.

IV.4   Evaluation

From the exploratory investigations and the exemplary project it is observed that post-tensioning a glass beam is a promising concept. The post-tensioning tendon(s) effectively enhance both the initial and post-breakage resistance of the glass beam. For the annealed float glass beams investigated in associated research, it is observed that the compressive pre-stress resulting from the post-tensioning tendon(s) increases the tensile strength of the glass and limits crack propagation upon glass failure. However, due to the persisting post-tensioning force, explosive final failure occurred. It is recommended to further investigate the structural response of post-tensioned glass beams and to focus on techniques to prevent or limit the explosive failure at the post-breakage stage.

Bibliography

Bibliography

Adams & Wake, 1984

Adams RD, Wake WC, 'Structural adhesive joints in engineering', London: Elsevier Applied Science, 1984, ISBN 0-85334-263-6.

Antonelli et al., 2008

Antonelli A, Cagnacci E, Giordano S, Orlando M, Spinelli P, 'Experimental and Theoretical Analysis of C-FRP Reinforced Glass Beams', Proceedings of ISAAG 2008 conference, pg. 171-182, Munich, 2008.

Ashby & Jones, 2006

Ashby MF, Jones DRH, 'Engineering materials 2: an introduction to microstructures, processing and design', 3rd edition, Oxford: Butterworth-Heinemann, 2006, ISBN 0-7506-6381-2.

Ashby, Shercliff & Cebon, 2010

Ashby M, Shercliff H, Cebon D, 'Materials: engineering, science, processing and design', 2nd edition, Oxford : Butterworth-Heinemann, 2010, ISBN 978-1-85617-895-2, 978-1-85617-743-6.

ASTM, B 117-03

ASTM International, 'ASTM-standard B 117 – 03, Standard Practice for Operating Salt Spray (Fog) Apparatus', United States.

Badheshia & Honeycombe, 2006

Badhesia HKDH, Honeycombe RWK, 'Steels: microstructure and properties', 3rd edition, Amsterdam: Elsevier, 2006, ISBN 0-7506-8084-9.

Beddoes, 1999

Beddoes J, Parr JG, 'Introduction to stainless steels', 3rd edition, Materials Park: ASM International, 1999, ISBN 0-87170-673-3.

Belis, 2005

Belis J, 'Kipsterkte van monolithische en gelamineerde glazen liggers', Dissertation, Ghent University, Belgium, 2005.

Belis et al., 2005

> Belis J, Impe R van, Louter PC, Veer, FA, Bos FP, 'Design and testing of glass purlins for a 100 m² transparent pavilion', In s.n. (Ed.), Proceedings of the 9th international conference on architectural and automotive glass: glass processing days (pg. 392-395). Tampere: GPD, 2005.

Belis et al., 2009a

> Belis J, Visscher K de, Callewaert D, Impe van R, 'Laminating metal-to-glass; preliminary results of case-study', Conference proceedings. Tampere: Glass performance days, Glaston Finland (Oy): 2009. pg. 191-193.

Belis et al., 2009b

> Belis J, Depauw D, Callewaert D, Delincé D, Impe van R, 'Failure mechanisms and residual capacity of annealed glass/SGP laminated beams at room temperature', Engineering Failure Analysis 2009; 16(6):1866-1875.

Belis et al., 2009c

> Belise J, Callewaert D, Delincé D, Impe van R, 'Experimental failure investigation of a hybrid glass/steel beam', Engineering Failure Analysis 2009; 16(4):1163-1173.

Bennison et al., 2002

> Bennison SJ, Smith CA, Duser A van, Jagota A, 'Structural Performance of Laminated Glass made with a "Stiff" Interlayer', presented at Glasstech Asia 2002.

Bernard, Gy & Daudeville, 2002

> Bernard F, Gy R, Daudeville L, 'Finite Element Computation of Residual Stresses Near Holes in Tempered Glass Plates' Glass Technology, 43C, 2002.

Betsch, 2004

> Betsch, 'Courtyard Roof Covering in Munich', journal DETAIL Review of Architecture 2004; 10:1145-1148.

Blaauwendraad, 2007

> Blaauwendraad J, 'Buckling of laminated glass columns', Heron 2007; 52(1/2):147-164.

Bos, 2007

> Bos FP, 'Towards a combined probabilistic / consequence-based safety approach of structural glass members', Heron 2007; 52(1/2):59-86.

Bos, 2009

> Bos FP, 'Safety Concepts in Structural Glass Engineering – Towards an Integrated Approach', Dissertation, Delft: TU Delft, 2009.

Bos et al., 2004

> Bos FP, Veer FA, Hobbelman GJ, Louter PC., 'Stainless steel reinforced and post-tensioned glass beams', In C Pappalettere (Ed.), International conference on experimental mechanics / icem12 / advances in experimental mechanics, pages #1-#9 (CD-rom), Bari: Politecnico di Bari, 2004.

Bos et al., 2005a

> Bos FP, Veer FA, Belis J, Nieuwenhuijzen van EJ, Louter PC, 'The joint for the all transparent pavilion', In J Vitkala (Ed.), Glass processing days, pg. 385-388, GPD, Tampere, Finland, 2005.

Bos et al., 2005b

> Bos FP, Veer FA, Hobbelman GJ, Romein T, Nijsse R, Belis J, Louter PC, Nieuwenhuijzen van EJ, 'Designing and planning the world's biggest experimental glass structure', In J Vitkala (Ed.), Glass processing days, pg. 401-405. GPD, Tampere, Finland, 2005.

Braam & Lagendijk, 2008

> Braam CR, Lagendijk P, 'Constructieleer gewapend beton', CB2, 4th revised edition, Cement&BetonCentrum, 's Hertogenbosch, The Netherlands, 2008.

Brockmann et al., 2009

> Brockmann W, Geiß PL, Klingen J, Schröder B, 'Adhesive bonding: materials, applications and technology', Rev. and updated translation of the German book, Weinheim: Wiley-VCH, 2009, ISBN 978-3-527-31898-8.

Bucak et al., 2009a

> Bucak Ö, Geiß PL, Kötter MP, Bues M, Illguth M, 'Geklebte Stahl-Glas-Verbundtragwerke', Stahlbau 2009; 78(S1):36–40.

Bucak et al., 2009b

> Bucak Ö, Bues M, Illguth M, Geiß PL, Kötter MP, 'Bonded steel glass hybrid beams', GPD 2009, pg. 318-320.

Bucak & Meissner, 2005

> Bucak Ö, Meissner M, 'Trag- und Resttragfähigkeitsuntersuchungen an Verbundglas mit den Zwisschenlage SentryGlas Plus –Abschlussbericht', München: AIF – Fachhochschule München; 2005.

Calderone & Jacob, 2001

> Calderone I, Jacob L, 'The Fallacy of the Weibull Distribution for Window Glass Design', In Proceedings of Glass Processing Days 2001, 18-21 June, Tampere, Finland, pg. 293–297, 2001.

Callewaert et al., 2008

> Callewaert D, Delincé D, Belis J, Van Impe R, (2008), 'Temperature-dependent behaviour of glass/ionomer laminates: preliminary test results', Proceedings of Challenging Glass, pg. 431-437, 2008.

Callister, 2000

> Callister WD, 'Materials science and engineering: an introduction', 5th edition, New York: Wiley, 2000, ISBN 0-471-32013-7.

Cardarelli, 2008

> Cardarelli F, 'Materials handbook: a concise desktop reference', 2nd edition, London: Springer, 2008, ISBN 978-1-84628-668-1, 978-1-84628-669-8 (e-ISBN).

Carré & Daudeville, 1998

> Carré H, Daudeville L, 'Thermal tempering simulation of glass plates: inner and edge residual stresses, Journal of Thermal Stresses, 21: pg. 667-689, 1998.

Carvalho, 2010

> Carvalho, 'Reinforced glass – Exploring architectonical, technological and structural aspects', Project sheet, COST Action TU 0905 Structural glass – Novel Design Methods and Next Generation Products aspects, internal document, 2010.

Charles & Hillig, 1962

> Charles RJ, Hillig WB, 'The kinetics of glass failure by stress corrosion', In Symposium on Mechanical Strength of Glass and Ways of Improving it, Charleroy, Belgium, 1962.

Cruz & Pequeno, 2008a

> Cruz P, Pequeno J, 'Timber-Glass Composite Beams: Mechanical Behaviour & Architectural Solutions, Proceedings of Challenging Glass, pg. 439-448, 2008.

Cruz & Pequeno, 2008b

> Cruz P, Pequeno J, 'Structural Timber-Glass Adhesive Bonding', Proceedings of Challenging Glass, pg. 205-214, 2008.

Cruz & Pequeno, 2008c

> Cruz P, Pequeno J, 'Timber-Glass Composite Structural Panels: Experimental Studies & Architectural Applications', Proceedings of Challenging Glass, pg. 449-458, 2008.

Davis, 2003

> Davis GD, 'Durability of Adhesive Joints', book chapter in Handbook of Adhesive Technology, second edition, revised and expanded, editors PIZZI, A., MITTAL, K.L., CRC Press 2003, Print ISBN: 978-0-8247-0986-0, eBook ISBN: 978-0-203-91222-5.

DeJong, Hendrinks & Rots, 2008

> DeJong MJ, Hendriks MAN, Rots JG, 'Sequentially linear analysis of fracture under non-proportional loading', Engineering Fracture Mechanics 2008; 75(18):5042-5056.

DELO, 2009

> DELO, Industrial Adhesives, 'Technical Information, DELO-PHOTOBOND® GB368, UV- and light curing acrylate adhesive, medium viscosity', document: DELO-PHOTOBOND 368 - 12.09 (revision 20), 2009, obtained through website www.delo.de.

Delincé et al., 2008a

> Delincé D, Callewaert D, Vanlaere W, Belis J, 'Plastic deformation of polymer interlayers during post-breakage behavior of laminated glass – partim 2: Experimental validation', Int J Mod Phys B 2008; 22:5447-5452.

Delincé et al., 2008b

> Delincé D, Callewaert D, Belis J, Van Impe R, 'Post-breakage behaviour of laminated glass in structural applications', Proceedings of Challenging Glass, pg. 459-467 Delft, 2008.

De Witte & Kikstra, 2002

    De Witte FC, Kikstra WP, 'Diana – Finite Element Analysis, User's manual, release 8.1', TNO Building and Construction Research, Department of Computational Mechanics, Delft, The Netherlands, 2002.

DuPont, 2009

    DuPont, 'DuPont^{TM} SentryGlas$^®$ architectural safety glass interlayer', EI du Pont de Nemours and company, 2009, obtained through website www.sentryglas.com.

Ebnesajjad, 2008

    Ebnesajjad S, 'Adhesives technology handbook', 2nd edition, Norwich, N.Y.: William Andrew, 2008, ISBN 978-0-8155-1533-3.

Ehrenstein, 2001

    Ehrenstein GW, 'Polymeric materials: structure-properties-applications', translated from German, Munich: Hanser, 2001, ISBN 3-446-21461-5.

EN 572-1:2004

    EN 572-1:2004, 'Glass in building - Basic soda lime silicate glass products - Part 1: Definitions and general physical and mechanical properties', July 2004.

EN 572-2:2004

    EN 572-2:2004, 'Glass in building - Basic soda lime silicate glass products - Part 2: Float glass', July 2004.

EN 10278:1999

    EN 10278:1999, 'Dimensions and tolerances of bright steel products', November 1999.

EN 10088-1: 2005

    EN 10088-1: 2005, 'Stainless steels - Part 1: List of stainless steels', June 2005.

EN 10088-2: 2005

    EN 10088-2: 2005, 'Stainless steels - Part 2: Technical delivery conditions for sheet/plate and strip of corrosion resisting steels for general purposes', June 2005.

EN-ISO 12543-4, 1998

>   European Standard EN ISO 12543-4, 'Glass in building - Laminated glass and laminated safety glass - Part 4: Test methods for durability' CEN European Committee for Standardization, 1998.

EOTA, 1999

>   European Organization for Technical Approvals (EOTA), 'ETAG 002, Edition November 1999, Guideline for European technical approval for structural sealant glazing systems (SSGS), Part 1: Supported and unsupported systems', Brussels, 1999.

Feirabend, 2010

>   Feirabend S, 'Steigerung der Resttragfähigkeit von Verbundsicherheitsglas mittels Bewehrung in der Zwischenschicht', Dissertation, Universität Stuttgart, Germany, 2010.

Feirabend & Sobek, 2008

>   Feirabend S, Sobek W, 'Bewehrtes Verbundsicherheitsglas', Stahlbau 2008; 77(S1):16–22.

Feirabend & Sobek, 2009

>   Feirabend S, Sobek W, 'Improved post-breakage behavior of laminated glass due to embedded reinforcement', GPD 2009, pg. 726-729.

Feldmann, Abeln & Baitinger, 2010

>   Feldmann M, Abeln B, Baittinger M, 'Analysis of bonded hybrid steel-glass-beams by small scale tests', Challenging Glass 2, pg. 249-258, 2010.

Freitag, 2004

>   Freitag B, 'Glass-Concrete Composite Technology', Structural Engineering International 2/2004, pg. 111-117.

Froli & Lani, 2010a

>   Froli M, Lani L,'Trabes Vitrea Tensegrity: an Example of Segmental Prestressed Glass Beams', Challenging Glass 2, pg. 415-426, 2010.

Froli & Lani, 2010b

>   Froli M, Lani L, 'Glass tensegrity trusses', Structural Engineering International 2010; 20(4):436-441.

Gacnacci et al., 2008

> Gacnacci E, Orlando M, Pecora ML, Spinelli P, 'Application of C-FRP Strengthened Glass Beams in Facade Design', Proceedings of ISAAG 2008, pg. 103-114.

Gacnacci, Orlando, Spinelli, 2009

> Gacnacci E, Orlando M, Spinelli P, 'Experimental campaign and numerical simulation of the behaviour of reinforced glass beams', Proceedings of Glass Performance Days 2009, pg. 484-487.

Grenet, 1899

> Grenet L, 'Mechanical Strength of Glass', Enc. Industr. Nat. Paris 1899; 5(4):838–848.

Griffith, 1920

> Griffith AA, 'The Phenomena of Rupture and Flow in Solids', Philosophical Transactions, Series A, 221:163–198, 1920.

Gy, 2003

> Gy R, 'Stress corrosion of silicate glass: a review', Journal of Non-Crystalline Solids 2003; 316(1):1–11.

Haldimann, 2006

> Haldimann M, 'Fracture Strength of Structural Glass Elements – Analytical and numerical modeling, testing and design', Dissertation No 3671, Lausanne: EPFL, 2006.

Haldimann, Luible & Overend, 2008

> Haldimann M, Luible A, Overend M, 'Structural Use of Glass', Structural Engineering Documents 10, IABSE, Zurich, Switzerland, 2008.SED.

Hamm, 2000

> Hamm J, 'Tragverhalten von Holz und Holzwerkstoffen im statischen Verbund mit Glas', Dissertation No 2065, IBOIS/EPFL, 2000.

Hartman, Greenwood & Miller, 1996

> Hartman DR, Greenwood ME, Miller DM, 'High Strength Glass Fibers', Owens-Corning Pub. No. 1-PL-19 025-A, 1996.

Hess, 2000

Hess R, 'Glasträger', Forschungsbericht des Instituts für Hochbautechnik, vdf Hochschulverlag AG der ETH Zürich, Zürich, 2000.

Heusden, 2005

Heusden van J, 'Constructief glazen element, Toepassen van voorspanning in glas', Master thesis, Faculty of Civil Engineering & Geosciences, TU Delft, 2005.

ISE, 1999

ISE, Institution of Structural Engineers, 'Guide to the structural use of adhesives', London: Institution of Structural Engineers, 1999, ISBN 1-874266-43-3.

Kasper & Stadelmann, 2002

Kasper A, Stadelmann H, 'Chemical behavior of nickel sulfide in soda-lime-silica glass melts', Glass Science and Technology: Glastechnische Berichte 2002; 75(1):1-11.

Kreher, Natterer & Natterer, 2004

Kreher K, Natterer Jul, Natterer Joh, 'Timber-Glass-Composite Girders for a Hotel in Switzerland', Structural Engineering International 2/2004: 149-151.

Kreher, 2004

Kreher K, 'Tragverhalten und Bemessung von Holz-Glass-Verbundträgern unter Berücksichtigung der Eigenspannungen im Glas', Dissertation Nr. 2999, IBIOS/EPFL 2004.

Laufs, 2000

Laufs W, 'Ein Bemessungskonzept zur Festigkeit thermisch vorgespannter Gläser', Dissertation, RWTH Aachen, Shaker Verlag, 2000.

Lawn, 1993

Lawn B, 'Fracture of brittle solids', Second Edition, Cambridge University Press, 1993.

Leung, 2010

Leung CCK, 'Reinforcing glass with glass, Application of transparent reinforcement in structural glass beams', Master thesis, Faculty of Civil Engineering & Geosciences, TU Delft, 2010.

Levengood, 1958

Levengood WC, 'Effect of origin flaw characteristics on glass strength', Journal of Applied Physics 1958; 29(5):820–826.

Loewenstein, 1983

Loewenstein KL, 'The manufacturing technology of continuous glass fibres', 2nd edition, Amsterdam: Elsevier, 1983.

Louter, 2004

Louter PC, 'Ontwikkeling van een glazen overkappingsconstructie', Master thesis.TU Delft, 2004.

Louter, 2007

Louter PC, 'Adhesively bonded reinforced glass beams', Heron 2007; 52(1/2):31-58.

Louter, 2008

Louter PC, 'Bewehrte Glasträger', Stahlbau 2008; 77(S1):23–27.

Louter, 2009

Louter PC, 'High-strength fibre rods as embedded reinforcement in SentryGlas-laminated glass beams', In the Proceedings of the Glass Performance Days 2009, pg. 285- 289, Tampere, Finland, 2009.

Louter et al., 2005

Louter PC, Belis J, Veer FA, Hobbelman GJ, 'Reinforced glass cantilever beams', In J Vitkala (Ed.), Glass processing days, pg. 429-433, Tampere: GPD, 2005.

Louter et al., 2006a

Louter PC, Herwijnen F van, Schetters L, Romein T, Veer FA, 'Experimental research on scale 1:8 models of an 18 m reinforced glass beam', In G Siebert (Ed.), International symposium on the application of architectural glass ISAAG 2006 : conference proceedings, pg. 215-222, Munchen: Universitat der Bundeswehr, 2006.

Louter et al., 2006b

Louter PC, Heusden J van, Veer FA, Vamberský JNJA, Boer HR de, Versteegen J, 'Post-tensioned glass beams', In EE Gdoutos (Ed.), Fracture of Nano and Engineering Materials and Structures, pg. 1-9, Dordrecht: Springer, 2006.

Louter et al., 2010a

Louter PC, Leung C, Kolstein H, Vamberský J, 'Structural glass beams with embedded glass fibre reinforcement', Proceedings of Challenging Glass 2, pg. 439-448 , TU Delft, 2010.

Louter et al., 2010b

Louter PC, Belis J, Bos FP, Callewaert D, Veer FA, 'Experimental investigation of the temperature effect on the structural response of SG-laminated reinforced glass beams', Engineering Structures 2010; 32(6):1590-1599.

Louter & Veer, 2007a

Louter PC, Veer FA, 'Experimental research on scale 1:4 models of an 18m reinforced glass beam, part I', In s.n. (Ed.), Glass performance days 2007, conference proceedings, pg. 87-92, Tampere: Glass performance days, 2007.

Louter & Veer, 2007b

Louter PC, Veer FA, 'Large span reinforced glass beams, prototype research', In s.n. (Ed.), IAAS 2007 Shell and Spatial Structures, pg. 1-10, 2007.

Louter, Van de Graaf & Rots, 2010

Louter PC, Graaf A van de, Rots JG, 'Modeling the structural response of reinforced glass beams using an SLA-scheme', Proceedings of Challenging Glass 2, pg. 427-438, TU Delft, 2010.

Louter, Veer & Belis, 2008

Louter PC, Veer FA, Belis J, 'Redundancy of reinforced glass beams: temperature, moisture and time dependent behaviour of the adhesive bond', Proceedings of Challenging Glass (pg. 479-490). Amsterdam: IOS Press TU Delft, 2008.

Lubin, 1969

Lubin G, 'Handbook of fiberglass and advanced plastics composites', New York: Van Nostrand Reinhold, 1969

Luible, 2004

Luible A, 'Stabilität von Tragelementen aus Glas', Dissertation EPFL 3014, Ecole polytechnique fédérale de Lausanne (EPFL), Lausanne, 2004.

Macfarlane, 1999

> Macfarlane T, 'Construction Details for Structural Glass Assemblies', Glass Processing Days, pg. 474-476, Tampere, Finland, 1999.

Meissner & Sackmann, 2006

> Meissner M, Sackmann V, 'On the effect of artificial weathering on the shear bond and the tear strength of two different interlayers of laminated glass', in the proceedings of ISAAG 2006 conference, Munich, 2006.

Michalske & Freiman, 1983

> Michalske TA, Freiman SW, 'A Molecular Mechanism for Stress Corrosion in Vitreous Silica', Journal of the American Ceramic Society 1983; 66(4):284–288.

Netusil & Eliasova, 2010a

> Netusil M, Eliasova M, 'Experimental and Numerical Analysis of Glued Steel-Glass Joints', Proceedings of Challenging Glass 2, pg. 269-276.

Netusil & Eliasova, 2010b

> Netusil M, Eliasova M, 'Adhesively bonded hybrid steel-glass beams', ICSA, abstract pg. 97-98.

Nielsen, 2009

> Nielsen JH, 'Tempered Glass: bolted connections and related problems', Dissertation, Technical University of Denmark, Department of Civil Engineering, 2009.

Nielsen & Olesen, 2007

> Nielsen JH, Olesen JF, 'Mechanically Reinforced Glass Beams', Proceedings of the 3rd Int. Conf. On Structural Engineering, Mechanics and Computations, Cape Town, South Africa, 2007.

Nieuwenhuijzen, Bos & Veer, 2005

> Nieuwenhuijzen EJ van, Bos FP & Veer FA, 'The laminated glass column', In J Vitkala (Ed.), Glass processing days (pg. 420-423). Tampere: GPD, 2005.

Nijsse, 2003

> Nijsse R, 'Glass in structures: elements, concepts, designs', Basel: Birkhäuser, 2003, ISBN: 3-7643-6439-4.

O'Callaghan, 2008

O'Callaghan J, 'Glass Structures from Stairs to Cubes', Proceedings of Challenging Glass, pg. 29-37, Delft, May 2008, www.bk.tudelft.nl/challengingglass.

Ølgaard et al., 2008

Ølgaard AB, Nielsen JH, Olesen JF, Stang H, 'Properties of an Adhesive for Structural Glass Applications', Proceedings of Challenging Glass, pg. 263-272.

Ølgaard, Nielsen & Olesen, 2009

Ølgaard AB, Nielsen JH, Olesen JF, 'Design of Mechanically Reinforced Glass Beams – Modelling and Experiments', Structural Engineering International, 2/2009, pg. 130-136, 2009.

Palumbo, Palumbo & Mazzuchelli, 2005

Palumbo D, Palumbo M, Mazzuchell M, 'A New Roof for the XIIIth Century "Loggia de Vicari" (Arquà Petrarca – PD – Italy) Based on Structural Glass Trusses: a Case Study', GPD 2005.

Peters et al., 2007

Peters S, Fuchs A, Knippers J, Behling S, 'Ganzglastreppe mit transparenten SGP-klebeverbindungen – Konstruktion and statische Berechnung', Stahlbau 2007; 76(3):151-156.

Petrie, 2007

Petrie EM, 'Handbook of adhesives and sealants', book, New York, McGraw-Hill, 2007, ISBN: 978-0-07-147916-5 / 0-07-147916-3.

prEN 13474-1: 1999

prEN 13474-1: 1999, 'Glass in building - Design of glass panes - Part 1: General basis of design', February 1999.

prEN 13474-2: 2000

prEN 13474-2: 2000, 'Glass in building - Design of glass panes - Part 2: Design for uniformily distributed loads', February 2000.

Puller, 2008

Puller K, Sobek W, 'Glass-Steel Connections Using Acrylate Adhesives', Proceedings of Challenging Glass, pg. 273-278, Delft, 2008.

Rademakers, 2008

> Rademakers M, Master thesis, Civil Engineering and Geosciences, TU Delft, 2008.

Rice & Dutton, 1995

> Rice P, Dutton H, 'Structural Glass', 2nd edition, London: Spon, 1995, ISBN: 0-419-19940-3.

Richemont & Veer, 2007

> Richemont S de, Veer FA, 'Glass-aluminium bonded joints; testing, comparing and designing for the ATP', Heron 2007; 52(1/2):105-122.

Rots, 1988

> Rots JG, 'Computational modelling of concrete fracture', Dissertation, TU Delft, 132 pp, 1988.

Rots, 2001

> Rots JG, Sequentially linear continuum model for concrete fracture. In Fracture mechanics of concrete structures: pg. 831-839. Rotterdam: Balkema, 2001.

Rots et al., 2009

> Rots JG, Invernizzi S, Belletti B, Hendriks MAN, 'Circumventing bifurcations in structural softening', In proceedings of the Computational Modeling Workshop on Concrete, Masonry and on Fiber-reinforced Composites, June 17-18, 2009, Delft, The Netherlands.

Rots, Belletti & Invernizzi, 2008

> Rots JG, Belletti B, Invernizzi S, 'Robust modeling of RC structures with an "event-by-event" strategy', Engineering Fracture Mechanics 2008; 75: 590-614.

Schetters, 2007

> Schetters LPT, 'Design and evaluation of a large span glass beam with a safe failure behaviour', Master thesis, Faculty of Architecture, Building and Planning, Eindhoven University of Technology, 2007.

Schittich et al., 2007

> Schittich C, Schuler M, Balkow D, Staib G, Sobek W, 'Glass Construction Manual',2nd edition, Basel: Birkhäuser, 2007, ISBN: 978-3-7643-8122-6.

Schlaich J, Schäfer K & Jennewein M, 1987

Schlaich J, Schäfer K, Jennewein M, 'Toward a Consistent Design of Structural Concrete' PCI Journal 1987; 32(3):74-150.

Schneider & Hilcken, 2010

Nickel Sulphide (NiS-) induced failure of glass: fracture mechanics model and verification by fracture data', in proceedings of Engineered Transparency Conference 2010, pg. 125-136, Schneider & Weller (eds.), 2010, ISBN 978-3-86780-177-5.

Schober, Gerber & Schneider, 2004

Schober RH, Gerber H, Schneider J, 'Ein Glashaus für die Therme in Badenweiler', Stahlbau 2004; 73(11):886–892.

Schober, Gerber & Schneider, 2007

Schober RH, Gerber H, Schneider J, 'Glass house Badenweiler', in CRISINEL M, EEKHOUT M, HALDIMANN M, VISSER R (editors), 'EU COST C13 Glass & Interactive Building Envelopes', IOS Press Amsterdam, 2007, ISBN: 978-1-58603-709-3, pg. 271-276.

Shelby, 2005

Shelby JE, 'Introduction to glass science and technology', Cambridge: Royal Society of Chemistry, 2005, ISBN: 0-85404-639-9.

Stelzer, 2010

Stelzer I, 'High Performance Laminated Glass', Challenging Glass 2, pg. 467-474, Delft, 2010.

Tasche, 2008

Tasche S, 'Strahlungshärtende Acrylate im Konstruktiven Glasbau', Dissertation, Technische Universität Dresden, Dresden, Germany, 2008, ISBN 978-3-86780-086-6.

Trovato, 2009

Trovato D, 'Sequentially linear analysis for a reinforced glass beam', Master thesis, Politecnico di Torino, 2009.

Ungermann & Preckwinkel, 2010

Ungermann D, Preckwinkel E, 'Structural Behaviour of Hybrid Steel-Glass Beams', Proceedings of Challenging Glass 2, pg. 485-495, 2010.

Van de Graaf, 2008

>   Van de Graaf AV, 'Sequentially linear analysis as an alternative to nonlinear analysis applied to a reinforced glass beam', 7th fib PhD Symposium (pg. 63-71), 2008.

Van de Graaf, Hendriks & Rots, 2009

>   Van de Graaf AV, Hendriks MAN, Rots JG, 'Sequentially linear analysis for modeling tunnelling-induced surface structure damage', 2nd Int. Conf. on computational methods in tunnelling, EURO: TUN 2009 (pg. 977-984). Freiburg, Germany: Aedificatio Publishers.

Van de Graaf, Hendriks & Rots, 2010

>   Van de Graaf AV, Hendriks MAN, Rots JG, 'A discrete cracking model for sequentially linear analysis', In Nenad Bicanic, Rene Borst, de, Herbert Mang & Gunther Meschke (Eds.), Computational modelling of concrete structures - euro-c 2010 (pg. 409-418). Leiden: CRC PRess - Taylor & Francis Group, 2010.

Veer, 2005

>   Veer FA, '10 years of zappi research', In J Vitkala (Ed.), Glass processing days (pg. 424-428). Tampere: GPD, 2005.

Veer, 2007

>   Veer FA, 'The strength of glass, a nontransparent value', Heron 2007; 52(1/2):87-104.

Veer et al., 2003a

>   Veer FA, Rijgersberg H, Ruytenbeek D, Louter PC, Zuidema J, 'Composite Glass Beams, The third Chapter', Proceedings of the 8th Glass Processing Days, Finland, 2003.

Veer et al., 2003b

>   Veer FA, Gross S, Hobbelman GJ, Vredeling M, Janssen MJHC, Van der Berg R, Rijgersberg HA, 'Spanning structures in glass', In J Vitkala (Ed.), Glass processing days / educational glass conference (pg. 78-81). Tampere, Finland: Glass processing days / tamglass ltd.Oy, 2003.

Veer, Janssen & Nägele, 2005

>   Veer FA, Janssen MJHC, Nägele T, 'The Possibilities of Glass Bond Adhesives', In J Vitkala (Ed.), Glass processing days (pg. 436-439). Tampere: GPD, 2005.

Veer, Louter & Bos, 2009

> Veer FA, Louter PC, Bos FP, 'The Strength of annealed, heat-strengthened and fully tempered float glass', Fatigue & Fracture of Engineering Materials & Structures 2009; 32(1):18–25.

Veer, Riemslag & Ting, 2001

> Veer FA, Riemslag AC, Ting CN, 'Structurally Efficient Glass Laminated Composite Beams' In J Vitkala (Ed.), Glass Processing Days (pg. 363-367). Tampere, Finland: Glass Processing Days/Tamglass Ltd.Oy, 2001.

Veer & Rodichev, 2009

> Veer FA, Rodichev Y, 'The strength of glass, size effects', In J Vitkala (Ed.), Proceedings of the Glass Performance Days 2009 (pg. 851-853). Tampere Finland: Glass PerformanceDays, Glaston Finland Oy. (TUD).

Veer & Zuidema, 2008

> Veer FA, Zuidema J, 'The relation between the adhesive application method and the fatigue lifetime for a photocatalytic adhesive joint', International Journal of Adhesion and Adhesives 2008; 28(6):291-295.

Vogt, 2009

> Vogt I, 'Strukturelle Klebungen mit UV- und lichthärtenden Acrylaten', Dissertation, Technische Universität Dresden, Dresden, Germany, 2009, ISBN 978-3-86780-129-4.

Wallenberger & Bingham, 2010

> Wallenberger FT, Bingham PA, 'Fiberglass and glass technology: energy-friendly compositions and applications', WALLENBERGER FT, BINGHAM PA (editors), New York: Springer, 2010, ISBN 978-1-4419-0735-6, 978-1-4419-0736-3 (eBook).

Walraven, 2006

> Walraven JC, 'College gewapend beton', reader to course CT2051B/3051B, Faculty of Civil Engineering, April 2006.

Weller, Meier & Weimar, 2010

> Weller B, Meier A, Weimar T, 'Glass-Steel Beams as Structural Members of Facades', Proceedings of Challenging Glass 2, pg. 517-524.

Weller & Tasche, 2009

>   Weller B, Tasche S, 'Experimental Evaluation of Ultraviolet and Visible Light Curing Acrylates for Use in Glass Structures', Journal of ASTM International 2009; 6(9).

Weller, Weimar & Meier, 2010

>   Weller B, Weimar T, Meier A, 'Hybrid façade system made of glass and steel', Proceedings of the Engineered Transparency Conference 2010, Dusseldorf, 2010.

Wellershoff & Sedlacek, 2003

>   Wellershoff F, Sedlacek G, 'Structural Use of Glass in Hybrid Elements: Steel-Glass-Beams, Glass-GFRP-Plates', Proceedings of GPD 2003, pg. 268-270.

Wellershoff, Sedlacek, & Kasper, 2004

>   Wellershoff F, Sedlacek G, Kasper R, 'Design of joints, members and hybrid elements for glass structures', Proceedings of ISAAG 2004, pg. unknown.

Wiederhorn & Bolz, 1970

>   Wiederhorn SM, Bolz LH, 'Stress corrosion and static fatigue of glass', Journal of the American Ceramic Society 1970; 53(10):543–548.

Wigginton, 1996

>   Wigginton M, 'Glass in Architecture', London: Phaidon, 1996, ISBN: 0-7148-2922-6.

Wörner, Schneider & Fink, 2001

>   Wörner JD, Schneider J, Fink A, 'Glasbau: Grundlagen, Berechnung, Konstruktion', Berlin: Springer, 2001, ISBN 3-540-66881-0.

Wurm, 2007

>   Wurm J, 'Glass structures: design and construction of self-supporting skins', Basel: Birkhäuser, 2007, ISBN: 978-3-7643-7608-6 / 978-3-7643-8317-6.

Curriculum Vitae

Curriculum Vitae

Christian Louter was born on 15 April 1979 in Papendrecht in the Netherlands. He grew up in Papendrecht and attended there the pre-university education at *De Lage Waard,* from which he graduated in 1997. Subsequently, he started his academic education at the Faculty of Architecture at the Delft University of Technology (TU Delft) in the Netherlands. During his studies he was member of the board of the student association *BouT* and responsible for the organisation of educational events, such as lectures and a study-trip to Finland. In 2004 he graduated with honourable mention in Building Technology. His MSc thesis project focused on the structural application of glass.

Later in 2004, Christian started as a research fellow at the structural glass research group at the department of Mechanics in Buildings at the Faculty of Architecture of the TU Delft. At that time the research group focused on the construction of an all glass pavilion. Within a team of researchers and students, Christian was responsible for the design, testing and construction of the main reinforced glass beams for this pavilion.

From 2005, Christian continued his structural glass research as a doctoral candidate on the topic of 'reinforced glass beams' at this same research group. During his doctoral research he was member of the CUR/KCG Working Group on Structural Glass. Furthermore, alongside the structural glass research at TU Delft, Christian and his close colleague Freek Bos, initiated and organized the international Challenging Glass conferences on the architectural and structural applications of glass.

Currently, Christian is employed at the Steel Structures Laboratory (ICOM) of the École Polytechnique Fédérale de Lausanne (EPFL) in Switzerland, where he continues his research on structural glass.

In addition, Christian is chairman of Working Group 4 'Novel Glass Assemblies' of the European Cost Action TU0905, member of the Scientific Committee to the ICSA 2013 conference, lector at the post-academic course on structural glass at the TU Delft (edition 2005, 2007 & 2009) and candidate-member of the IABSE Working Group on Structural Glass.

Education

1997 - 2004	**Master of Science**, at the department of Building Technology, Faculty of Architecture, TU Delft, the Netherlands
1991 - 1997	**Preuniversity education** De Lage Waard, Papendrecht, the Netherlands

Working experience

2010 - present	**Research Engineer** at the Steel Structures Laboratory (ICOM), École Polytechnique Fédérale de Lausanne (EPFL), Switzerland
2005 - 2010	**PhD candidate** at the chair of Mechanics in Buildings, Faculty of Architecture, TU Delft, the Netherlands
2004 - 2005	**Research fellow** at the chair of Mechanics in Buildings, Faculty of Architecture, TU Delft, the Netherlands

Committees & other

- **European COST Action TU 0905**
  Structural Glass - Novel Design Methods and Next Generation Products
  Chairman of Working Group 4 Novel Glass Assemblies (2010 – ongoing)
- **ICSA 2013 Conference**
  International Conference on Structures and Architecture
  Member of the international Scientific Committee (2010 - 2013)
- **Challenging Glass Conference**
  International Conference on Architectural and Structural Applications of Glass
  Co-chairman of the Challenging Glass Conference series (2008, 2010)
- **IABSE, International Association for Bridge and Structural Engineering**
  International Working Group Structural Glass
  Candidate Member of the Committee (2007 – ongoing)
- **CUR & Kenniscentrum Glas**
  National Working Group Structural Glass
  Member of the Committee (2005-2007)
- **PAO course**
  Post Academic Course on Structural Glass
  Lecturer at the structural glass course (2005, 2007 and 2009)

Journal Publications

- P.C. Louter, J. Belis, F. Bos, D. Callewaert and F. Veer, 'Experimental investigation of the temperature effect on the structural response of SG-laminated reinforced glass beams' *Engineering Structures*, 32(6), 1590-1599, 2010.
- P.C. Louter, 'Bewehrte Glasträger', *Stahlbau -Berlin-*, 77(S1), 23-27, 2008
- P. C. Louter, 'Adhesively bonded reinforced glass beams', *Heron*, 52(1/2), 31-58, 2007